Scalar Dissipation Rate based Flamelet Modelling of Turbulent Premixed Flames

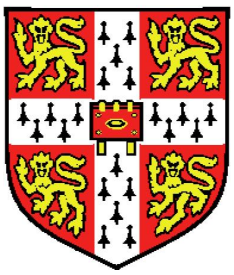

Hemanth Kolla

Department of Engineering

University of Cambridge
(Trinity Hall)

A dissertation submitted for the degree of

Doctor of Philosophy

November 2009

Declaration

This dissertation is the result of my own work and includes nothing which is the outcome of work done in collaboration except where specifically indicated in the text.

This dissertation contains approximately 35000 words and includes 49 figures.

Hemanth Kolla
February 1, 2010

To my motherland, for the warmth of her womb

and

To Nalanda, for the warmth of her embrace

Acknowledgements

I would like to express my sincere gratitude to Dr. N. Swaminathan for his constant support, advice and encouragement. I have learnt a great deal under his tutelage and benefited immensely from his supervision. I would also like to thank Professors Stewart Cant and Nondas Mastorakos for their invaluable guidance throughout the course of my PhD. Acknowledgements are due to Cambridge Commonwealth Trust and Cambridge Nehru Trust whose generous financial support helped fund my studies. Conference grants from Cambridge University Engineering Department, Trinity Hall and Combustion Institute are also gratefully acknowledged. Acknowledgements are also due to Rolls–Royce plc. and in particular Dr. Ruud Eggels for the technical support.

A special note of thanks to Mrs. Kate Graham and Mr. Peter Benie of Hopkinson laboratory without whose help finishing my PhD would have been very arduous. Friends and colleagues have greatly contributed to making my stay in Cambridge a memorable experience. I will forever cherish my association with members of Heat Gallery: Dr. Jim Rogerson, Olliver, Mark, Inkyu, Tristan, Tee, Larry, Shokri and Shaohong. In addition, I would like to thank my fellow Indian scholars at Cambridge who have helped me on various occasions and in particular Pashmina, Sriram and Sandeep for being such dependable buddies.

I'm deeply indebted to my parents and my brother for their continued love and support and their faith in my endeavours. And finally I'd like to thank my wife Nalanda for being a patient companion and making it all worthwhile.

Scalar Dissipation Rate based Flamelet Modelling of Turbulent Premixed Flames

Hemanth Kolla

Lean premixed combustion has potential for reducing emissions from combustion devices without compromising fuel efficiency, but it is prone to instabilities which presents design difficulties. From emissions point of view reliable predictions of species formation rates in the flame zone are required while from the point of view of thermo–acoustics the prediction of spatial variation of heat release rate is crucial; both tasks are challenging but imperative in CFD based design of combustion systems. In this thesis a computational model for turbulent premixed combustion is proposed in the RANS framework and its predictive ability is studied.

The model is based on the flamelet concept and employs strained laminar flamelets in reactant–to–product opposed flow configuration. The flamelets are parametrised by scalar dissipation rate of progress variable which is a suitable quantity to describe the flamelet structure since it is governed by convection–diffusion–reaction balance and represents the flame front dynamics. This paramaterisation is new. The mean reaction rate and mean species concentrations are obtained by integrating the corresponding flamelets quantity weighted by the joint pdf of the progress variable and its dissipation rate. The marginal pdf of the progress variable is obtained using β–pdf and the pdf of the conditional dissipation rate is presumed to be log–normal. The conditional mean dissipation rate is obtained from unconditional mean dissipation rate which is a modelling parameter. An algebraic model for the unconditional mean scalar dissipation rate is proposed based on the relevant physics of reactive scalar mixing in turbulent premixed flames. This algebraic model is validated directly using DNS data. An indirect validation is performed by deriving a turbulent flame speed expression using the Kolmogorov–Petrovskii–Piskunov analysis and comparing its predictions with experimental data from a wide range of flame and flow conditions.

The mean reaction rate closure of the strained flamelets model is assessed using RANS calculations of statistically planar one–dimensional flames in corrugated flamelets and thin reaction zones regimes. The flame speeds predicted by this

closure were close to experimental data in both the regimes. On the other hand, an unstrained flamelets closure predicts flame speed close to the experimental data in the corrugated flamelets regime, but overpredicts in the thin reaction zones regime indicating an overprediction of the mean reaction rate.

The overall predictive ability of the strained flamelets model is assessed via calculations of laboratory flames of two different configurations: a rod stabilised V–flame and pilot stabilised Bunsen flames. For the V–flame, whose conditions correspond to the corrugated flamelets regime, the strained and unstrained flamelets models yield similar predictions which are in good agreement with experimental measurements. For the Bunsen flames which are in the thin reaction zones regime, the unstrained flamelet model predicts a smaller flame brush while the predictions of the strained flamelets model are in good agreement with the experimental data. The major and minor species concentrations are also reasonably well predicted by the strained flamelets model, although the minor species predictions seem sensitive to the product stream composition of the laminar flamelets.

The fluid dynamics induced attenuation of the reaction rate is captured by the strained flamelets model enabling it to give better predictions than the unstrained flamelets model in the thin reaction zones regime. The planar flames and laboratory flames calculations illustrate the importance of appropriately accounting for fluid dynamic effects on flamelet structure and the scalar dissipation rate based strained flamelet model seems promising in this respect. Furthermore, this model seems to have a wide range of applicability with a fixed set of model parameters.

Contents

List of Figures viii

Nomenclature xiv

1 Introduction 1

2 Background on Premixed Flame Modelling 6

2.1 Laminar Flames 7

2.2 Turbulent Flames 10

2.2.1 RANS Governing Equations 10

2.2.2 Regimes of Turbulent Premixed Combustion 13

2.2.3 Bray–Moss–Libby Model 16

2.2.4 Flame surface density models 19

2.2.5 G–Equation Level Set Formalism 21

2.2.6 PDF transport approach 22

2.2.7 Presumed PDF approaches 23

2.2.8 Conditional Moment Closure 24

2.2.9 Chemistry Tabulation 26

3 Scalar Dissipation Rate 28

3.1 Definition and Physical Meaning 28

3.2 Role in Turbulent Combustion Modelling 30

3.2.1 Non–Premixed Combustion 32

3.2.2 Premixed Combustion 33

3.2.3 Stratified/Partially Premixed Combustion 34

3.3 Summary 35

4 Strained Flamelet Formulation for Premixed Flames **36**
4.1 Scalar Dissipation Parametrisation 38
4.1.1 Motivation 39
4.2 Choice of Flamelet Configuration 40
4.2.1 Reactant–to–Reactant Flamelet 41
4.2.2 Reactant–to–Product Flamelet 42
4.3 Shapes of the PDFs 46
4.4 Conditional Mean Scalar Dissipation Rate 49
4.5 Summary 52

5 Modelling of Mean Scalar Dissipation Rate **53**
5.1 Transport Equation 54
5.2 Modelling of Dominant Terms 55
5.2.1 Dissipation–Dilatation correlation, T_2 55
5.2.2 Turbulence–Scalar interaction, T_{32} 57
5.2.3 Flame front curvature, $(T_4 - D_2)$ 59
5.3 Algebraic Model for $\widetilde{\epsilon_c}$ 59
5.3.1 Realisability 61
5.4 Validation 62
5.4.1 Attributes of DNS data 62
5.4.2 Comparisons with DNS data 64
5.5 Summary 66

6 Turbulent Flame Speed **67**
6.1 Expression for Turbulent Flame Speed 67
6.1.1 Analysis of the Flame Speed expression 69
6.2 Flame Speed definitions in Experiments 72
6.3 KPP analysis 75
6.3.1 KPP analysis of a planar one–dimensional flame 75
6.3.2 Applicability to multi–dimensional flames 76
6.4 Comparisons with experimental data 78
6.4.1 Flame speed datasets 80
6.4.2 Results 84

6.5 Summary 89

7 Application of Strained Flamelet Formulation 96

7.1 Computational methodology 96

7.1.1 Overview of modelling closures 98

7.2 RANS of planar one–dimensional flames 99

7.2.1 Computational details 99

7.2.2 Results and discussion 104

7.3 RANS of laboratory flames 113

7.3.1 Computational details 114

7.3.1.1 V–flame calculations 114

7.3.1.2 Bunsen flames calculations 116

7.3.2 Results and discussion 120

7.3.2.1 V–flame 120

7.3.2.2 Bunsen flames 122

7.4 Summary 143

8 Conclusions and Future work 146

8.1 Recommendations for future work 147

8.1.1 Lewis number effects 148

8.1.2 Sensitivity to turbulence closure 148

8.1.3 Unsteady strain, non–adiabaticity and curvature 149

8.1.4 Stratified combustion 150

8.1.5 Statistically non–planar flames 150

8.1.6 Modelling for CMC 150

8.1.7 Modelling for LES 151

A Relations between Reynolds and Favre averaged quantities 152

B List of Publications 154

References 155

List of Figures

2.1 Turbulent combustion regime diagram of Peters (2000). 15

4.1 Schematic of purely strained planar laminar flamelet configurations: (a) Reactant–to–Reactant (RtR) and (b) Reactant–to–Product (RtP). 41

4.2 Normalised reaction rate, $\dot{\omega}^+$, profiles of RtP flames of lean CH_4–air mixture ($\phi = 0.6$), at various strain rates, plotted against the distance from the stagnation plane. 43

4.3 The surface of $\dot{\omega}^+(c, N_c^+)$ from RtP flame calculations of lean CH_4–air mixture, $\phi = 0.6$. 45

4.4 The surface of $\dot{\omega}^+(c, N_c^+)$ from RtP flame calculations of lean C_3H_8–air mixture, $\phi = 0.8$. 46

4.5 Representative curves of $\dot{\omega}^+$ vs N_c^+ conditioned on the progress variable ζ for three cases: (a) methane–air, $\phi = 0.6$, Le = 0.96, (b) propane–air, $\phi = 0.8$, Le = 1.83 and (c) methane–air, $\phi = 1.4$, Le = 1.17 . The $\zeta = 0.7$ curve for the propane–air case is shown in (d) and its integration is discussed in the text. 47

4.6 Profiles of $N_c(\zeta)/N_c(\zeta^*)$ for three mixtures: (a) CH_4–air of $\phi = 0.6$; (b) CH_4–air of $\phi = 1.0$ and (c) C_3H_8–air of $\phi = 0.8$. The unstrained flame is the solid and strained flames are dashed curves. 50

5.1 Attributes of the DNS data on the combustion regime diagram. . 63

5.2 Comparisons of $\widetilde{\epsilon_c}$ predicted by various models with DNS data. . . 65

6.1 Typical prediction of Eq. (6.3) for three different values of Λ/δ_L^o with $\tau = 5$. 71

6.2 Schematic showing a turbulent flame brush. The thick solid curves denote the flame brush boundaries and the dashed line denotes an iso–surface of $\tilde{c}$ inside the flame brush. The thin solid line denotes an instantaneous c iso–contour with displacement speed s_d. The orthogonal curvilinear coordinate system (η, ξ, ζ) is attached locally to the $\tilde{c}$ iso–surface. 73
6.3 Typical comparisons of turbulent flame speed expressions to the experimental data of Shepherd & Cheng (2001). 79
6.4 Turbulent combustion regime diagram (Peters, 2000) with attributes of various experimental flames: $*$ Smith & Gouldin (1978); ♦ Aldredge *et al.* (1998); $\triangle$ Kobayashi *et al.* (1996); $\triangledown$ Savarianandam & Lawn (2006); $\circ, \bullet$ Il'yashenko & Talantov (1966). 83
6.5 The predictions of turbulent flame speed expressions are compared to the experimental data of Smith & Gouldin (1978) for various equivalence ratios: (a)–(c) correspond to $\phi = 0.75$; (d)–(f) correspond to $\phi = 0.85$ and (g)–(i) correspond to $\phi = 1.0$. The comparisons on the left, center and right columns correspond to $\Lambda =$ 0.69mm, 0.95mm and 1.49mm respectively. 91
6.6 The predictions of turbulent flame speed expressions are compared to the experimental data of Aldredge *et al.* (1998) for various equivalence ratios: (a) $\phi = 1.0$; (b) 1.1; (c) 1.2; (d) 1.3; (e) 1.4; (f) 1.5; (g) 0.8; (h) 0.9. 92
6.7 The variation of turbulent flame speed with u'/s_L^o at different pressures: (a) 0.1 MPa; (b) 0.5 MPa; (c) 1 MPa; (d) 2 MPa; (e) 3 MPa. The experimental data of Kobayashi *et al.* (1996) are compared to the flame speed expression. 93
6.8 Comparisons of turbulent flame speed prediction to the experimental data of Savarianandam & Lawn (2006). 94
6.9 Comparisons of turbulent flame speed prediction to the experimental data of Il'yashenko & Talantov (1966). 94
6.10 Comparison of turbulent flame speed expressions to the experimental database of Abdel-Gayed *et al.* (1987) for two values of flame stretch parameter, K: (i) K = 0.053 and (ii) K = 0.15. 95

7.1 The regime diagram with the parameters of the one–dimensional computational flames for two values of flame stretch parameter K: 0.15 (⧫) and 1.0 (•). 101
7.2 The progress of the solution in a typical one–dimensional flame calculation. Starting from an arbitrary initial profile (dashed line), the flame brush travels from right to left. 102
7.3 History of displacement speed, S_d, in m/s for three $\tilde{c}$ values in two flames: (a) $u'/s_L^o = 4$, K = 0.15 (b) $u'/s_L^o = 12$, K = 1.0. The results are shown for the algebraic closure of the mean reaction rate. 103
7.4 The spatial profiles of $\tilde{c}$ predicted by the various models plotted against the normalised distance for two cases: (a) $u'/s_L^o = 4$, K = 0.15 (b) $u'/s_L^o = 16$, K = 1.0. The location of $\tilde{c} = 0.5$ in each case is denoted by x_1. 105
7.5 The normalised flame brush thickness, δ_t/δ_L^o, predicted by various models at different u'/s_L^o, for two values of flame stretch parameter: (a) K = 0.15 and (b) K = 1. 106
7.6 The shape of the density weighted pdf of progress variable, $\widetilde{p}(\zeta)$, at three locations in the flame brush ($\tilde{c}$ = 0.1, 0.5 and 0.9) from the strained flamelet calculations for two cases : (a) $u'/s_L^o = 3$, K = 0.15 and (b) $u'/s_L^o = 24$, K = 1. The inset in (b) shows the values of $\int_{0.1}^{0.9} \widetilde{p}(\zeta;\tilde{c})\, d\zeta$ for the two cases. 108
7.7 Comparisons of predicted flame speeds with the experimental data of Abdel-Gayed *et al.* (1987) for two values of flame stretch parameter: (a) K = 0.15 and (b) K = 1. 110
7.8 Flame speeds predicted by the strained flamelet closure for two mixtures: stoichiometric methane–air with K = 1.0 (•) and lean propane–air with KLe = 1.0 (◊). The experimental data of Abdel-Gayed *et al.* (1987) for K = 1.0 are also shown (○). 111
7.9 The comparisons of flame speeds predictions with the predictions of Bradley *et al.* (1994) for two values of flame stretch parameter: (a) KLe = 0.15 and (b) KLe = 1. 112

7.10 The regime diagram with conditions of the V–flame (•) of Robin *et al.* (2008) and the Bunsen flames (⧫) of Chen *et al.* (1996). . . 114
7.11 The schematic of the computational domain for the V–flame calculation. The 'O'–grid in the region close to the rod is also shown. 115
7.12 The schematic of the computational domain for the Bunsen flames calculations. The diameter of the nozzle jet is D. 117
7.13 The calculated longitudinal (left) and transverse velocities (right) in m/s using the unstrained flamelets (dashed lines) and strained flamelets (solid lines) models are compared with the experimental data (∘) for the V–flame (Robin *et al.*, 2008) at three downstream locations. 121
7.14 The calculated mean progress variable using the unstrained flamelets (dashed lines) and strained flamelets (solid lines) models are compared with the experimental data (dots) of the V–flame (Robin *et al.*, 2008) at two streamwise locations. 122
7.15 The contours of $\overline{\dot{\omega}}/\overline{\rho}$ (s^{-1}) from the V–flame calculations. The contours in $x < 0$ region are for the strained flamelets while those in $x > 0$ region are for the unstrained flamelets. 123
7.16 The normalised mean axial velocity and normalised mean turbulent kinetic energy from non–reacting flow calculations (solid lines) of case F2 are compared with the experimental data (∘) of Chen *et al.* (1996). 124
7.17 The normalised mean axial velocity and normalised mean turbulent kinetic energy from non–reacting flow calculations (solid lines) of case F1 are compared with the experimental data (∘) of Chen *et al.* (1996). 126
7.18 The normalised mean axial velocity and normalised mean turbulent kinetic energy from non–reacting flow calculations (solid lines) of case F3 are compared with the experimental data (∘) of Chen *et al.* (1996). 127
7.19 The normalised mean axial velocity from reacting flow calculations of flames F1 (left), F2 (center) and F3 (right) are compared with the experimental data of Chen *et al.* (1996). 128

7.20 The normalised mean turbulent kinetic energy from reacting flow calculations using the strained flamelets model of flames F1 (left), F2 (center) and F3 (right) are compared with the experimental data of Chen *et al.* (1996). 129
7.21 The contour plot of temperature (K) from the Bunsen flame calculations for case F3. The plot for the entire computational domain (top) and the region close to the nozzle exit (bottom) are shown. 130
7.22 The mean progress variable, $\overline{c}$, using the strained flamelets model is compared with the experimental data of Chen *et al.* (1996) for flames F1 (left), F2 (center) and F3 (right). 133
7.23 The mean CH_4 mass fractions from strained flamelets calculations are compared with the experimental data of Chen *et al.* (1996) for flames F1 (left), F2 (center) and F3 (right). 134
7.24 The root mean square progress variable fluctuations, $\sqrt{\overline{c'^2}}$, from strained flamelets calculations are compared with the experimental data of Chen *et al.* (1996) for flames F1 (left), F2 (center) and F3 (right). 135
7.25 The turbulent flame brush thicknesses, δ_t (mm), from the strained flamelets calculations are compared with the experimental data (•) of Chen *et al.* (1996) for flames F1 (left), F2 (center) and F3 (right). 136
7.26 The mean progress variable, $\overline{c}$, (left) and mean CH_4 mass fraction (right) from the unstrained flamelet calculations are compared with the experimental data of Chen *et al.* (1996) for flame F2. 137
7.27 The major species mass fractions: O_2 (○, _ _ _), CO_2 (•, ___) and H_2O (△, _ _), from strained flamelets calculations are compared with the experimental data (symbols) of Chen *et al.* (1996) for flames F1 (left), F2 (center) and F3 (right). 139
7.28 The minor species mass fractions: 10×CO (○, _ _ _) , 100×H_2 (•, ___) and 75×OH (△, _ _), from strained flamelets calculations are compared with the experimental data (symbols) of Chen *et al.* (1996) for flames F1 (left), F2 (center) and F3 (right). 140

7.29 The predictions of $10 \times Y_{\mathrm{CO}}$ using strained flamelets model (__) are compared with predictions of Herrmann (2006) (_ _ _) and Lindstedt & Vaos (2006) (_ _) for flame F3 at $x/D = 4.5$. The sensitivity of strained flamelets predictions to RtP flamelet boundary conditions are shown: (a) equilibrium mixture composition for product stream, (b) product stream comprising of only CO_2 and H_2O. . . 141

7.30 The predictions of $10 \times$CO from strained flamelet calculations using two definitions of progress variable: c_f (_ _ _) and c_p (_ _) are compared with the experimental data of Chen *et al.* (1996) for flame F2. 142

Nomenclature

Roman Symbols

a_T Tangential strain rate

c Reaction progress variable

C_3, C_4 Constants in the model for T_{32}

$\mathfrak{L}$ Markstein length

c_f Progress variable based on fuel mass fraction

C_p Mixture specific heat

c_p Progress variable based on mass fraction of CO and CO_2

$C_{p,\alpha}$ Specific heat at constant pressure of species α

D_2, T_2, T_{32}, T_4 Unclosed leading order terms in $\widetilde{\epsilon_c}$ transport equation

Da Damköhler number

D_α Equivalent diffusion coefficient of species α

D_c Diffusivity of the progress variable

$D_{k\alpha}$ Binary diffusion coefficient of species k and α

D_{th} Thermal diffusivity

e Internal energy

g Normalised progress variable variance

h_α Total enthalpy of species α

K Flame stretch factor

Ka Karlovitz number

K_c, K_c^* Constants in the model for T_2

$K_{f,j}$ Forward rate of reaction j

$K_{r,j}$ Reverse rate of reaction j

Le_α Lewis number of species α

Le Mixture Lewis number

m Mass flux eigen value in KPP analysis

N_c Instantaneous scalar dissipation rate of c

p Hydrostatic pressure

Pr Prandtl number

Q_α Conditional mean of species α

q_i Component of heat flux vector in direction i

Re Turbulent Reynolds number

R_u Universal gas constant

s_c Laminar flame consumption speed

$\mathrm{Sc_c}$ Schmidt number of c

s_d Laminar flame displacement speed

S_{GC} Global consumption speed in a turbulent flame brush

S_{LC} Local consumption speed in a turbulent flame brush

s_L^o Unstrained laminar flame speed

S_T Turbulent flame speed

T Temperature

t time

$\tilde{k}$ Favre average turbulent kinetic energy

u_i Velocity component in direction i; i = 1 3

$\widetilde{u_i'' c''}$ Turbulent flux of the progress variable

u' Turbulent r.m.s velocity

$V_{\alpha,i}$ Diffusion velocity of species α in direction i

W_α Molecular weight of species α

X_α Mole fraction of species α

$[X_\alpha]$ Molar concentration of species α

x_i Spatial coordinate in direction i

Y_a Mass fraction of species α

y_α Fluctuation about the conditional mean of species α

Greek Symbols

β' Constant in the model for $(T_4 - D_2)$

$\alpha^*, \beta^*, \gamma^*$ Contributions of the unburnt, fully burnt and burning gases in the BML pdf

δ Zeldovich flame thickness

$\Delta h^o_{f,\alpha}$ Formation enthalpy of species α

δ_{ij} Kronecker delta; $\delta_{ij} = 1$ if $i = j$ and 0 otherwise

δ^o_L Laminar flame thermal thickness

$\widetilde{\varepsilon}$	Favre average turbulent kinetic energy dissipation rate
η_k	Kolmogorov length scale
κ	Fluid dynamic stretch rate
Λ	Integral length scale
λ	Thermal conductivity
μ	Dynamic viscosity
μ_t	Turbulent viscosity
ν	Kinematic viscosity
ν_t	Turbulent diffusivity
$\dot{\omega}_\alpha$	Mass rate of production of species α by chemical reactions
$\dot{\omega}$	Reaction rate of the progress variable
$\dot{\omega}_o$	Reaction rate of an unstrained planar flame
ϕ	Equivalence ratio
ψ	Sample space variable for N_c
ρ	Density
Σ	Flame surface density
σ_{ij}	Stress tensor
τ	Heat release parameter
τ_c	Chemical time scale
τ_{ij}	Viscous stress tensor
τ_k	Kolmogorov time scale
τ_t	Integral time scale

$\widetilde{\epsilon_c}$ Favre averaged scalar dissipation rate of c

(η, ξ, ζ) Orthogonal curvilinear coordinate system attached to $\tilde{c}$ iso–surface

Ξ Flame wrinkling factor

ξ Mixture fraction

ζ Sample space variable for c

Chapter 1

Introduction

Combustion is a phenomenon that occurs all around us: a burning candle, a domestic boiler, an aircraft engine etc., to name a few instances. Since the dawn of the industrial age, energy derived from combustion of fuels has improved the quality of human life in almost every respect, albeit with consequences for the environment. Until the 1990s the main concerns with fossil fuel combustion were emissions of Oxides of Sulphur and Nitrogen which are known to cause atmospheric pollution (smog, acid rain, ozone layer depletion etc.). The scenario, however, has since emerged to be more dire. It is now widely accepted that emission of green house gases (GHG) is having a calamitous impact on our environment. According to IPCC (2007) "many natural systems are being affected by regional climate changes, particularly temperature raise" and "most of the observed increase in global average temperatures since the mid–20^{th} century is *very likely* due to increase in anthropogenic green house gas concentrations". This report estimates that combustion of fossil fuels in the domestic, industrial, energy and transportation sectors contributes the most (71%) to total GHG emissions of which CO_2 constitutes a major portion (57%). While alternative energy sources such as wind, tidal and solar energy are being widely explored, because of economic and technological reasons fossil fuels and alternative hydrocarbon fuels such as bio–fuels are likely to provide a bulk of the growing energy demand for the foreseeable future. This is particularly true for high power density applications, such as transportation. It is hence imperative that combustion devices are designed to be cleaner and more efficient, as recommended by IPCC (2007), to

help mitigate the effects of GHG emissions.

Lean premixed combustion, which burns a homogeneous mixture of fuel and excess oxidiser, has the potential for significantly reducing emissions from combustion devices while improving their efficiency (Correa, 1992; Heywood, 1976; Lefebvre, 1999). Land based gas turbine engines in the energy sector that burn gaseous fuel are already able to operate in this mode (Davis & Washam, 1988). This has not yet been realised for aircraft engines since they burn liquid fuels that require a substantial amount of time to vaporise and mix which can result in operational difficulties such as autoignition or flashback (Correa, 1992; Lefebvre, 1999). Instead, a fuel rich mixture is first burnt in a primary zone followed by the injection of additional air to burn the residual fuel and achieve an overall lean combustion (Mongia, 1998). The reacting mixture in such a scenario is not perfectly premixed and has compositional inhomogeneities but future technologies in the aviation sector are likely to move towards premixed combustion (Correa, 1998; Rolls-Royce, 2005). Current generation reciprocating engines: spark ignition (Takagi, 1998; Zhao *et al.*, 1999) and compression ignition engines (Lee & Lee, 2007; Yao *et al.*, 2009) also burn inhomogeneous mixtures that are lean overall. However, even in combustion of inhomogeneous mixtures, the classical premixed mode is expected to play a major role in determining the overall combustion characteristics (Westbrook *et al.*, 2005). While attractive from the efficiency and emissions point of view, lean premixed combustion is very susceptible to instabilities (Lieuwen *et al.*, 1998; Shih *et al.*, 1996) due to the high sensitivity of heat release rate to mixture composition, and this can contribute to rough combustion, unless sufficient care is taken in the design.

Computational simulations are widely used in the design of combustion devices as they greatly reduce the time and expense of the design cycle and provide information at a level of detail that is difficult to obtain from experiments. However, most combustion devices operate in the turbulent regime and numerically resolving the entire range of spatial and temporal scales that characterise turbulent flames in realistic geometries is not computationally tractable even with the state–of–art computing resources. To circumvent this, modelling strategies are employed whereby the need to resolve all the scales is avoided by mathematical treatments such as averaging, filtering, of the governing equations. As a result of

these treatments, terms arise representing the interaction among various physical processes: fluid dynamics, thermodynamics, molecular transport and chemical reactions. These interactions are quite complex in turbulent combustion and not well understood. Consequently, computations of turbulent combustion rely heavily on theoretical and mathematical models that provide a description of these underlying physical processes. Hence, the study of turbulent combustion modelling is important, not only because it helps us to understand the fundamental physics, but because it is essential in the design process. It is evident that the premixed mode of combustion is likely to play a major role in the drive towards efficient, clean and quiet combustion devices. While significant advances have been made in understanding and modelling turbulent premixed combustion (Borghi, 1988; Bray, 1980; Peters, 2000; Veynante & Vervisch, 2002) a lot remains to be achieved. For instance the prediction of heat release rates and species concentrations, important from the noise and emissions perspectives, presents a formidable challenge which is yet to be satisfactorily addressed. The development of a predictive model for turbulent premixed combustion applicable over wide range of conditions encountered in practical devices is an ongoing activity in the combustion research community. The present study attempts a contribution to this endeavour.

In Direct Numerical Simulations (DNS), which represent one extreme of the computational paradigm, all the scales of the flow and flame are resolved. Although this is attractive, the inclusion of detailed chemical kinetics and transport processes in DNS tremendously increases the computational expense restricting the computational domain size to typically few cm^3. At the other extreme, Reynolds–Averaged Navier–Stokes (RANS) simulations solve governing equations for average quantities with no attempt to resolve any of the scales. The unclosed terms arising in the RANS governing equations, typically involving correlations of turbulence and thermochemical quantities, require modelling. The most challenging aspect of RANS is the modelling of terms that are dictated by the turbulence–chemistry interactions since these interactions are highly non–linear. In Large Eddy Simulations (LES) governing equations of filtered quantities representing the dynamics of energy containing large scale motions of turbulent flow are solved. The influence of smaller scales are represented using

models. However, the chemical scales are typically smaller than the smallest turbulent scale, the Kolmogorov scale, in turbulent flames of practical interest and the turbulence–chemistry interaction is unresolved and requires modelling even in LES (Pope, 1990). Most LES models are extensions of RANS modelling ideas (Poinsot & Veynante, 2001) and hence turbulent combustion modelling in the RANS paradigm is pivotal.

Many concepts/quantities in the realm of combustion modelling embody turbulence–chemistry interactions; one such quantity, the *scalar dissipation rate*, is the focus of this work. The mean scalar dissipation rate is the average rate of decay of scalar fluctuations and denotes the rate of scalar mixing at the smallest scales. Conventionally, mixture fraction, a conserved scalar, is employed to describe the thermochemical state in non–premixed flames, and its dissipation rate is dictated entirely by the turbulence. The scenario is different for premixed flames (Bilger, 2004b) whose thermochemical description is usually via the reaction progress variable, a reactive scalar, whose dissipation rate is dictated by the turbulence as well as the flame front dynamics. While the modelling of mean dissipation rate of the mixture fraction is well understood, that of the progress variable is not. Nonetheless, scalar dissipation rate is a central parameter in most modelling approaches (Bilger, 1976; Bray, 1980; Klimenko & Bilger, 1999; Pope, 1985) since it is linked to the fundamental quantities in turbulent combustion (Veynante & Vervisch, 2002). The main objectives of this work are:

(i) to formulate a RANS computational model for turbulent premixed combustion based on scalar dissipation rate,

(ii) to study the associated problem of mean scalar dissipation rate modelling in turbulent premixed flames, and

(iii) to validate the models using DNS and experimental data over wide range of turbulent flame conditions.

The outline of this thesis is as follows. The background on premixed flame modelling is first presented in Chapter 2 giving an overview of the available modelling methodologies. The discussion is restricted to laminar flames and RANS modelling of turbulent premixed flames. Chapter 3 focuses on scalar dissipation

rate; its physical meaning, significance in turbulent combustion and its modelling challenges. The formulation of a turbulent premixed combustion model based on the scalar dissipation rate is presented in Chapter 4. This model is based on the "flamelet" concept which views turbulent flame as an ensemble of laminar–like reaction layers - flamelets. Strained laminar flames in an appropriate configuration are chosen to represent the flamelets and the choice of scalar dissipation rate to parametrise these flamelets results in a wide range of applicability of the model.

The closure of mean scalar dissipation rate, required in the formulation presented in Chapter 4, is studied in Chapter 5 and a new algebraic closure is proposed based on recent findings. This model is validated using DNS data. Validation using experimental data is not possible since direct measurements of this quantity are scarce. However, its indirect validation is performed in Chapter 6 by obtaining an expression for turbulent flame speed from the scalar dissipation rate model and comparing it with experimental data from a wide range of configurations and conditions.

The computational model is applied to turbulent flame calculations and results are presented in Chapter 7. The calculations of a test problem: planar one–dimensional flame are discussed first. The results of laboratory flame calculations of different configurations are discussed and conclusions are drawn regarding the regime of applicability of the model. Some limitations of flamelet modelling in predicting pollutants are identified and possible ways to improve this are discussed. Chapter 8 discusses the scope for future work.

Chapter 2

Background on Premixed Flame Modelling

The classical modes, namely premixed and non–premixed, are logical starting points to study combustion. In non–premixed flames the fuel and oxidiser enter the combustion zone from separate streams and the flame is located at the stoichiometric interface. The oxidiser and fuel are supplied to the flame zone via diffusion. In premixed flames the fuel and oxidiser are mixed at the molecular level prior to entering the combustion zone and the flame propagates into the unburnt mixture at a speed, relative to the fluid motion, determined by the rates of reaction and thermal diffusion. The conventional compression ignition engine is a typical example of the former while a spark ignition engine is an example of the latter.

However, in practice one mostly encounters combustion situations that lie in between these two classical extremes. As noted in the introduction, many practical devices involve combustion of inhomogeneous reacting mixtures, which is broadly called as *partially premixed* combustion, which can be further categorised into *stratified premixed* and *premixed/non–premixed* combustion (Bilger *et al.*, 2005). In stratified premixed combustion the inhomogeneous mixture is either entirely fuel–lean or fuel–rich and the local flame structures are only of the premixed type whereas in premixed/non–premixed combustion the mixture includes both rich and lean compositions and flame structures of both premixed and non–premixed type are likely to occur. The role of premixed mode in partially premixed combustion is evident and the implications for modelling are obvious.

Premixed combustion models are often, though not always, an integral part of the modelling strategies for partially premixed combustion (Domingo *et al.*, 2002; Hélie & Trouvé, 2000; Jiménez *et al.*, 2002; Peters, 2000).

The focus of this work is premixed flame modelling and in this chapter an overview of the existing models is presented. The term 'modelling' is best described as an effort to provide a mathematical description for physical phenomena. The modelling of the fundamental phenomena in laminar flames is discussed first and then the Reynolds–Averaged–Navier–Stokes (RANS) modelling of turbulent flames is presented.

2.1 Laminar Flames

The mathematical framework for laminar combustion is provided by the governing equations of fluid motion: mass and momentum conservation, and the transport of thermochemical quantities: species concentrations and energy. For a multi–component gaseous reacting system with N species and M reactions these equations written in tensorial notation are (Williams, 1985a) :

- continuity equation
$$\frac{\partial \rho}{\partial t} + \frac{\partial \rho u_i}{\partial x_i} = 0, \tag{2.1}$$

- momentum conservation
$$\frac{\partial \rho u_i}{\partial t} + \frac{\partial \rho u_i u_j}{\partial x_j} = -\frac{\partial \sigma_{ij}}{\partial x_j} + \rho \sum_{\alpha=1}^{N} Y_\alpha f_{\alpha,i}, \tag{2.2}$$
where $f_{\alpha,i}$ is the i^{th} component of the body force acting on species α. The stress tensor is defined in terms of the pressure and viscous stress tensors as $\sigma_{ij} = p\delta_{ij} - \tau_{ij}$ where $\tau_{ij} = -\frac{2}{3}\mu\frac{\partial u_k}{\partial x_k}\delta_{ij} + \mu\left(\frac{\partial u_i}{\partial x_j} + \frac{\partial u_j}{\partial x_i}\right)$;

- conservation of species α
$$\frac{\partial \rho Y_\alpha}{\partial t} + \frac{\partial}{\partial x_i}\left[\rho(u_i + V_{\alpha,i})Y_\alpha\right] = \dot{\omega}_\alpha, \quad \alpha = 1....N, \tag{2.3}$$
where $V_{\alpha,i}$ is the molecular diffusion velocity and $\dot{\omega}_\alpha$ is the total rate of mass production by chemical reactions.

- conservation of energy

$$\frac{\partial \rho e}{\partial t} + \frac{\partial \rho u_i e}{\partial x_i} = -\frac{\partial q_i}{\partial x_i} - \sigma_{ij}\frac{\partial u_i}{\partial x_j} + \rho \sum_{\alpha=1}^{N} Y_\alpha f_{\alpha,i} V_{\alpha,i} + \dot{\mathcal{Q}}, \tag{2.4}$$

  where q_i is the energy flux in direction i due to thermal conduction and $\dot{\mathcal{Q}}$ includes effects such as ignition source, radiative flux etc. The energy equation is often recast in terms of enthalpy or temperature using the identity $e = \sum_\alpha Y_\alpha h_\alpha - p/\rho$ and the caloric equation of state $h_\alpha = \Delta h^o_{f,\alpha} + \int_{T^o}^{T} C_{p,\alpha} dT$.

The pressure is obtained from the equation of state

$$p = \rho R_u T \sum_{\alpha=1}^{N} \frac{Y_\alpha}{W_\alpha} \ . \tag{2.5}$$

For multi–component mixtures simplifications are often made for the molecular diffusive flux terms q_i and $V_{\alpha,i}$. Typically Dufour effects are neglected and the heat flux vector is expressed as $q_i = -\lambda(\partial T/\partial x_i) + \rho \sum_\alpha h_\alpha Y_\alpha V_{\alpha,i}$. The expression for species diffusive velocity, after neglecting Soret effects, is very complicated and usually the approximation of Curtiss & Hirschfelder (1949) is employed which yields the Fickian form

$$V_{\alpha,i} = -D_\alpha \frac{1}{X_\alpha}\frac{\partial X_\alpha}{\partial x_i} = -D_\alpha \frac{1}{Y_\alpha}\frac{\partial Y_\alpha}{\partial x_i}$$

where the equivalent diffusivity, D_α, is given by $D_\alpha = (1 - Y_\alpha)/(\sum_{k\neq\alpha} X_i/D_{k\alpha})$ and $D_{k\alpha}$ is the binary diffusivity of species k and α. This expression is based on the approximation that all the species are in trace quantities relative to one major species, which is reasonable since in most cases air is used as the oxidiser and the Nitrogen concentration is much larger compared to the rest of the species. The relative magnitude of the thermal and mass diffusivities is given by the Lewis number of a species defined as $\mathrm{Le}_\alpha \equiv D_{th}/D_\alpha$ where the thermal diffusivity is defined as $D_{th} \equiv \lambda/(\rho C_p)$ and C_p is the mixture specific heat. The Prandtl number is the ratio of the momentum and thermal diffusivities and is defined as $\mathrm{Pr} \equiv \nu/D_{th}$ where the kinematic viscosity is $\nu \equiv \mu/\rho$.

If the system of M reversible reactions is expressed using the stoichiometric coefficients as $\sum_\alpha \nu'_{\alpha j}\mathcal{M}_\alpha \rightleftharpoons \sum_\alpha \nu''_{\alpha j}\mathcal{M}_\alpha$ for $j = 1, ...M$ where $\mathcal{M}_\alpha$ is the chemical symbol for species α, then the total mass production rate of species α is given by

$$\dot{\omega}_\alpha = W_\alpha \sum_{j=1}^{M} (\nu''_{\alpha j} - \nu'_{\alpha j}) \left[K_{f,j} \prod_{\alpha=1}^{N} [X_\alpha]^{\nu'_{\alpha j}} - K_{r,j} \prod_{\alpha=1}^{N} [X_\alpha]^{\nu''_{\alpha j}} \right]. \qquad (2.6)$$

The forward reaction rates are usually expressed in the Arrhenius form, $K_{f,j} = A_j T^{\beta_j} \exp(-T_{a,j}/R_u T)$ where A_j and β_j are constants and $T_{a,j}$ is the activation temperature for reaction j. The reverse reaction rate is obtained from $K_{r,j} = K_{f,j}/K_{eq,j}$ where $K_{eq,j}$ is the equilibrium constant.

The above mathematical framework is not specific to a combustion mode and the differences between the premixed and non–premixed modes emerge only through the boundary conditions. In principle the above system of equations can be solved numerically if appropriate initial and boundary conditions are specified. In practice the detailed chemical mechanisms for typical hydrocarbons involve tens of species and hundreds of reactions which means the dimension of the system of equations (2.1)–(2.4), equal to $(N + 5)$, is large. Furthermore the system of equations is stiff due to the exponential dependence of reaction rates on temperature and a wide range of length and time scales are involved. This requires special numerical techniques to obtain a solution. Nonetheless computational codes for canonical flame configurations have been developed (Bradley *et al.*, 1996; Kee *et al.*, 1985; Lutz *et al.*, 1997; Somers, 1994) and are widely used. Canonical flames are usually one–dimensional (1D) or quasi–one–dimensional and their spatial scales are relatively small; the thickness of a freely propagating planar unstrained flame, which is a canonical flame, is typically less than a millimetre. Multi–dimensional flames are seldom computed with the detailed thermochemistry due to the enormous computational cost involved. Instead the thermochemistry is tabulated using a set of reduced number of representative scalars (Maas & Pope, 1994; van Oijen & de Goey, 2000) and only transport equations of these scalars are solved along with equations describing the fluid flow. Such a strategy is also widely used in turbulent flame computations which are discussed next.

2.2 Turbulent Flames

For turbulent flames the computational expense is further compounded because they are inherently unsteady and are comprised of cascade of eddies that span a wide range of length and time scales. Direct numerical simulations solve the full set of equations described in Sec. 2.1 and resolve all the scales[1] involved. Hence they are prohibitively expensive and are restricted to computational domains that are orders of magnitude smaller than engineering devices. However, for engineering applications one is mostly interested in the statistical moments rather than the instantaneous values of temperature, velocity etc. These statistical moments are obtained economically by solving the Reynolds–Averaged Navier–Stokes (RANS) equations.

2.2.1 RANS Governing Equations

By averaging Eqs. (2.1) and (2.2) one obtains, respectively, the continuity equation

$$\frac{\partial \overline{\rho}}{\partial t} + \frac{\partial \overline{\rho}\widetilde{u}_i}{\partial x_i} = 0 \tag{2.7}$$

and the momentum equation

$$\frac{\partial \overline{\rho}\widetilde{u}_i}{\partial t} + \frac{\partial \overline{\rho}\widetilde{u}_i\widetilde{u}_j}{\partial x_j} = -\frac{\partial \overline{p}}{\partial x_i} + \frac{\partial}{\partial x_j}\left(\overline{\tau}_{ij} - \overline{\rho}\widetilde{u_i''u_j''}\right) \ , \tag{2.8}$$

for the mean motion, when the body forces are assumed to be negligible. The over bar denotes Reynolds averaging and tilde denotes density weighted (Favre) averaging: $\widetilde{u}_i \equiv \overline{\rho u_i}/\overline{\rho}$. The Favre fluctuation is denoted by a double prime i.e. $u_i'' = u_i - \widetilde{u}_i$. In the above equation the Reynolds stresses, $\widetilde{u_i''u_j''}$, are unclosed. One could solve transport equations for the six components of the symmetric Reynolds stress tensor, but these equations contain further unclosed terms and at some point modelling closures will be required[2]. Instead a two–equation approach

[1] for reacting flows the numerical resolution requirement is more stringent compared to non–reacting flows since the scales of chemical reactions are often smaller than the turbulence scales.

[2] the transport equations for $\widetilde{u_i''u_j''}$ contain the triple correlations $\widetilde{u_i''u_j''u_k''}$. In general transport equations of correlations of fluctuating quantities will contain higher order correlations.

(Jones & Launder, 1972) is widely followed whereby the Reynolds stresses are closed using the Boussinesq approximation

$$\widetilde{\overline{\rho} u_i'' u_j''} = -\mu_t \left(\frac{\partial \widetilde{u}_i}{\partial x_j} + \frac{\partial \widetilde{u}_j}{\partial x_i} - \frac{2}{3} \frac{\partial \widetilde{u}_k}{\partial x_k} \delta_{ij} \right) + \frac{2}{3} \overline{\rho} \tilde{k} \delta_{ij} \ , \tag{2.9}$$

and the turbulent viscosity is modelled as $\mu_t = \overline{\rho} C_\mu \tilde{k}^2 / \widetilde{\varepsilon}$. Modelled transport equations are solved for the Favre averaged turbulent kinetic energy, $\tilde{k}$ (Bray *et al.*, 1992)

$$\frac{\partial \overline{\rho} \tilde{k}}{\partial t} + \frac{\partial \overline{\rho} \widetilde{u}_i \tilde{k}}{\partial x_i} = \frac{\partial}{\partial x_i} \left[\left(\mu + \frac{\mu_t}{\mathrm{Sc}_k} \right) \frac{\partial \tilde{k}}{\partial x_i} \right] + \mathcal{P}_k + \overline{p' \frac{\partial u_k''}{\partial x_k}} - \overline{\rho} \widetilde{\varepsilon} \ , \tag{2.10}$$

and its dissipation rate, $\widetilde{\varepsilon}$,

$$\frac{\partial \overline{\rho} \widetilde{\varepsilon}}{\partial t} + \frac{\partial \overline{\rho} \widetilde{u}_i \widetilde{\varepsilon}}{\partial x_i} = \frac{\partial}{\partial x_i} \left[\left(\mu + \frac{\mu_t}{\mathrm{Sc}_\varepsilon} \right) \frac{\partial \widetilde{\varepsilon}}{\partial x_i} \right] + C_{\varepsilon 1} \mathcal{P}_k \frac{\widetilde{\varepsilon}}{\tilde{k}} - C_{\varepsilon 2} \overline{\rho} \frac{\widetilde{\varepsilon}^2}{\tilde{k}} \ . \tag{2.11}$$

The production term in the above equations is $\mathcal{P}_k = -\overline{\rho} \widetilde{u_i'' u_j''} (\partial \widetilde{u}_i / \partial x_j) - \overline{u_i''} (\partial \overline{p} / \partial x_i)$. The values for the model constants in Eqs. (2.9)-(2.11) are: $C_\mu = 0.09$, $\mathrm{Sc}_k = 1.0$, $\mathrm{Sc}_\varepsilon = 1.3$, $C_{\varepsilon 1} = 1.44$ and $C_{\varepsilon 2} = 1.92$. This two–equation approach, known as $\tilde{k}$–$\widetilde{\varepsilon}$ approach, was originally proposed (Jones & Launder, 1972) for non–reacting turbulent flows but it is retained in many turbulent flame calculations due to its simplicity and low computational expense. However, the pressure related terms are usually neglected for non–reacting flows.

As noted earlier, computations of turbulent flames can be made tractable by describing the thermochemistry via few representative scalars instead of solving for all the reactive species. For premixed flames the most commonly used scalar for this purpose is the reaction progress variable, c. The progress variable is typically defined as either normalised fuel mass fraction or normalised temperature[3] such that it takes a value of zero in unburnt mixture and 1 in the burnt mixture. Alternative definitions of progress variable have also been proposed (Bilger, 2004a; Bilger *et al.*, 1991). Here we use the temperature based definition,

$$c \equiv \frac{T - T_u}{T_b - T_u} \ , \tag{2.12}$$

[3]The two definitions are equivalent strictly for the case of a single step irreversible reaction and when the Lewis number of the fuel is equal to 1 (Poinsot & Veynante, 2001).

where T_u is the unburnt mixture temperature and T_b is the adiabatic flame temperature. The transport equation for the instantaneous progress variable is

$$\frac{\partial \rho c}{\partial t} + \frac{\partial \rho u_i c}{\partial x_i} = \frac{\partial}{\partial x_j}\left(\rho D_c \frac{\partial c}{\partial x_j}\right) + \dot{\omega} \ , \tag{2.13}$$

which can be obtained from Eq. (2.4) (Poinsot & Veynante, 2001) by setting the body forces and $\dot{\mathrm{Q}}$ to zero and assuming that the work done by pressure and viscous stresses are negligibly small, which is reasonable for flames in low Mach number flows. The diffusivity and the reaction rate of the progress variable are D_c and $\dot{\omega}$ respectively. If the specific heats of all the species are assumed to be equal to the mixture specific heat, C_p, then D_c is equal to the thermal diffusivity D_{th}. The reaction rate can be written from Eq. (2.6) as

$$\dot{\omega} = \frac{-\sum_{\alpha=1}^{N} h_\alpha \dot{\omega}_\alpha}{C_p(T_b - T_u)} \ . \tag{2.14}$$

The transport equation for the Favre averaged progress variable, $\tilde{c}$, is

$$\frac{\partial \overline{\rho}\tilde{c}}{\partial t} + \frac{\partial \overline{\rho}\widetilde{u}_i\tilde{c}}{\partial x_i} = \frac{\partial}{\partial x_i}\left(\overline{\rho D_c \frac{\partial \tilde{c}}{\partial x_i}} - \overline{\rho}\widetilde{u_i'' c''}\right) + \overline{\dot{\omega}}. \tag{2.15}$$

The two terms, the turbulent scalar flux, $\widetilde{u_i'' c''}$, and the mean reaction rate, $\overline{\dot{\omega}}$, on the right hand side in Eq. (2.15) are unclosed. The turbulent scalar flux can be closed similar to the Reynolds stresses using a gradient transport hypothesis as

$$\overline{\rho}\widetilde{u_i'' c''} = -\frac{\mu_t}{\mathrm{Sc_c}}\left(\frac{\partial \tilde{c}}{\partial x_i}\right) \ . \tag{2.16}$$

However this closure contradicts the phenomenon of counter–gradient transport (Bray *et al.*, 1981; Moss, 1980) which is known to occur in turbulent premixed flames and will be discussed in Section 2.2.3.

A closure for mean reaction rate, $\overline{\dot{\omega}}$, is more challenging and is the primary concern of premixed flame modelling. The difficulty in closing $\overline{\dot{\omega}}$ can be illustrated using a simple case involving single irreversible reaction between fuel (F) and oxidiser (O) giving rise to a product (P). The mean reaction rate in this case is related to the mean fuel consumption rate via $\overline{\dot{\omega}} = Q\overline{\dot{\omega}}_F / C_p(T_b - T_u)$, where Q is the heat

released per unit mass of fuel consumption. Using an Arrhenius form for the rate constant the fuel consumption rate is written as $\dot{\omega}_F = A\rho^2 T^\beta Y_F Y_O \exp(-T_a/T)$. The mean of this quantity, and hence $\overline{\dot{\omega}}$, cannot be expressed as a simple function of $\widetilde{Y}_F$, $\widetilde{Y}_O$ and $\widetilde{T}$ mainly because of the non–linear exponential term. Using a Taylor series expansion for the mean fuel consumption rate gives (Libby & Williams, 1980; Poinsot & Veynante, 2001)

$$\overline{\dot{\omega}}_F = A\overline{\rho}^2 \widetilde{T}^\beta \widetilde{Y}_F \widetilde{Y}_O \exp\left(-\frac{T_a}{\widetilde{T}}\right)\left[1 + \left(\frac{T_a}{\widetilde{T}}\right)^2 \frac{\widetilde{T''^2}}{\widetilde{T}^2} + \frac{\widetilde{Y''_F Y''_O}}{\widetilde{Y}_F \widetilde{Y}_O} + ...\right]. \qquad (2.17)$$

The second term in the square brackets is not small compared to the first term since T_a is usually large, and it can only be neglected for unrealistically small temperature fluctuations (Libby & Williams, 1980). The higher order terms in such an expansion involve powers of $(T_a/\widetilde{T})$ and neglecting these terms results in large truncation errors. The third term involving $\widetilde{Y''_F Y''_O}$ is also not negligible and its closure is difficult. Furthermore, for a general case involving multi–step chemistry this expression becomes more complicated and difficult to estimate. Thus, the closure of $\overline{\dot{\omega}}$ using the moments is difficult and alternative methods are employed. Modelling of this quantity is usually based on physical ideas of the interaction between the turbulent flow and the chemical reactions; the turbulence–chemistry interaction. A laminar premixed flame has a well defined velocity and length scale while turbulent flows are characterised by a range of length and time scales. The influence of turbulent flow on a premixed flame can be qualitatively described by the relative magnitude of the flame and the turbulent flow scales. This gives rise to the concept of turbulent combustion regimes which forms a first basis for model development.

2.2.2 Regimes of Turbulent Premixed Combustion

Damköhler (1940) was among the first to describe turbulent flame behaviour based on combustion regimes. He envisaged a regime where all the scales of the turbulent eddies are much larger than the flame scales and inner structure of the flame front is virtually undisturbed in the "flamelet" limit. This occurs when the Damköhler number, Da, is much greater than 1. The Damköhler number is the

ratio of the integral turbulent time scale to the chemical time scale

$$\mathrm{Da} \equiv \frac{\tau_t}{\tau_c} = \frac{\Lambda/u'}{\delta/s_L^o} \tag{2.18}$$

where Λ is the integral length scale, u' is the turbulent root mean square (RMS) velocity and s_L^o is the laminar flame speed. The Zeldovich flame thickness is defined as $\delta \equiv D_{th_u}/s_L^o$ where the thermal diffusivity of the unburnt mixture is D_{th_u}. In the other extreme, Da < 1, all the turbulent time scales are smaller than the chemical time scale and the species are mixed by the turbulent motions at a rate faster than the chemical reactions. This limit is called "perfectly stirred" limit (Libby & Williams, 1980). In the flamelet regime the turbulence wrinkles and contorts the flame front which increases its area and results in greater reactant consumption per unit time. The flame brush propagates at a greater speed, S_T, than the laminar flame speed, s_L^o. A simple expression proposed by Damköhler (1940) gives $S_T/s_L^o \simeq A_T/A_c = 1 + (u'/s_L^o)$, where A_T is the area of the wrinkled turbulent flame and A_c is its projected area. Thus, the turbulent flame speed, S_T, incorporates the influences of turbulence as well as chemistry and has been the subject of many theoretical and experimental studies. This quantity is studied in more detail in Chapter 6.

The Klimov–Williams criterion (Klimov, 1963; Williams, 1976) introduces the notion that even when Da > 1, the smallest eddies which are of the Kolmogorov scale, η_k, can penetrate and disturb the flame front. This occurs when the Karlovitz number, Ka, defined as (Peters, 1986)

$$\mathrm{Ka} \equiv \frac{\tau_c}{\tau_k} = \left(\frac{\delta}{\eta_k}\right)^2 \tag{2.19}$$

is larger than unity implying that the Kolmogorov eddies are smaller than the flame thickness. The Kolmogorov time scale is τ_k. Peters (2000) refines this idea by noting that the laminar flame has three distinct layers: a preheat layer, an inner reaction layer and an oxidation layer. The reaction layer is typically one–tenth of the flame thickness and hence the Kolmogorov eddies have to be much smaller to penetrate this layer. The regime diagram of Peters (2000) is shown in Fig. 2.1. The turbulent Reynolds number is defined as

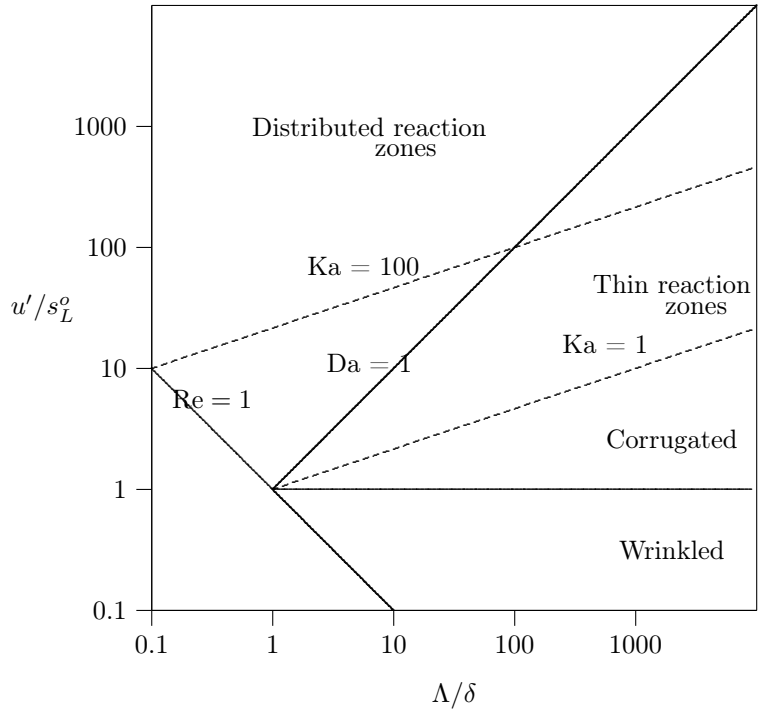

Figure 2.1: Turbulent combustion regime diagram of Peters (2000).

$$\mathrm{Re} = \frac{u'\Lambda}{\nu_u}, \tag{2.20}$$

and for a unity Prandtl number, $\mathrm{Re} = (u'\Lambda)/(s_L^o\delta)$. The region bounded by the Ka = 1 and Ka = 100 lines is the "thin reaction zones" regime where the Kolmogorov eddies are smaller than the flame thickness and enter the preheat layer but are unable to penetrate the reaction layer. For Ka > 100 the entire flame structure is disturbed by the turbulent eddies and reactions occur over a distributed region in space. Below the Ka = 1 line lie the "corrugated" and "wrinkled flamelets" regimes which are separated by $u'/s_L^o = 1$ line. In the former the flame front is likely to be corrugated with possibility of isolated pockets of burning mixture while in the latter the flame front is merely wrinkled with its layer like structure intact. It must be stressed that the regimes in Fig. 2.1 are based on qualitative ideas and make many simplifying assumptions. Modified combustion diagrams based on experimental observations have been proposed by Chen & Bilger (2001b). Poinsot *et al.* (1991) construct a regime diagram

using rigorous analysis of flame/vortex interactions from DNS data. Nonetheless, such qualitative ideas are widely used in model formulation and as guidelines to estimate the regimes of applicability of various models.

Interesting modelling simplifications can be made in the classical limits of combustion regimes. In the perfectly stirred limit the turbulent time scales are faster than the chemical processes and fluctuations in the thermochemical quantities are small since they are quickly mixed by the turbulent motions. The mean reaction rate in Eq. (2.17) can then be reasonably approximated to that evaluated using only the mean quantities (Libby & Williams, 1980). On the other hand, in the flamelet limit it can be assumed that the flame front structure is laminar–like; the "laminar flamelet" approximation. The mean reaction rate can then be deduced from the reaction rate in a laminar flame - typically a canonical flame - and the statistics of the flamelets at a given location. The perfectly stirred limit is unlikely to be attained in practical devices and in most cases the scenario is somewhat closer to the flamelet regime (Peters, 1986). Many turbulent premixed (and non–premixed) combustion models are based on the flamelet concept. These and other models, specifically for premixed flames, are discussed below.

2.2.3 Bray–Moss–Libby Model

The Bray–Moss–Libby (BML) model (Bray, 1980; Bray & Libby, 1976; Bray & Moss, 1977) provides a thermochemical closure centred on the progress variable pdf. This pdf is expressed as the sum of the probabilities of finding unburnt, fully burnt and the burning gases at a location by

$$p(c=\zeta;\mathbf{x},t) = \underbrace{\alpha^*(\mathbf{x},t)\delta(\zeta)}_{\text{unburnt gases}} + \underbrace{\beta^*(\mathbf{x},t)\delta(1-\zeta)}_{\text{burnt gases}} + \underbrace{\gamma^*(\mathbf{x},t)f(\zeta)}_{\text{burning gases}} , \tag{2.21}$$

where $\delta(\zeta)$ and $\delta(1-\zeta)$ are the Dirac delta functions and ζ is the sample space variable for c. Normalisation of the pdf yields the conditions:

$$\alpha^* + \beta^* + \gamma^* = 1, \quad \text{and} \quad \int_0^1 f(\zeta)\, d\zeta = 1. \tag{2.22}$$

The mean value of a thermochemical quantity, Φ_α, can be written as

$$\overline{\Phi}_\alpha = \int_0^1 \Phi_\alpha(\zeta)\; p(\zeta)\; d\zeta \;, \tag{2.23}$$

which upon substituting Eq. (2.21) gives

$$\overline{\Phi}_\alpha \;=\; \alpha^* \Phi_\alpha(0) + \beta^* \Phi_\alpha(1) + \gamma^*(\mathbf{x}, t) \int_0^1 \Phi_\alpha(\zeta)\; f(\zeta)\; d\zeta. \tag{2.24}$$

For flames with large Reynolds and Damköhler numbers that are well within the flamelet regime, the flame front is thin and the probability of finding the burning gases is small compared to the probabilities of unburnt or burnt gases. The burning gas component $\gamma^* \sim \mathcal{O}(1/\mathrm{Da})$, is negligible compared to α^* and β^* and the mean quantity $\overline{\Phi}_\alpha$ has contributions mostly from the unburnt and fully burnt gases when Da is large.

Simple relations can be obtained by noting that the Favre averaged progress variable $\tilde{c}$ is

$$\overline{\rho}\tilde{c} \equiv \overline{\rho c} = \int_0^1 \rho(\zeta)\; \zeta\; p(\zeta)\; d\zeta = \rho_b \beta^* \tag{2.25}$$

where ρ_b is the density of the burnt gases. If the combustion occurs in low Mach number flows then the density can be expressed as $\rho = \rho_u T_u / T = \rho_u / (1 + \tau\zeta)$, where ρ_u is the unburnt density and the heat release parameter is defined as $\tau \equiv T_b / T_u - 1 = \rho_u / \rho_b - 1$. This yields (Bray, 1980)

$$\overline{\rho} = \rho_u \int_0^1 \frac{1}{1 + \tau\zeta}\; p(\zeta)\; d\zeta \quad \text{and} \quad \overline{\rho}\tilde{c} = \rho_u \int_0^1 \frac{\zeta}{1 + \tau\zeta}\; p(\zeta)\; d\zeta\;, \tag{2.26}$$

which can be combined to give

$$\overline{\rho} = \frac{\rho_u}{1 + \tau\tilde{c}}\;, \tag{2.27}$$

and

$$\beta^* = \frac{(1+\tau)\tilde{c}}{1 + \tau\tilde{c}} \quad \text{and} \quad \alpha^* = \frac{1 - \tilde{c}}{1 + \tau\tilde{c}}\;. \tag{2.28}$$

Thus, the thermochemical state of the mixture is completely determined by $\tilde{c}$ which can be obtained from its transport equation, Eq. (2.15), provided the turbulent scalar flux and the mean reaction rate are modelled.

The turbulent scalar flux in Eq. (2.15) is sometimes closed via a gradient transport hypothesis as noted in Section 2.2.1 which assumes that, by analogy to molecular transport, the turbulent transport is positive in the direction of negative gradient of $\tilde{c}$. However, counter–gradient transport, where the scalar flux is positive along positive $\tilde{c}$ gradient, has been observed in experiments (Bray

et al., 1981). This is explained in BML framework by noting that the scalar flux can be expanded as

$$\widetilde{u_i''c''} \;=\; (\widetilde{u_i c} - \widetilde{u}_i\tilde{c}) \;=\; \tilde{c}(1-\tilde{c})(\overline{u}_i^b - \overline{u}_i^u), \tag{2.29}$$

where $\overline{u}_i^b$ and $\overline{u}_i^u$ are the mean velocities conditioned in the burnt and the unburnt gases respectively. Since the burnt gases have lower density they are preferentially accelerated by the pressure gradient compared to unburnt gases i.e., $\overline{u}_i^b > \overline{u}_i^u$. Hence $\widetilde{u_i''c''}$ is positive in the direction going from the unburnt to the burnt side; the direction of positive mean pressure gradient as well as positive $\tilde{c}$ gradient. Thus the BML model provides a theoretical basis for the correct behaviour of turbulent scalar flux, however, the conditional mean velocities need to be modelled.

The main modelling challenge, the closure of $\overline{\dot{\omega}}$, remains unresolved in the BML approach. This is because the mean reaction rate, when evaluated using Eq. (2.24), will be $\mathcal{O}(\gamma^*)$, which is assumed to be negligible. Alternative approaches have been developed to close the mean reaction rate.

Bray (1979) analyses the transport equations of $\tilde{c}$ and $\widetilde{c''^2}$ and deduces that, under the BML assumptions, the mean reaction rate is proportional to the mean scalar dissipation rate, $\widetilde{\epsilon_c}$, as

$$\overline{\dot{\omega}} = \frac{2}{2C_m - 1}\overline{\rho}\widetilde{\epsilon_c} \tag{2.30}$$

where

$$C_m \equiv \frac{\int_0^1 \zeta\ \dot{\omega}(\zeta)\ p(\zeta)\ d\zeta}{\int_0^1 \dot{\omega}(\zeta)\ p(\zeta)\ d\zeta}\ , \tag{2.31}$$

and the value of C_m is typically 0.7. The mean scalar dissipation rate is defined as

$$\overline{\rho}\widetilde{\epsilon_c} = \overline{\rho D_c \frac{\partial c''}{\partial x_i}\frac{\partial c''}{\partial x_i}}\ . \tag{2.32}$$

Unfortunately, the mean scalar dissipation rate is an unclosed quantity and its closure for premixed flames is challenging. One could use classical models developed for passive scalars in non–reacting turbulence which give $\overline{\rho}\widetilde{\epsilon_c} = \overline{\rho}\widetilde{c''^2}/\tau_t$. Under the BML assumptions $\widetilde{c''^2} \approx \tilde{c}(1-\tilde{c})$, and by estimating the turbulence

time scale as $\tau_t \simeq \tilde{k}/\widetilde{\varepsilon}$, one recovers the Eddy–Break–Up (EBU) model of Mason & Spalding (1973)

$$\overline{\dot{\omega}} \approx C_{\mathrm{EBU}} \frac{\overline{\rho}}{\tau_t} \widetilde{c''^2} \approx C_{\mathrm{EBU}}\ \overline{\rho}\ \frac{\widetilde{\varepsilon}}{\tilde{k}}\ \tilde{c}(1-\tilde{c}). \tag{2.33}$$

An obvious limitation of the EBU model is that it contains no information about the chemistry. In the above framework this stems from the modelling of $\widetilde{\epsilon_c}$ based on passive scalar mixing concepts and further details on this will be discussed in Chapter 5.

Another approach is to estimate the mean reaction rate from the number of times the flame front crosses a given point (Bray *et al.*, 1984). Mathematically, this is expressed as

$$\overline{\dot{\omega}} = \dot{\omega}_f \nu_f \tag{2.34}$$

where ν_f is the flame crossing frequency and $\dot{\omega}_f$ is the reaction rate per flame crossing. If the flame front is infinitely thin the progress variable signal at a location resembles a telegraph signal whose analysis yields

$$\nu_f = 2\ \frac{\overline{c}(1-\overline{c})}{\hat{T}} \tag{2.35}$$

where the mean period of the telegraph signal, $\hat{T}$, is typically set equal to τ_t. The reaction rate per flame crossing is expressed as

$$\dot{\omega}_f = \frac{\rho_u s_L^o}{|\sigma_f|} \tag{2.36}$$

where $|\sigma_f|$ is a flamelet orientation factor (Bray *et al.*, 1984).

2.2.4 Flame surface density models

Perhaps the most widely employed approach, which is complementary to the BML methodology, is to express the mean reaction rate per unit volume as a product of reaction rate per unit flame area times flame surface density, Σ (Marble & Broadwell, 1977)

$$\overline{\dot{\omega}} = \rho_u \langle s_c \rangle_s \Sigma\ , \tag{2.37}$$

where s_c is the flame consumption speed and the notation $\langle\ \rangle_s$ denotes averaging over the flame surface. The flame surface density is the mean flame surface area

per unit volume. Algebraic expressions for the flame surface density have been proposed based on the flame crossing frequency analysis (Bray *et al.*, 1989) and fractal theories (Gouldin *et al.*, 1989).

Pope (1988) presents a definition for the surface density of $c = \zeta$ iso–surface as,

$$\Sigma = \langle |\nabla c| c = \zeta \rangle \; p(\zeta) \; , \tag{2.38}$$

where $\langle |\nabla c| c = \zeta \rangle$ is the average of $|\nabla c|$ conditioned on $c = \zeta$, and $p(\zeta)$ is the marginal pdf. A balance equation for Σ is given by (Candel & Poinsot, 1990; Pope, 1988; Trouvé & Poinsot, 1994)

$$\frac{\partial \Sigma}{\partial t} + \frac{\partial \langle u_i \rangle_s \Sigma}{\partial x_i} + \frac{\partial}{\partial x_i} \left[\langle s_d n_i \rangle_s \Sigma \right] = \langle a_T + s_d \frac{\partial n_i}{\partial x_i} \rangle_s \Sigma, \tag{2.39}$$

where s_d is the flame surface displacement speed, a_T is the tangential strain rate and n_i is the i^{th} component of the unit vector normal to the flame surface. These quantities are defined as (Poinsot & Veynante, 2001)

$$a_T = (\delta_{ij} - n_i n_j) \frac{\partial u_i}{\partial x_j} \; , \qquad s_d = \left(\frac{1}{|\nabla c|} \frac{Dc}{Dt} \middle| \, c = \zeta \right) \; . \tag{2.40}$$

In typical implementation of this equation in turbulent flame calculations the last term on the left hand side (LHS), the normal propagation term, is neglected. The convective term is written as $\langle u_i \rangle_s = \widetilde{u_i} + \langle u_i'' \rangle_s$, and the tangential strain rate term is split into terms corresponding to the mean flow field and turbulent fluctuations. The last term in the right hand side (RHS), the curvature term, is treated as a destruction term which is modelled such that it prevents the transport equation from predicting an infinite growth of flame surface area. Numerous modelling closures for the tangential strain rate and the destruction terms have been proposed and these are summarised by Poinsot & Veynante (2001) and Veynante & Vervisch (2002).

If the flame front is assumed to be planar unstrained laminar flame then the consumption speed in Eq. (2.37), s_c, is close to s_L^o. However the turbulence eddies are likely to wrinkle and stretch the flame front and alter its consumption speed. Bray & Cant (1991) account for the stretch rate, κ, via $\langle s_c \rangle_s = I_o s_L^o$, where the "stretch factor", defined as

$$I_o = \frac{1}{s_L^o} \int s_c(\kappa) \; p(\kappa) \; d\kappa \; , \tag{2.41}$$

is the ratio of the mean flamelet consumption speed to unstrained laminar flame speed.

2.2.5 G–Equation Level Set Formalism

Peters (2000) developed a level set formalism based on the well known G–equation (Williams, 1985b) that describes the kinematics of flame front propagation. The scalar G is defined such that its value is G_o at the flame front, but away from the flame front its value is not uniquely defined. To ascribe a meaningful field value in a turbulent flame, the fluctuating scalar G is interpreted as the distance between the mean and the instantaneous flame front measured in the direction normal to the mean turbulent flame. The mean flame front location is given by $\widetilde{G} = G_o$. The variance $\widetilde{G''^2}$ thus becomes a measure of the flame brush thickness. The transport equation for $\widetilde{G}$ is (Peters, 1999)

$$\overline{\rho}\frac{\partial \widetilde{G}}{\partial t} + \overline{\rho}\widetilde{u}_i\frac{\partial \widetilde{G}}{\partial x_i} = \overline{\rho}S_T\left|\frac{\partial \widetilde{G}}{\partial x_i}\right| - \mu_t\mathcal{K}\left|\frac{\partial \widetilde{G}}{\partial x_i}\right| \quad . \tag{2.42}$$

The first term on the RHS represents the normal propagation of the turbulent flame front while the second is a curvature term. The turbulent flame speed, S_T, needs to be modelled and it is obtained as $S_T = s_L^o(1 + \widetilde{\sigma}_t)$ where $\widetilde{\sigma}_t$ is the ratio of the increase in turbulent flame surface area to that of the laminar flame. A balance equation for $\widetilde{\sigma}_t$, valid in the corrugated and thin reaction zones regimes, was derived by Peters (1999) leading to algebraic expressions for the turbulent flame speed, S_T.

To describe the thermochemical state of the mixture, a rescaled quantity x_n is derived from the scalar G as

$$x_n = \frac{G - G_o}{|\nabla G|} \ , \tag{2.43}$$

where x_n is the normal distance from the flame front. One–dimensional laminar flamelet equations are solved to yield Φ_α as a function of x_n which, along with presumed pdfs are used to obtain the mean quantities, $\overline{\Phi}_\alpha$, in the turbulent flame (Herrmann, 2006).

2.2.6 PDF transport approach

The motivation behind the pdf transport approach is that an exact closure for the mean reaction rate can be obtained if the joint pdf of all the thermochemical scalars is known. Revisiting the case of the single step reaction in Section 2.2.1, the mean fuel consumption rate can be closed exactly as

$$\overline{\dot{\omega}}_F = \int\int\int \dot{\omega}_F(Y_F, Y_O, T)\ p(Y_F, Y_O, T)\ dY_F\ dY_O\ dT\ , \tag{2.44}$$

where $p(Y_F, Y_O, T)$ is the joint pdf of the species mass fractions and temperature. Thus, for a multi–component system with N species, the one–point joint composition pdf, $p(\underline{\Phi})$, provides a closed form expression for the reaction rates, where the vector $\underline{\Phi} = (Y_1, Y_2, ...Y_N, T)$. An evolution equation for the mass–weighted joint pdf, $\tilde{p}(\underline{\Phi})$, is (O'Brien, 1980; Pope, 1985)

$$\begin{aligned}\frac{\partial\ \overline{\rho}\ \tilde{p}(\underline{\Phi})}{\partial t} + \frac{\partial}{\partial x_i}\left[\overline{\rho}\widetilde{u_i}\ \tilde{p}(\underline{\Phi})\right] + \sum_{\alpha=1}^{N}\frac{\partial}{\partial \Phi_\alpha}\left[\frac{1}{\rho}\dot{\omega}_\alpha(\underline{\Phi})\ \overline{\rho}\ \tilde{p}(\underline{\Phi})\right] = \\ -\frac{\partial}{\partial x_i}\left[\langle u_i''|\underline{\Phi}\rangle\ \overline{\rho}\ \tilde{p}(\underline{\Phi})\right] + \sum_{\alpha=1}^{N}\frac{\partial}{\partial \Phi_\alpha}\left(\left\langle\frac{1}{\rho}\frac{\partial J_{i,\alpha}}{\partial x_i}\ \middle|\ \underline{\Phi}\right\rangle\ \overline{\rho}\ \tilde{p}(\underline{\Phi})\right)\ ,\end{aligned} \tag{2.45}$$

where the molecular diffusion flux is $J_{i,\alpha} = V_{i,\alpha}Y_\alpha$. The three terms on the LHS, including the reaction source term, are closed. The first term on the RHS denotes the turbulent transport in the physical space and it is usually modelled using the gradient transport hypothesis. However, the need to model this term, as well as the unclosed terms in the momentum equation, can be avoided if the evolution of the joint velocity–composition pdf is solved. The second term on the RHS denotes molecular mixing in composition space and poses the main modelling challenge for this approach (Pope, 1990).

The joint pdf at each location has a large dimension, $(N+1)$, and conventional numerical techniques such as finite differences are unsuitable for solving the pdf equation. Instead, Monte–Carlo methods are employed whereby a large number of notional fluid particles are introduced whose compositional distribution approximates the joint pdf. The advantage of this method is that the computational expense increases only linearly with the pdf dimension (Pope, 1985) making

the approach computationally tractable for any arbitrarily large chemical mechanism. However, in practice, the implementation of pdf transport approach is complicated and expensive compared to other approaches discussed earlier.

2.2.7 Presumed PDF approaches

The two main difficulties associated with the pdf transport approach: numerical solution of the pdf equation and the large dimension of the joint pdf, can be simplified by representing the thermochemistry using fewer scalars and by presuming a shape for the scalar pdf. The BML model and the G–equation approach described earlier are examples of this where the progress variable and the scalar G, respectively, determine the thermochemical state. Presuming a pdf shape also allows separating the complex thermochemistry calculation from the flow field calculation. The mean thermochemical quantities, including mean density and reaction rates, can be calculated *a priori* and tabulated as functions of scalar moments and looked up during the turbulent flame calculations. The number of scalar moments required for the tabulation is dictated by the presumed pdf shape. For instance, the BML pdf requires only the first moment, $\tilde{c}$, whereas the beta–pdf, which is widely employed (Bradley *et al.*, 1994; Poinsot & Veynante, 2001; Schneider *et al.*, 2005), requires the first two moments: $\tilde{c}$ and $\widetilde{c''^2}$. These need to be obtained from their transport equations.

Fundamental differences between various presumed pdf approaches arise depending on the number and definition of the representative scalars employed, and their relationship to the thermochemistry. In the laminar flamelet models, which are based on the flamelet approximation, the relationship is constructed from canonical laminar flame calculations. For example, the mean quantities can be evaluated from Eq. (2.23) by presuming $p(\zeta)$ and taking $\Phi_\alpha(\zeta)$ to correspond to a laminar flame. Similarly, the mean reaction rate can be obtained from laminar flame values, $\dot{\omega}(\zeta)$, as

$$\overline{\dot{\omega}} = \int \dot{\omega}(\zeta)\ p(\zeta)\ d\zeta. \tag{2.46}$$

This is the basis of the laminar flamelet approaches proposed by Bradley *et al.* (1994), van Oijen & de Goey (2000) and Gicquel *et al.* (2000). However, other approaches to construct the mapping exist, as will be discussed in Section 2.2.9.

2.2.8 Conditional Moment Closure

Conditional Moment Closure (CMC) is based on the hypothesis that in turbulent flames the fluctuations of all thermochemical quantities are well correlated with the fluctuations of just one scalar: mixture fraction in non–premixed and progress variable in premixed flames. Hence, while the fluctuations about the unconditional mean can be significant, the fluctuations about a mean conditioned on such a scalar are small. The unconditional mean is related to the conditional mean as

$$\overline{\Phi}_\alpha = \int \langle \Phi_\alpha | c = \zeta \rangle \; p(\zeta) \; d\zeta \; . \tag{2.47}$$

Note that the above equation, which is mathematically exact, is very similar to Eq. (2.23) which is an approximation. In CMC the conditional mean scalar values, $Q_\alpha \equiv \langle \Phi_\alpha | c = \zeta \rangle$, are obtained from their respective transport equations. For the case of premixed flames this equation is written as (Klimenko & Bilger, 1999)

$$\langle \rho|\zeta\rangle \frac{\partial Q_\alpha}{\partial t} + \langle \rho u_i|\zeta\rangle \frac{\partial Q_\alpha}{\partial x_i} = \langle \rho|\zeta\rangle \langle N_c|\zeta\rangle \frac{\partial^2 Q_\alpha}{\partial \zeta^2} + \langle \dot{\omega}_\alpha|\zeta\rangle - \langle \dot{\omega}|\zeta\rangle \frac{\partial Q_\alpha}{\partial \zeta} + e_{Q_\alpha} + e_{y_\alpha}, \tag{2.48}$$

where the reaction rate terms, $\dot{\omega}_\alpha$ and $\dot{\omega}$, are as in Eqs. (2.3) and (2.13) respectively and the instantaneous scalar dissipation rate is

$$N_c \equiv D_c \frac{\partial c}{\partial x_i} \frac{\partial c}{\partial x_i} \tag{2.49}$$

Equation (2.48) has been arrived at independently by Klimenko (1990) using the joint pdf equation, and by Bilger (1993) using a decomposition about the conditional mean as $Y_\alpha(\mathbf{x}, t) = Q_\alpha(\zeta, \mathbf{x}, t) + y_\alpha(\mathbf{x}, t)$, where y_α is the conditional fluctuation. The term e_{Q_α} is (Swaminathan & Bilger, 2001a)

$$e_{Q_\alpha} \equiv \frac{\partial}{\partial x_i}\left(\rho D_\alpha \frac{\partial Q_\alpha}{\partial x_i}\right) + \left\langle \frac{\partial Q_\alpha}{\partial \zeta} \frac{\partial}{\partial x_i}\left([1 - Le_\alpha]\rho D_\alpha \frac{\partial c}{\partial x_i}\right) + \rho D_\alpha \frac{\partial c}{\partial x_i}\frac{\partial}{\partial x_i}\left(\frac{\partial Q_\alpha}{\partial \zeta}\right) \middle| \zeta \right\rangle \tag{2.50}$$

and it represents the contribution of molecular diffusion which becomes negligible when Re is large. However, the second term in the above equation arises from

differential diffusion effects and might have to be cautiously considered (Swaminathan & Bilger, 2001a). The last term on the RHS in Eq. (2.48) is

$$e_{y_\alpha} \equiv -\left\langle \rho\frac{\partial y_\alpha}{\partial t} + \rho u_i\frac{\partial y_\alpha}{\partial x_i} - \frac{\partial}{\partial x_i}\left(\rho D_\alpha\frac{\partial y_\alpha}{\partial x_i}\right)\middle|\zeta\right\rangle \tag{2.51}$$

and it can be modelled as (Klimenko & Bilger, 1999)

$$e_{y_\alpha} \approx \frac{1}{p(\zeta)}\frac{\partial}{\partial x_i}(\langle\rho\mathbf{u}_i''y_\alpha|\zeta\rangle p(\zeta)) \tag{2.52}$$

where $\mathbf{u}_i''$ is the conditional fluctuation of velocity u_i.

Modelling of the conditional velocity, $\langle\rho u_i|\zeta\rangle$, was investigated by Swaminathan & Bilger (2001a) and some simple closures seem promising. On the other hand, modelling of the conditional mean scalar dissipation rate, $\langle N_c|\zeta\rangle$, is yet to be addressed satisfactorily (Swaminathan & Bilger, 2001b)[4] and it appears to be inextricably linked to the unconditional mean dissipation rate, $\widetilde{\epsilon_c}$. For the conditional reaction rates a first order closure can be obtained by writing a Taylor series expansion of $\langle\dot{\omega}_\alpha|\zeta\rangle$, similar to Eq. (2.17), and noting that the conditional fluctuations are negligible which gives (Klimenko & Bilger, 1999)

$$\langle\dot{\omega}_\alpha(Y_1,....Y_N,T)|\zeta\rangle \approx \langle\dot{\omega}_\alpha(Q_1,....Q_N,Q_T)|\zeta\rangle = \dot{\omega}_\alpha(Q_1,....Q_N,Q_T). \tag{2.53}$$

This first order closure has been found to be remarkably good for the conditional reaction rates of major species and progress variable, but not so for minor species since their conditional fluctuations are not small (Swaminathan & Bilger, 2001a). For such species, conditioning on more than one scalar might be necessary.

Apart from modelling of the conditional scalar dissipation rate, the main difficulty in implementing CMC for premixed flames seems to be with the suitable definition of the progress variable (Klimenko & Bilger, 1999). It is worth noting that CMC is considerably more expensive than the approaches discussed earlier, except possibly the transported pdf approach. The number of transport equations to be solved for the thermochemistry is equal to $(N + 1)$ times the number of

[4]For non–premixed flames the conditioning variable, the mixture fraction, is a conserved scalar and its pdf equation leads to an expression for the conditional scalar dissipation rate under certain conditions (Klimenko & Bilger, 1999). This is considerably more difficult when the conditioning variable is a reactive scalar, such as c for premixed flames.

points in the conditioning variable space. However, the rigorous mathematical framework of the CMC is likely to provide better predictions of pollutants and their formation rates compared to other approaches that are based on physical or phenomenological arguments.

2.2.9 Chemistry Tabulation

Tabulating the thermochemistry is a crucial aspect of most of the modelling approaches described in the previous sections, with the exception of CMC[5]. In the pdf transport approach an on–the–fly computation of the reaction rates in the $(N + 1)$–dimensional composition space is time consuming unless a reduced chemical mechanism is considered. In presumed pdf approaches (G–equation and flamelet) chemistry tabulation is an integral part of their formulation. Hence strategies have been developed to simplify the detailed chemical kinetics and tabulate the chemistry as functions of few scalars.

The Intrinsic Low Dimensional Manifold (ILDM) approach identifies that for every reacting system of N species, there exists subspaces of much smaller dimension, n_s, in which reactions proceed according to slow time scales (Maas & Pope, 1992b). At each point in this subspace there is local equilibrium with respect to $(N - n_s)$ fastest time scales and any point away from this subspace is attracted to it via these faster processes. Hence the dynamic evolution of the reacting system can be parametrised in terms of only n_s variables and these completely determine the thermochemical state of the mixture. The physical and mathematical foundation of this approach and its implementation are discussed in (Maas & Pope, 1992a,b, 1994). ILDM performs a simplification of the detailed chemical mechanism as opposed to reducing it. In reduced chemical mechanisms certain fast chemical reactions are identified and the assumption of partial equilibrium for these reactions is invoked at the start of the reduction process. These assumptions provide poor approximations beyond certain composition range. In ILDM, the chemical reactions corresponding to the fast time scales are identified locally at each point in the subspace and different initial compositions optimally approach this manifold.

[5]The BML model also does not require the tabulation since it does not attempt to resolve the chemical structure of the flame front.

Gicquel *et al.* (2000) note that at low temperatures the chemical time scales are not disparate and hence ILDM provides a poor approximation in such regions. This is remedied by a Flame Prolongation of ILDM (FPI) (Gicquel *et al.*, 2000) which is conceptually similar to the Flamelet–Generated Manifolds (FGM) approach of van Oijen & de Goey (2000). Both involve generating a manifold from freely propagating unstrained planar laminar flame calculations, which is used to tabulate the thermochemistry in terms of a progress variable. Physically, when applied to turbulent flame calculations, FPI and FGM can be viewed as laminar flamelet models where the turbulent flame front has the same structure as that of an unstrained laminar flame. Bradley *et al.* (1994) propose a stretched laminar flamelet model that accounts for the influence of fluid–dynamic stretch rate on the reaction rate. While the focus of their approach was on the closure of the mean reaction rate, $\overline{\dot{\omega}}$, it could be extended to provide a closure for the mean species concentrations also. In Chapter 4, an alternative flamelet approach based on the scalar dissipation rate will be presented. This approach is motivated by physical considerations. But first it is worth emphasising the role played by scalar dissipation rate in turbulent premixed flame modelling, and this is discussed in the next chapter.

Chapter 3

Scalar Dissipation Rate

This chapter focuses on the scalar dissipation rate which is unclosed yet central in many modelling approaches. The mathematical definition and physical meaning of this quantity will be discussed first. Simple relations between chemical reaction rates and the scalar dissipation rate in premixed and non–premixed flames will be presented. The role of mean scalar dissipation rate in turbulent combustion modelling will then be illustrated. Although the main interest of this study is lean premixed flames, non–premixed flames are discussed for the sake of completeness and to emphasise the central role of the scalar dissipation rate in turbulent combustion in general.

3.1 Definition and Physical Meaning

It is worthwhile to examine the balance equation for the scalar variance, $\widetilde{c''^2}$. By substituting $c = \tilde{c} + c''$ in Eq. (2.13), multiplying by c'' and then averaging the result leads to the exact equation (Bray, 1980; Veynante & Vervisch, 2002)

$$\frac{\partial \overline{\rho}\widetilde{c''^2}}{\partial t} + \frac{\partial \overline{\rho}\widetilde{u}_i\widetilde{c''^2}}{\partial x_i} + \frac{\partial \overline{\rho}\widetilde{u''_i c''^2}}{\partial x_i} = \frac{\partial}{\partial x_j}\overline{\left(\rho D_c \frac{\partial c''^2}{\partial x_j}\right)} + 2\overline{c''\frac{\partial}{\partial x_j}\left(\rho D_c \frac{\partial \tilde{c}}{\partial x_j}\right)} - \underbrace{2\overline{\rho}\widetilde{u''_i c''}\frac{\partial \tilde{c}}{\partial x_i}}_{\text{production}} + \underbrace{2\overline{\dot{\omega}'' c''}}_{\text{reaction}} - \underbrace{2\overline{\rho D_c \frac{\partial c''}{\partial x_i}\frac{\partial c''}{\partial x_i}}}_{\text{dissipation}}. \quad (3.1)$$

Modelled form of the above equation is particularly relevant to presumed pdf approaches since the pdf shapes requiring the first two moments are popular

choice among modellers. The three terms in the LHS denote the unsteady, mean convection and the turbulent transport terms. The first two terms in the RHS denote the influence of molecular transport, and are negligible for large Reynolds numbers. The third term denotes a production of scalar fluctuations due to gradients in the mean, if the scalar flux, $\overline{\rho}\widetilde{u_i''c''}$, is gradient type. The fourth term denotes the reaction rate contribution and needs to be modelled. This term is related to the mean reaction rate (Bray, 1979) by

$$\overline{\dot{\omega}''c''} = \overline{\dot{\omega}c} - \overline{\dot{\omega}}\tilde{c} = (C_m - \tilde{c})\overline{\dot{\omega}} \ . \tag{3.2}$$

The last term in the RHS of Eq. (3.1) is the mean scalar dissipation rate, $\widetilde{\epsilon_c}$, defined earlier by Eq. (2.32) and it is unclosed. This term has a negative sign in Eq. (3.1) and for a simplified homogeneous case with no $\tilde{c}$ gradients and no reaction, it denotes one half of the rate of decay of scalar fluctuations. Since the absence of fluctuations implies a well mixed fluid, the mean scalar dissipation rate can be physically interpreted as the rate at which turbulent mixing occurs at the molecular level (Cant & Mastorakos, 2008). Mathematically, it is the average of the instantaneous dissipation rate

$$\overline{\rho N_c} = \overline{\rho D_c}\frac{\partial\tilde{c}}{\partial x_i}\frac{\partial\tilde{c}}{\partial x_i} + \overline{2\rho D_c\frac{\partial c''}{\partial x_i}\frac{\partial\tilde{c}}{\partial x_i}} + \overline{\rho D_c\frac{\partial c''}{\partial x_i}\frac{\partial c''}{\partial x_i}}, \tag{3.3}$$

since the contribution of the gradients of mean progress variable is negligible compared to the gradients of fluctuations. Hence $\overline{\rho N_c} \approx \overline{\rho}\widetilde{\epsilon_c}$.

The EBU model of Mason & Spalding (1973), mentioned in Section 2.2.3, is based on the physical idea that in the limit of fast chemistry, the mean reaction rate is limited by the rate at which the reactants are brought into contact with hot products by the turbulent mixing. Bilger (1976) provided a mathematical basis for this physical argument by considering the mixture fraction formulation in non–premixed flames. Considering a two–feed problem, assuming all species have equal diffusivities, Bilger (1976) defines the mixture fraction as

$$\xi = \frac{Z_i - Z_{i_2}}{Z_{i_1} - Z_{i_2}} \ , \tag{3.4}$$

where Z_i is the mass fraction of any element i, and the subscripts 1 and 2 denote the two feeds. The mixture fraction is a conserved scalar and satisfies $L(\xi) = 0$

where the linear operator

$$L \equiv \rho\frac{\partial}{\partial t} + \rho u_i \frac{\partial}{\partial x_i} - \frac{\partial}{\partial x_i}\left(\rho D \frac{\partial}{\partial x_i}\right). \tag{3.5}$$

The conservation equation for species α can be written as $L(Y_\alpha) = \dot{\omega}_\alpha$. If the species concentrations are assumed to be functions of mixture fraction alone, then through simple transformation one obtains (Bilger, 1976)

$$\dot{\omega}_\alpha = \frac{\partial Y_\alpha}{\partial \xi} L(\xi) - \frac{\partial^2 Y_\alpha}{\partial \xi^2}\left(\rho D \frac{\partial \xi}{\partial x_i}\frac{\partial \xi}{\partial x_i}\right) = -\frac{\partial^2 Y_\alpha}{\partial \xi^2}\ \rho N_\xi \tag{3.6}$$

and the mean reaction rate is directly proportional to the mean scalar dissipation rate i.e. $\overline{\dot{\omega}}_\alpha \sim \widetilde{\epsilon}_\xi$. The definitions of N_ξ and $\widetilde{\epsilon}_\xi$ are analogous to N_c and $\widetilde{\epsilon}_c$ respectively. For premixed flames, one can similarly work with the progress variable and, noting that $L(c) = \dot{\omega}$ from Eq. (2.13), obtain

$$\dot{\omega}_\alpha = \frac{\partial Y_\alpha}{\partial c}\ \dot{\omega} - \frac{\partial^2 Y_\alpha}{\partial c^2}\ \rho N_c\ . \tag{3.7}$$

Again the dependence of mean species reaction rates on the mean scalar dissipation rate, $\widetilde{\epsilon}_c$, is apparent. However, this analysis leads nowhere useful for premixed flame modelling since, in the first instance, closure of $\overline{\dot{\omega}}$ is itself unknown and, further, the modelling of $\widetilde{\epsilon}_c$ is challenging. In contrast, modelling of $\widetilde{\epsilon}_\xi$ is relatively easier. Nonetheless, these simple results suggest that the mean scalar dissipation rate fundamentally represents the turbulence–chemistry interaction both in premixed and non–premixed scenarios. Inevitably, it appears directly or indirectly in most combustion modelling approaches, as we shall see in the next section.

3.2 Role in Turbulent Combustion Modelling

Veynante & Vervisch (2002) analyse the various mathematical tools of turbulent combustion and conclude that the scalar dissipation rate is a key parameter and often a stumbling block in modelling. In presumed pdf approaches, which are conceptually the simplest, the mean scalar dissipation rate is required in the variance equation, Eq. (3.1). Provided the turbulent scalar flux and reaction terms are closed for the $\tilde{c}$ equation, the scalar dissipation rate presents the only additional closure problem. In CMC the conditional mean scalar dissipation rate

appears as an unclosed term in Eq. (2.48) and it is related to the mean scalar dissipation rate as (Swaminathan & Bilger, 2001b)

$$\widetilde{\epsilon_c} \;=\; \int_0^1 \langle N_c|\zeta\rangle \; \tilde{p}(\zeta) \; d\zeta. \tag{3.8}$$

For transported pdf approaches, as discussed in Section 2.2.6, the only unclosed term is the molecular mixing term which is the last term in the RHS of Eq. (2.45). An elementary implementation of this approach would involve solving the transport equation of the pdf of a single scalar. The molecular mixing term for such a case becomes equal to (Klimenko & Bilger, 1999; O'Brien, 1980; Swaminathan & Bilger, 2001b; Veynante & Vervisch, 2002)

$$-\frac{1}{\langle\rho|\zeta\rangle}\frac{\partial}{\partial\zeta}\left[\langle\nabla\cdot(\rho D_c\nabla c)\mid\zeta\rangle\; p(\zeta)\right] \approx -\frac{\partial^2}{\partial\zeta^2}\left[\langle\rho\; N_c|\zeta\rangle\; p(\zeta)\right] \tag{3.9}$$

involving only the conditional mean dissipation rate, when the Reynolds number is large. On the other hand, in solving transport equations of multi–component pdfs, stochastic mixing models are used to mimic the molecular mixing process. A key ingredient of these models is the scalar mixing frequency, τ_c^{-1}, which is the inverse of the decay time scale of scalar fluctuations and is related to the scalar dissipation rate by

$$\tau_c^{-1} \equiv \frac{\widetilde{\epsilon_c}}{\widetilde{c''^2}} \;. \tag{3.10}$$

The mixing frequency is usually estimated from the decay time scale for turbulent velocity fluctuations, τ_t, via

$$\tau_c^{-1} = C_\phi \tau_t^{-1} = C_\phi \frac{\widetilde{\varepsilon}}{\widetilde{k}} \;, \tag{3.11}$$

and for a passive scalar C_ϕ is about 1.0 (Spalding, 1971). Bilger *et al.* (2005) point out that such mixing models based on passive scalar dynamics involve no explicit coupling between reaction and mixing, although pdf simulations have been successful in predicting complex phenomena such as local extinction in non–premixed turbulent flames. However, the need to include the coupling is acknowledged by Subramaniam & Pope (1998) and Mitarai *et al.* (2005).

3.2.1 Non–Premixed Combustion

Passive scalar mixing models have been quite useful in non–premixed flame modelling. In the class of laminar flamelet models, spawned by the work of Peters (1984), the dissipation rate of mixture fraction assumes a special role. Attaching a coordinate system to the stoichiometric mixture fraction surface, Peters (1984) performs a Crocco–type transformation from (x_1, x_2, x_3, t) system to (ξ, Z_2, Z_3, t_1) system where, by definition, ξ is locally normal and Z_2 and Z_3 are locally tangential to the stoichiometric surface. This leads to the flamelet equations in terms of the mixture fraction

$$\rho \frac{\partial Y_\alpha}{\partial t_1} = \rho N_\xi \frac{\partial^2 Y_\alpha}{\partial \xi^2} + \dot{\omega}_\alpha - R(Y_\alpha) \ . \tag{3.12}$$

The derivatives with respect to Z_2 and Z_3, denoted by the operator R, and the unsteady term are of lower order in the inner reaction zone (except close to extinction) (Peters, 1984). Under such conditions the structure of a burning flamelet that defines $Y_\alpha(\xi)$ is parametrised only by the dissipation rate, N_ξ. This is identical to Bilger's result, Eq. (3.6), except for the unsteady term. Thus the statistics of the mixture fraction and its dissipation rate are sufficient to describe the thermochemistry of a turbulent flame via

$$\overline{\Phi}_\alpha = \int_0^{N_{\xi,q}} \int_0^1 \Phi_\alpha(\xi, N_\xi)\ p(\xi, N_\xi)\ d\xi\ dN_\xi \ , \tag{3.13}$$

where $N_{\xi,q}$ is the dissipation rate at extinction. The mean dissipation rate, $\widetilde{\epsilon_\xi}$, required for the statistics of N_ξ can be obtained from a transport equation but it is usually closed algebraically using a simple model

$$\widetilde{\epsilon_\xi} \approx C_\xi \frac{\widetilde{\varepsilon}}{\widetilde{k}}\ \widetilde{\xi''^2} \ , \tag{3.14}$$

where $C_\xi = 1.0$[1] and it is obtained from Eq. (3.11) .

[1] the definition of scalar dissipation rate in (Peters, 1984) includes a factor of 2, i.e., $N_\xi = 2D(\partial\xi/\partial x_i)^2$. Accordingly the constant C_ξ takes a value of 2.0 in that work.

3.2.2 Premixed Combustion

Bilger (2004b) suggests that the heat release is unlikely to influence the fine–scale structure of turbulence strongly in non–premixed flames since the local dilatation at the flame front is much smaller than the turbulence strain rate. However, in premixed flames, the strong local dilatation will be subdued only under intense turbulence conditions. Hence, models based on passive scalar ideas might be reasonable for the former but are unjustifiable for the latter. Furthermore, the parametrising scalars for premixed flame modelling are invariably reactive. In flamelet combustion the gradients of reactive scalars are steepened by chemical reactions which is not incorporated in the current mixing models (Subramaniam & Pope, 1998). Consequently, attempts at tailoring the stochastic mixing models for premixed flame calculations have been few. Pope & Anand (1984) solve the transport equation of $p(\zeta)$ for a single step chemistry, and consider the closure of the mixing term for the two extreme conditions: distributed reaction zones and wrinkled flamelets regimes. For the former regime passive scalar type mixing models were retained. For the latter, the mixing term was not explicitly modelled. Instead, invoking the flamelet assumption, the mixing term combined with the reaction term was expressed as a local function of the progress variable and was obtained from planar laminar flame results. Lindstedt & Vaos (2006) report premixed flame calculations for conditions that are far from the classical extremes, with a mixing model using modified model constant C_ϕ which includes a chemical time scale.

Despite its modelling difficulties, the scalar dissipation rate is mathematically linked to the fundamental quantities in premixed combustion (Veynante & Vervisch, 2002). The direct relation between the mean reaction rate, $\overline{\dot{\omega}}$, and the mean scalar dissipation rate, $\widetilde{\epsilon_c}$, is already shown in Eq. (2.30). When combined with Eq. (3.7) it shows that the mean reaction rate of species α, $\overline{\dot{\omega}}_\alpha$, is proportional to $\widetilde{\epsilon_c}$, similar to the case of non–premixed flames. It is also related to the flame surface density from Eq. (2.38) as

$$\Sigma = \left\langle \sqrt{(N_c/D_c)} \middle| c = \zeta \right\rangle p(\zeta) \ . \tag{3.15}$$

3.2.3 Stratified/Partially Premixed Combustion

Recent modelling strategies for partially premixed combustion have employed both reactive and passive scalars: progress variable to track the reaction zones and mixture fraction to denote the local stoichiometry. Bray *et al.* (2005) suggest that an appropriately defined progress variable can be a suitable scalar to represent the thermochemistry in partially premixed flames. One possible definition, suggested therein, is as a normalised fuel mass fraction with a mixture fraction dependence. The reaction source term for such a progress variable then introduces a dependence on the mixture fraction dissipation rate, N_ξ, and an additional parameter; the cross scalar dissipation rate[2],

$$N_{\xi c} \equiv D \frac{\partial \xi}{\partial x_i} \frac{\partial c}{\partial x_i}. \tag{3.16}$$

Libby & Williams (2000) and subsequently Ribert *et al.* (2004) have formulated a presumed pdf approach for partially premixed systems where the joint pdf, $p(\xi, c)$, consists of two Dirac delta functions in the (ξ, c) space. The strength and the location of the delta functions are determined by, in the least, $\widetilde{\xi}$, $\widetilde{\xi''^2}$, $\tilde{c}$ and $\widetilde{c''^2}$ for which transport equations are solved. The shape presumed for the pdf constrains the cross correlation to satisfy

$$\widetilde{\xi'' c''} = \sqrt{\widetilde{\xi''^2}\,\widetilde{c''^2}} \tag{3.17}$$

which is not necessarily physical. Robin *et al.* (2006) attempt to relax this constraint by presuming a pdf shape with four Dirac delta functions and solving a transport equation for the cross correlation, $\widetilde{\xi'' c''}$, which requires the closure of the mean cross scalar dissipation, $\overline{\rho N_{\xi c}}$. Thus, it appears that models of partially premixed flames need to address the closure of the mean cross scalar dissipation, apart from the mean dissipation rates of individual scalars.

The cross scalar dissipation rate can be expressed as (Bray *et al.*, 2005)

$$N_{\xi c} = (\hat{e}_\xi \cdot \hat{e}_c) \sqrt{N_\xi N_c} \tag{3.18}$$

where $\hat{e}_\xi$ and $\hat{e}_c$ are the unit vectors normal to the ξ and c iso–surfaces. The dot product $(\hat{e}_\xi \cdot \hat{e}_c)$ could assume a value between -1 and 1 in a turbulent flame and

[2]for the simple case of all species having unity Lewis numbers $D_\xi = D_c = D$.

it is possible that the mean value is negligible (Bray *et al.*, 2005). However, this is only speculative and further study is required to justify any assumptions of the magnitude of the cross scalar dissipation on physical grounds.

3.3 Summary

The role of scalar dissipation rate in turbulent combustion was studied in this chapter. Simple mathematical relations that link the scalar dissipation rate to the fundamental quantities in turbulent combustion were presented. From modelling point of view, conditional and unconditional mean scalar dissipation rates are central to most modelling methodologies. For premixed flames, closures for the reaction rates of chemical species and the progress variable are of interest and these are seen to be proportional to the progress variable dissipation rate, N_c. It is instructive to study a balance equation for N_c. Swaminathan & Bray (2005) present the equation

$$\begin{aligned}\frac{\partial \rho N_c}{\partial t} + \frac{\partial \rho u_i N_c}{\partial x_i} = \frac{\partial}{\partial x_j}\left(\rho D_c \frac{\partial N_c}{\partial x_j}\right) - 2\rho\left(D_c \frac{\partial^2 c}{\partial x_j \partial x_k}\right)^2 \\ -\rho D_c \frac{\partial c}{\partial x_j}\left[\frac{\partial u_j}{\partial x_k} + \frac{\partial u_k}{\partial x_j}\right]\frac{\partial c}{\partial x_k} + 2\rho N_c \frac{\partial u_i}{\partial x_i} + 2D_c \frac{\partial c}{\partial x_k}\frac{\partial \dot{\omega}}{\partial x_k}\,,\end{aligned} \tag{3.19}$$

where the dependence of D_c on temperature is assumed to be negligible. In the above equation the first and second terms in the RHS denote the diffusive flux and dissipation respectively. The third term is governed by the interaction of the fluid–dynamic strain rate with the gradients of progress variable. The fourth term arises due to density jump across the flame front and the last term represents the correlation between progress variable gradient and chemical reaction. This equation suggests that the balance of N_c is intricately linked to the fundamental processes that affect the flame front dynamics. The observations on the central role of N_c and its close coupling to the physical processes influencing the dynamics of the flame front provide motivation for formulating a flamelet model based on the scalar dissipation rate, which is discussed in the next chapter.

Chapter 4

Strained Flamelet Formulation for Premixed Flames

In this chapter the formulation of a mathematical model for turbulent premixed flame computations is developed using the flamelet concept. The objective is to describe how the mutual influence of turbulence and flamelets at the scales relevant to combustion can be captured, with a specific interest on the mean reaction rate modelling, within the framework of the laminar flamelets approach. The existing models based on flamelet ideas will be briefly summarised before presenting a new formulation which is based on a scalar dissipation rate parametrisation. Closures for the unknown terms, the joint pdf of progress variable and scalar dissipation rate and the requisite moments, will be discussed. The choice of a canonical laminar flamelet configuration will then be discussed which results in the final closure.

In laminar flamelet modelling the turbulent flame is viewed as an ensemble of thin locally one–dimensional laminar structures called flamelets. Experimental studies (Chen *et al.*, 1996; Dunn *et al.*, 2007, 2009) indicate that even at very high turbulence intensities, while the flame front is disrupted by the turbulence, flamelet–like structures can still be discerned. Numerical studies (Poinsot *et al.*, 1991) have demonstrated that flamelet type combustion is likely to extend to regimes well beyond those suggested by classical ideas. However, the success of this modelling method depends on the approach used to ascribe the influence of turbulence on flamelets. The flame front is contorted and strained by the eddies but if the flame scales are much smaller than the typical small (Kolmogorov)

scales of turbulence, such as in the wrinkled flamelets regime, then the effects of turbulent straining can be ignored. Some existing models such as FGM (van Oijen & de Goey, 2000), FPI (Gicquel *et al.*, 2000) and the flamelet model of Bradley *et al.* (1988) are based on such an implicit assumption; the turbulent flamelet structure corresponds to a freely propagating planar unstrained laminar flame. They provide a closure for the mean reaction rate as

$$\overline{\dot{\omega}} = \int_0^1 \dot{\omega}_o(\zeta)\ p(\zeta)\ d\zeta, \tag{4.1}$$

where $\dot{\omega}_o(\zeta)$ is the reaction rate in an unstrained planar laminar flame.

At higher turbulence intensities, such as in the thin reaction zones regime, the influence of turbulence straining is unlikely to be negligible. It is well known from asymptotic theories (Clavin, 1985) that the consumption speed, s_c, depends on the fluid dynamic stretch rate, κ, as

$$s_c(\kappa) = s_L^o - \mathfrak{L}\kappa, \tag{4.2}$$

where $\mathfrak{L}$ is the Markstein length. The stretch rate can be written as (Candel & Poinsot, 1990)

$$\kappa = a_T + s_d/r \tag{4.3}$$

and it incorporates the effects of both the strain rate, a_T, and the flame front curvature, r. The displacement speed, s_d, denotes the speed of advancement of the flame relative to unburnt mixture while the consumption speed, s_c, denotes the rate of reactants consumption by the flame. Bradley (1992) and co–workers (Bradley *et al.*, 1994, 1998, 2005) propose a flamelet model that accounts for the stretch rate effects as

$$\overline{\dot{\omega}} = \int\int \dot{\omega}(\zeta,\kappa)\ p(\zeta,\kappa)\ d\zeta\ d\kappa\ . \tag{4.4}$$

They assume that ζ and κ are statistically independent which allows the joint pdf to be decomposed as $p(\zeta,\kappa) = p(\zeta)\ p(\kappa)$. Further, noting that there is a correspondence between consumption speeds and reaction rate profiles, they write, by analogy to Eq. (4.2),

$$\dot{\omega}(\zeta,\kappa) = \widehat{f}(\kappa)\ \dot{\omega}_o(\zeta)\ . \tag{4.5}$$

Empirical correlations for $\widehat{f}(\kappa)$ in terms of $\mathfrak{L}$ were obtained from numerical calculations of spherical laminar flames (Bradley *et al.*, 1996, 1998). Their final closure for the mean reaction rate can be expressed as

$$\overline{\dot{\omega}} = P_b \int \dot{\omega}_o(\zeta)\ p(\zeta)\ d\zeta, \tag{4.6}$$

and the "burning rate factor",

$$P_b = \int_{\kappa_q^-}^{\kappa_q^+} \widehat{f}(\kappa)\ p(\kappa)\ d\kappa, \tag{4.7}$$

incorporates the stretch effects and is analogous to the factor I_o in Eq. (2.41). The positive and negative extinction stretch rates are denoted by κ_q^+ and κ_q^- respectively.

4.1 Scalar Dissipation Parametrisation

The stretch rate dependence of the consumption speed given by Eq. (4.2) is strictly valid for low stretch rates (Poinsot & Veynante, 2001). Accordingly, at high stretch rates the validity of the analogous relationship, Eq. (4.5), as well as Eq. (2.41) might be questionable. Bradley *et al.* (1998) indicate that the Markstein number correlations proposed for $\widehat{f}(\kappa)$ are likely to be valid only for weakly curved corrugated flames. On the other hand, a recent DNS study (Hawkes & Chen, 2006) showed significant burning in turbulent flames at strain rates much larger than the extinction strain rates of symmetric counterflow laminar flames. Therefore, it is proposed to use a scalar dissipation rate parametrisation, instead of the stretch rate, in the form of

$$\overline{\dot{\omega}} = \int\int \dot{\omega}(\zeta,\psi)\ p(\zeta,\psi)\ d\psi\ d\zeta\ , \tag{4.8}$$

where ψ is the sample space variable for the scalar dissipation rate N_c. Physically, this implies that the influence of turbulence dynamics on the flame front is tracked using the local scalar dissipation rate.

4.1.1 Motivation

There are many reasons for choosing the scalar dissipation rate to parametrise the flamelets. To emphasise a few of these:

- On a physical basis, the mixing of cold and hot fluid parcels on the flame surface is required to sustain combustion and the rate of this mixing is given by the scalar dissipation rate.
- As discussed in Section 3.3, scalar dissipation rate is governed by the convection–diffusion–reaction balance and represents the flame front dynamics whereas the stretch rate represents flame front kinematics.
- The progress variable gradients, and hence N_c, are mainly produced by chemical reactions. It can be expected, as is also evident from Eq. (3.7), that locally the reaction rate is strongly correlated with the dissipation rate.
- It can be inferred from the asymptotic analyses of Libby & Williams (1982) and Libby *et al.* (1983) that the flamelet structure is closely related to gradient of c, and hence N_c, both at low and high stretch rates.

Furthermore, in the implementation of the stretch rate parametrisation, when one considers the distribution of stretch rates acting on a turbulent flame front at a given spatial location, it is not distinguished whether the stretch rate corresponds to a location on the burnt side, the unburnt side or within the flame front. When embedding the laminar flamelets, however, the stretch rate characterising a flamelet is defined at a location on the unburnt side only according to Bradley *et al.* (1996). On the other hand, the use of a scalar dissipation rate parametrisation automatically allows such a distinction to be accounted for. This is because the scalar dissipation rate is defined at every location in the laminar flamelet. One could also define a stretch rate at every location in the laminar flamelet but existing models do not follow such an approach.

The scalar dissipation rate parametrisation proposed here is some what similar to the non–premixed laminar flamelets formulation of Peters (1984), Eq. (3.13). However, in Eq. (3.13), the flamelet structure is characterised by a single dissipation rate value, that at the stoichiometric mixture fraction, whereas here the

dissipation rate at every location in the flamelet is considered. Also, statistical independence between the mixture fraction and its dissipation rate is typically assumed which is strictly valid when the mixture fraction pdf is Gaussian (Gao & O'Brien, 1991). Such an assumption might be drastic for the progress variable since it is a reactive scalar and its pdf is unlikely to resemble a Gaussian. The assumption of statistical independence is eschewed and the joint pdf is written using the Bayes theorem as

$$p(\zeta, \psi) = p(\zeta)\ p(\psi|\zeta)\ . \tag{4.9}$$

The mean reaction rate in Eq. (4.8) now becomes

$$\overline{\dot{\omega}} = \int \left[\int_0^{N_{max}} \dot{\omega}(\zeta, \psi)\ p(\psi|\zeta)\ d\psi \right]\ p(\zeta)\ d\zeta\ . \tag{4.10}$$

One could solve for the pdfs from the transport equations but a simpler framework to test the scalar dissipation rate parametrisation is followed by presuming these pdfs which will be discussed in Section 4.3. The quantity $\dot{\omega}(\zeta, \psi)$ is to be obtained from strained laminar flames which is the focus of the next section.

4.2 Choice of Flamelet Configuration

To put the current reaction rate closure in perspective it is helpful to write Eq. (4.10) as

$$\overline{\dot{\omega}} = \int_0^1 \langle \dot{\omega}|\zeta \rangle\ P(\zeta)\ d\zeta\ . \tag{4.11}$$

The difference in various modelling methodologies can be illustrated in the way the conditional mean reaction rate, $\langle \dot{\omega}|\zeta \rangle$, is evaluated[1]. In the unstrained flamelets closure given by Eq. (4.1), $\langle \dot{\omega}|\zeta \rangle = \dot{\omega}_o(\zeta)$, whereas the stretch rate based closure of Bradley and co–workers is equivalent to $\langle \dot{\omega}|\zeta \rangle = P_b\ \dot{\omega}_o(\zeta)$. But, in the current closure

$$\langle \dot{\omega}|\zeta \rangle = \int_{N_1}^{N_2} \dot{\omega}(\zeta, \psi)\ P(\psi|\zeta)\ d\psi\ . \tag{4.12}$$

[1] As noted in Section 2.2.8, in CMC a closure for $\langle \dot{\omega}|\zeta \rangle$ is obtained by evaluating the Arrhenius type reaction rate expression using the conditional mean species mass fractions and temperature.

The value of $\dot{\omega}(\zeta, \psi)$ and the limits N_1 and N_2 will be dictated by the choice of the flamelet configuration as different configurations exhibit different responses to stretching (Law, 2006). Since stretched premixed flamelets can be established in a variety of configurations such as spherical flames, planar flames in Reactant–to–Reactant or Reactant–to–Product opposed flows etc., it is important to choose a configuration that reasonably represents the turbulent flame characteristics (Peters, 1984). Two configurations that are widely considered (Dixon-Lewis, 1990) in the context of flamelet modelling are the purely strained steady planar flames; the opposed flow symmetric Reactant–to–Reactant (RtR) and asymmetric Reactant–to–Product (RtP) flamelets shown schematically in Fig. 4.1. In these flamelets, the stretch rate is equal to the strain rate as there is no curvature. It is worth discussing the salient characteristics of these flamelets and their response to straining before identifying the configuration of choice.

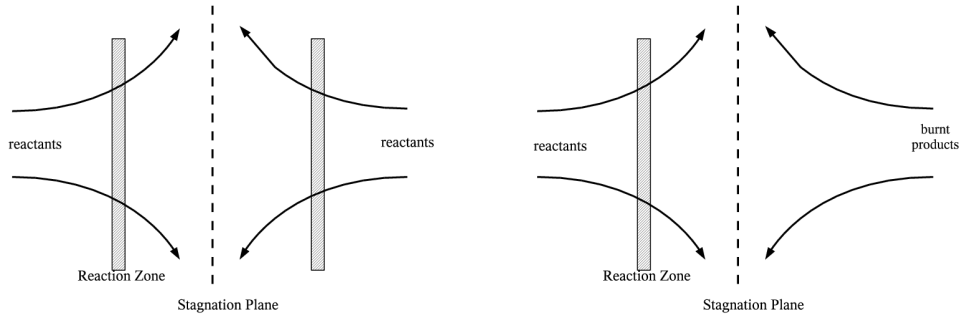

(a) (b)

Figure 4.1: Schematic of purely strained planar laminar flamelet configurations: (a) Reactant–to–Reactant (RtR) and (b) Reactant–to–Product (RtP).

4.2.1 Reactant–to–Reactant Flamelet

In the RtR configuration the reaction zones move towards the stagnation plane as the strain rate is increased. The response of the flame structure - the reaction rate or species concentration profiles versus a flame coordinate - to strain rate depends on the mixture Lewis number, Le. The mixture Lewis number is defined as the ratio of thermal diffusivity of unburnt mixture, D_{th_u}, to the diffusivity of

the deficient species. For equidiffusive mixtures (Le = 1) the flame structure is insensitive to strain rate changes (Dixon-Lewis, 1990; Law *et al.*, 1994) whereas for non–equidiffusive mixtures the burnt temperature, T_b, and the reaction rate, $\dot{\omega}$, decrease (increase) with strain rate for mixtures with Le greater (less) than unity (Sung *et al.*, 1996). When the strain rate is high enough the reaction zone reaches the stagnation plane and is progressively truncated leading to an abrupt extinction caused by the depletion of the radical pool by the diverging streamlines (Dixon-Lewis, 1990).

4.2.2 Reactant–to–Product Flamelet

In RtP flames at low strain rates the reaction zone is on the reactants side far from the stagnation plane and is characterised by reactive–diffusive balance with convection of lower order. As the strain rate is increased the reaction zone progressively moves closer to the stagnation plane and at sufficiently high strain rates it crosses over and locates on the products side. Under such conditions the convective flux of reactants is away from the reaction zone but the diffusion is able to overcome the negative convection and ensure a net positive flux of reactants enabling an attenuated chemical reaction (Libby & Williams, 1982). This is evident in Fig. 4.2 which shows $\dot{\omega}^+$ profiles of lean methane–air flames in RtP configuration at various strain rates as a function of distance from the stagnation plane located at $x = 0$. The equivalence ratio, ϕ, of the mixture is 0.6. The superscript + denotes a quantity normalised appropriately using ρ_u, s_L^o and δ_L^o. The thermal thickness is defined based on the temperature gradient in the unstrained laminar flame as (Poinsot & Veynante, 2001)

$$\delta_L^o = \frac{T_b - T_u}{(dT/dx)_{max}} \tag{4.13}$$

The reactants stream is in the region $x < 0$ and the products stream is in the region $x > 0$. The strain rate, a, corresponding to each profile is noted in the figure and its value, as per convention, is equal to the maximum velocity gradient on the unburnt side of the flame. These profiles are calculated using the OPPDIF code (Lutz *et al.*, 1997) and the GRI–3.0 chemical mechanism. The product

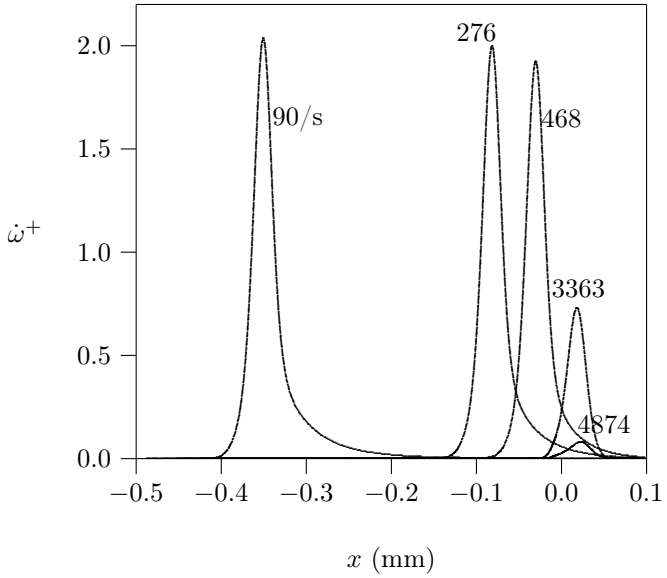

Figure 4.2: Normalised reaction rate, $\dot{\omega}^+$, profiles of RtP flames of lean CH_4–air mixture ($\phi = 0.6$), at various strain rates, plotted against the distance from the stagnation plane.

stream boundary conditions i.e. equilibrium compositions and temperature are obtained using the STANJAN code (Reynolds, 1986).

In RtP flames there is no abrupt extinction as in RtR flames but an extinction regime can be identified when the reaction rate becomes negligible and there is no net additional product creation (Libby & Williams, 1982). The approach to this regime is smooth for adiabatic equidiffusive flames, although, abrupt extinction could occur if the Lewis number is sufficiently far from 1 or under non–adiabatic conditions (Libby *et al.*, 1983). In this work however, only adiabatic flames are considered. Another distinction is that RtP flames have a negative displacement speed when the reaction zone is located on the products side whereas negative displacement speed is not possible in RtR flames.

Hawkes & Chen (2006) used DNS data to examine the suitability of the RtR and RtP configurations for flamelet modelling and found that the RtP configuration reproduced the overall turbulent flame characteristics well over a range of conditions. The trends of displacement and consumption speeds versus the strain rate in turbulent flames were in reasonable agreement with those in the RtP

flames, whereas, the RtR configuration showed trends that were qualitatively opposite to the DNS data. Furthermore, the turbulent flames were observed to burn at strain rates much larger than the extinction value of RtR flames and burning at such high strain rates was better explained by the RtP flames. This too is evident from Fig. 4.2 which shows considerable reaction rate even at $a = 3363/\text{s}$ whereas the extinction strain rate for the lean methane–air flame ($\phi = 0.6$) in RtR configuration is about 200/s (Law *et al.*, 1986). Also, negative displacement speeds observed in DNS studies by Gran *et al.* (1996) and Hawkes & Chen (2006) can be explained by the RtP but not the RtR configuration. Based on the above considerations the RtP configuration is chosen in the present formulation.

The quantity $\dot{\omega}(c = \zeta, N_c = \psi)$, required to evaluate $\overline{\dot{\omega}}$, is obtained from a series of RtP flame calculations i.e. $\dot{\omega}(\zeta, \psi) = \dot{\omega}_{RP}(\zeta, \psi)$ in Eq. (4.12), where the subscript RP denotes RtP flamelets. It is clear from Eq. (4.8) that $\overline{\dot{\omega}}$ is equal to the volume under the surface defined by the product of $\dot{\omega}_{RP}(\zeta, \psi)$ with the pdf $p(\zeta, \psi)$. The surface of $\dot{\omega}^+(c, N_c^+)$ obtained from RtP flamelets is shown in Fig. 4.3 for the lean methane–air mixture and in Fig. 4.4 for lean propane–air mixture. For lean methane–air mixture having Lewis number, Le, less than 1, the surface has a simply connected topology since the value of N_c increases monotonically with strain rate for all c. However, for the lean propane–air mixture having Le $>$ 1, as the strain rate increases N_c decreases first as noted by Sung *et al.* (1996) and then increases. Hence, the surface in Fig. 4.4 is folded but it is still integrable.

The response of $\dot{\omega}(c, N_c)$ to the strain rate is better understood when these surfaces are viewed as a series of $\dot{\omega}$ vs N_c curves for different values of the sample space variable ζ as shown in Fig. 4.5. Data from the laminar flame calculations are used to plot representative curves in this figure. The area under each curve weighted by the conditional pdf, $p(\psi|\zeta)$, is equal to $\langle\dot{\omega}|\zeta\rangle$ in Eq. (4.12). It is also worth noting that the limits N_1 and N_2 are in general different for different ζ. The curves shown in Fig. 4.5a are for Le $<$ 1 case and those in 4.5b and 4.5c are for Le $>$ 1 cases. The unstrained flame value, N_o, gives N_1 and the extinction limit gives N_2 for the Le $<$ 1 case. However, for the Le $>$ 1 case the upper limit N_2 corresponds to the extinction limit but the lower limit N_1 corresponds to an intermediately strained value since N_o lies between the two. This results in the reaction rate being multivalued for a certain range of the dissipation rate.

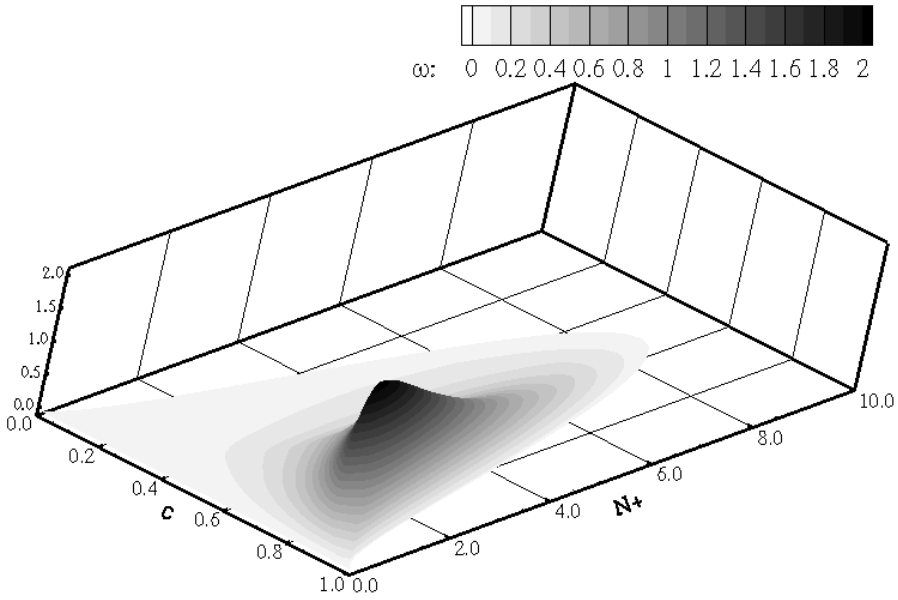

Figure 4.3: The surface of $\dot{\omega}^+(c, N_c^+)$ from RtP flame calculations of lean CH_4–air mixture, $\phi = 0.6$.

Physically, this implies that in the domain $\psi \in [N_1, N_o]$, there exist two states: a higher and a lower burning state. Mathematically, the integration of such a curve, shown schematically in Fig. 4.5d, can be performed in two ways:

(i) The total integral can be written as $I_1 + I_2$. The area of the "C" portion, bounded by the solid curve and the dashed line, is I_1 and I_2 is the area under the solid curve in the domain $\psi > N_o$. The dashed line is defined by $\psi = N_o$.

(ii) Either the upper or lower branches of the "C" portion can be neglected which yields a single–valued curve in the domain $\psi \in [N_1, N_o]$. The integral of this single–valued curve will be I_1 and I_2 is the same as before. It is more likely that the higher burning state occurs in turbulent flames of large Damkohler number and hence neglecting the lower branch is probably more physical.

Preliminary calculations show that the two approximations above yield mean

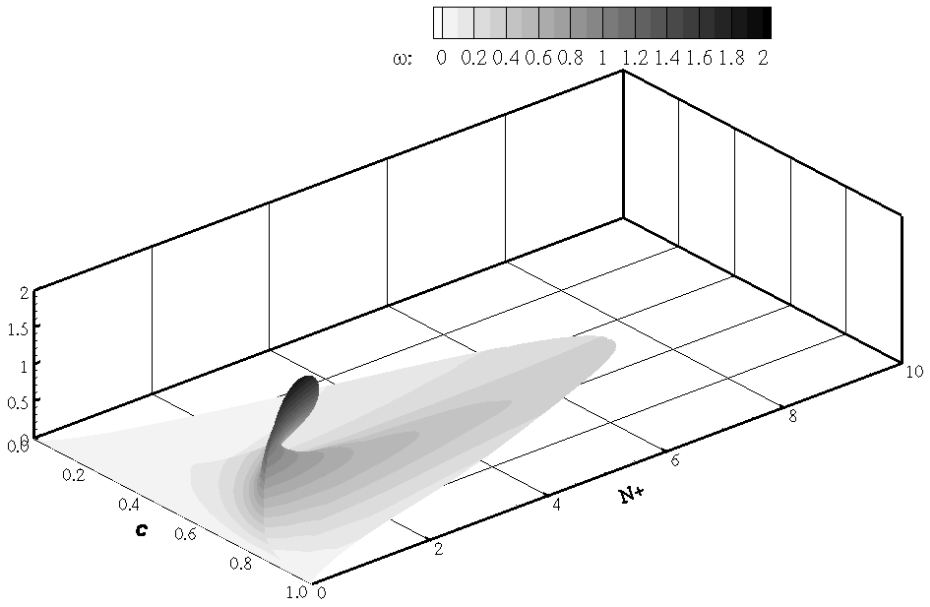

Figure 4.4: The surface of $\dot{\omega}^{+}(c, N_c^{+})$ from RtP flame calculations of lean C_3H_8–air mixture, $\phi = 0.8$.

reaction rate values very close to each other for Le > 1 mixture. This will be evident from calculations of statistically planar one–dimensional flames in Chapter 7. It must be noted that the characteristics of a $\dot{\omega}(c, N_c)$ surface are governed by the mixture Lewis number and not its equivalence ratio. Rich methane–air mixtures with Le > 1 have the same characteristics as the lean propane–air mixture and this is evident from Figs. 4.5b and 4.5c. The proposed modelling formulation is equally applicable for both rich and lean mixtures. We now turn the attention to the other unknown quantities in Eq. (4.11); the pdfs $p(\zeta)$ and $p(\psi|\zeta)$.

4.3 Shapes of the PDFs

As noted in Section 2.2.3, a BML type shape for $p(\zeta)$ has the drawback that it neglects the contributions from the reacting part of the flamelet, $0 < \zeta < 1$ yielding a zero mean reaction rate value. One approach to overcome this is to relate the burning mode, $f(\zeta)$ in Eq. (2.21), to the inverse of the progress variable

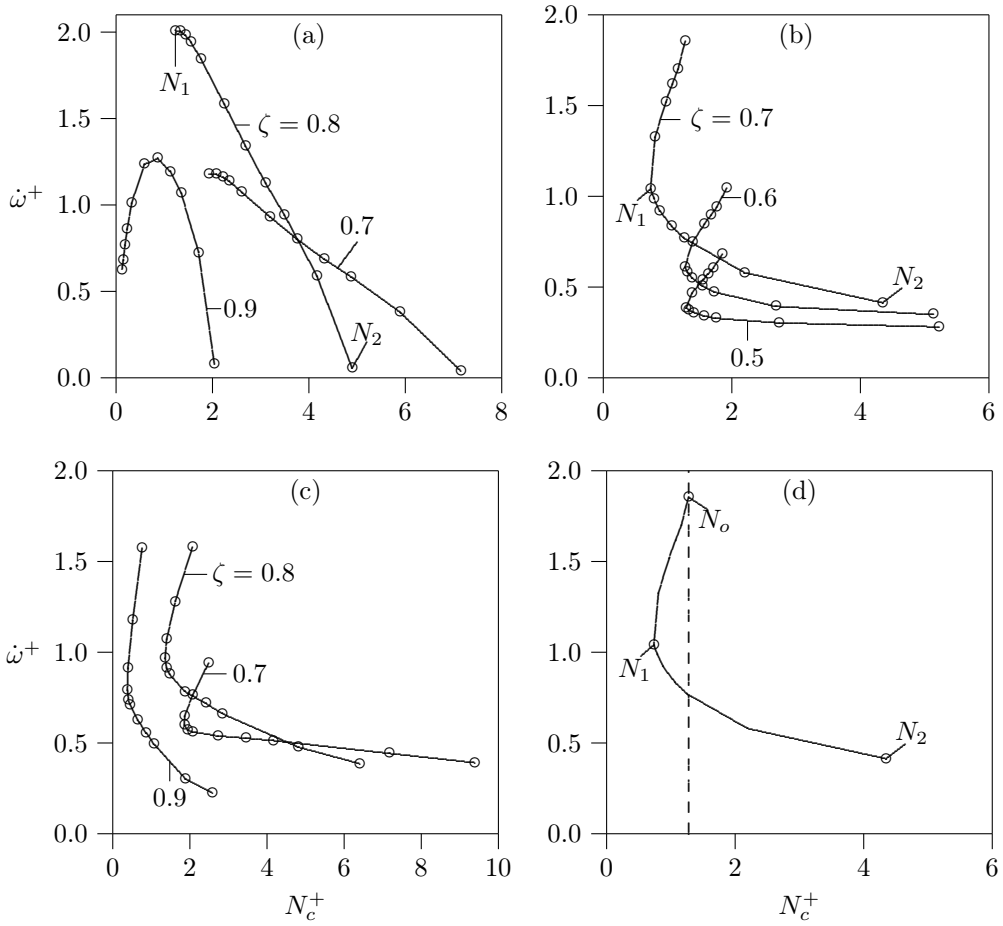

Figure 4.5: Representative curves of $\dot{\omega}^+$ vs N_c^+ conditioned on the progress variable ζ for three cases: (a) methane–air, $\phi = 0.6$, Le = 0.96, (b) propane–air, $\phi = 0.8$, Le = 1.83 and (c) methane–air, $\phi = 1.4$, Le = 1.17 . The $\zeta = 0.7$ curve for the propane–air case is shown in (d) and its integration is discussed in the text.

gradient in an unstrained laminar flame (Bray, 1980; Bray *et al.*, 2006)

$$f(\zeta) = \left[\frac{d\zeta}{d(x/\delta)}\right]^{-1} \quad . \tag{4.14}$$

Another alternative is to reasonably presume $p(\zeta)$ to be a beta–pdf (Poinsot & Veynante, 2001) as has been done in many earlier works (Bradley *et al.*, 1994; Schneider *et al.*, 2005). The BML–pdf is valid in the limit of large Da and in this limit the normalised variance, $g \equiv \widetilde{c''^2}/\tilde{c}(1-\tilde{c})$, becomes nearly equal to 1. However, experimental studies of Chen & Bilger (2001a, 2002) show that for flames with moderate Da, even though the pdf resembles the BML model with peaks at 0 and 1, the contribution of the burning mode is non–negligible. Furthermore, the peak values of g in the flame brush were as low as 0.4 and the beta–pdf reasonably represents the experimental pdfs (Chen & Bilger, 2002). Accordingly, the beta shape is presumed for the density weighted pdf

$$\tilde{p}(\zeta) = \frac{\Gamma(a+b)}{\Gamma(a)\,\Gamma(b)}\,\zeta^{a-1}\,(1-\zeta)^{b-1}\ , \tag{4.15}$$

where the parameters are

$$a = \tilde{c}\left(\frac{\tilde{c}(1-\tilde{c})}{\widetilde{c''^2}} - 1\right)\ , \quad \text{and,} \quad b = a\left(\frac{1}{\tilde{c}} - 1\right)\ . \tag{4.16}$$

The gamma function is defined as

$$\Gamma(x) = \int_0^{+\infty} e^{-t}\,t^{x-1}\,dt. \tag{4.17}$$

Note that $p(\zeta)$ is related to the density weighted pdf via (Swaminathan *et al.*, 1997)

$$p(\zeta) = \frac{\overline{\rho}\,\tilde{p}(\zeta)}{\rho} = \frac{1+\tau\zeta}{1+\tau\tilde{c}}\ \tilde{p}(\zeta)\ . \tag{4.18}$$

Since the progress variable gradient is produced by chemical reactions and the flamelets are spatially intermittent inside the flame–brush, one can take the conditional dissipation rate pdf, $p(\psi|\zeta)$, to be log-normal. Experimental (Chen & Bilger, 2002) and DNS (Swaminathan & Bilger, 2001b) studies show that the scalar dissipation is log–normally distributed. However, this is an open issue and

further experimental and DNS studies examining this pdf are required. Presuming the log–normal shape one can write

$$p(\psi|\zeta) = \frac{1}{(\psi|\zeta)\ \sigma_{N_c}\ \sqrt{2\pi}} \exp\left\{-\frac{1}{2\sigma_{N_c}^2}[\ln(\psi|\zeta) - \mu_{N_c}]^2\right\}\ , \tag{4.19}$$

where the mean and variance of natural logarithm of the conditional dissipation rate, $\ln(\psi|\zeta)$, are respectively denoted by μ_{N_c} and $\sigma_{N_c}^2$. These two quantities are related to the conditional mean, $\langle N_c|\zeta\rangle$, and conditional variance, $G_{N_c}^2$, of the dissipation rate respectively through the relations (Peters, 1984)

$$\langle N_c|\zeta\rangle = \exp(\mu_{N_c} + 0.5\sigma_{N_c}^2) \quad \text{and} \quad G_{N_c}^2 = \langle N_c|\zeta\rangle^2(\exp\sigma_{N_c}^2 - 1)\ . \tag{4.20}$$

A nominal value of σ_{N_c} is taken to be 0.3 and this value is found (Rogerson *et al.*, 2007) by analysing the DNS data of Nada *et al.* (2004). The sensitivity of the model predictions to the value of σ_{N_c} is a subject for future studies. Now, it is clear that only the conditional mean dissipation rate $\langle N_c|\zeta\rangle$ is required to get the pdf using Eq. (4.19).

4.4 Conditional Mean Scalar Dissipation Rate

Klimenko & Bilger (1999) consider the closure of the conditional mean scalar dissipation rate in the context of CMC and prescribe an approach based on the pdf transport equation. The equation for $p(\zeta)$ can be written as (Veynante & Vervisch, 2002)

$$\frac{\partial}{\partial t}\left[\rho\ p(\zeta)\right] + \frac{\partial}{\partial x_i}\left[\rho\ \langle u_i|\zeta\rangle\ p(\zeta)\right] + \frac{\partial}{\partial \zeta}\left[\dot{\omega}\ p(\zeta)\right] = -\frac{\partial^2}{\partial \zeta^2}\left[\rho\ \langle N_c|\zeta\rangle\ p(\zeta)\right]\ . \tag{4.21}$$

The terms in the LHS can be integrated twice to yield closed form expression for $[\langle N_c|\zeta\rangle\ p(\zeta)]$, subject to the appropriate pdf boundary conditions. The resulting closure for $\langle N_c|\zeta\rangle$ will be consistent with the pdf equation. This approach was originally developed for the mixture fraction pdf, $p(\xi)$, whose transport equation has no reaction term. Although more rigorous, this is difficult to adopt for the case of a progress variable due to the presence of the reaction term. However, it is worth exploring in future studies.

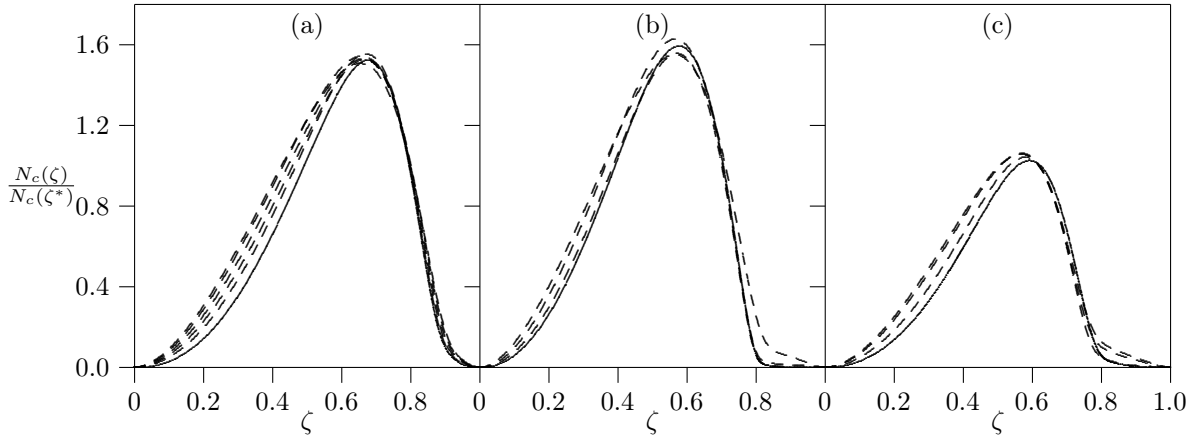

Figure 4.6: Profiles of $N_c(\zeta)/N_c(\zeta^*)$ for three mixtures: (a) CH_4–air of $\phi = 0.6$; (b) CH_4–air of $\phi = 1.0$ and (c) C_3H_8–air of $\phi = 0.8$. The unstrained flame is the solid and strained flames are dashed curves.

Alternatively, a closure based on physical arguments can be developed. In the context of strained flamelet approach, since the turbulent flame is treated as an ensemble of strained laminar flamelets, the conditional dissipation rate can be taken to be

$$\langle N_c|\zeta\rangle \approx \int N_c(\zeta, a)\; p(a)\; da\;, \tag{4.22}$$

where $N_c(\zeta, a)$ is the scalar dissipation rate in a flamelet subject to a strain rate a. The asymptotic studies of RtP flames (Libby & Williams, 1982; Libby *et al.*, 1983) showed that the strain rate primarily influences the progress variable gradient at the inner reaction zone, denoted by ζ^* in the discussion below, which in turn dictates the gradient at other locations. Thus, one may expect

$$N_c(\zeta, a) \approx N_c(\zeta^*, a) f(\zeta)\;. \tag{4.23}$$

This approximation is evaluated in Fig 4.6 using the results of laminar flames calculations for different values of a and for three mixtures; lean ($\phi = 0.6$) and stoichiometric ($\phi = 1.0$) methane–air and lean ($\phi = 0.8$) propane–air mixtures. Figure 4.6a and 4.6b are for the methane–air flames and Fig. 4.6c is for the propane–air flame. These curves are obtained from calculations using the PREMIX (Kee *et al.*, 1985) and OPPDIF codes and detailed chemical mechanisms. The mechanism of Sung *et al.* (1998) for propane–air mixtures is used. The solid curve in Fig. 4.6 corresponds to the unstrained laminar flame while the dashed

curves correspond to increasing strain rates upto a point where the reaction zone just reaches the stagnation plane in an RtP opposed flow configuration. This strain rate value is 500/s for lean CH_4–air, 1800/s for stoichiometric CH_4–air and 1200/s for lean C_3H_8–air respectively. The inner reaction zone corresponds to the location of maximum fuel consumption rate and it remains reasonably constant at $\zeta^* \approx 0.8$, 0.7 and 0.62 respectively, over the range of strain rates considered in these flames. Although the collapse of the curves in the thermal regions is not ideal, it is reasonable for the most part of flames where chemical reactions are expected to be intense, providing good support for the approximation in Eq. (4.23).

Substituting the approximation (4.23) into Eq. (4.22) results in $\langle N_c|\zeta\rangle \approx \langle N_c|\zeta^*\rangle f(\zeta)$, which, when combined with Eq. (3.8), gives

$$\widetilde{\epsilon}_c \approx \int_0^1 \langle N_c|\zeta^*\rangle \; f(\zeta) \; \tilde{p}(\zeta) \; d\zeta \tag{4.24}$$

leading to

$$\langle N_c|\zeta\rangle \approx \frac{\widetilde{\epsilon}_c \; f(\zeta)}{\int_0^1 f(\zeta) \; \tilde{p}(\zeta) \; d\zeta}. \tag{4.25}$$

Any of the curves in Fig. (4.6) can be taken to approximate $f(\zeta)$ and hence we choose the curve corresponding to the unstrained flame.

The Eqs. (4.11), (4.12), (4.18), (4.19) and (4.25) constitute a closure for the mean reaction rate $\overline{\dot{\omega}}$ provided a model for the mean scalar dissipation rate, $\widetilde{\epsilon}_c$, is available. The mean reaction rate can be calculated *a priori* and tabulated as a function of $\tilde{c}$, $\widetilde{c''^2}$ and $\widetilde{\epsilon}_c$. The progress variable mean, $\tilde{c}$, and variance, $\widetilde{c''^2}$, can be obtained from solving their transport equations (2.15) and (3.1) respectively. The mean scalar dissipation rate, $\widetilde{\epsilon}_c$, can also be obtained from a modelled transport equation or an algebraic model. However, as noted in Chapter 3, existing models are based on passive scalar ideas whereas c is a reactive scalar. The next chapter is devoted to the challenging but important task of providing a closure for $\widetilde{\epsilon}_c$.

A consistent closure can also be written for the mean species mass fraction as

$$\overline{Y}_\alpha = \int_0^1 \langle Y_\alpha|\zeta\rangle \; p(\zeta) \; d\zeta, \quad \text{where,} \; \langle Y_\alpha|\zeta\rangle = \int_{N_1}^{N_2} Y_{\alpha_{RP}}(\zeta,\psi) \; p(\psi|\zeta) \; d\psi. \tag{4.26}$$

The upper limit, N_2, is determined using the extinction limit given by (Libby & Williams, 1982)

$$\frac{\int_0^1 \dot{\omega}_{RP}(\zeta)\ d\zeta}{\int_0^1 \dot{\omega}_o(\zeta)\ d\zeta} \leq 0.1\ . \tag{4.27}$$

This criterion is a practical limit and not a theoretical one. The upper limit, N_2, can be infinity in principle but for $\psi > N_2$ there is negligible chemical reaction. Also, the limits N_1 and N_2 do not cover the negative stretch rate regime and this is a limitation of the RtP configuration.

4.5 Summary

A strained flamelet model for turbulent premixed combustion is proposed. The flamelets are parametrised using the scalar dissipation rate, N_c, since the stretch rate parametrisation is not valid for high values of stretch. The scalar dissipation rate is defined at every location in the flame front and asymptotic studies (Libby & Williams, 1982) have shown that N_c is closely related to the flamelet structure both at low and high stretch rates which motivated its choice as a parameter. Strained laminar flames in Reactant–to–Product (RTP) opposed flow configuration are chosen to represent the flamelets since recent DNS studies (Hawkes & Chen, 2006) have shown that they reproduce the turbulent flame characteristics well. A closure for the mean reaction rate, $\overline{\dot{\omega}}$, of the progress variable, c, is obtained using Eq. (4.8) and presuming shapes for the pdfs of the progress variable and the conditional scalar dissipation rate. A β–pdf is used for the marginal pdf $\widetilde{p}(\zeta)$ and a log–normal pdf is used for $p(N_c|\zeta)$. The required conditional mean scalar dissipation rate, $\langle N_c|\zeta\rangle$, is to be obtained from the mean scalar dissipation rate, $\widetilde{\epsilon_c}$, which needs to be modelled. The modelling of $\widetilde{\epsilon_c}$ is studied in the next chapter.

Chapter 5

Modelling of Mean Scalar Dissipation Rate

The modelling of unconditional mean dissipation rate of the progress variable is addressed in this chapter. This quantity is a central modelling parameter in the flamelet formulation described in the previous chapter, as well as other modelling approaches. An exact transport equation for this quantity, which was derived in a recent work (Swaminathan & Bray, 2005), will be presented first. Modelling of various leading order terms of this transport equation will be discussed leading to an algebraic closure for the mean dissipation rate. The algebraic model will be validated by making comparisons with DNS data.

It is worthwhile to make a few observations on the common practices of mean scalar dissipation rate modelling. By far the most popular closure is the classical passive scalar model given in Eq. (3.11), with the constant $C_\phi = 1.0$. The quantity $C_\phi \equiv (\widetilde{\epsilon_c}/\widetilde{c''^2})/(\widetilde{\varepsilon}/\tilde{k})$ is the ratio of turbulence–to–scalar time scales and a constant value is based on the notion that the scalar fluctuations decay rate is proportional to the velocity fluctuations decay rate. Hence this model is sometimes referred to as "linear relaxation model". Based on an initial survey of experimental data, Pope (1985) questions the universality of value of C_ϕ, especially for scalar fields in decaying turbulence. However, the DNS study of Eswaran & Pope (1988) later confirmed that, even for a wide variation in the initial value of scalar integral length scale, C_ϕ tends to a value of about 1.0 after some early transients. Although this model is applied in a variety of scenarios, it is strictly valid for a passive scalar transport in incompressible turbulence. However, it has often been used to

model the mean and the cross dissipation rates involving reactive scalars without sufficient justification. Chomiak *et al.* (1991) prescribe a modification to C_ϕ with a dependence on the Prandtl number, Pr, and the Reynolds number, Re, but suggest that the reactiveness of a scalar has no influence. It will be shown later that when the physics of reactive scalars are appropriately accounted, a chemical time scale appears in the scalar dissipation rate model naturally.

5.1 Transport Equation

An exact transport equation for $\widetilde{\epsilon_c}$ was derived by Swaminathan & Bray (2005) :

$$\frac{\partial \overline{\rho}\widetilde{\epsilon_c}}{\partial t} + \frac{\partial \overline{\rho}\widetilde{u}_j\widetilde{\epsilon_c}}{\partial x_j} = \underbrace{\frac{\partial}{\partial x_j}\left(\overline{\rho D_c}\frac{\partial \widetilde{\epsilon_c}}{\partial x_j}\right)}_{\mathrm{D_1}} \underbrace{- \overline{2\rho\left(D_c\frac{\partial^2 c''}{\partial x_j\,\partial x_k}\right)^2}}_{\mathrm{D_2}} + T_1 + T_2 + T_3 + T_4 \quad (5.1)$$

$$\begin{aligned}
T_1 &\equiv -\frac{\partial \overline{\rho u_j'' \epsilon_c}}{\partial x_j} - 2\overline{\rho D_c}\left(\widetilde{u_j''\frac{\partial c''}{\partial x_k}}\right)\frac{\partial^2 \widetilde{c}}{\partial x_j\,\partial x_k} \\
T_2 &\equiv 2\overline{\rho\epsilon_c\frac{\partial u_i}{\partial x_i}} \\
T_3 &\equiv \underbrace{-2\overline{\rho D_c}\frac{\partial \widetilde{c}}{\partial x_j}\left(\widetilde{\frac{\partial c''}{\partial x_k}\frac{\partial u_j''}{\partial x_k}}\right)}_{\mathrm{T_{31}}} \underbrace{-2\overline{\rho D_c}\left(\widetilde{\frac{\partial c''}{\partial x_j}\frac{\partial u_j''}{\partial x_k}\frac{\partial c''}{\partial x_k}}\right)}_{\mathrm{T_{32}}} \underbrace{-2\overline{\rho D_c}\left(\widetilde{\frac{\partial c''}{\partial x_j}\frac{\partial c''}{\partial x_k}}\right)\frac{\partial \widetilde{u_j}}{\partial x_k}}_{\mathrm{T_{33}}} \\
T_4 &\equiv 2\left(\overline{D_c\frac{\partial c''}{\partial x_k}\frac{\partial \dot{\omega}''}{\partial x_k}}\right),
\end{aligned}$$

when the diffusivity D_c has a weak dependence on temperature. A similar equation was also derived earlier but with a constant density approximation by Borghi and co-workers (Borghi, 1990; Mantel & Borghi, 1994; Mura & Borghi, 2003). The various terms in Eq. (5.1) have the following meaning. The left hand side represents temporal and convective changes of $\widetilde{\epsilon_c}$. The molecular diffusion and dissipation are denoted by D_1 and D_2 respectively. The effects of dilatation rate is represented by T_2 which results from the density change across the flame front and hence this term is absent in the equation derived by Mantel & Borghi (1994). This term is generally positive representing a source contribution to $\widetilde{\epsilon_c}$ evolution.

The turbulence–scalar interaction is represented by T_3 and the predominant contribution to this term comes from T_{32} (Chakraborty & Swaminathan, 2007a; Swaminathan & Grout, 2006) which is traditionally considered to be positive. The influence of chemical reaction is denoted by T_4.

For large Reynolds and Damköhler numbers, the order of magnitude analysis (Swaminathan & Bray, 2005) showed the following balance at leading order:

$$T_2 + T_{32} + T_4 - D_2 \simeq 0. \tag{5.2}$$

All of these terms are unclosed and need to be modelled. Swaminathan & Bray (2005) discussed the past modelling studies underpinned by passive scalar turbulence physics. It has been recognised recently (Chakraborty & Swaminathan, 2007a; Swaminathan & Grout, 2006) that the heat release strongly influences turbulence scalar interaction and models based on passive scalar ideas need to be revised. Accounting for these findings led to precise modelling of these terms by Chakraborty *et al.* (2008). Our interest is on a simple algebraic model for the mean scalar dissipation rate which can be obtained from the leading order balance in Eq. (5.2). Modelling of the terms in this equation follows the study of Chakraborty *et al.* (2008) in a broad sense and the details of these models are discussed in the next section.

5.2 Modelling of Dominant Terms

The modelling of each of the terms in Eq. (5.2) is considered in this section.

5.2.1 Dissipation–Dilatation correlation, T_2

The term T_2 denotes the correlation between dissipation and dilatation rates and a model for this term can be obtained by adopting the BML–type pdf from Eq. (2.21). Since the dilatation rate is zero everywhere except inside the flame front, T_2 must be proportional to γ^* as

$$T_2 = 2\gamma^* \int \rho N_c \nabla \cdot \mathbf{u}\, f(\zeta)\, d\zeta\ . \tag{5.3}$$

In the limit of large Da the internal structure of the flamelet is less likely to be disturbed by the turbulence and hence, making use of Eq. (2.30), Swaminathan & Bray (2005) propose:

$$T_2 = \frac{4K_c}{(2C_m - 1)} \left(\frac{s_L^o}{\delta_L^o}\right) \overline{\rho}\widetilde{\epsilon_c} \ , \tag{5.4}$$

where

$$K_c \equiv \left(\frac{\delta_L^o}{s_L^o}\right) \frac{\int \{\rho N_c (\nabla \cdot \mathbf{u})\}_L^o \ f(\zeta) \ d\zeta}{\int \dot{\omega}_o \ f(\zeta) \ d\zeta} \ . \tag{5.5}$$

The notation $\{\}_L^o$ denotes quantities corresponding to an unstrained laminar flame. It is clear that the values of K_c cannot be chosen arbitrarily once the internal flamelet structure is specified. The values of K_c for methane–air and propane–air mixtures at various equivalence ratios are given in Table 5.1. These are calculated from planar laminar flame results. The values for stoichiometric methane–air flames at elevated pressures are also given in Table 5.1.

Table 5.1: T_2 Model constants K_c and K_c^*.

CH_4–air, p = 1 atm				CH_4–air, $\phi = 1$				C_3H_8–air, p = 1 atm			
ϕ	τ	K_c/τ	K_c^*/τ	p (atm)	τ	K_c/τ	K_c^*/τ	ϕ	τ	K_c/τ	K_c^*/τ
0.6	4.58	0.24	0.82	1	6.48	0.18	0.87	0.6	4.74	0.27	0.85
0.7	5.17	0.21	0.83	1.5	6.51	0.18	0.86	0.7	5.36	0.23	0.86
0.8	5.70	0.19	0.84	2	6.52	0.19	0.85	0.8	5.91	0.20	0.88
0.9	6.17	0.18	0.85	3	6.54	0.20	0.85	0.9	6.36	0.19	0.90
1.0	6.48	0.18	0.87	5	6.56	0.21	0.85	1.0	6.62	0.18	0.92
1.1	6.42	0.19	0.88	10	6.59	0.23	0.84	1.1	6.59	0.20	0.94
1.2	6.17	0.23	0.89	20	6.62	0.24	0.84	1.2	6.36	0.24	0.96
1.4	5.64	0.29	0.91					1.4	5.83	0.31	0.99

It was shown in earlier studies (Chakraborty *et al.*, 2008; Rogerson & Swaminathan, 2007) that for large Da flames the weight of the burning mode can be expressed as $\gamma^* = \overline{\rho\epsilon_c}/\int \rho N_L^o f(\zeta) \ d\zeta$. Using this γ^* one obtains

$$T_2 = 2 \left(\frac{s_L^o}{\delta_L^o}\right) K_c^* \ \overline{\rho} \ \widetilde{\epsilon}_c, \tag{5.6}$$

where

$$K_c^* = \left(\frac{\delta_L^o}{s_L^o}\right) \frac{\int \{\rho N (\nabla \cdot \mathbf{u})\}_L^o \ f(\zeta) \ d\zeta}{\int \{\rho N\}_L^o \ f(\zeta) \ d\zeta} \ . \tag{5.7}$$

The model in Eq. (5.6) is similar to that in Eq. (5.4) but with a distinctly different model constant. The values of K_c^* for various cases are also listed in Table 5.1 and it is evident that the variation in K_c^*/τ with equivalence ratio, ϕ, is less than 10%, while the variation in K_c/τ is nearly 60% in methane–air flames. A similar trend is also noted for propane–air flames. Even for elevated pressures, K_c/τ varies substantially whereas K_c^*/τ remains almost constant. The sensitivity of K_c/τ to the equivalence ratio is because of N_L^o sensitivity to the flamelet structure. This high sensitivity is not desirable from the modelling point of view and thus the model in Eq. (5.6) is preferred. The comparison of this model with DNS data was observed to be very good in earlier studies (Kolla *et al.*, 2009; Rogerson & Swaminathan, 2007).

5.2.2 Turbulence–Scalar interaction, T_{32}

The tensor scalar product of turbulent strain rate and scalar gradient represents the turbulence–scalar interaction denoted by T_{32} in Eq. (5.1). This term can be written as

$$T_{32} = \overline{-2\rho\epsilon_c(\alpha\cos\theta_\alpha + \beta\cos\theta_\beta + \gamma\cos\theta_\gamma)} \ , \tag{5.8}$$

using the eigenvalue decomposition, where α, β and γ are the eigen values of the turbulent strain tensor $\partial u_i''/\partial x_j$. The eigen values are ranked as $\alpha > \beta > \gamma$, α being the most extensive principal strain rate and γ being the most compressive principal strain rate. The relative orientation of the scalar gradient vector with respect to the eigen vector corresponding to α strain rate is denoted by θ_α. Thus it is clear that the source or sink nature of T_{32} is dictated by the predominant alignment of the scalar gradient with the eigen vectors. It is well known (Ashurst *et al.*, 1987; Batchelor, 1952) that the scalar gradient preferentially aligns with the most *compressive* principal strain rate in turbulent flows yielding a source contribution from T_{32}. Recent studies (Chakraborty & Swaminathan, 2007a; Hartung *et al.*, 2008; Swaminathan & Grout, 2006) clearly showed that the scalar gradient aligns preferentially with the most *extensive* principal strain rate in regions of intense heat release. This is because of the competition between dilatation rate and turbulent strain rate (Swaminathan & Grout, 2006).

The dilatation rate can be scaled as $\sim \tau s_L^o/\delta_L^o$ while the turbulent strain rate can be scaled as $\sim \widetilde{\varepsilon}/\widetilde{k}$. When the dilatation rate overcomes the turbulence strain rate, T_{32} becomes negative and it dissipates the scalar gradient. To capture this behaviour, a model for T_{32} is proposed as below following recent studies (Chakraborty & Swaminathan, 2007b; Chakraborty *et al.*, 2008). The turbulent strain rate effect is modelled as $C_3\overline{\rho}\widetilde{\epsilon_c}(\tilde{\varepsilon}/\tilde{k})$ while the strain rate due to heat release is modelled as $-\tau C_4\overline{\rho}\widetilde{\epsilon_c}(s_L^o/\delta_L^o)$, where C_3 and C_4 are model constants. Combining these two contributions, one gets:

$$T_{32} = \left[C_3 - \tau C_4 \mathrm{Da_L}\right] \left(\frac{\widetilde{\varepsilon}}{\widetilde{k}}\right) \overline{\rho}\, \widetilde{\epsilon_c}, \tag{5.9}$$

where

$$\mathrm{Da_L} \equiv \frac{(s_L^o/\delta_L^o)}{(\tilde{\varepsilon}/\tilde{k})} \tag{5.10}$$

is the local Damköhler number. In a similar expression proposed earlier (Chakraborty & Swaminathan, 2007b; Chakraborty *et al.*, 2008), a density weighted Damköhler number $\mathrm{Da_L^*} = (\rho_\mathrm{u}\mathrm{Da_L}/\overline{\rho})$ was used instead of $\mathrm{Da_L}$. The model constants

$$C_3 = 1.5 \quad \text{and} \quad C_4 = 1.1\,(1 + \mathrm{Ka})^{-0.4} \tag{5.11}$$

are suggested by Chakraborty & Swaminathan (2007b). These forms were proposed so that Eq. (5.9) reduces to the classical expression signifying a source, when $\mathrm{Da}_L \rightarrow 0$ and/or $\mathrm{Ka} \rightarrow \infty$. Also, the classical form is recovered when $\tau = 0$.

The classical model for $\widetilde{\epsilon_c}$ from Eq. (3.11), which is strictly for a passive scalar, can be written as $\widetilde{\epsilon_c} = C_\phi(\widetilde{\varepsilon}/\tilde{k})\widetilde{c''^2}$, where, as noted earlier, C_ϕ is the ratio of integral time scales of turbulent velocity fluctuation to scalar fluctuation. This model can also be obtained by balancing T_{32} and D_2 in Eq. (5.2) when the scalar is passive (Mantel & Borghi, 1994). Hence C_3 in Eq. (5.9) is directly related to the time scale ratio, C_ϕ. For a passive scalar the time scale ratio is typically about 1 but in premixed flames its variation is large (Mantel & Bilger, 1995; Swaminathan & Bray, 2005). These analyses showed that $C_\phi \approx 0.05$ within the flame–brush. The classical model with $C_\phi \approx 1$ will over predict the scalar dissipation rate and it is also evident that this model is strictly not valid for turbulent premixed flames.

In order to satisfy this change in the time scale ratio the model constant C_3 is modified as

$$C_3 = \frac{1.5}{(1 + \mathrm{Ka}^{-m})} \tag{5.12}$$

so that $C_3 \approx 1.5$ when Ka is large and C_3 would decrease as Ka decreases. For the present work m is taken to be 0.5.

5.2.3 Flame front curvature, $(T_4 - D_2)$

It was shown by Mantel & Borghi (1994), Mura & Borghi (2003) and Swaminathan & Bray (2005) that $(T_4 - D_2 + D_1)$ is related to the flame front curvature contribution and accordingly an algebraic model was proposed for this using flamelet theories. However, D_1 is a closed term and the order of magnitude analysis by Swaminathan & Bray (2005) showed that it is not of leading order when the Damköhler and Reynolds numbers are large. Thus, after excluding D_1 a revised model was proposed by Chakraborty *et al.* (2008) based on DNS data analysis. This model is

$$(T_4 - D_2) = -\beta' \, \overline{\rho} \, \frac{\widetilde{\epsilon_c}^2}{\tilde{c}(1 - \tilde{c})}, \tag{5.13}$$

where $\beta' = 6.7$, is a model constant. Since $\widetilde{c''^2} \approx \tilde{c}(1 - \tilde{c})$ for high Da flames, Eq. (5.13) can be rewritten as

$$(T_4 - D_2) = -\beta' \, \overline{\rho} \, \frac{\widetilde{\epsilon_c}^2}{\widetilde{c''^2}} \, . \tag{5.14}$$

The recent analysis by Chakraborty *et al.* (2008) showed that dissipative nature of D_2 overwhelms contribution from T_4 thereby making $(T_4 - D_2)$ negative throughout the flame brush, which justifies the negative sign in Eq. (5.13).

5.3 Algebraic Model for $\widetilde{\epsilon_c}$

Apart from the classical model, algebraic models for $\widetilde{\epsilon_c}$ have been proposed in the past. The recent models are briefly discussed first before deriving and analysing a

new model. Combining the relation $\overline{\dot{\omega}} \approx \rho_u s_L^o \Sigma$ (Bray *et al.*, 1989) with Eq. (2.30), Vervisch *et al.* (2004) obtained

$$\overline{\rho}\widetilde{\epsilon_c} = \left(\frac{2C_m - 1}{2}\right) \rho_u s_L^o \Xi |\nabla \overline{c}| \left(\frac{\overline{c'^2}}{\overline{c}(1-\overline{c})}\right), \tag{5.15}$$

where $\Xi \equiv \Sigma/|\nabla \overline{c}|$ is the flame wrinkling factor commonly used in the flame surface density modelling. However, to evaluate $\widetilde{\epsilon_c}$ from Eq. (5.15) one requires to model Ξ which is beyond the scope of this study. Furthermore, such modelling attempts can be viewed as relating two unknowns, $\widetilde{\epsilon_c}$ and Σ, via a third unknown $\overline{\dot{\omega}}$. The last factor containing $\overline{c'^2}$ is introduced intuitively to ensure that $\widetilde{\epsilon_c}$ goes to zero when $\overline{c'^2}$ goes to zero. An interesting comparison of this model to DNS data is shown by Vervisch *et al.* (2004). Fiorina *et al.* (2005) employ this model for RANS calculations with a nominal value for the unknown quantity Ξ.

Borghi and his co-workers (Borghi, 1990; Mantel & Borghi, 1994; Mura & Borghi, 2003) proposed a model:

$$\widetilde{\epsilon_c} \simeq \left(1 + \frac{2C_{\epsilon_c} s_L^o}{3\sqrt{\widetilde{k}}}\right) \left(C_D \frac{\widetilde{\varepsilon}}{\widetilde{k}}\right) \widetilde{c''^2}, \quad C_{\epsilon_c} = 0.1,\ C_D = 0.21, \tag{5.16}$$

when $\left(\sqrt{\widetilde{k}}/s_L^o\right) > 0.067$, based on the analysis of $\widetilde{\epsilon_c}$ transport equation but with constant density assumption. This limitation is remedied by Swaminathan & Bray (2005) in the following model by allowing the density to vary across the flame front:

$$\widetilde{\epsilon_c} \simeq \left(1 + \frac{2}{3} C_{\epsilon_c} \frac{s_L^o}{\sqrt{\widetilde{k}}}\right) \left(C_{D_c} \frac{s_L^o}{\delta_L^o} + C_D \frac{\widetilde{\varepsilon}}{\widetilde{k}}\right) \widetilde{c''^2}, \quad C_{D_c} = 0.24. \tag{5.17}$$

The relaxation of the constant density assumption allowed a chemical time scale to appear naturally and explicitly in the model. If the laminar flame scales are used to normalise Eq. (5.17), it follows that $\widetilde{\epsilon_c}$ scales as (s_L^o/δ_L^o) for large Da flames (Bray & Swaminathan, 2006). Such explicit scaling is not apparent in the other models for the scalar dissipation rate.

The model constant C_{D_c} is proportional to K_c in Eq. (5.4) and hence the scalar dissipation rate model given by Eq. (5.17) is sensitive to the flamelet structure. Furthermore, the classical model for T_{32} based on the alignment of scalar

gradient with the most compressive eigen vector of turbulent strain rate, is used to deduce Eq. (5.17). Thus this model does not incorporate the change in the alignment characteristics noted earlier in subsection 5.2.2. To account for the correct physics, a new model is derived by using Eqs. (5.6), (5.9) and (5.13) in Eq. (5.2):

$$\widetilde{\epsilon_c} \simeq \frac{1}{\beta'}\left(2K_c^*\frac{s_L^o}{\delta_L^o} + [C_3 - \tau C_4 \mathrm{Da_L}]\frac{\widetilde{\varepsilon}}{\widetilde{k}}\right)\widetilde{c''^2}. \tag{5.18}$$

It should be noted here that this model is strictly valid for large Damköhler number and it is straightforward to see that $\widetilde{\epsilon_c}$ scales as (s_L^o/δ_L^o) in this limit. It is worth mentioning that Eq. (5.18) includes the chemical time scale, which is important (Swaminathan & Bray, 2005), and it incorporates the correct physics of turbulence-scalar interaction which is absent in Eq. (5.17). Furthermore, the heat release parameter τ appears explicitly in Eq. (5.18) unlike in the earlier models. These models predictions will be compared to DNS data in Section 5.4 while our immediate attention is focussed on realisability of the model given by Eq. (5.18).

5.3.1 Realisability

Duclos *et al.* (1993) noted that $\int \overline{\dot{\omega}}\ dv$ given by various flame surface density models has to be finite for realisability. This condition from Eq. (2.30) implies that $\widetilde{\epsilon_c}$ must be bounded within the flame brush. Furthermore, Eq. (2.30) suggests that $\widetilde{\epsilon_c}$ should be zero at the flame brush boundary. Also, $\widetilde{\epsilon_c} \to 0$ when $\overline{c'^2} \to 0$ as noted by Vervisch *et al.* (2004) which is equivalent to the condition given by Duclos *et al.* (1993). This was the reason for adding the last factor proportional to $\overline{c'^2}$ in Eq. (5.15). It is straightforward to see that Eq. (5.18) satisfies all of these criteria. The remaining concern is on simple physical realisability, i.e., the semi-positive definiteness ($\widetilde{\epsilon_c} \geq 0$) of the scalar dissipation rate. Equation (5.17) automatically satisfies this criterion but it is not obvious for Eq. (5.18).

This equation is rearranged as

$$\widetilde{\epsilon_c} \simeq \frac{1}{\beta'}\left([2K_c^* - \tau C_4]\frac{s_L^o}{\delta_L^o} + C_3\frac{\widetilde{\varepsilon}}{\widetilde{k}}\right)\widetilde{c''^2}. \tag{5.19}$$

It is clear that a sufficient condition for the physical realisability is

$$\frac{2K_c^*}{\tau} - C_4 \geq 0 \ . \tag{5.20}$$

The constant C_4 is $1.1(1 + \mathrm{Ka})^{-0.4}$ and thus $C_4 \leq 1.1$ for any value of Ka. On the other hand $K_c^*/\tau > 0.8$ for methane-air and propane–air mixtures as in Table 5.1[1]. For hydrogen-air mixtures, the laminar flame calculations yield $K_c^*/\tau \simeq 0.65$ (Rogerson & Swaminathan, 2007). Hence, although K_c^* is weakly dependent on fuel, the sufficient condition $(2K_c^*/\tau - C_4) \geq 0$ will always be satisfied thereby making the current model *unconditionally realisable*. It is worth noting that while the models for T_2 and T_{32} along with their respective constants were proposed independently to capture the relevant physics, the algebraic model for $\widetilde{\epsilon_c}$ is automatically unconditionally realisable. Furthermore, if a density weighted Damköhler number is used instead of $\mathrm{Da_L}$ in Eqs. (5.9) or (5.18), then the sufficient condition becomes $[2K_c^*/\tau - (\rho_u/\overline{\rho})C_4] \geq 0$ which is not guaranteed always since $\rho_u/\overline{\rho} = (1 + \tau\widetilde{c})$. The unconditional realisability of Eq. (5.18) noted above is an indication that correct physics is captured by the model. However, DNS comparisons presented in the next section provide more rigorous validation for the model.

5.4 Validation

The algebraic scalar dissipation rate model derived in the previous section is validated using DNS data in this section. Before discussing these results, the attributes of the DNS data are briefly discussed first.

5.4.1 Attributes of DNS data

Five different DNS datasets are considered in this study. The main attributes of these data sets are given in Table 5.2 and are also shown in the regime diagram in Fig. 5.1. All these cases directly simulated the propagation of a premixed flame in three dimensional homogeneous turbulence. Turbulence inflow and outflow

[1]It is believed that even for higher hydrocarbons including paraffins and aliphatic compounds,$K_c^*/\tau \simeq 0.8$ to 0.9. This needs to be verified with either flame calculations or experiments.

boundary conditions were applied in the direction of mean flame propagation and periodic boundary conditions were used in the other two directions. It is evident from Table 5.2 and Fig. 5.1 that the flames cover a range of combustion conditions, viz. the wrinkled flamelets, the corrugated flamelets and the thin reaction zones regime, all with Da>1.

Table 5.2: Initial parameters of DNS data used.

Flame	u'/s_L^o	Λ/δ	Re	Da	Ka
R1	1.41	28.3	56.7	20.1	0.37
R2a	0.85	78.0	106.8	91.8	0.2
R2b	1.70	39.0	106.8	22.9	0.8
R2c	3.40	19.5	106.2	5.7	3.2
R2d	3.38	41.5	201.7	12.3	1.5

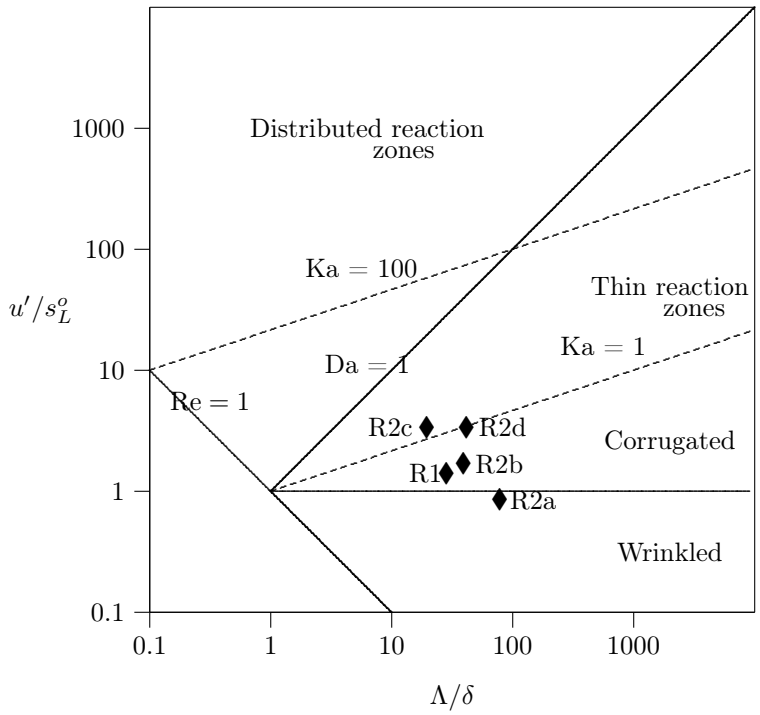

Figure 5.1: Attributes of the DNS data on the combustion regime diagram.

The case R1 was simulated by Rutland & Cant (1994) using a single irreversible reaction with large activation energy. In R2 cases a stoichiometric

hydrogen-air flame was simulated (Nada *et al.*, 2004) with detailed kinetic mechanism involving 27 reactions and 12 reactive species. Reactant mixtures preheated to 700 K were used. The DNS data at about 4.4 initial eddy turnover time from the case R1, and at about 2.5 initial eddy turnover time from the set of R2 cases are considered for the present analysis. Full details of these DNS can be found elsewhere (Nada *et al.*, 2004; Rutland & Cant, 1994).

5.4.2 Comparisons with DNS data

It is to be noted that the models discussed in Sections 5.2 and 5.3 were developed using DNS data which are completely different from the DNS data used here. The predictions of various scalar dissipation rate models given in Section 5.3 are compared to the DNS results in Fig. 5.2. The superscript '+' denotes that $\widetilde{\epsilon}_c$ is normalised using s_L^o and δ_L^o appropriately. The progress variable c_1 is the local temperature increment $(T - T_u)$ normalised by the maximum temperature increment observed in the respective DNS. Since model of Ξ is kept beyond the scope of the present study, model prediction of Eq. (5.15) is not shown. One–fourth of the values predicted by the classical model, Eq. (3.11), are also shown in Fig. 5.2. The values of model constants used are those given in Section 5.3. Since the R2 DNS considered hydrogen-air mixture, $K_c^*/\tau = 0.65$ is used but for R1 case $K_c^*/\tau = 0.85$. It is evident from Fig. 5.2 that Eq. (5.18) satisfactorily predicts the scalar dissipation rate demonstrating the model capability across the combustion regimes. While there is a slight over prediction for the R1 and an under prediction for the R2b and R2d cases, the overall agreement might be considered reasonable. The predictions of Eq. (5.17) also appear reasonable although an over prediction is observed for the R2a case. However, this model does not incorporate the correct scalar gradient alignment physics as noted in Section 5.2. Figure 5.2 also shows that Eq. (5.16) under predicts the scalar dissipation rate while the classical model over predicts the values by nearly a factor of four. It was observed that the Ka dependence of C_3 in Eq. (5.9) is required for correct prediction of $\widetilde{\epsilon}_c$ by the model in Eq. (5.18). This modification to C_3 allows for a slow change of T_{32} effects across the flame–brush.

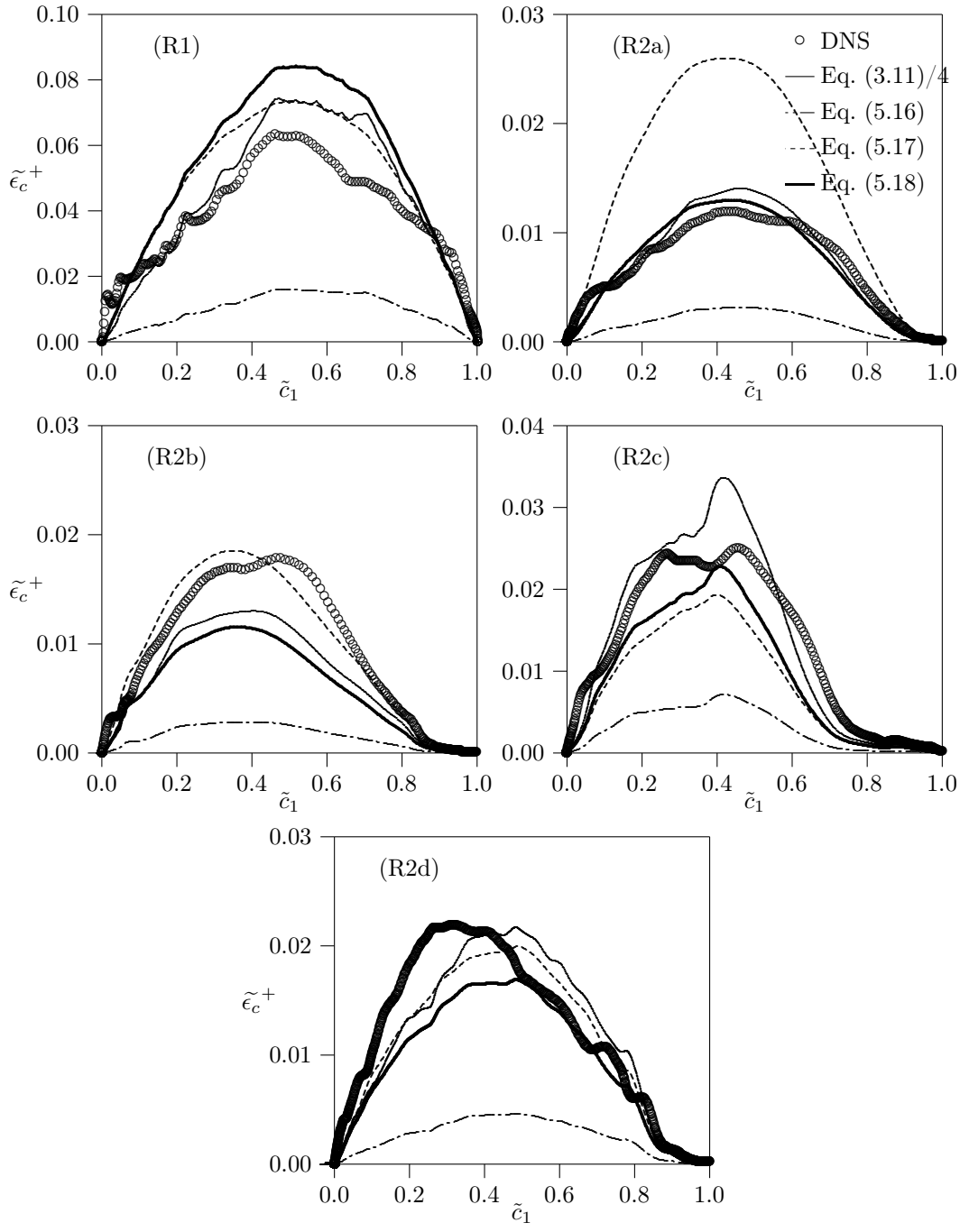

Figure 5.2: Comparisons of $\widetilde{\epsilon_c}$ predicted by various models with DNS data.

5.5 Summary

An algebraic model for the Favre averaged scalar dissipation rate, $\widetilde{\epsilon_c}$, is derived for high Damköhler number turbulent premixed flames. This model is based on the leading order balance of an exact transport equation for $\widetilde{\epsilon_c}$, which includes the effects of dilatation, interaction of turbulence and scalar gradients, chemical reaction and dissipation processes. The model for $\widetilde{\epsilon_c}$ is examined for its physical realisability and it is shown that the proposed model is always unconditionally realisable. Predictions of this new algebraic model are compared to DNS data of turbulent premixed combustion in different regimes and the agreement is found to be satisfactory.

Direct validation of the $\widetilde{\epsilon_c}$ model with experimental data could not be performed since extensive measurements of this quantity are currently scarce. Accurate measurement of $\widetilde{\epsilon_c}$ is made difficult by the stringent resolution requirements for measuring the steep scalar gradients (Bilger, 2004b). However, an indirect experimental validation is possible via the turbulent flame speed; a quantity which has been widely measured in a variety of flame configurations and over a wide range of conditions. Such an indirect validation is performed in the next chapter.

Chapter 6

Turbulent Flame Speed

The aim of this chapter is to provide an indirect experimental validation for the algebraic mean scalar dissipation rate model via turbulent flame speed. The analytical framework that establishes a mathematical link between these two quantities is presented first that yields an algebraic expression for the latter from the model for the former. The characteristics of this flame speed expression will be examined in relation to some well known theories. Attention is then paid to the various definitions of turbulent flame speed adopted in experiments so as to identify the definition that corresponds to the algebraic expression being considered. Experimental data are accordingly chosen for validation and comparisons, which will be discussed.

6.1 Expression for Turbulent Flame Speed

Turbulent flame speed, S_T, is a fundamental quantity in turbulent premixed flames. It signifies the intensity of burning and it is influenced by the dynamics of both large and small scales of turbulence, and turbulence–chemistry interaction. It has been the subject of a large number of theoretical and experimental studies (see for example Bradley (2002); Driscoll (2008)) and it is known to be central in many premixed flame modelling methods such as the Flame Surface Density (FSD) models (Veynante & Vervisch, 2002), the Turbulent Flame speed Closure (TFC) (Zimont, 2000) and the G–equation approach (Peters, 1999). Many of the existing flame speed expressions are based on semi–empirical scaling laws (Gülder,

1990) while others have used the physics of passive scalar dynamics (Kerstein & Ashurst, 1992; Ronney & Yakhot, 1992; Yakhot, 1988). As noted in Chapter 3 the fine scale mixing rate strongly influences the burning rate in turbulent flames and hence the flame speed. Consequently, the reactive scalar physics inherent in the $\widetilde{\epsilon_c}$ model discussed in the previous chapter will have implications on S_T as well. This provides the motivation to test the $\widetilde{\epsilon_c}$ model by making turbulent flame speed predictions. This is made possible by the Kolmogorov–Petrovskii–Piskunov (KPP) analysis (Duclos *et al.*, 1993; Lipatnikov & Chomiak, 2002) which yields:

$$S_T = 2\sqrt{\frac{\nu_t}{(\rho_u \, \mathrm{Sc_c})} \left(\frac{\partial \overline{\dot{\omega}}}{\partial \tilde{c}}\right)_{\tilde{c}\to 0}} \, , \tag{6.1}$$

where $\nu_t \equiv \mu_t/\overline{\rho}$ is the turbulent diffusivity. From Eq. (2.30) one can write

$$\left(\frac{\partial \overline{\dot{\omega}}}{\partial \tilde{c}}\right)_{\tilde{c}\to 0} = \frac{2}{2C_m - 1} \, \rho_u \, \left(\frac{\partial \widetilde{\epsilon_c}}{\partial \tilde{c}}\right)_{\tilde{c}\to 0} \tag{6.2}$$

for large Damköhler number flames. Substituting for the $\widetilde{\epsilon_c}$ model from Eq. (5.18) in the above two equations, and noting that for large Da, $\widetilde{c''^2} \approx \tilde{c}(1-\tilde{c})$, yields after some algebra

$$\left(\frac{S_T}{s_L^o}\right) = \left\{ \frac{18 C_\mu}{(2C_m - 1)\beta'} \left[[2K_c^* - \tau C_4] \left(\frac{u' \Lambda}{s_L^o \delta_L^o}\right) + \frac{2C_3}{3} \left(\frac{u'}{s_L^o}\right)^2 \right] \right\}^{1/2} . \tag{6.3}$$

In obtaining the above equation the standard closure for turbulent diffusivity $\nu_t = C_\mu \tilde{k}^2/\widetilde{\varepsilon}$ (see Eq. (2.9)) is employed and the simple scaling laws; $\tilde{k} = 3u'^2/2$, $\widetilde{\varepsilon} = u'^3/\Lambda$ are used. The value of $\mathrm{Sc_c}$ is taken to be 1. Apart from the standard modelling constants C_μ and C_m, all the constants in Eq. (6.3) are from the $\widetilde{\epsilon_c}$ model. To reiterate, each of these constants represents an important aspect of scalar mixing physics: K_c^* denotes the effects of dilatation rate, C_3 and C_4 represent the interaction between turbulence strain and the scalar gradient, β' denotes flamelet curvature contribution. The KPP analysis will be closely examined in Section 6.3 in light of the various definitions of turbulent flame speed in experiments. But first we turn our focus on the characteristics of the algebraic flame speed expression

6.1.1 Analysis of the Flame Speed expression

In Eq. (6.3) one can see the dependence of S_T on u' and Λ coming out naturally from the modelling of $\widetilde{\epsilon_c}$. The role of turbulence length scale on the flame propagation is well established (Abdel-Gayed *et al.*, 1987; Bray, 1990; Peters, 1999). Dependence on τ is also seen in Eq. (6.3) which is not shown by many existing expressions. Although Eq. (6.3) seems to involve many parameters, a close study shows that only three parameters: u', Λ and the fuel type can be varied independently. From an experimental point of view this corresponds to two independent conditions, the turbulence (with two independent parameters u' and Λ) and the fuel mixture (characterising the thermo–chemistry with s_L^o, δ_L^o, τ and K_c^*).

For a scalar propagating passively, Eq. (6.3) reduces to $(S_T/s_L^o) \sim (u'/s_L^o)$ since $K_c^* = C_4 = 0$. A similar scaling is seen in the classical expression (Lipatnikov & Chomiak, 2002): $(S_T/s_L^o) = 1 + C(u'/s_L^o)^n$ when $(u'/s_L^o) \gg 1$. Hence Eq. (6.3) can be seen as a special case of the classical form with the constant C dependent on the length scale ratio (Λ/δ_L^o). In his seminal work, Damköhler (1940) proposed that for low turbulence intensities $(S_T/s_L^o) \simeq (A_T/A_c)$ where A_T is the area of the wrinkled flame surface and A_c is its projected area. This yields the linear dependence:

$$\frac{S_T}{s_L^o} = 1 + \frac{u'}{s_L^o} \ . \tag{6.4}$$

For high turbulence intensity cases, Damköhler postulated that

$$\frac{S_T}{s_L^o} \sim \left(\frac{\nu_t}{D_{th_u}}\right)^{0.5} \sim \left(\frac{u'\Lambda}{s_L^o \delta}\right)^{0.5} \ . \tag{6.5}$$

The similarity of this result to the first term on the right hand side of Eq. (6.3) is to be noted. The second term can be seen to correspond to the linear dependence noted above. Kerstein & Ashurst (1992) consider the flame as a passive interface and study its dynamics in turbulent flow. Their analysis yields a scaling $(S_T/s_L^o) \sim (u'/s_L^o)^{4/3}$ in the limit $u' << s_L^o$, and in the limit $u' >> s_L^o$ the scaling $S_T \sim u'$ multiplied by a factor $\ln(u'/s_L^o)^{-3/4}$ was reported.

To further examine the characteristics of Eq. (6.3) in the two limiting cases, i.e. small and large u'/s_L^o, let us consider Λ/δ_L^o to be fixed. For a given experiment this is a reasonable assumption since Λ is usually a function of geometrical parameters

and δ_L^o is constant for a given mixture. For a fixed Λ/δ_L^o, Eq. (6.3) becomes $S_T/s_L^o \sim \sqrt{(A+B)(u'/s_L^o)^2}$ where $A = (2K_c^* - \tau C_4)\mathrm{Da}$ represents the influence of thermo–chemistry and $B = 2C_3/3$ represents the influence of turbulence. The group of constants $18C_\mu/(2C_m - 1)\beta'$ is of order unity and it does not depend on turbulence characteristics or thermo–chemistry. Thus it is excluded in A and B above.

- When u'/s_L^o is small the Karlovitz number, Ka, is also small in high Da flames. This gives $C_4 \approx 1$ and $C_3 \sim \sqrt{\mathrm{Ka}}$. Since $2K_c^* \sim \tau$, in this limit A is one order smaller than Da and one can expect $\mathcal{O}(B) \approx \mathcal{O}(A)$. Thus one recovers the linear dependence $(S_T/s_L^o) \sim (u'/s_L^o)$, which is consistent with Damköhler's result. Physically, it implies that the influence of thermo–chemistry is comparable to the effects of turbulence.

- In the other limit of large u'/s_L^o, Ka is large. Thus $C_4 \approx 0$ and $C_3 \approx 1.5$. Hence $A \sim \tau\mathrm{Da}$ and $B \sim 1$ which implies that

$$\frac{S_T}{s_L^o} \sim \sqrt{\mathcal{O}(\tau)\ \frac{u'\Lambda}{s_L^o \delta_L^o}\ +\ \mathcal{O}(1)\ \left(\frac{u'}{s_L^o}\right)^2}.$$

  While Damköhler's result in this limit shows a dependence only on the first term inside the square root, Eq. (6.3) suggests that the second term is also comparable. Mathematically, this scaling is similar to the result of Kerstein & Ashurst (1992).

The well known "bending" phenomena at high turbulence intensities, reported in many works, is consistent with Damköhler's square–root dependence. Following the analysis of Peters (1999), the behaviour of Eq. (6.3) for a fixed Λ/δ_L^o value is examined to study if it predicts the bending. The predictions of Eq. (6.3) for $\tau = 5$, for three values of Λ/δ_L^o, are shown in Fig. 6.1. The similarity of this figure to Fig. 5 of Peters (1999), and the associated discussion therein, indicates that Eq. (6.3) does predict bending. One conclusion often drawn in literature is that the bending phenomena indicates that at high enough u'/s_L^o values, the S_T/s_L^o curve should level off. This trend however is not apparent for Eq. (6.3) from Fig. 6.1.

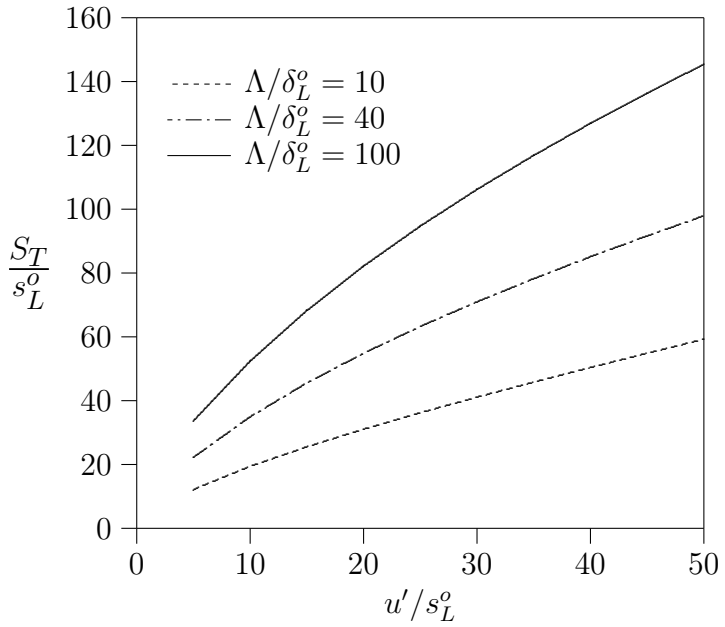

Figure 6.1: Typical prediction of Eq. (6.3) for three different values of Λ/δ_L^o with $\tau = 5$.

It is interesting to note some qualitative agreement of Eq. (6.3) with the classical analyses (Damköhler, 1940; Kerstein & Ashurst, 1992). However, it must be noted that when $u'/s_L^o = 0$, these analyses recover the laminar flame speed i.e. $S_T = s_L^o$. This is not so for Eq. (6.3) and for other KPP expressions derived by Duclos *et al.* (1993) which lead Kolla *et al.* (2009) to surmise that the KPP expression is inapplicable in the limit $u'/s_L^o = 0$. However, the reason for this apparent inapplicability is clarified by Libby (1989) who points out that such a behaviour is expected since the molecular diffusivity is assumed to be negligible in the KPP analysis. If the molecular diffusivity is included and the total diffusivity is taken to be $(\nu_t + \nu)$, then for $u'/s_L^o = 0$ an estimate for (S_T/s_L^o) from Eq. (6.3) is

$$\left(\frac{S_T}{s_L^o}\right) = \left\{\left[\frac{2K_c^* - \tau C_4}{(2C_m - 1)\beta'}\right]\frac{8\nu}{s_L^o \delta_L^o}\right\}^{1/2} \sim \mathcal{O}(1) \ .$$

However, our interest is on turbulent flames with large Re for which the assumption $\nu_t >> \nu$ is reasonable and hence we exclude the molecular diffusivity from the total diffusivity. Equation (6.3) will be compared with experimental data in

Section 6.4. However, it is essential to note that the definition of turbulent flame speed is integral to this task.

6.2 Flame Speed definitions in Experiments

A precise definition of turbulent flame speed is crucial while making comparisons with experimental data since the measured values can be based on quite different definitions. Here we adopt the definitions of Driscoll (2008) :

- Global Consumption Speed, S_{GC}: It is defined as the total mass consumption rate of reactants expressed as a velocity and it is given by

$$S_{GC} = \frac{\iiint \overline{\dot{\omega}} \; dV}{\rho_u \; A_{ref}} \; , \tag{6.6}$$

  where dV is an elemental volume of the flame brush and A_{ref} is the area of a reference iso–surface of $\tilde{c}$.

- Local Consumption Speed, S_{LC}: It is defined as the local mass consumption rate per unit area of the flame brush and it is given by

$$S_{LC} = \frac{\int_{-\infty}^{\infty} \overline{\dot{\omega}} \; dx_n}{\rho_u} \; , \tag{6.7}$$

  where x_n is the local normal coordinate to the flame brush.

- Leading Edge Displacement Speed, S_T: It is defined as the speed of propagation of the flame brush leading edge ($\tilde{c} \approx 0$ iso–surface) relative to the unburnt mixture velocity. This quantity is referred to as turbulent flame speed in this study and is illustrated schematically in Fig. 6.2.

It is to be noted that the quantity s_d used in the flame surface density modelling is also commonly referred to as displacement speed and it corresponds to the advancement speed of an instantaneous iso–contour of c. This quantity is defined by combining the two terms on the r.h.s of Eq. (2.13); the diffusive flux and the reaction rate terms:

$$\frac{\partial}{\partial x_j}\left(\rho D_c \frac{\partial c}{\partial x_j}\right) + \dot{\omega} = \rho s_d |\nabla c| \tag{6.8}$$

Hence s_d pertains to the instantaneous c iso–surface while S_T pertains to the iso–surface of $\tilde{c}$, as shown in Fig. 6.2. In this study, the leading edge displacement speed is called as turbulent flame speed and it is denoted as S_T.

The three quantities: S_{GC}, S_{LC} and S_T, are equal only for the case of a statistically stationary planar one–dimensional flame brush. The $\tilde{c}$ equation for this case is

$$\overline{\rho}\tilde{u}\frac{\partial \tilde{c}}{\partial x} = -\frac{\partial}{\partial x}(\overline{\rho u'' c''}) + \overline{\dot{\omega}}. \tag{6.9}$$

Integrating from the reactant ($x = -\infty$) to the product side ($x = +\infty$) and noting that $\overline{\rho}\tilde{u} = \rho_u S_T = \text{constant}$, by mass conservation, yields $\overline{\rho}\tilde{u} = \int_{-\infty}^{\infty} \overline{\dot{\omega}}\, dx$. Thus

$$S_T = \frac{1}{\rho_u}\int_{-\infty}^{\infty} \overline{\dot{\omega}}\, dx \tag{6.10}$$

which by definition is equal to S_{LC}. In this case S_{LC} is the same as S_{GC} since A_{ref} does not depend on the choice of $\tilde{c}$ iso–surface.

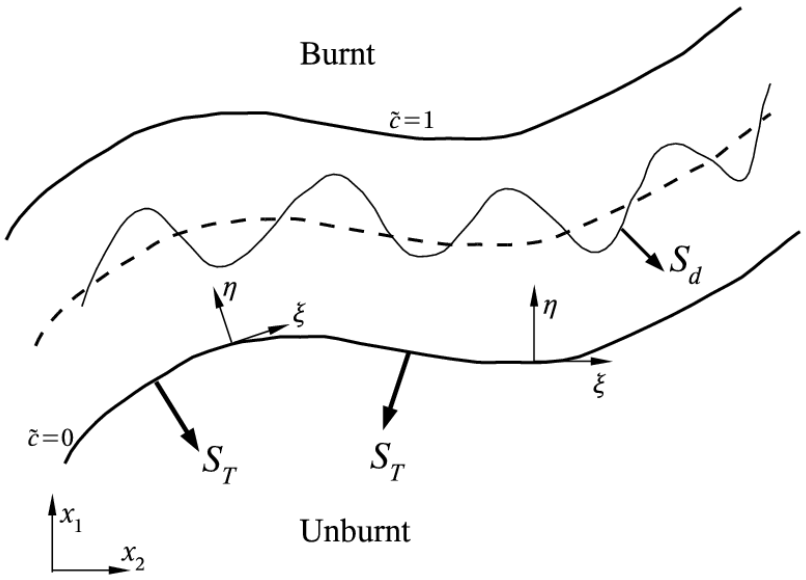

Figure 6.2: Schematic showing a turbulent flame brush. The thick solid curves denote the flame brush boundaries and the dashed line denotes an iso–surface of $\tilde{c}$ inside the flame brush. The thin solid line denotes an instantaneous c iso–contour with displacement speed s_d. The orthogonal curvilinear coordinate system (η, ξ, ζ) is attached locally to the $\tilde{c}$ iso–surface.

In real turbulent flames the scenario is different from the statistically planar one–dimensional case. In general S_{GC} is not equal to S_{LC}. The thickness of a turbulent flame brush is considerable and area of different $\tilde{c}$ iso–surfaces can be quite different. This implies that the value of S_{GC} depends on the choice of the $\tilde{c}$ iso–surface that defines A_{ref} as pointed out by Lipatnikov & Chomiak (2002). Driscoll (2008) suggests that $\tilde{c} = 0.5$ iso–surface can be adopted as a convention. Kim & Bilger (2007) showed that even the local consumption speed, S_{LC}, can vary with locations on the flame brush in multi–dimensional flames. Furthermore, if the mean flow is strained on the unburned side, the diverging streamlines result in a reactant flux in the transverse direction within the flame brush. In such cases the normal mass flux of the reactants at the flame brush leading edge can be greater than the reactant mass consumption rate per unit area in the flame brush and therefore $S_T > S_{LC}$. Shepherd & Kostiuk (1994) illustrate this clearly using the example of a stagnation point flame. Also, it can be envisaged from Fig. 6.2 that in multi–dimensional flames, S_T is likely to vary from one location to another even at the leading edge which is less likely in a statistically planar one–dimensional flame.

The leading edge displacement speed, S_T, is relatively easy to measure in experiments. In statistically stationary flames, S_T is the component of local mean flow velocity in the direction normal to the flame brush at the leading edge. Measurements of the mean flow velocity and the flame brush orientation are sufficient to obtain S_T at a given location on the leading edge. On the other hand, due to the reasons described above, measurements of S_{LC} and S_{GC} have to account for factors such as flame geometry, flow divergence and the various turbulent scalar fluxes involved. In envelope flames, such as a Bunsen flame or the slot flame of Filatyev *et al.* (2005), the flame geometry ensures that all the reactants are consumed by the flame and $S_{GC} = \dot{m}_R/(\rho_u A_{ref})$, where $\dot{m}_R$ is the mass flow rate of reactants into the burner which is known. Shepherd and co–workers (Shepherd & Cheng, 2001; Shepherd & Kostiuk, 1994; Shepherd *et al.*, 1998) measured the reactant mass fluxes over a control volume along the local flame brush normal direction in axisymmetric flames and the integral of these fluxes gives $\int \overline{\dot{\omega}}\, dx_n$ and hence the local consumption speed, S_{LC}. Another approach to obtain S_{LC} is from measurements of the mean flame surface density

Σ (Shepherd & Cheng, 2001) via $S_{LC} = s_L^o I_o \int \Sigma dx_n$ since the mean reaction rate can be modelled as $\overline{\dot{\omega}} = \rho_u s_L^o I_o \Sigma$ (see Eq. 2.41). Gouldin (1996) also obtained the burning rate integral $\int \overline{\dot{\omega}}\, dx_n$ by appropriately integrating the measured convective and diffusive fluxes in a V–flame. The understanding of these subtleties are important for interpreting whether a particular experimental study gives S_T, S_{GC} or S_{LC}. Furthermore, since the focus here is on a flame speed expression which is derived from the KPP analysis, it is equally important to ascertain which of these three quantities the KPP expression corresponds to. This is examined in the next section.

6.3 KPP analysis

Equation (6.3) was derived using the KPP analysis. The application of this analysis to a laminar flame (Zeldovich *et al.*, 1985) gives a flame speed expression as a solution to an eigenvalue problem and shows that the flame speed depends on conditions at the leading edge. An analogous turbulent case is the statistically planar one–dimensional flame for which the KPP analysis has been applied in earlier works (Corvellec *et al.*, 2000; Duclos *et al.*, 1993; Lipatnikov & Chomiak, 2002). As noted earlier, for this flame $S_T = S_{LC} = S_{GC}$ and there is a single flame speed which is an eigenvalue of the flame propagation problem. However, this is not the case in a multi–dimensional flame. Thus, it is important to examine the applicability of the KPP analysis and to understand whether the resulting expression gives S_T, S_{LC} or S_{GC}. To distinguish from the multi–dimensional case, we will refer to the eigenvalue in the planar one–dimensional case as burning velocity.

6.3.1 KPP analysis of a planar one–dimensional flame

It is well known that Eq. (6.9) can be reduced to (see for example Lipatnikov & Chomiak (2002))

$$\frac{dy}{d\tilde{c}} = \frac{my - \Omega}{y}, \tag{6.11}$$

by taking the turbulent scalar flux to be of gradient type and defining it as

$$y \equiv -\overline{\rho u'' c''} = \overline{\rho} \frac{\nu_t}{\mathrm{Sc_c}} \frac{\partial \tilde{c}}{\partial x} \ . \tag{6.12}$$

The quantity Ω is defined as $\Omega \equiv \overline{\rho} \nu_t \dot{\overline{\omega}} / \mathrm{Sc_c}$ and the mass flux $m = \rho_u S_T$ is an eigenvalue of the problem. The well known analysis by Zeldovich *et al.* (1985) gives $m = 2\sqrt{\Omega'(0)}$, which yields Eq. (6.1) for the burning velocity. The prime here denotes a derivative with respect to $\tilde{c}$. When the turbulent scalar flux is counter–gradient, the turbulent diffusivity changes sign at some location $\tilde{c} = c^*$ in the flame brush. Corvellec *et al.* (2000) point out that the burning velocity may be dictated by $\Omega'(1)$ rather than by $\Omega'(0)$ when the turbulent scalar flux is counter–gradient. On the other hand, Bray (1990) points out that earlier studies (for instance Libby (1989)) accounting for counter–gradient transport arrive at burning velocity expressions which are equivalent to the KPP expression.

6.3.2 Applicability to multi–dimensional flames

For statistically stationary, multi–dimensional turbulent flame, the transient terms are zero in the Favre averaged continuity equation, Eq. (2.7), and the $\tilde{c}$ equation, Eq. (2.15). Furthermore for large Reynolds numbers the molecular diffusion term in Eq. (2.15) is negligible compared to the other terms. Consider a curvilinear orthogonal coordinate system (η, ξ, ζ) attached to the flame brush, in which η is the coordinate locally normal to an iso–surface of $\tilde{c}$ and ξ, ζ are the local tangential coordinates as shown in Fig. 6.2. By definition $\tilde{c}$ varies only in the η direction. In such an orthogonal curvilinear coordinate system the above continuity and $\tilde{c}$ equations transform to (Gouldin, 1996)

$$\frac{1}{h_\eta h_\xi h_\zeta} \left[\frac{\partial}{\partial \eta} h_\xi h_\zeta \overline{\rho} \tilde{u_\eta} + \frac{\partial}{\partial \xi} h_\zeta h_\eta \overline{\rho} \tilde{u_\xi} + \frac{\partial}{\partial \zeta} h_\eta h_\xi \overline{\rho} \tilde{u_\zeta} \right] = 0 \tag{6.13}$$

and

$$\overline{\rho} \tilde{u_\eta} \frac{1}{h_\eta} \frac{\partial \tilde{c}}{\partial \eta} + \frac{1}{h_\eta h_\xi h_\zeta} \left[\frac{\partial}{\partial \eta} h_\xi h_\zeta \overline{\rho u_\eta'' c''} + \frac{\partial}{\partial \xi} h_\zeta h_\eta \overline{\rho u_\xi'' c''} + \frac{\partial}{\partial \zeta} h_\eta h_\xi \overline{\rho u_\zeta'' c''} \right] = \dot{\overline{\omega}} \tag{6.14}$$

respectively, where h_η, h_ξ, h_ζ are the corresponding scale factors. The scale factors are defined by the partial derivative of the position vector $\vec{\mathbf{r}}(x_1, x_2, x_3)$. Note

that Eq. (6.13) and the conditions $(\partial\tilde{c}/\partial\xi) = (\partial\tilde{c}/\partial\zeta) = 0$ are made use of in obtaining Eq. (6.14). Gouldin (1996) examines the conditions under which Eq. (6.14) poses an eigenvalue problem and notes that the sufficient condition for this arises when Eq. (6.13) reduces to $\overline{\rho}\tilde{u}_\eta =$ constant. This is satisfied only for a planar one–dimensional flame (Gouldin, 1996) while for a multi–dimensional flame this condition is usually not met.

The studies of Shepherd and co–workers (Shepherd & Cheng, 2001; Shepherd & Kostiuk, 1994; Shepherd *et al.*, 1998) indicate that the tangential turbulent fluxes, $\overline{\rho u_\xi{}'' c''}$ and $\overline{\rho u_\zeta{}'' c''}$, are negligibly small compared to the convective flux and the normal turbulent flux $\overline{\rho u_\eta{}'' c''}$. This plausible assumption seems to be supported by the experimental measurements of Gouldin (1996). However, more experimental studies on this issue would be enlightening. Here, this experimental observation is used to reduce Eq. (6.14) as

$$\overline{\rho}\tilde{u}_\eta \frac{1}{h_\eta}\frac{\partial\tilde{c}}{\partial\eta} + \frac{1}{h_\eta}\frac{\partial}{\partial\eta}\overline{\rho u_\eta{}'' c''} + \overline{\rho u_\eta{}'' c''}\frac{1}{h_\eta h_\xi h_\zeta}\frac{\partial h_\xi h_\zeta}{\partial\eta} = \overline{\dot{\omega}}. \tag{6.15}$$

If $\hat{e}_i$ is the unit vector in direction i then

$$\frac{1}{h_\eta h_\xi h_\zeta}\frac{\partial h_\xi h_\zeta}{\partial\eta} = \nabla\cdot\hat{e}_\eta = \frac{1}{R}$$

where R is the curvature of the $\tilde{c}$ iso–surface [1]. This reduces Eq. (6.15) to a quasi–1D form

$$\overline{\rho}\tilde{u}_\eta \frac{1}{h_\eta}\frac{\partial\tilde{c}}{\partial\eta} + \frac{\overline{\rho u_\eta{}'' c''}}{R} = -\frac{1}{h_\eta}\frac{\partial}{\partial\eta}(\overline{\rho u_\eta{}'' c''}) + \overline{\dot{\omega}}. \tag{6.16}$$

If the turbulent scalar flux is of gradient type and one defines y as before: $y \equiv \overline{\rho}(\nu_t/\mathrm{Sc_c})(\partial\tilde{c}/h_\eta\partial\eta)$ and uses the transformation

$$\frac{1}{h_\eta}\frac{\partial}{\partial\eta} = \frac{1}{h_\eta}\frac{\partial\tilde{c}}{\partial\eta}\frac{d}{d\tilde{c}} = \frac{y\,\mathrm{Sc_c}}{\overline{\rho}\nu_t}\frac{d}{d\tilde{c}}$$

then the following equation results

$$\frac{dy}{d\tilde{c}} = \frac{\hat{m}y - \Omega}{y}.$$

[1] The vector $\hat{e}_\eta$ points in the direction of increasing $\tilde{c}$.

where $\hat{m} = \overline{\rho}\tilde{u_\eta} - (\overline{\rho}\nu_t/R\mathrm{Sc_c})$ and Ω is defined as before. It is to be noted that $\hat{m} \neq$ constant and thus it is not an eigenvalue of the problem. Also $\hat{m}$, y and Ω depend on the ξ and ζ coordinates as well, but for the moment it is enough to focus on the dependence on η alone. By writing the Taylor's series expansions for these quantities about $\tilde{c} = 0$, following Hakberg & Gosman (1984), one obtains

$$s^2 - \hat{m}(0)s + \Omega'(0) = 0$$

where $s \equiv y'(0)$. Note that $\Omega(0) = 0$. Now, the condition for real roots becomes $\hat{m}^2(0) \geq 4\Omega'(0)$ and the minimum of which gives $\rho_u S_T - (\overline{\rho}\nu_t/R\ \mathrm{Sc_c})_{\tilde{c}=0} = 2\sqrt{\Omega'(0)}$. Thus

$$S_T = 2\sqrt{\frac{\nu_t}{(\rho_u\ \mathrm{Sc_c})}\left(\frac{\partial\overline{\dot{\omega}}}{\partial\widetilde{c}}\right)_{\widetilde{c}\to 0}} + \left(\frac{\nu_t}{R\ \mathrm{Sc_c}}\right)_{\tilde{c}=0}. \tag{6.17}$$

If the mean curvature is negligible, one readily recovers Eq. (6.1) which indicates that the KPP expression corresponds to the leading edge displacement speed, S_T. It is worth mentioning that the above analysis can also be performed when the turbulent flux is counter–gradient, following Corvellec *et al.* (2000). It is interesting to note from Eq. (6.17) that the leading edge displacement speed is enhanced by positive curvature. However, in the present study we focus on the case of zero curvature for which Eq. (6.3) is directly applicable. Comparisons of this expression with experimental data are considered next.

6.4 Comparisons with experimental data

Many flame speed expressions have been proposed earlier and they are investigated in detail in the review by Lipatnikov & Chomiak (2002). While some expressions correspond to the leading edge displacement speed, other expressions correspond to consumption speed. Their analysis of large number of experimental data revealed qualitative trends that were reproduced by only few flame speed expressions. The typical comparison of two such expressions with the experimental data of Shepherd & Cheng (2001) is shown in Fig. 6.3. The comparisons of Eq. (6.3) are also shown in the same figure. The data corresponds to S_T of lean methane–air flames of equivalence ratio $\phi = 0.7$ stabilised on a low–swirl burner.

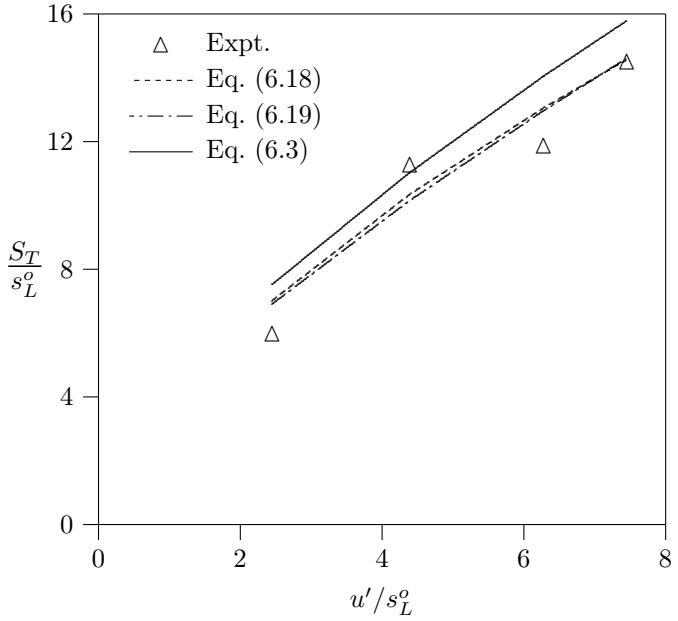

Figure 6.3: Typical comparisons of turbulent flame speed expressions to the experimental data of Shepherd & Cheng (2001).

Shepherd & Cheng (2001) compare their experimental data with the expressions of Peters (1999) and Zimont & Lipatnikov (1995). The expression given by Peters (1999) is

$$\frac{S_T}{s_L^o} = 1 - \frac{0.78}{2b_1}\frac{\Lambda}{\delta} + \left[\left(\frac{0.78}{2b_1}\frac{\Lambda}{\delta}\right)^2 + 0.78\frac{u'\Lambda}{s_L^o\delta}\right]^{0.5}, \tag{6.18}$$

where b_1 is a model constant. The expression of Zimont & Lipatnikov (1995) is

$$\frac{S_T}{s_L^o} = 1 + \kappa\frac{u'}{s_L^o}\mathrm{Da}^{0.25}, \tag{6.19}$$

where κ is a model constant. The values of these constants as proposed by the original authors are $b_1 = 2.0$ (Peters, 1999) and $\kappa = 0.51$ (Zimont & Lipatnikov, 1995). The expression of Gülder (1990) is very similar to Eq. (6.19). Note that the values of the model constants had to be adjusted to $b_1 = 3.4$ and $\kappa = 0.85$ to get good agreement with experimental data by Shepherd & Cheng (2001). However, none of the constants in Eq. (6.3) have been altered to obtain the result in Fig. 6.3 and the agreement is acceptable. Comparisons of Eq. (6.3) with a range of experimental data will be discussed next without changing these model

constants. Comparisons with other flame speed expressions are not attempted since the values of their model constants may have to be adjusted from one experiment to the other.

As noted earlier, the turbulent flame speed S_T in this study is the propagation speed of the leading edge of the mean flame brush and the flame speeds measured in experiments can sometimes correspond to S_{LC} or S_{GC}. Accordingly experimental studies which reported S_T have been chosen after careful scrutiny for comparison. The objective is to compare the flame speed values obtained using Eq. (6.3), while keeping the model constants fixed, with data representing a wide range of experimental conditions, burner geometry, flame configuration and measurement technique. These considerations guide the choice of experimental data sets, which are briefly discussed below with the relevant details.

6.4.1 Flame speed datasets

Table 6.1: Salient characteristics of various experimental S_T data sets.

Flame	Burner configuration	Mixture	ϕ	Pressure	Measurement location	Source
V–shape	Rod stabiliser at nozzle exit	CH_4–Air	0.75–1.0	Ambient	$\overline{c} = 1/\tau$	Smith & Gouldin (1978)
Planar	Taylor-Couette apparatus	CH_4–Air	0.8–1.5	Ambient	Leading edge	Aldredge *et al.* (1998)
Conical	Nozzle burner in high pressure	CH_4–Air	0.9	0.1–3.0 MPa	$\overline{c} = 0.5$	Kobayashi *et al.* (1996)
Planar	Diverging duct	CH_4–Air	0.75–0.95	Ambient	$\overline{c} = 0.5$	Savarianandam & Lawn (2006)
Right Cone	Parallel plates at square channel exit	City gas–Air	-	Ambient	Leading edge	Il'yashenko & Talantov (1966)

The configuration and conditions of various experimental data sets considered in the present study are listed in Table 6.1. As one can see, these experiments

correspond to a variety of flame configurations and burner geometry. The relevant attributes of these flames are given in Table 6.2.

Table 6.2: Attributes of various experimental S_T data.

Source	s_L^o (m/s)	δ_L^o (mm)	u' (m/s)	Λ (mm)	Re	Da
Smith & Gouldin (1978)	0.25–0.40	0.45–0.67	0.095–1.13	0.69–1.49	3–75	3-39
Aldredge *et al.* (1998)	0.17–0.48	0.37–0.92	0.2–1.06	5.5	50–265	5-219
Kobayashi *et al.* (1996)	0.06–0.34	0.095–0.5	0.053–0.83	1.0–1.5	7–830	6-97
Savarianandam & Lawn (2006)	0.19–0.32	0.51–0.79	0.01–0.26	3–36	7-497	142-4535
Il'yashenko & Talantov (1966)	0.2	0.7	0.22–10.5	6.8–11.2	114–3230	1.2-92

The study of Smith & Gouldin (1978) considered V–shaped rod stabilised methane–air flames of three equivalence ratios: $\phi = 0.75$, 0.85 and 1. They measured the orientation of the $\overline{T} = 2\ T_u$ isotherm, which corresponds to the $\overline{c} = 1/\tau$ iso–surface in the flame brush. This surface is not strictly the flame brush leading edge and this is to be noted while comparing the turbulent flame speed. Smith & Gouldin (1978) reported the component of local mean velocity normal to the above iso–surface as the turbulent flame speed for each ϕ and three different values of turbulence integral length scale, Λ: 0.69, 0.95 and 1.49mm. As established in Section 6.3, this normal mean velocity corresponds to the turbulent flame speed. Smith & Gouldin (1978) identify that S_T varies locally on the iso–surface and they clearly note the importance of correlating measurements of S_T at a location where u' and Λ are also measured.

Aldredge *et al.* (1998) measured both laminar and turbulent flame speeds of methane–air mixtures with equivalence ratio ranging from 0.8 to 1.5, varied in

steps of 0.1, in a Taylor–Couette (TC) apparatus. This apparatus consisted of two vertical concentric counter–rotating cylinders with an annular gap of 1.1cm. The planar flame, ignited at the open end, propagates into the nearly stationary turbulent mixture in the annulus. The rate of displacement of the propagating flame, which was calculated from video record, was reported as the flame speed. Clearly, this speed is the turbulent flame speed, S_T.

Kobayashi *et al.* (1996) measured the turbulent flame speed for lean methane–air mixture with $\phi = 0.9$ at pressures ranging from 0.1 to 3 MPa. The turbulence measurements under these conditions were reported in another study (Kobayashi *et al.*, 1997). A Hydrogen pilot flame was used to stabilise the turbulent flame at the exit of a nozzle in high pressure environment. Unlike the combustion bombs and SI engines in which the pressure change is unsteady and brief, the apparatus of Kobayashi *et al.* (1996) was designed to maintain high pressures for long durations. From instantaneous tomographic images of flame, the mean flame cone was identified and the flame speed was calculated as the component of the mean flow velocity normal to the mean flame cone, which corresponds to S_T as noted in sub–section 6.3.2.

Savarianandam & Lawn (2006) focussed on the weakly wrinkled flame regime ($u'/s_L^o < 1$) where the Darrieus–Landau (DL) instabilities have dominant influence on S_T. While the analysis of Damköhler suggests that S_T/s_L^o should be relatively closer to unity in this regime, other studies (Cambray & Joulin, 1992; Paul & Bray, 1996) indicate that Darrieus-Landau hydrodynamic instabilities result in S_T/s_L^o value significantly greater than unity. Flame speeds of nearly planar flames stabilised in a wide angled diffuser at very low turbulence intensities, reported by Savarianandam & Lawn (2006), provide evidence for this. Three methane–air mixtures of $\phi = 0.75$, 0.85 and 0.95 were used and values of u'/s_L^o ranged from 0.05 to 1.37. The flame speed was estimated to be the mean flow velocity at the mean flame height location. As noted by Savarianandam & Lawn (2006), this velocity is the leading edge displacement velocity S_T.

Il'yashenko & Talantov (1966) measured turbulent flame speeds in a flame configuration which was obtained in the region confined between two parallel plates, at the exit of a square channel. Ignition flames were used on two opposite sides of the channel exit and the other two sides were extended as walls. This

resulted in a symmetric configuration of two flame surfaces at an angle to the flow and intersecting at a downstream location. The experiments were done with both a smooth channel and a channel with turbulising grid at the exit, which allowed very high turbulence level to be achieved. They used city gas (a mixture of natural gas and coke gas) as the fuel and measured flame speeds up to $u'/s_L^o \sim 50$. The flame speed was estimated from the mean flow velocity and inclination angle of the flame surfaces. As established in Section 6.3.2, this normal velocity corresponds to the turbulent flame speed S_T.

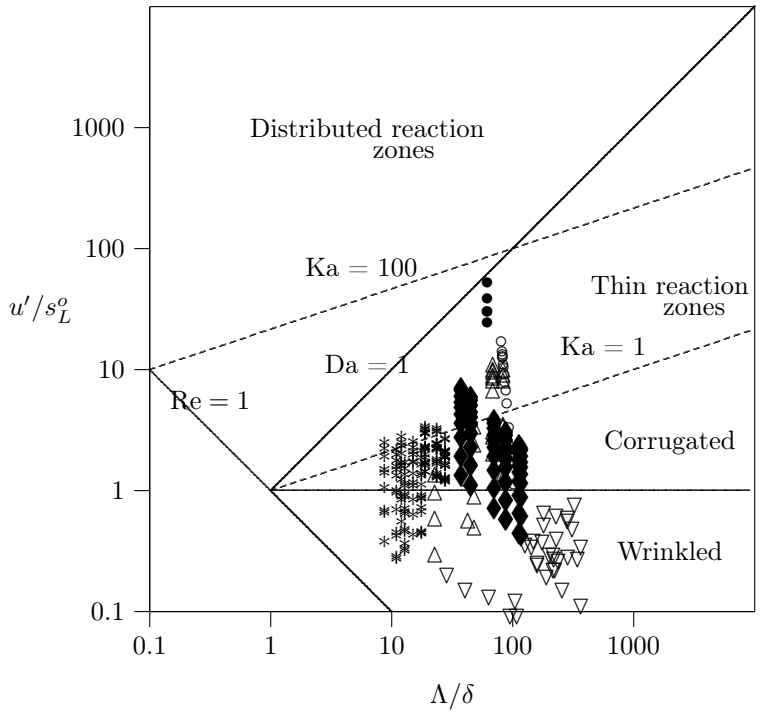

Figure 6.4: Turbulent combustion regime diagram (Peters, 2000) with attributes of various experimental flames: $*$ Smith & Gouldin (1978); ♦ Aldredge *et al.* (1998); $\triangle$ Kobayashi *et al.* (1996); $\triangledown$ Savarianandam & Lawn (2006); $\circ, \bullet$ Il'yashenko & Talantov (1966).

Figure 6.4 shows the above five data sets in the combustion regime diagram, which is adapted from Peters (2000). Although most of the experimental flames are within the corrugated and the wrinkled flamelets regimes, there are some cases spanning the thin reaction zones regime. More experimental data in this

regime would be very useful for model validation. Comparisons between Eq. (6.3) and the above data sets are discussed next.

6.4.2 Results

Equation (6.3) is strictly valid for a flame brush with zero curvature and it is clear from the foregoing discussion that the experimental flames in Table 6.1 are free from effects of mean curvature. The flame speed values obtained using Eq. (6.3) are compared to the measured values in these experiments in Figs. 6.5 - 6.9. It is worth emphasising that the constants in Eq. (6.3) remain the same in all the comparisons shown in Figs. 6.5 - 6.9. The thermal thickness of laminar flame is obtained using (Poinsot & Veynante, 2001)

$$\frac{\delta_L^o}{\delta} = 2(1+\tau)^{0.7} \ , \tag{6.20}$$

where the Zeldovich thickness, δ, is obtained using the thermal diffusivity ($\simeq 2.2 \times 10^{-5} \mathrm{m}^2/\mathrm{s}$ for atmospheric methane–air flames) and the laminar flame speed measured in the respective experimental work. If s_L^o is not measured, for example in the work of Smith & Gouldin (1978), then the values reported by Law (1993) are used. The Karlovitz number required for the constants C_3 and C_4 in Eq. (6.3) is evaluated as (Swaminathan & Bray, 2005)

$$\mathrm{Ka} = \left\{ \frac{(u'/s_L^o)^3}{(\Lambda/\delta)} \right\}^{0.5} \ . \tag{6.21}$$

The V–flame data of Smith & Gouldin (1978), shown in Fig. 6.5, are from measurements at $\overline{T} = 2T_u$ isotherm which corresponds to $\overline{c} = 1/\tau$ iso-surface as noted earlier. V–flames are characterised by increasing flame brush thickness with downstream distance, which implies that different $\overline{c}$ iso-surfaces have different inclinations. However, since $\tau \sim 5.5$, the $\overline{c} = 1/\tau$ iso-surface is reasonably close to, but not exactly at, the leading edge of the flame brush. As evident from Fig. 6.5, Eq. (6.3) compares well with the experimental data.

The flame speed predicted by Eq. (6.3) is compared to the data of Aldredge *et al.* (1998) in Fig. 6.6 and it is clear that Eq. (6.3) compares well with the experimental data. While the quantitative agreement is good for rich equivalence ratios, the predictions are slightly higher for lean mixtures as in Figs. 6.6(g) and

6.6(h). The laminar flame speed values, s_L^o, measured by Aldredge *et al.* (1998) for lean mixtures are much lower than those measured in other studies (Andrews & Bradley, 1972; Vagelopoulos *et al.*, 1994). Hence for comparisons of lean cases shown in Figs. 6.6(g) and 6.6(h), the planar laminar flame speed values reported by Law (1993) are used. For all other cases the values of s_L^o measured by Aldredge *et al.* (1998) are used. If one uses the measured s_L^o for the lean cases, then an underprediction of $\sim 30\%$ (maximum) is observed.

The effect of pressure on the turbulent flame speed was attributed by Kobayashi and his co–workers (Kobayashi & Kawazoe, 2000; Kobayashi *et al.*, 1996, 1997, 2002) to laminar flame instabilities. These studies observed that increasing pressure resulted in a decrease of the characteristic scale of flame instability, l_i, while the integral length scale Λ was not affected much. At elevated pressures, $l_i < \Lambda$ and hence flame instabilities are the predominant cause of the increase in S_T/s_L^o for a given u'/s_L^o (Kobayashi & Kawazoe, 2000). The characteristic flame instability scale l_i is dictated by both the Darrieus–Landau hydrodynamic instabilites and the thermal–diffusive effects and hence it is a function of δ, s_L^o, τ and the Lewis number Le. The effects of non–unity Lewis number were not considered in (Kolla *et al.*, 2009) and hence Le does not appear explicitly in Eq. (6.3). Nonetheless, for a given mixture, while Le does not depend on pressure, the other relevant parameters (δ, s_L^o, τ and Λ) appear in Eq. (6.3). Furthermore, Le is close to unity for the mixtures considered by Kobayashi and co–workers and hence it is expected that the pressure effects on S_T/s_L^o reported by them are likely to be captured by Eq. (6.3). This is evident from the comparisons shown in Fig. 6.7. Using the TFC closure and empirical correlations given by this experiment for the flame wrinkling ratio, Muppala *et al.* (2005) show an interesting comparison with this data. Kobayashi *et al.* (1996) note that the mean flame cone corresponds to the $\overline{c} = 0.5$ iso-surface and S_T estimated from the inclination of flame brush leading edge might be higher because of the difference in the inclination angles. Nonetheless, it is encouraging to note that the effect of pressure on S_T is well captured by Eq. (6.3). However, the comparison for 1 MPa is not so good and the reason for this is unclear at this time.

In the high pressure studies, the laminar flame instabilities were predominant in $u'/s_L^o > 1$ regime, due to a decrease in l_i at elevated pressures. On the other

hand, Savarianandam & Lawn (2006) studied the effects of instabilities at atmospheric pressure in $u'/s_L^o < 1$ regime, by studying weakly turbulent flames with very large turbulence integral length scale, Λ. For the planar flames stabilised in a wide angled diffuser (Savarianandam & Lawn, 2006) the turbulent flame speed was taken to be the flow velocity at the mean flame height location. This data is compared to the predictions of Eq. (6.3) in Fig. 6.8. The large scatter in the experimental data is because of large variation in the integral length scale. Bychkov (2000) notes that theories that ignore the effects of dilatation due to heat release, would not predict the influence of flame instabilities. Savarianandam & Lawn (2006) found good agreement of their experimental data with the theory of Akkerman & Bychkov (2005) which explicitly includes the density ratio, $(\tau + 1)$. Figure 6.8 shows that Eq. (6.3) compares well with the experimental data even though the instability effects were not explicitly considered in the analysis. In particular it is interesting to note that Eq. (6.3) is able to capture the sensitivity to the turbulence integral length scale observed in the experimental data. As mentioned earlier, the KPP result will not yield $S_T = s_L^o$ when $u'/s_L^o = 0$ unless the molecular diffusivity is included in the total diffusivity. However, the comparison with this data at small u'/s_L^o will not be erroneous here since the Re values are sufficiently large as can be seen from Fig. 6.4.

The values of u'/s_L^o in the study of Il'yashenko & Talantov (1966) are much higher than in most other investigations of turbulent flame speed. This data is shown in Fig. 6.9, which corresponds to a mixture with $s_L^o = 20$cm/s and the width of the channel is 40mm. The smooth channel data are denoted by open circles and the data with turbulence generating grid are denoted by closed circles. Because of this difference in the experimental arrangements, one can expect the integral length scales to be different. Unfortunately the values of the length scales are not reported by Il'yashenko & Talantov (1966). Here, the approach of Abdel-Gayed & Bradley (1981) is followed to obtain Λ. For the smooth channel case the turbulence Reynolds number is related to a Reynolds number, $\mathrm{Re_P}$, which is based on the mean flow velocity and hydraulic diameter (Abdel-Gayed & Bradley, 1981) via the correlation

$$u'\Lambda/\nu = 0.0153(\mathrm{Re_P})^{0.911}. \tag{6.22}$$

The values of $\mathrm{Re_P}$ are reported by Il'yashenko & Talantov (1966) and thus for the given values of u' and ν the turbulence integral length scale can be obtained from Eq. (6.22). For the case with turbulence generating grid the following correlation suggested by Abdel-Gayed & Bradley (1981), is used:

$$\Lambda/d = 0.155(x/d)^{0.452}, \tag{6.23}$$

where d is the diameter of the rod in the turbulence generating grid and x is the measurement location downstream of the channel exit. The experimental data is compared to the predictions of Eq. (6.3) in Fig. 6.9. The experimental results are shown as two different sets to signify the difference in the experimental set–up and thus in the turbulence integral length scale. Accordingly, the theoretical curves (solid lines) are broken around $u'/s_L^o \sim 20$. The following observations can be made from Fig. 6.9.

(i) The prediction of Eq. (6.3) shown in Fig. 6.9 is very good. The dotted lines extended from the solid lines in Fig. 6.9 are the predictions by Eq. (6.3) if one were to use the same integral length scale over the whole range of u'/s_L^o. The upper dotted line is for Λ/δ_L^o obtained from Eq. (6.22), while the lower dotted line is for Λ/δ_L^o obtained from Eq. (6.23). This clearly shows the sensitivity of S_T/s_L^o predicted by Eq. (6.3) to the turbulence integral length scale.

(ii) The expression of Klimov (1983): $S_T/s_L^o = 3.5(u'/s_L^o)^{0.7}$, is developed specifically for this experiment and thus the prediction is close to the experimental data.

(iii) Figure 6.9 supports the linear dependence of S_T/s_L^o on u'/s_L^o for large values of u'/s_L^o noted earlier in subsection 6.1.1. The levelling off of the S_T/s_L^o curve, as suggested by the bending phenomenon, is not seen in Fig. 6.9. If one considers the data only in the region of $u'/s_L^o < 20$ then there is some semblance of bending. But upon further increase of u'/s_L^o, the data shows a persistent increase in S_T/s_L^o with no sign of bending. It would appear that more experimental S_T measurements at such high u'/s_L^o values are needed to provide conclusive evidence (or lack thereof) of the bending phenomenon.

Furthermore, this phenomenon is seen to depend on whether the velocity ratio or the length scale ratio is held constant as noted by Bray (1990).

The comparison between predictions of Eq. (6.3) and various experimental data is consistently good. While only few data sets amongst large number available are considered in the present work, these data sets are representative to show the influence of various factors affecting turbulent premixed flame speed and its behaviour. However, it is worth considering the experimental database of Abdel-Gayed *et al.* (1987). This compilation is based on the dimensionless parameter K, known as the "flame stretch factor", which seems to be a useful basis for turbulent flame speed comparison. The flame stretch parameter quantifies the effect of stretch on the flame propagation and is defined as (Abdel-Gayed *et al.*, 1987)

$$\mathrm{K} \equiv \frac{u'\delta}{\lambda s_L^o} = 0.157 \left(\frac{u'}{s_L^o}\right)^2 \mathrm{Re}^{-0.5} \,, \tag{6.24}$$

where λ is the Taylor microscale. The vast experimental data of turbulent flame speed was correlated with u'/s_L^o for different values of the stretch parameter by Abdel-Gayed *et al.* (1987). This compilation is shown in Fig. 6.10 for K = 0.053 and 0.15. Figure 6.10 also compares the prediction of Eqs. (6.3), (6.18) and (6.19) with the experimental data. For this comparison, the values of constants used in Eqs. (6.18) and (6.19) are $b_1 = 2.0$ and $\kappa = 0.51$ as originally proposed. For small values of K the collapse of experimental data of Abdel-Gayed *et al.* (1987) seems reasonable, but the scatter in the experimental data seems large for high K values. However, it must be noted that the experimental data span a narrow range of K values: $0.045 \leq \mathrm{K} \leq 0.06$ in Fig. 6.10(i) and $0.12 \leq \mathrm{K} \leq 0.17$ in Fig. 6.10(ii). Furthermore, Driscoll (2008) points out that the scatter is possibly because the database includes measurements of both displacement and consumption speeds. This comparison suggests that Eq. (6.3) predicts the experimental data well for low K but the flame speed seems to be overpredicted for high K. This is expected since Eq. (2.30), which is central to the derivation of Eq. (6.3), is strictly valid for low stretch (when γ^* is small). As the stretch parameter increases validity of Eq. (2.30) progressively diminishes since the flame front thickens.

Nonetheless, Eq. (6.3) seems to be showing the correct physical behaviour and parametric dependence observed in a number of experiments and the predicted

S_T compares well with those experimental data. Driscoll (2008) suggests that the turbulent flame speed, S_T, is not just a function of the local fluid–dynamic and thermochemical parameters alone but burner geometry has a significant influence since the wrinkling processes in turbulent flames are geometry–dependent. Hence models that are obtained from differential equations that simulate the flame wrinkling are likely to perform better than empirical models. Our approach is similar since the scalar dissipation rate is related to the flame surface density and in the present work, the flame speed expression is derived from a model for scalar dissipation rate that accounts for the dominant terms in its transport. Furthermore Driscoll (2008) prescribes that flame speed databases should be categorised based on the flame geometry and S_T expressions should include an appropriate geometric parameter to account for geometry–dependent wrinkling. However the comparisons with various experiments shown here have demonstrated that Eq. (6.3) gives good predictions for flames with different geometry. This is because the small–scale mixing rate and thus the chemical reaction rate are independent of large scales in turbulent flows with sufficient scale separation. The success of Eq. (6.3) underscores the importance of the scalar dissipation rate and confirms the hypothesis that a deep understanding of its physics can help in predicting the turbulent flame speed reliably.

6.5 Summary

An expression for turbulent flame speed, S_T, is studied as a means of providing an indirect experimental validation for the mean scalar dissipation rate, $\widetilde{\epsilon}_c$, model derived in Chapter 5. Unlike many of the earlier turbulent flame speed expressions, this expression has no adjustable parameters and the model constants carry specific physical significance and they are related to the physics of scalar dissipation rate. The turbulent flame speed expression explicitly includes the influence of the heat release parameter, τ, the fuel type, the velocity ratio u'/s_L^o and the length scale ratio Λ/δ_L^o. These parameters signify the influences of thermo–chemical and turbulence processes, which can be altered independently in experiments. The current expression agrees qualitatively with the classical flame speed theories such as those of Damköhler (1940) and Kerstein & Ashurst

(1992). In the wrinkled flamelets regime i.e. for low turbulence level, the normalised turbulent flame speed, S_T/s_L^o, varies almost linearly with the normalised turbulence RMS velocity, u'/s_L^o, for a given value of the length scale ratio Λ/δ_L^o. However Damköhler's result gives a square–root dependence for S_T/s_L^o on u'/s_L^o for high levels of turbulence while the current expression suggests a combination of linear and square–root dependence similar to the result of Kerstein & Ashurst (1992).

The flame speed expression is derived using the KPP theorem which has hitherto been applied for the case of a statistically planar one–dimensional flame. Analysis of multidimensional flame brush in a local curvilinear orthogonal coordinate system attached to a $\tilde{c}$ iso–surface suggests that a quasi one–dimensional structure can be observed when the turbulent scalar flux in the tangential directions of the $\tilde{c}$ iso–surface is negligible. The analysis of the quasi one–dimensional equation gives an expression for S_T, which is similar to the KPP result if the mean curvature of the flame brush is negligible. Including the mean flame brush curvature in the analysis shows explicitly that increasing positive curvature causes an almost linear increase of the flame speed. Since the flame brush curvature was excluded in the development of Eq. (6.3), which is analysed here, the experimental data sets are chosen such that they are meaningful for its validation.

The S_T/s_L^o values predicted by the current expression, with fixed model constants, compare well with a wide range of experimental data from various flow configurations and conditions. Notably, the comparisons are good with data upto $u'/s_L^o \simeq 50$. The increase in S_T due to laminar flame instabilities for unity Lewis number mixtures, which are expected to be significant in the weakly wrinkled regime and at elevated pressures, is also well predicted by the current flame speed expression. The ability of the flame speed expression to predict values in close agreement with experimental data over a wide range of conditions indicates that the correct physics are incorporated into the mean scalar dissipation rate model. This model is a central modelling parameter in the strained laminar flamelet formulation described in Chapter 4. In the next chapter the strained flamelet formulation will be applied for turbulent premixed flame calculations to test its predictive capability.

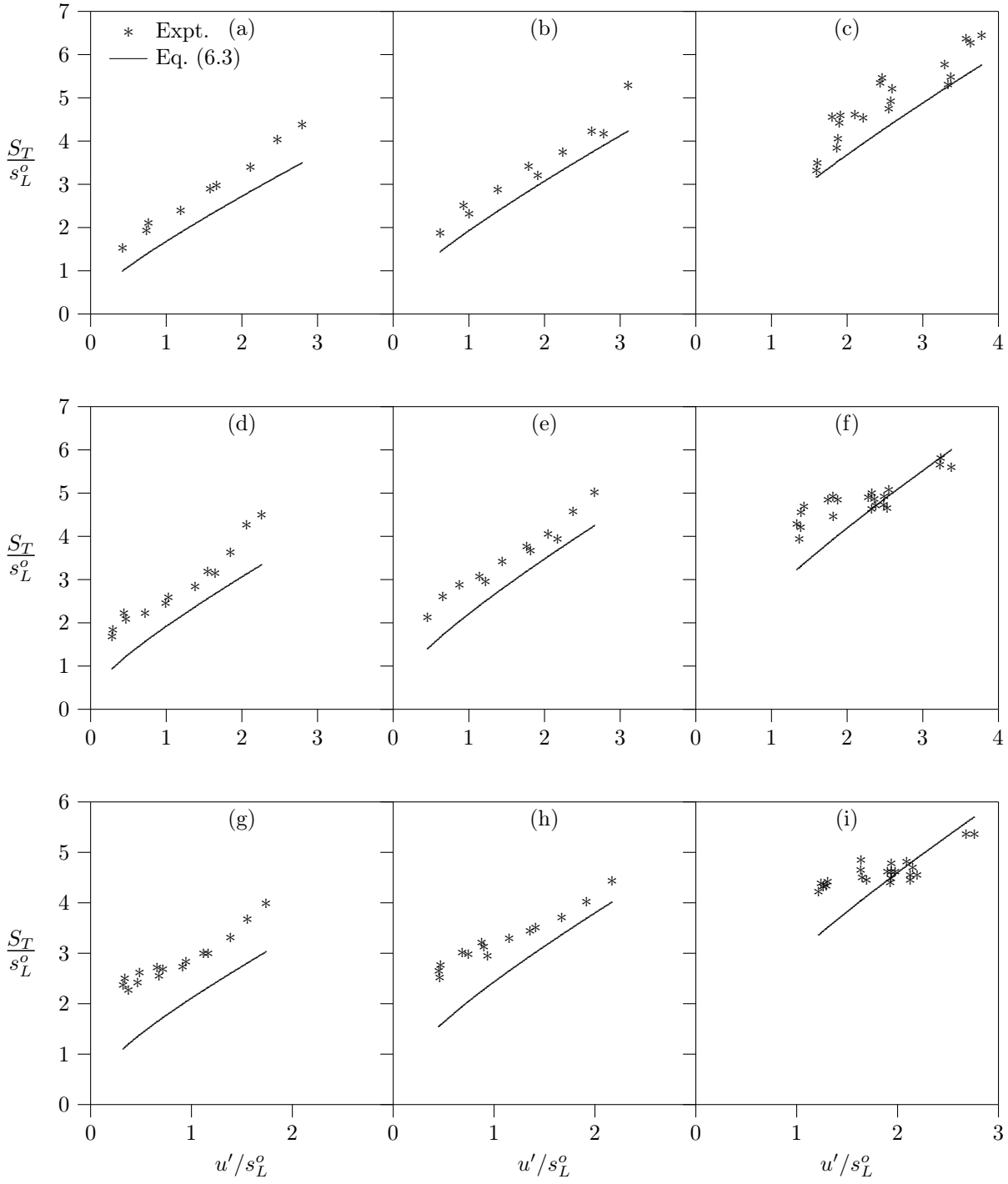

Figure 6.5: The predictions of turbulent flame speed expressions are compared to the experimental data of Smith & Gouldin (1978) for various equivalence ratios: (a)–(c) correspond to $\phi = 0.75$; (d)–(f) correspond to $\phi = 0.85$ and (g)–(i) correspond to $\phi = 1.0$. The comparisons on the left, center and right columns correspond to $\Lambda = 0.69$mm, 0.95mm and 1.49mm respectively.

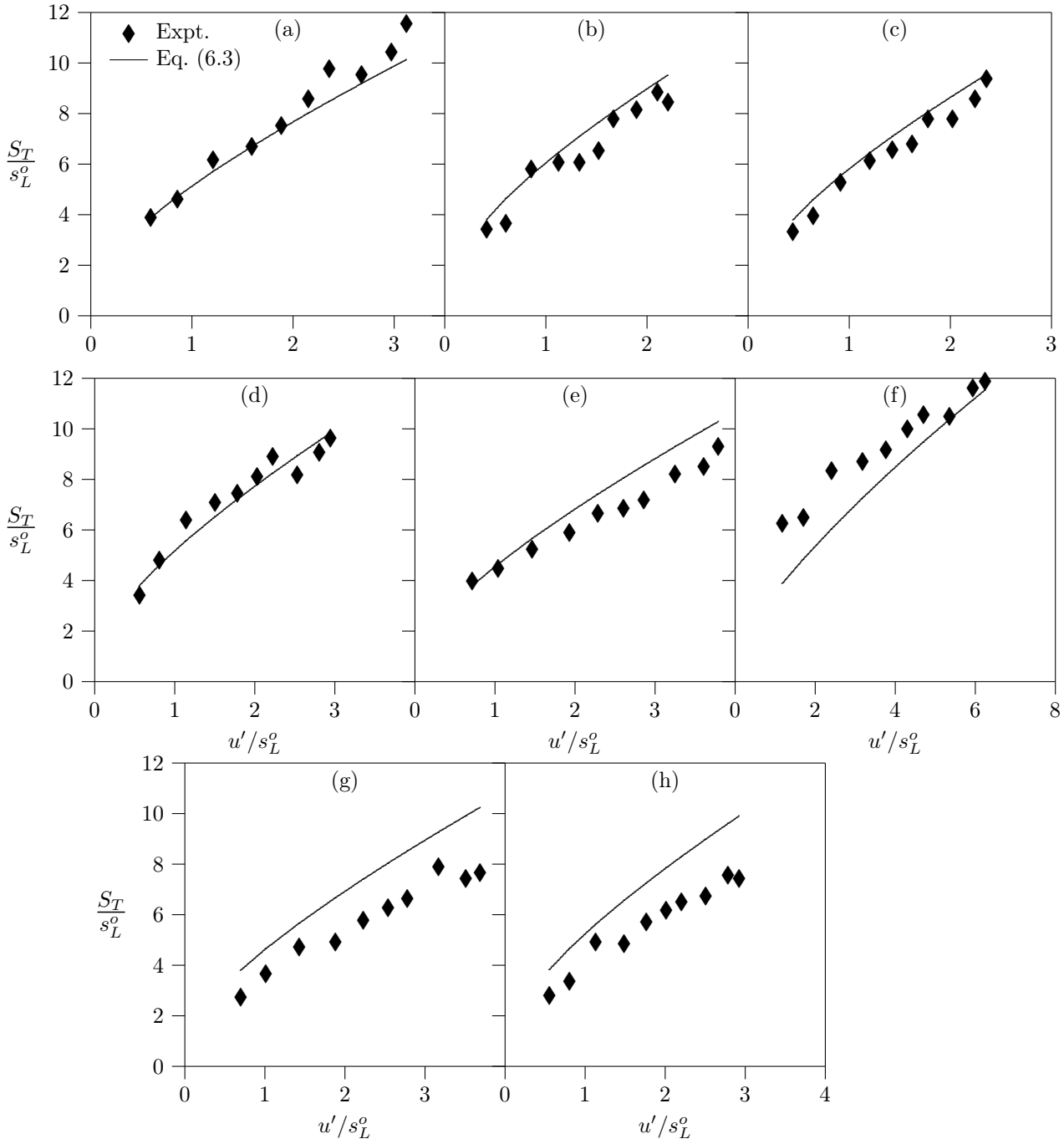

Figure 6.6: The predictions of turbulent flame speed expressions are compared to the experimental data of Aldredge *et al.* (1998) for various equivalence ratios: (a) $\phi = 1.0$; (b) 1.1; (c) 1.2; (d) 1.3; (e) 1.4; (f) 1.5; (g) 0.8; (h) 0.9.

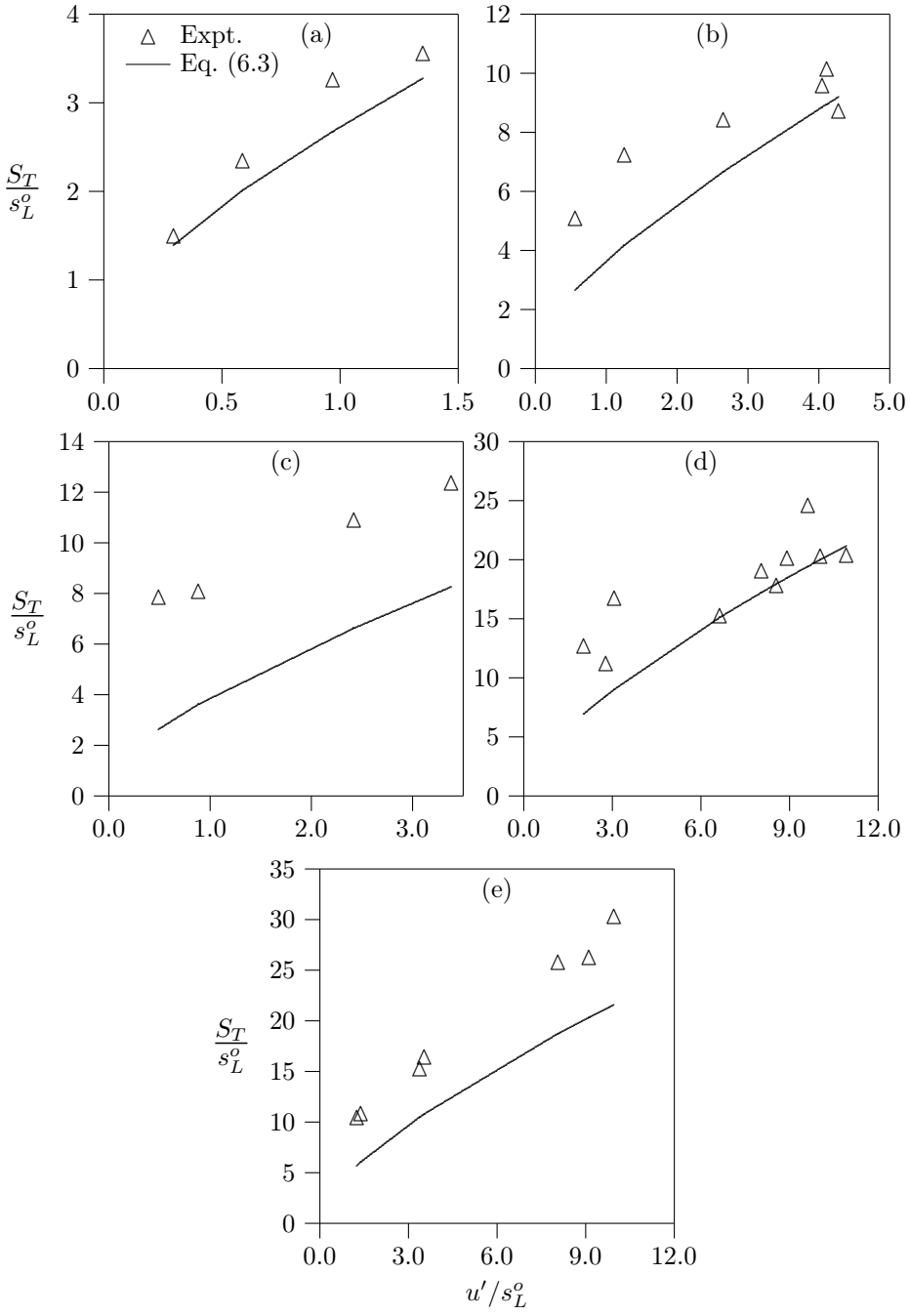

Figure 6.7: The variation of turbulent flame speed with u'/s_L^o at different pressures: (a) 0.1 MPa; (b) 0.5 MPa; (c) 1 MPa; (d) 2 MPa; (e) 3 MPa. The experimental data of Kobayashi *et al.* (1996) are compared to the flame speed expression.

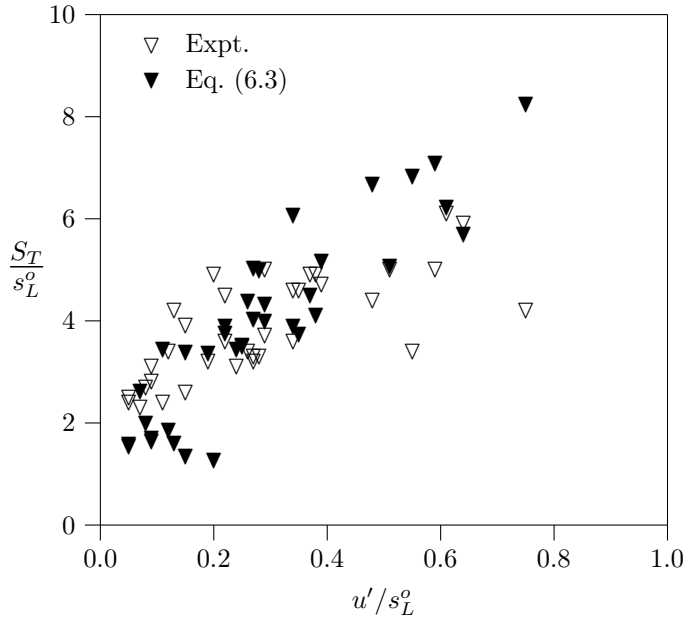

Figure 6.8: Comparisons of turbulent flame speed prediction to the experimental data of Savarianandam & Lawn (2006).

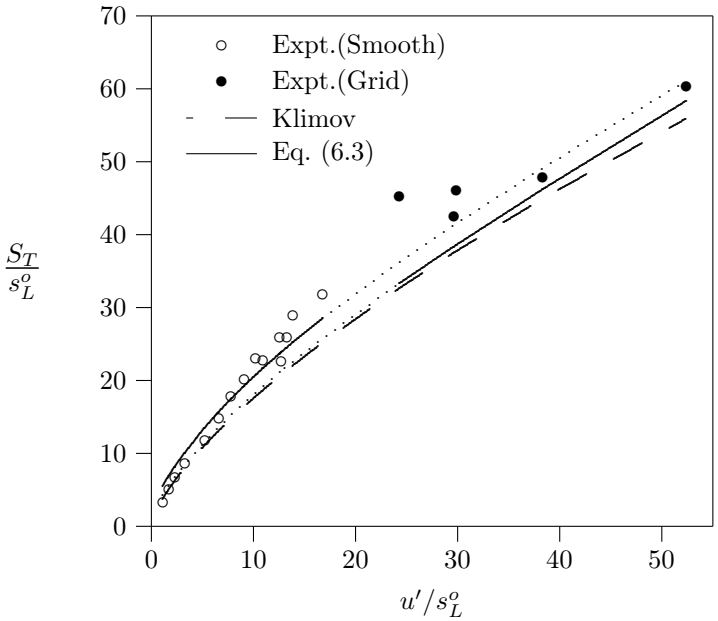

Figure 6.9: Comparisons of turbulent flame speed prediction to the experimental data of Il'yashenko & Talantov (1966).

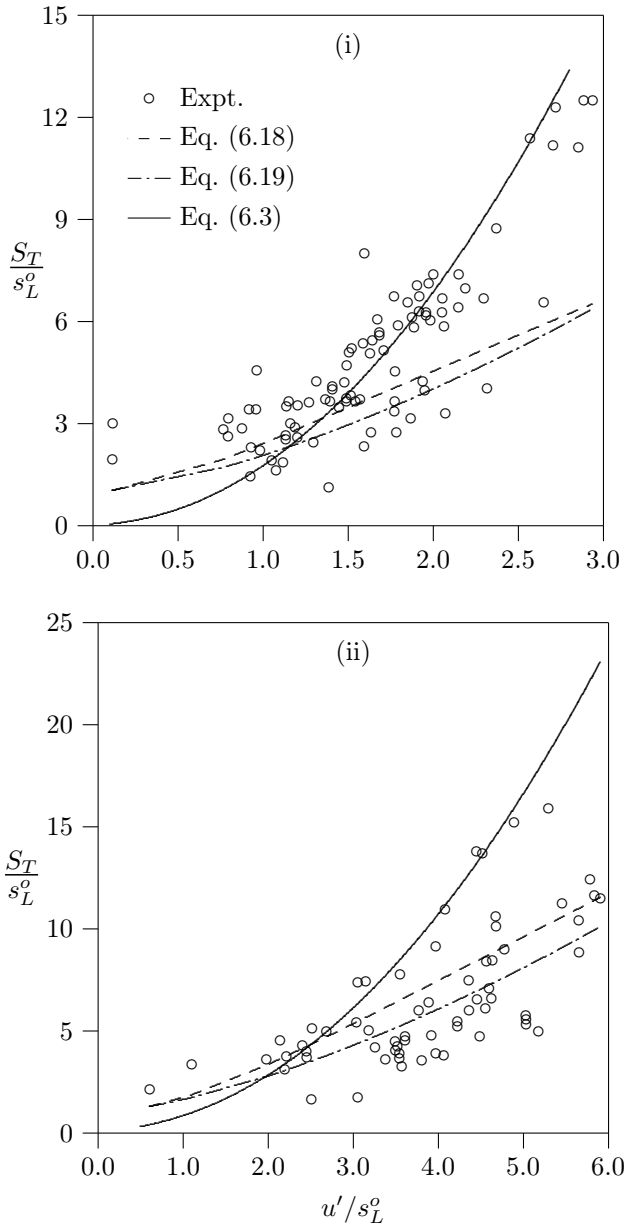

Figure 6.10: Comparison of turbulent flame speed expressions to the experimental database of Abdel-Gayed *et al.* (1987) for two values of flame stretch parameter, K: (i) K = 0.053 and (ii) K = 0.15.

Chapter 7

Application of Strained Flamelet Formulation

The strained flamelet formulation described in Chapter 4 is applied for turbulent premixed flame calculations in this chapter, to test its predictive ability. Calculations of statistically planar one–dimensional flames are considered first to compare the predictions of the strained flamelet mean reaction rate closure with other closures. Calculations of laboratory flames of different configurations are then performed and predictions of the flame brush structure and species concentrations are compared with experimental data. An overview of the computational methodology adopted in the present calculations is described in the next section.

7.1 Computational methodology

The calculations performed are in the Reynolds–Averaged–Navier–Stokes (RANS) paradigm with the standard $\tilde{k} - \widetilde{\varepsilon}$ turbulence closure (see Section 2.2.1). The governing equations solved are:

- Favre averaged continuity equation; Eq. (2.7)
- Favre averaged momentum equation; Eq. (2.8)
- Favre averaged turbulent kinetic energy equation; Eq. (2.10)
- Favre averaged kinetic energy dissipation rate equation; Eq. (2.11)

- Favre averaged progress variable equation; Eq. (2.15)
- Progress variable variance equation; Eq. (3.1)

These governing equations can be cast in a generalised form as

$$\frac{\partial \overline{\rho}\Psi}{\partial t} + \frac{\partial \overline{\rho}\widetilde{u}_j\Psi}{\partial x_j} = \frac{\partial}{\partial x_j}\left(\Gamma\frac{\partial \Psi}{\partial x_j}\right) + S_\Psi \tag{7.1}$$

where $\Psi = \widetilde{u}_i,\ \tilde{k},\ \widetilde{\varepsilon},\ \tilde{c}$, etc., and $\Psi = 1$ for mass conservation equation. The term involving Γ represents the diffusive flux typically including the turbulent and laminar diffusivities and S_Ψ represents the source terms. For example, when $\Psi = \widetilde{\varepsilon}$, from Eq. (2.11), $\Gamma = \mu + \mu_t/Sc_\varepsilon$ and $S_\Psi = C_{\varepsilon 1}\mathcal{P}_k\widetilde{\varepsilon}/\tilde{k} - C_{\varepsilon 2}\overline{\rho}\widetilde{\varepsilon}^2/\tilde{k}$.

The governing equations are discretised using the finite–volume formulation described by Patankar (1980). The pressure correction approach of Patankar (1980) is employed to obtain a solution for the flow field. This approach, applicable for low Mach number flows, allows a guessed pressure field to be corrected by the continuity equation, such that the resulting velocity field from the momentum equations satisfy the continuity equation. This iterative algorithm is described in detail by Patankar (1980) but it essentially involves the following steps:

1. Guess a mean pressure field p^*
2. Using the guessed pressure field, solve the momentum equations to obtain a velocity field $\widetilde{u}_i^*$.
3. Solve the equation for pressure correction p'. This equation is obtained from the continuity equation in terms of the velocities $\widetilde{u}_i^*$.
4. Correct the velocities $\widetilde{u}_i^*$ and pressure p^* using p'.
5. Solve the equations for other Ψ.
6. Treating the corrected pressure as p^*, return to step 2 and repeat until convergence.

In turbulent flame calculations, the flame influences the flow field via the mean density, $\overline{\rho}$, which is calculated using the equation of state and this is incorporated at step 5 in the above sequence of calculation.

7.1.1 Overview of modelling closures

As noted earlier, the standard $\tilde{k} - \widetilde{\varepsilon}$ turbulence closure is employed and the Reynolds stresses are closed using Eq. (2.9). Two additional unclosed terms remain in Eqs. (2.10) and (2.11). The first of these - the pressure–dilatation term - is closed using the model of Zhang & Rutland (1995):

$$\overline{p' \frac{\partial u_k''}{\partial x_k}} = 0.5 \, \tilde{c} \, (\tau s_L^o)^2 \, \overline{\dot{\omega}} \; . \tag{7.2}$$

The second term, $\overline{u''}$, is closed as (Jones, 1994)

$$\overline{u''} = \tau \, \frac{\widetilde{u'' c''}}{1 + \tau \tilde{c}} \; . \tag{7.3}$$

The turbulent scalar flux is closed using the gradient transport hypothesis; Eq. (2.16). The turbulent flux term in the $\widetilde{c''^2}$ equation - the third term on the l.h.s of Eq. (3.1) - is also closed using the gradient type closure as

$$\overline{\rho} \widetilde{u_i'' c''^2} = -\frac{\mu_t}{\mathrm{Sc_c}} \left(\frac{\partial \widetilde{c''^2}}{\partial x_i} \right) \; . \tag{7.4}$$

The mean scalar dissipation rate term in Eq. (3.1) is closed using the algebraic model described in Chapter 5; Eq. (5.18). The values of the various model constants are given in Table 7.1.

Table 7.1: Values of model constants.

Constant	Equation	Value
C_μ	Eq. (2.9)	0.09
$\mathrm{Sc_k}$	Eq. (2.10)	1.0
Sc_ε	Eq. (2.11)	1.3
$C_{\varepsilon 1}$	Eq. (2.11)	1.44
$C_{\varepsilon 2}$	Eq. (2.11)	1.92
β'	Eq. (5.18)	6.7
C_3	Eq. (5.18)	$1.5\sqrt{\mathrm{Ka}}/(1+\sqrt{\mathrm{Ka}})$
C_4	Eq. (5.18)	$1.1(1+\mathrm{Ka})^{-0.4}$
K_c^*/τ	Eq. (5.18)	0.85 (hydrocarbon–air)

7.2 RANS of planar one–dimensional flames

A test case of statistically planar one–dimensional flames propagating into homogeneous isotropic turbulence, is considered following many earlier studies (Anand & Pope, 1987; Bradley *et al.*, 1994; Swaminathan & Bray, 2005). Physically, this problem corresponds to premixed flame propagating into a grid generated turbulence in a wind tunnel. This problem is inherently unsteady and thus one needs to consider spatio–temporal evolution of the flame brush. This problem offers a simple way to test reaction rate closures without clouding it with uncertainties in turbulence modelling since simple turbulence closure can be used.

7.2.1 Computational details

The discretised governing equations and the computational algorithm described in Section 7.1 are implemented as a computer code using FORTRAN–77. This code was employed for one–dimensional flame calculations in the earlier study of Swaminathan & Bray (2005). The present formulation seems similar to the study of Swaminathan & Bray (2005), but it differs in the following respects, viz.,

(i) the turbulence in the reactant is not considered to be frozen,

(ii) the variance transport equation, Eq. (3.1), is solved using the new scalar dissipation rate model in Eq. (5.18), whereas in Swaminathan & Bray (2005) the variance was taken to be $\tilde{c}(1-\tilde{c})$, and

(iii) the reaction rate closures used here are entirely different.

The mean reaction source terms, $\overline{\dot{\omega}}$ and $\overline{\dot{\omega}''c''}$, appearing respectively in Eqs. (2.15) and (3.1), are related via Eq. (3.2). Three closures for these terms are studied for the one–dimensional flame calculations:

1. Algebraic closure of Bray (1979); $\overline{\dot{\omega}}$ closed via Eq. (2.30) and $\overline{\dot{\omega}''c''} = (C_m - \tilde{c})\overline{\dot{\omega}}$ with $C_m = 0.7$. The dissipation rate is obtained using Eq. (5.18).

2. Unstrained Flamelet model (UF) given by Eq. (4.1). According to this model

$$\overline{\dot{\omega}c} = \int_0^1 \zeta \; \dot{\omega}_o(\zeta) \; p(\zeta) \; d\zeta. \tag{7.5}$$

3. Strained Flamelet model (SF) using RtP flamelets given by Eq. (4.11). This model gives

$$\overline{\dot{\omega}c} = \int_0^1 \zeta \, \langle \dot{\omega} | \zeta \rangle \, p(\zeta) \, d\zeta. \tag{7.6}$$

The algebraic closure from the BML description of turbulent premixed flame is valid in the large Da limit and the turbulent flame front is treated to be a thin interface. The unstrained flamelet model allows one to include the flame front structure without the stretch effects. The strained flamelet model accounts for the stretch effects also. These effects can be clearly seen in the results to be presented in the next section. As noted in Section 4.3, the pdf $p(\zeta)$ is obtained from $\widetilde{p}(\zeta)$ which is presumed to be a β–pdf.

Table 7.2: Attributes of the one–dimensional flame cases.

	u'/s_L^o	Λ/δ	Da	Ka
K=0.15	2.00	8.764	4.382	0.955
	3.00	29.579	9.860	0.955
	4.00	70.113	17.528	0.955
	5.00	136.939	27.388	0.955
	6.00	236.630	39.438	0.955
	6.50	300.855	46.285	0.955
K=1.0	8.0	12.620	1.578	6.369
	12.0	42.593	3.549	6.369
	16.0	100.962	6.310	6.369
	18.0	143.753	7.986	6.369
	20.0	197.192	9.860	6.369
	24.0	340.748	14.198	6.369

Turbulent combustion of stoichiometric methane–air mixture at 298 K and atmospheric pressure are considered. The thermo–chemical characteristics of this mixture are $s_L^o = 0.40$ m/s, $\delta_L^o = 0.41$ mm and $\tau = 6.48$. Flames corresponding to two values of the flame stretch factor, K: 0.15 and 1.0, are computed. It is evident from Eqs. (6.21) and (6.24) that K = 0.157 Ka. The attributes of the various cases computed are given in Table 7.2. The combustion conditions of these flames are also marked in the regime diagram in Fig. 7.1. It is evident from this figure that the flames with $K = 0.15$ are at the upper limit of the corrugated flamelets regime and the flames with $K = 1.0$ are in the thin reaction zones

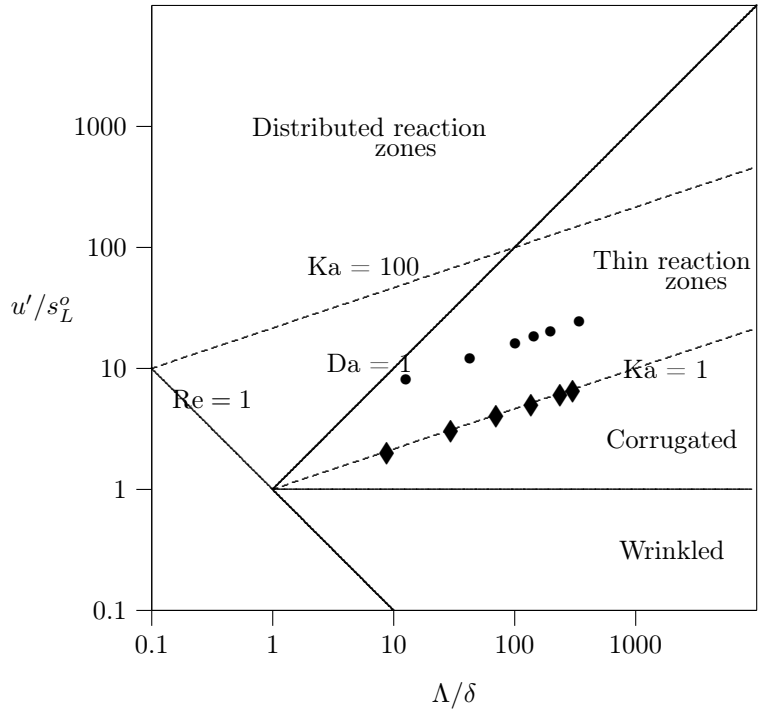

Figure 7.1: The regime diagram with the parameters of the one–dimensional computational flames for two values of flame stretch parameter K: 0.15 (⧫) and 1.0 (•).

regime. The length of the computational domain varies from 0.125m to 1.0m and the grid spacing varies from 0.13mm to 1.25mm and these values are dictated by the turbulent flame conditions. The turbulence characteristics in the unburnt mixture are specified by $\tilde{k} = 3u'^2/2$ and $\widetilde{\varepsilon} = u'^3/\Lambda$ for these flames. The grid spacing in the calculations is uniform and the number of cells is chosen to ensure that atleast 10 cells are inside $\min(\Lambda, \delta_t)$. The turbulent flame brush thickness, δ_t, is defined as

$$\delta_t \equiv \frac{1}{(\partial\tilde{c}/\partial x)_{\max}} \ . \tag{7.7}$$

Two and three dimensional look up tables of $\overline{\dot{\omega}}$ are calculated *a priori* for the unstrained and strained flamelet models respectively. The tables have a resolution of 0.01 in the $\tilde{c}$ dimension and 0.02 in the g dimension. For the strained flamelet model the third dimension is $\widetilde{\epsilon_c}$ and the resolution is 5/s. Values of $\overline{\dot{\omega}}$ from the table are obtained using linear interpolations for the values of $\tilde{c}$, g and $\widetilde{\epsilon_c}$ realised

in the RANS calculation.

The unsteady calculations are initialised using an arbitrary $\tilde{c}$ profile going from 0 to 1 in the computational domain (see Fig. 7.2). The turbulence quantities, $\tilde{k}$ and $\widetilde{\varepsilon}$, are set equal to the unburnt mixture values in the entire domain at the start of the calculations. Initial profiles of mean density and mean velocity are specified according to the $\tilde{c}$ profile. The mean velocity on the unburnt side of the flame brush remains zero at all times. The simulations are run until a steady propagation is observed and the time period for this depends on the flame and turbulence conditions specified at the start of the simulation. A value of 0.1 microsecond is used to time advance the equations in all cases. The time evolution is shown in Fig. 7.2 for the flame with $K = 1$ and $u'/s_L^o = 12$ in the form of spatial variation of $\tilde{c}$ after every millisecond. The grid nodes are plotted for the last instant and it is evident that the flame brush is well resolved. After

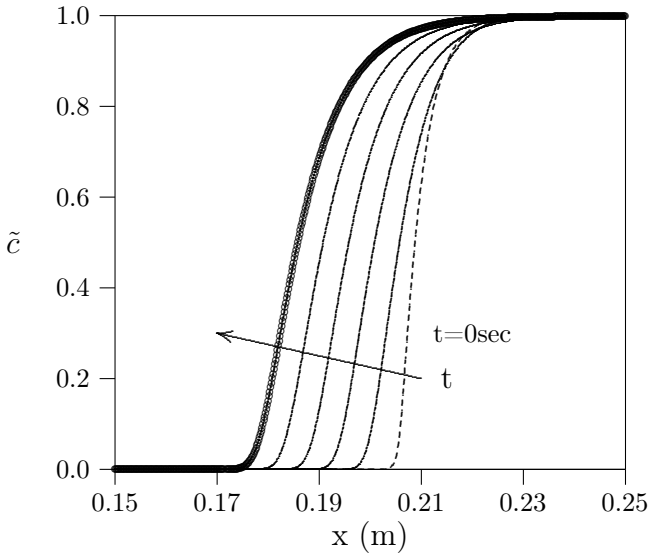

Figure 7.2: The progress of the solution in a typical one–dimensional flame calculation. Starting from an arbitrary initial profile (dashed line), the flame brush travels from right to left.

some initial transients the flame propagation is steady and all the points on the $\tilde{c}$ profile move at the same speed. This is verified by tracking $\tilde{c} = 0.3$, 0.5 and 0.7 with time. The rate of change of displacement of these tracked locations, $S_d \equiv dx(\tilde{c})/dt$, is shown in Fig. 7.3 for two flames having $u'/s_L^o = 4$, K = 0.15

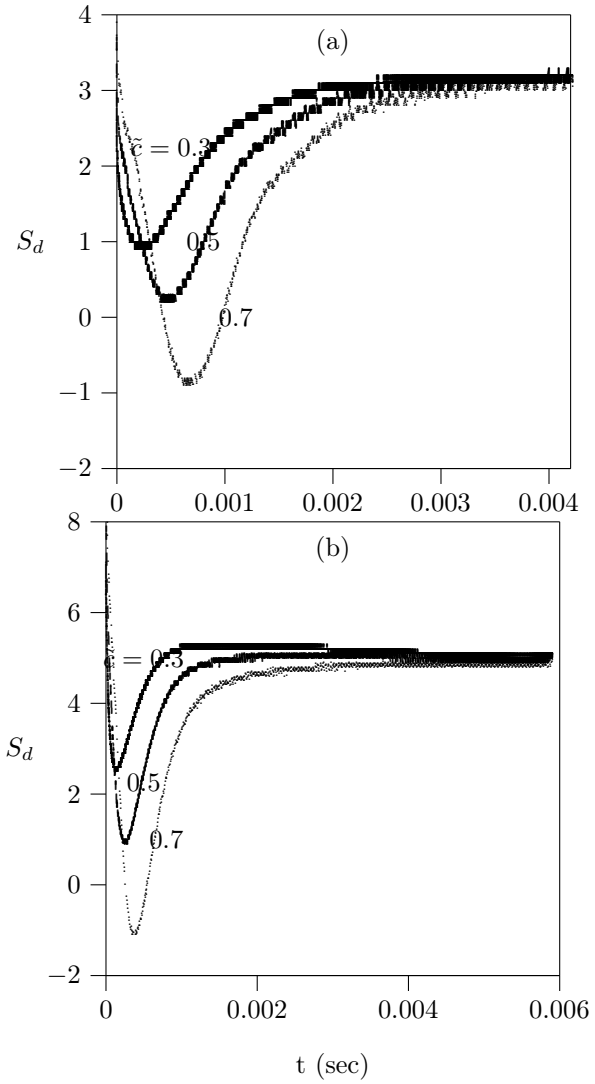

Figure 7.3: History of displacement speed, S_d, in m/s for three $\tilde{c}$ values in two flames: (a) $u'/s_L^o = 4$, K = 0.15 (b) $u'/s_L^o = 12$, K = 1.0. The results are shown for the algebraic closure of the mean reaction rate.

and $u'/s_L^o = 12$, K = 1.0. These two flames are close to the two extremes of the twelve flames marked in Fig. 7.1. The results shown in Figs. 7.2 and 7.3 are from algebraic model calculations and the similar behaviour is observed in all cases and with other models. The movement of iso–$\tilde{c}$ value is controlled by the diffusion and chemical reactions and thus the speed noted in Fig. 7.3 is the displacement speed, S_d. It is easy to show that this speed corresponds to the turbulent flame speed, S_T, for the statistically planar flames considered here. Thus the stationary values such as those observed in Fig. 7.3 are taken to be S_T. Equation (6.10), which is valid for this flame configuration, can be rewritten as

$$S_T = \frac{1}{\rho_u} \int_0^1 \overline{\dot{\omega}}(\tilde{c})\, d\tilde{c} \ ,$$

and hence the S_T values will be dictated by the mean reaction rate closure. The S_T values from calculations are compared to the experimental compilation Abdel-Gayed *et al.* (1987) and earlier computations of Bradley *et al.* (1994) in the next section.

7.2.2 Results and discussion

Before comparing the turbulent flame speeds, let us study the structure of the flame brush predicted by the three reaction rate closures. In Fig. 7.4 the $\tilde{c}$ profiles of two flames with $u'/s_L^o = 4$, $K = 0.15$ and $u'/s_L^o = 16$, $K = 1.0$ are plotted as a function of a normalised spatial coordinate $(x - x_1)/\delta_L^o$, where x_1 corresponds to the location of $\tilde{c} = 0.5$. The thickness of the profile given by the algebraic model is the largest and that given by the strained flamelet model is the smallest in Fig. 7.4. The normalised flame brush thickness, δ_t/δ_L^o, shown in Fig. 7.5 confirms this observation for all cases. Alternative definitions of δ_t, such as that of Bray (1990):

$$\delta_t = \int_{-\infty}^{\infty} \widetilde{c''^2} dx \ , \tag{7.8}$$

or a definition based on mean reaction rate profile, yield the same trends as in Fig. 7.5. This figure shows that for a given K value, δ_t increases as u'/s_L^o is increased. On the other hand for a given u'/s_L^o, δ_t decreases as K is increased. The flame brush thickness, δ_t, is expected (Bradley *et al.*, 1994; Peters, 2000) to

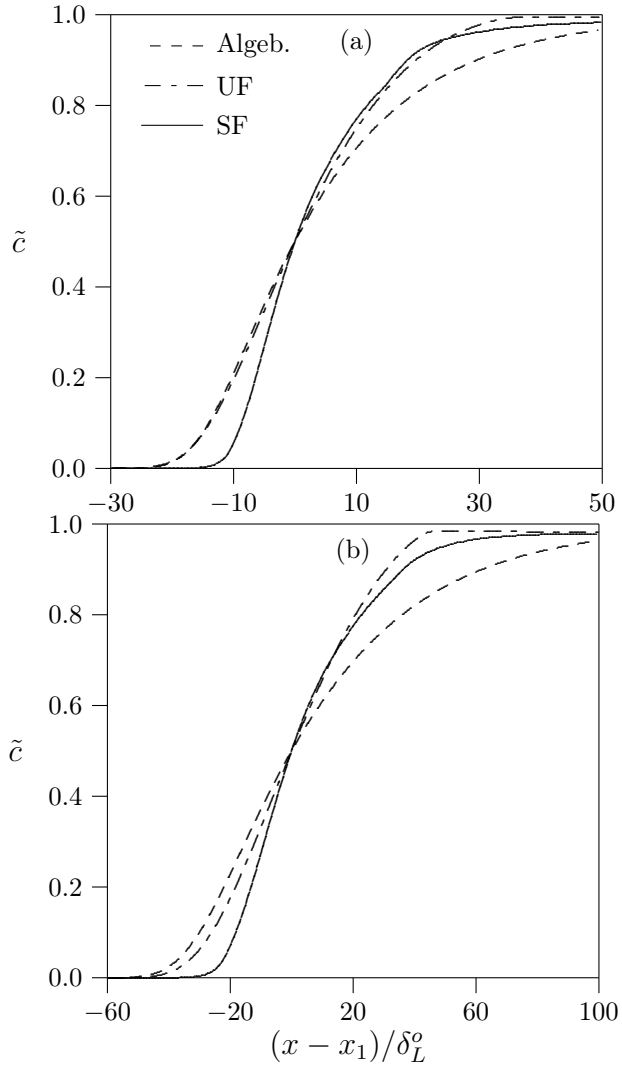

Figure 7.4: The spatial profiles of $\tilde{c}$ predicted by the various models plotted against the normalised distance for two cases: (a) $u'/s_L^o = 4$, K = 0.15 (b) $u'/s_L^o = 16$, K = 1.0. The location of $\tilde{c} = 0.5$ in each case is denoted by x_1.

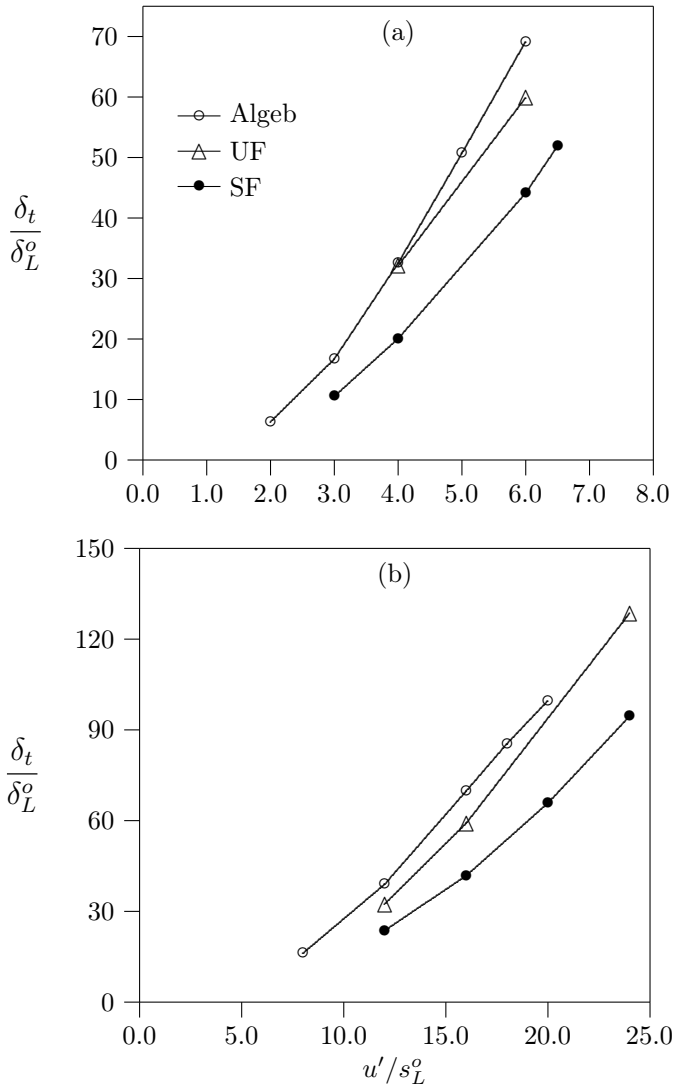

Figure 7.5: The normalised flame brush thickness, δ_t/δ_L^o, predicted by various models at different u'/s_L^o, for two values of flame stretch parameter: (a) K = 0.15 and (b) K = 1.

scale with the integral length scale, Λ. From the definition of the flame stretch factor it can be seen that $(\Lambda/\delta) \sim (u'/s_L^o)^3/\mathrm{K}^2$. Hence, for a fixed K value, Λ/δ increases with increase in u'/s_L^o whereas, for a fixed u'/s_L^o, Λ/δ decreases with increase in K. The present calculations hence seem to reproduce the scaling of δ_t with Λ. On the other hand, when Λ/δ is fixed, the calculations suggest that the flame brush thickness increases with u'/s_L^o. This is evident by comparing the K = 0.15, $u'/s_L^o = 5$ case with $\Lambda/\delta = 136.9$ and the K = 1.0, $u'/s_L^o = 18$ case with $\Lambda/\delta = 143.7$. From Fig. 7.5 it can be seen that δ_t/δ_L^o for the former case is 32 while for the latter it is 54. This trend is consistent with that observed in the DNS study of Veynante & Poinsot (1997). A higher turbulence intensity causes a greater wrinkling of the flame front resulting in a thicker flame brush (Veynante & Poinsot, 1997) which explains such a trend. Comparison of predicted flame brush thickness to its measured value for multidimensional laboratory flames will be discussed in Section 7.3.2.2.

The density weighted pdf, $\widetilde{p}(\zeta)$, from the strained flamelet calculations are shown in Fig. 7.6 for two cases at three locations inside the flame brush; $\tilde{c}$ = 0.1, 0.5 and 0.9. It is evident from this figure that there is a large contribution from the reactants compared to that from the products for the location near the unburnt side, $\tilde{c} = 0.1$, and vice–versa for $\tilde{c} = 0.9$. The contribution from the burning gases is non–negligible for $\tilde{c} = 0.5$. This contribution can be quantified using $\int_{0.1}^{0.9} \widetilde{p}(\zeta)\ d\zeta$, whose values are shown in the inset in Fig. 7.6b. A careful scrutiny of this figure shows that the burning mode contribution is increased at all locations inside the flame brush, which is more apparent for $\tilde{c} = 0.5$, when the stretch rate K is increased. This is because of the flame front thickening at high stretch rates. The similarity of the pdfs in Fig. 7.6 to the experimental pdfs of Chen & Bilger (2002) is worth noting.

The flame propagation speeds using the three $\overline{\dot{\omega}}$ closures are compared with the experimental data of Abdel-Gayed *et al.* (1987) in Fig. 7.7. The predictions of the algebraic flame speed expression, Eq. (6.3), are also shown. The KPP analysis assumes a gradient transport for $\widetilde{u''c''}$ and the variance is assumed to be given by the BML limit: $\widetilde{c''^2} = \tilde{c}(1-\tilde{c})$. The present calculations with the algebraic reaction rate closure indeed yield $\widetilde{c''^2}$ values close to the BML values

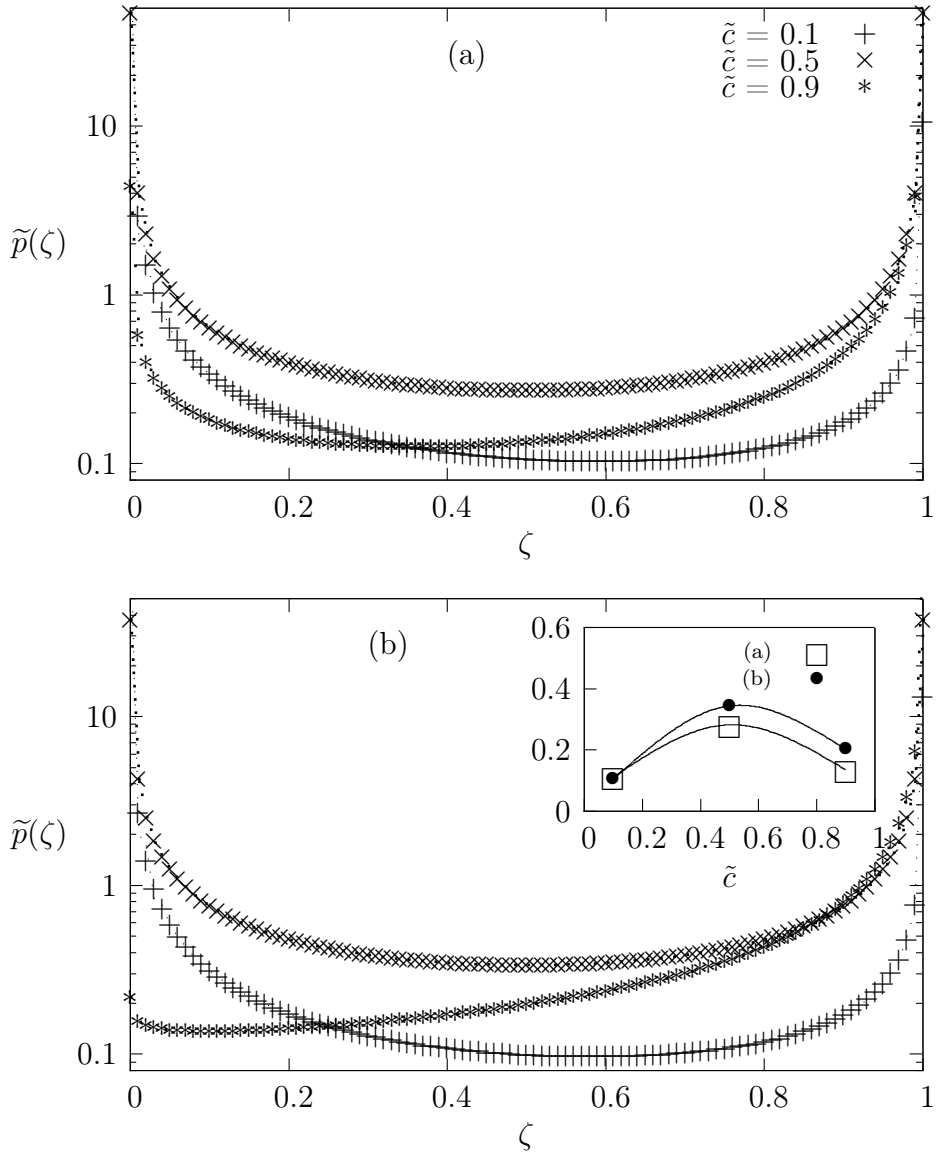

Figure 7.6: The shape of the density weighted pdf of progress variable, $\widetilde{p}(\zeta)$, at three locations in the flame brush ($\tilde{c} = 0.1$, 0.5 and 0.9) from the strained flamelet calculations for two cases : (a) $u'/s_L^o = 3$, K = 0.15 and (b) $u'/s_L^o = 24$, K = 1. The inset in (b) shows the values of $\displaystyle\int_{0.1}^{0.9} \widetilde{p}(\zeta;\tilde{c})\, d\zeta$ for the two cases.

and thus it is not surprising to see the flame speeds predicted by this closure close to the KPP values in Fig. 7.7. In general, the curves in Fig. 7.7a suggest that for a given stretch value $\overline{\dot{\omega}}_{\mathrm{SF}} < \overline{\dot{\omega}}_{\mathrm{UF}} < \overline{\dot{\omega}}_{\mathrm{Algeb}}$ with the inequality becoming larger as u'/s_L^o increases. The difference in the mean reaction rate values and thus the turbulent flame speeds increases further in highly stretched flames when u'/s_L^o is large as shown in Fig. 7.7b. This is because of greater influence of the fluid dynamic stretch effects in highly strained flames. Consequently, the algebraic closure overpredicts the mean reaction rate and the flame speed at high u'/s_L^o as depicted in Fig. 7.7. A similar trend is seen for the unstrained flamelets (UF) closure. The prediction by this model seems acceptable as in Fig. 7.7a when the combustion is in the corrugated flamelets regime. However, for flames in the thin reaction zones regime there is a large over–prediction. The flame speeds predicted by the strained flamelets (SF) closure are closer to the experimental data as in Fig. 7.7, when the combustion is in the corrugated flamelets as well as in thin reaction zones regimes. Also, the departure of results for the algebraic, UF and SF closures from one another reinforces that the stretch effects become prominent at large u'/s_L^o. The strained flamelets model using the scalar dissipation rate is shown to capture these variations nicely.

Bradley *et al.* (1992) observe that the experimental data of S_T are correlated better with the parameter KLe instead of K as in (Abdel-Gayed *et al.*, 1987). The compiled data, when grouped based on KLe, shows far less scatter than when grouped on K (Bradley *et al.*, 1992). The basis for this lies in the fact that the stretch rate effect on the burning velocity of a laminar flame has a dependence on the Lewis number, as noted in Section 4.2.1[1]. This can be verified in the one–dimensional flame calculations by considering mixtures of different Lewis numbers. Accordingly, a few cases of propane–air mixture of equivalence ratio 0.8, with Le = 1.83, were considered. Three cases corresponding to KLe = 1.0 and u'/s_L^o = 6, 8 and 12 were computed. The choice of lean propane–air mixture was also driven by the need to validate the strained flamelet closure for Le > 1 mixtures. As noted in Section 4.2.2, when Le > 1, the integration of the $\dot{\omega}$ vs N_c curve to obtain $\langle\dot{\omega}|\zeta\rangle$ requires approximations (see Fig. 4.5b and associated

[1]This is also manifest in Eq. (4.2). The Markstein length, $\pounds$, has a dependence on the Lewis number (Law, 2006).

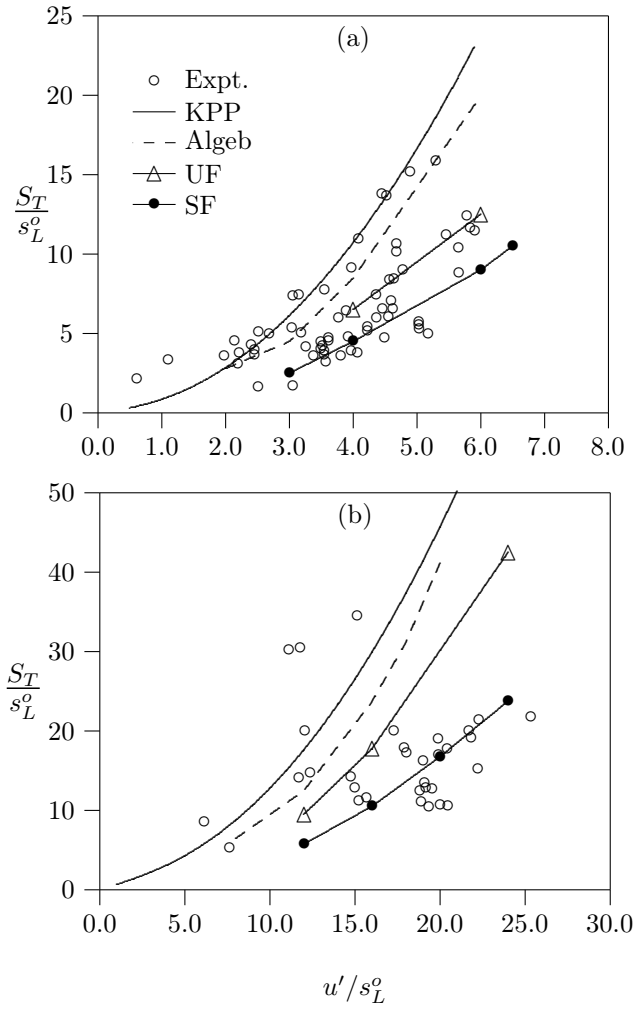

Figure 7.7: Comparisons of predicted flame speeds with the experimental data of Abdel-Gayed *et al.* (1987) for two values of flame stretch parameter: (a) K = 0.15 and (b) K = 1.

discussion). For the cases considered, the two approaches prescribed in Section 4.2.2, yield S_T values that are nearly equal (within 5%). The S_T values computed using approximation (ii) in Section 4.2.2 are plotted in Fig. 7.8, and these are compared with the values corresponding to KLe = 1 case of the stoichiometric methane–air mixture. Note that for the methane–air mixture, KLe ≈ K since Le ≈ 1. Figure 7.8 indeed suggests that for mixtures with different Lewis numbers, the flame speed is very well parametrised by KLe, as observed by Bradley *et al.* (1992).

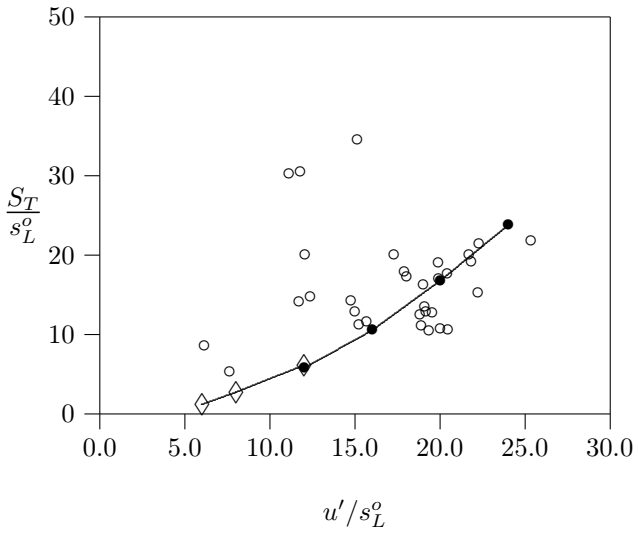

Figure 7.8: Flame speeds predicted by the strained flamelet closure for two mixtures: stoichiometric methane–air with K = 1.0 (•) and lean propane–air with KLe = 1.0 (◊). The experimental data of Abdel-Gayed *et al.* (1987) for K = 1.0 are also shown (○).

The predictions of the SF closure are compared with the results of Bradley *et al.* (1994) in Fig. 7.9. The mean reaction rate closure in Eq. (4.6) is used by Bradley *et al.* (1994) and the results were reported based on a parameter KLe. Their results for KLe = 0.14 and 1.0 are compared with the current results for KLe = 0.15 and 1.0 respectively in Fig. 7.9. As noted earlier, Eq. (4.6) includes the stretch effects via the burning rate factor, P_b. More importantly, second order turbulence closures are used by Bradley *et al.* (1994) by solving the transport equations for the Reynolds stresses and turbulent scalar flux as opposed

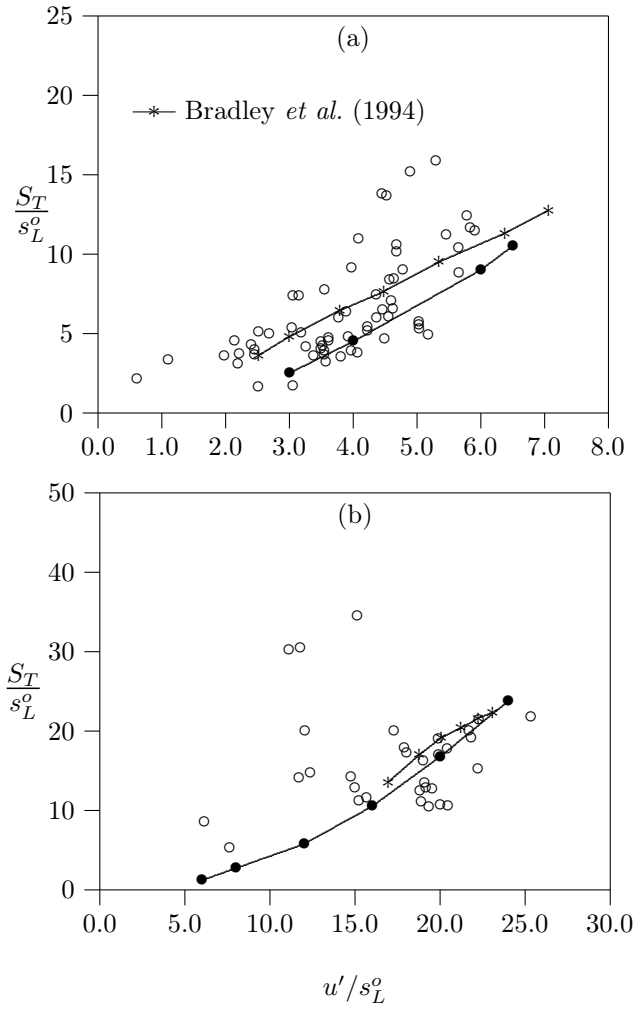

Figure 7.9: The comparisons of flame speeds predictions with the predictions of Bradley *et al.* (1994) for two values of flame stretch parameter: (a) KLe = 0.15 and (b) KLe = 1.

to the simple closures used in the present calculations, and the dissipation rate of $\widetilde{c''^2}$ in Eq. (3.1) is modelled by the classical linear relaxation model by Bradley *et al.* (1994). The calculations with the standard $\tilde{k}$–$\widetilde{\varepsilon}$ closure in the work of Bradley *et al.* (1994) yielded higher flame speeds than with second order closures. Figure 7.9 suggests that the present calculations agree very well with the results of Bradley *et al.* (1994), which is surprising given the many differences in the implementation and details of turbulence and combustion models. Quantitatively,

the mean reaction rate across the flame brush depends on $\widetilde{c''^2}$, $\tilde{k}$ and $\tilde{\varepsilon}$ values inside the flame brush. This is evident from Eqs. (5.18) and (4.11) for the SF closure. For the closure of Bradley *et al.*, this dependence arises via the pdf $p(\zeta)$ and the factor P_b. It is likely that the quantitative differences in the resulting $\overline{\dot{\omega}}$ values are not large, and this could explain the agreement seen in Fig. 7.9. The comparisons in Figs. 7.7 and 7.9 clearly illustrate the benefit of accounting for local fluid–dynamic effects on the reaction rate for turbulent premixed flames. This becomes more important at high turbulence conditions because it can be expected that the local flamelet structure is disturbed by the straining induced by turbulence eddies to a larger extent from that of a freely propagating unstrained laminar flame. Flamelet models based on steady strained laminar flames seem promising in this respect.

7.3 RANS of laboratory flames

The planar one–dimensional flame calculations clearly showed the benefits of strained flamelets and the use of scalar dissipation rate, by capturing the reduction in burning rate and the flame speed as stretch rate increases. This behaviour is captured well for both the corrugated flamelets and thin reaction zones regimes of turbulent premixed combustion. In this section, calculations of laboratory flames are discussed with the aim of examining the predictive ability of this strained flamelets approach across the combustion regimes by using a single set of values for model parameters. Two different laboratory flames: a rod stabilised V–flame of Robin *et al.* (2008) and pilot stabilised Bunsen flames of Chen *et al.* (1996) are considered. The V–flame conditions correspond to the corrugated flamelets regime and the Bunsen flame conditions correspond to the thin reaction zones regimes in the combustion regime diagram shown in Fig. 7.10. While the applicability of flamelet models in the former regimes is intuitive, their applicability to the latter requires a suitable description of fluid–dynamics influence on the laminar flame structure. This was appropriately addressed in the strained flamelets model and this will be tested using the Bunsen flames calculations.

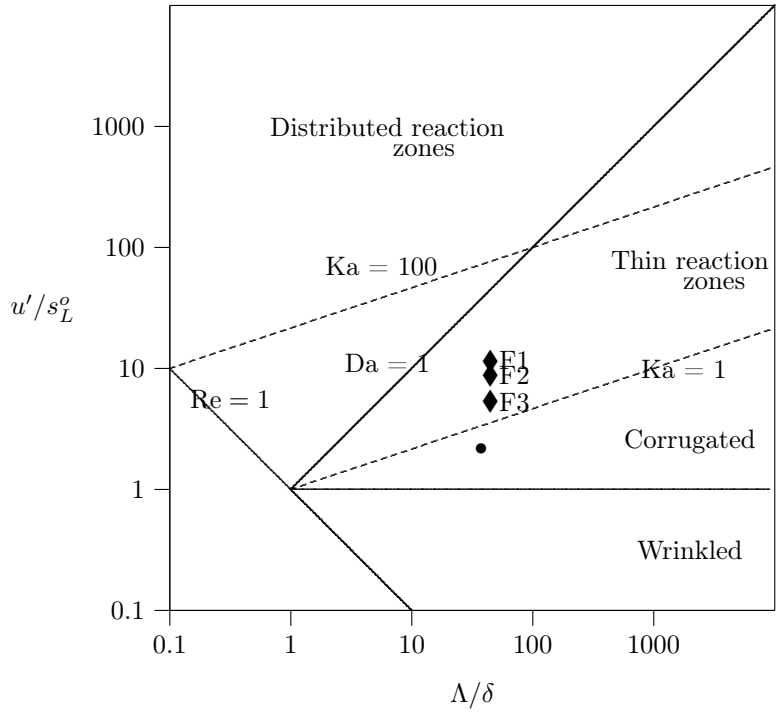

Figure 7.10: The regime diagram with conditions of the V–flame (•) of Robin *et al.* (2008) and the Bunsen flames (⧫) of Chen *et al.* (1996).

7.3.1 Computational details

The finite volume form of the discretised transport equations are implemented in Rolls-Royce proprietary CFD code PRECISE (Anand *et al.*, 1999). Appropriate sub–routines were added to this code for the implementation of the strained flamelets reaction rate model.

7.3.1.1 V–flame calculations

The V–flame experiments of Robin *et al.* (2008) were designed mainly to study stratified flames but measurements for premixed flames were also reported. A schematic of the flame and the coordinate directions are shown in Fig. 7.11. The z direction is the streamwise direction and x is the transverse direction. The origin of the coordinate system is located at the centre of the stabilising rod. The mean quantities are assumed not to vary much in the y direction and hence the flames can be treated as two–dimensional with symmetry about the $x = 0$ plane.

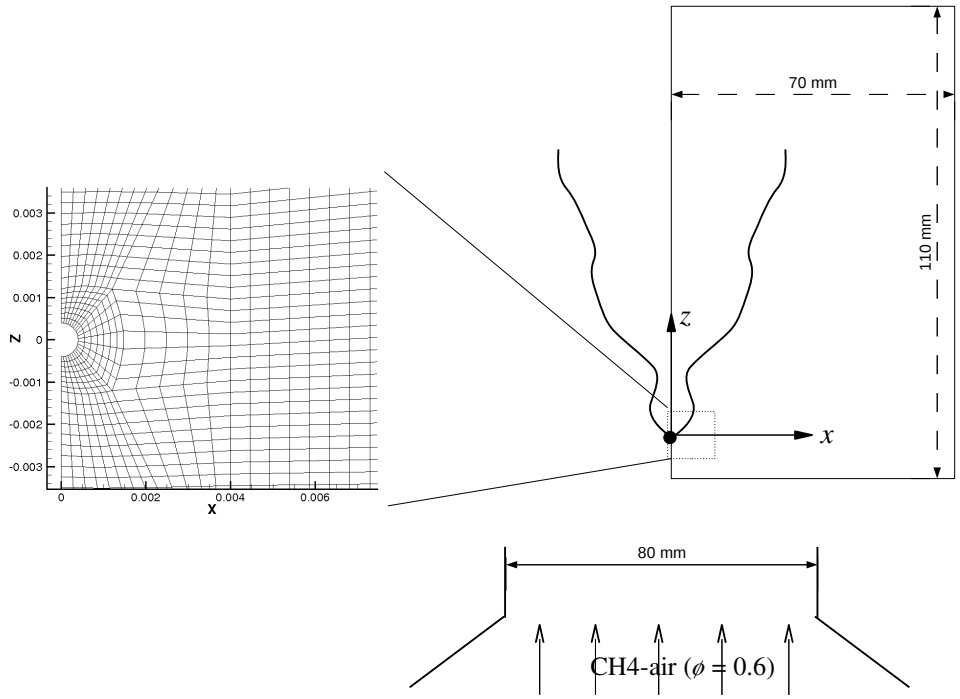

Figure 7.11: The schematic of the computational domain for the V–flame calculation. The 'O'–grid in the region close to the rod is also shown.

A rectangular computational domain in the region -10 mm $\leq z \leq$ 100 mm and $0 \leq x \leq$ 70mm is considered as shown in Fig. 7.11. Note that in the x direction the computational domain is wider than the half burner width (40mm) to allow for the entrainment of ambient air. The computational domain is discretised into a structured grid of nearly 30000 cells with the smallest cell size of 0.05mm $\times$ 0.1mm nearest to the rod and the cell size gradually increases away from the rod as shown in Fig. 7.11. The grid generation is performed using the 'O'–grid utility of the commercial package ANSYS–ICEMCFD.

The flame calculated in the present study is that designated as "HE06" by Robin *et al.* (2008) and it is shown in the regime diagram in Fig. 7.10. It corresponds to a lean methane–air mixture of equivalence ratio $\phi = 0.6$ with unstrained laminar flame speed of $s_L^o = 0.13$ m/s and the Zeldovich thickness of $\delta = 0.163$

mm. Turbulence at the burner exit was generated by different grids and for the flame HE06 the mean exit velocity is U = 3.14 m/s, the normalised turbulence RMS velocity is $u'/s_L^o = 2.14$ and the turbulence integral length scale is 6.1 mm. In the calculations, uniform conditions at the inlet boundary (z = -10 mm, 0 $\leq x \leq$ 40 mm) are specified based on the values reported by Robin *et al.* (2008) and they are, $\tilde{k}$ = 0.15 m^2/s^2 and $\widetilde{\varepsilon}$ = 10 m^2/s^3. The entrainment is facilitated by setting a small inlet velocity of 0.3 m/s in the region $x > 40$ mm.

The fluid density can be influenced by combustion as well as mixing with ambient air. To account for this mixing, the transport equation for mean mixture fraction, $\widetilde{\xi}$ is also solved and it's inlet values are specified to be $\widetilde{\xi} = 1$ for $0 \leq x \leq$ 40mm and $\widetilde{\xi} = 0$ for $x >$ 40mm. Note that $\widetilde{\xi} = 1$ here corresponds to a reacting mixture of equivalence ratio 0.6. It was assumed that the flame brush never interacts with the entrainment air which was verified from the $\widetilde{\xi}$ field calculations. Such an assumption simplifies the calculation of the mean density via the formula

$$\overline{\rho} = \left[\frac{(1-\widetilde{\xi})}{\rho_{air}} + \frac{\widetilde{\xi}}{\overline{\rho}_{reac}} \right]^{-1} , \tag{7.9}$$

where the density of air is ρ_{air} and the density of the reacting mixture, $\overline{\rho}_{reac}$, is related only to $\tilde{c}$ via Eq. (2.27). The unburnt density of the reacting mixture is ρ_u. Hence the combustion affects the flow field only via $\overline{\rho}$ which is related to $\widetilde{\xi}$ and $\tilde{c}$ using the above relations. The flame is anchored numerically by patching a small region of cells (5 $\times$ 5) just adjacent to the rod with burnt conditions ($\tilde{c} = 1$). This is reasonable since the flame is anchored by a heated rod in the experiment. The grid independence of the solution is also verified.

7.3.1.2 Bunsen flames calculations

The pilot stabilised Bunsen flames of Chen *et al.* (1996) have been computed in earlier studies using different modelling approaches such as the Flame Surface Density approach (Prasad & Gore, 1999), the level set G–equation approach both in RANS (Herrmann, 2006; Schneider *et al.*, 2005) and LES (De & Acharya, 2008; Pitsch & de Lageneste, 2002) contexts and the transported PDF approach (Lindstedt & Vaos, 2006). The flames correspond to stoichiometric methane air mixtures and the same mixture is used for the pilot flames (Chen *et al.*, 1996).

Here, all three flames designated as F1, F2 and F3 by Chen *et al.* (1996) are calculated. The Reynolds number based on jet exit diameter and bulk mean velocity is 52000, 40000 and 24000 for flames F1, F2 and F3 respectively. These flame conditions, shown in Fig. 7.10, lie in the thin reaction zones regimes and are challenging to compute with flamelet models in RANS as noted earlier. The centreline value of the turbulence RMS velocity, u', and the lateral integral length scale of 2.4 mm measured (Chen *et al.*, 1996) near the nozzle exit are used to calculate the flame conditions in Fig. 7.10.

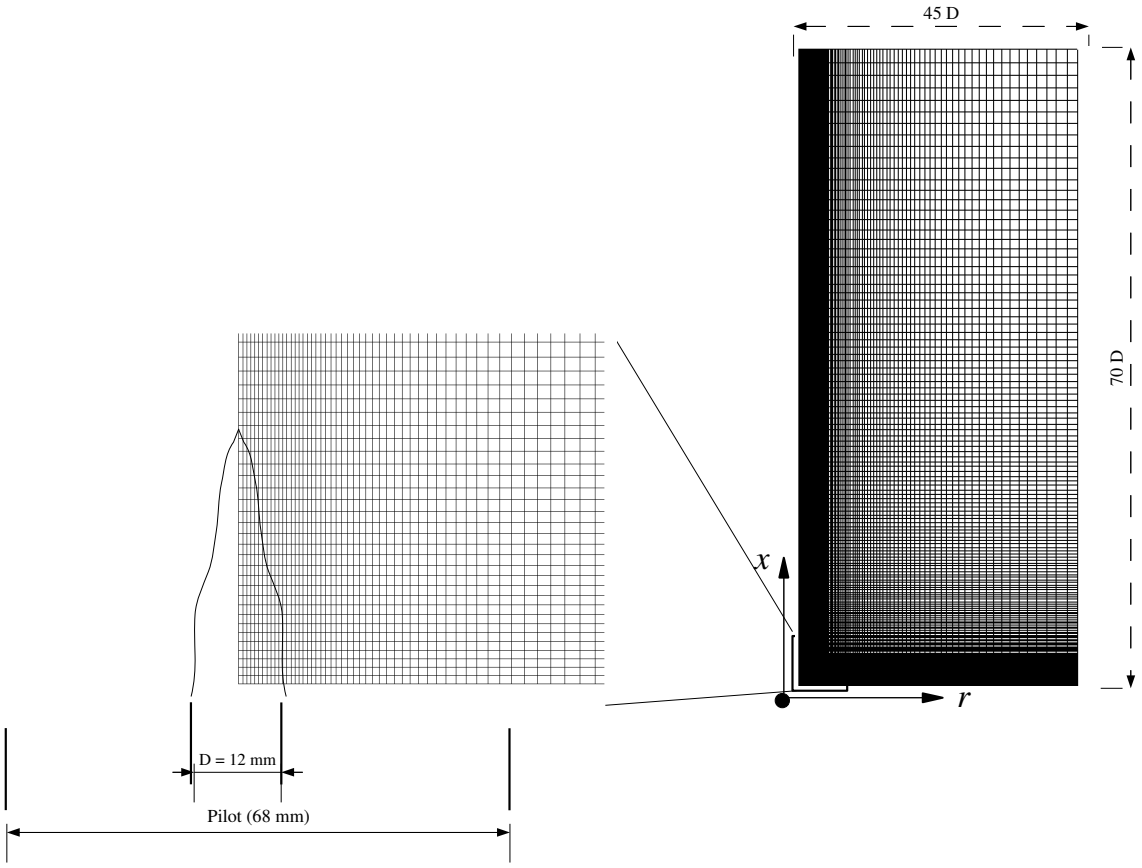

Figure 7.12: The schematic of the computational domain for the Bunsen flames calculations. The diameter of the nozzle jet is D.

A two–dimensional axisymmetric computational domain of $70D$ in the axial direction, x, and $45D$ in the radial direction, r, was considered where $D = 12$

mm is the diameter of the nozzle jet. The diameter of the pilot is 68 mm. The domain was discretised into a structured grid of non–uniform cell sizes with the smallest cells of 0.5mm×1.0mm close to the nozzle inlet plane. The schematic of the computational domain is shown in Fig. 7.12. The value of the standard $\tilde{k}$–$\widetilde{\varepsilon}$ model constant C_{ε_1} is changed from 1.44 to 1.52 to account for the round–jet anomaly (Pope, 1978). The mean axial velocity profiles measured at the nozzle exit (Chen *et al.*, 1996) are used to set the correpsonding velocity boundary conditions. The measured turbulent RMS velocity profiles and the longitudinal length scale are used to set the boundary conditions for $\tilde{k}$ and $\widetilde{\varepsilon}$. A uniform velocity for the pilot stream was set based on the volume flow rate through the pilot. A small velocity of 0.2 m/s was specified for the coflow air to allow for ambient air entrainment.

The experimental conditions present a difficulty for modelling with adiabatic flamelets since the temperatures of the pilot stream are sub–adiabatic due to losses to the burner wall and the presence of a cooling water circuit. To overcome this difficulty the following methodology is adopted. Transport equations for the mean and variance of the normalised fuel mass fraction, $c_f = 1 - Y_f/Y_{f_u}$ are solved instead of the progress variable based on the temperature. The equations of $\widetilde{c_f}$ and $\widetilde{c_f''^2}$ are identical to that of $\tilde{c}$ and $\widetilde{c''^2}$ since the Lewis number is close to unity for the reactant mixtures. Adiabatic flamelets are still used but to account for sub–adiabatic temperatures at the pilot boundary, the transport of the Favre averaged total enthalpy, $\tilde{h}$, is considered. The transport equation of $\tilde{h}$ for low speed flows is (Libby & Williams, 1980)

$$\frac{\partial \overline{\rho}\tilde{h}}{\partial t} + \frac{\partial \overline{\rho}\tilde{u}_i\tilde{h}}{\partial x_i} = \frac{\partial}{\partial x_i}\left[\frac{\mu_t}{\mathrm{Pr}}\frac{\partial \tilde{h}}{\partial x_i}\right] \ . \tag{7.10}$$

In the above equation, the effects of viscous dissipation, body forces and radiation have been assumed to be negligible.

The total enthalpy is defined as the sum of sensible and chemical enthalpies of the mixture,

$$\tilde{h} = C_{p_{mix}}(\widetilde{T} - T^o) + \Delta h^o_{f_{mix}} \tag{7.11}$$

where

$$C_{p_{mix}} = \sum_{\alpha} \widetilde{Y}_\alpha \, C_{p,\alpha} \ , \tag{7.12}$$

and,

$$\Delta h^o_{f_{mix}} = \sum_{\alpha} \widetilde{Y}_\alpha \, \Delta h^o_{f,\alpha} \; . \tag{7.13}$$

The reference temperature is T^o (298 K). Here too it is assumed that the entrained ambient air mixes only with the fully burnt mixture since the pilot is large compared to the main jet. Similar to the V–flame calculations, the effect of entrainment is accounted via the mean mixture fraction, $\tilde{\xi}$, whose value is 1 in the main jet and the pilot stream and 0 in the ambient air stream. The values of $C_{p_{mix}}$ and $\Delta h^o_{f_{mix}}$ are then approximated as:

$$\begin{aligned} C_{p_{mix}} \; &\approx \; \tilde{\xi} \, C_{p_{reac}} \; + \; (1 - \tilde{\xi}) \, C_{p_{air}}, \\ \Delta h^o_{f_{mix}} \; &\approx \; \tilde{\xi} \, \Delta h^o_{f_{reac}} \; + \; (1 - \tilde{\xi}) \, \Delta h^o_{f_{air}}, \end{aligned} \tag{7.14}$$

where $C_{p_{reac}}$ and $\Delta h^o_{f_{reac}}$ are for the reacting component of the mixture and $C_{p_{air}}$ and $\Delta h^o_{f_{air}}$ are for the air. Since the air stream is assumed to be comprised of only O_2 and N_2 at 298 K, $\Delta h^o_{f_{air}} = 0$. The values of $C_{p_{reac}}$ and $\Delta h^o_{f_{reac}}$ are obtained from laminar flame calculations and tabulated along with the mean reaction source terms as functions of $\widetilde{c_f}$, $\widetilde{c''^2_f}$ and $\widetilde{\epsilon_{c_f}}$. Thus the temperature is calculated from the local values of $\widetilde{c_f}$, $\widetilde{c''^2_f}$, $\widetilde{\epsilon_{c_f}}$, $\tilde{\xi}$ and $\tilde{h}$ via Eqs. (7.11) and (7.14). The mean density is then obtained from the ideal gas relation.

Such a formulation allows for specification of sub–adiabatic temperature boundary conditions in the pilot region through $\tilde{h}$. However, the measurements of Chen *et al.* (1996) indicate a radial variation in the pilot temperature values. At a radial location of 10 mm ($r/D \sim 0.83$) the measurements indicate that the temperature is less than 1500 K while at 20 mm it is about 2000 K. Lindstedt & Vaos (2006) considered two values for the pilot temperature: 1785 K and 2005 K in their calculations while Herrmann (2006) used a value of 1936 K. Measurements of the radial variation of the pilot stream temperature, ideal from the boundary condition point of view, have not been reported by Chen *et al.* (1996). In the present calculations we choose an ad–hoc value of 1950 K as the uniform pilot temperature in the reacting flow calculations.

The approach described above in Eq. (7.14) is an approximate way to account for the influence of the ambient air whilst using a purely premixed model for

turbulent combustion. The calculations of Herrmann (2006) support such an approximation for the lower Reynolds number flame F3. For higher Reynolds numbers the entrainment is larger and there could be some interaction of the ambient air with the flame front, especially at locations far from the nozzle. A more accurate way to account for this mixing is to consider the influence of stratification on the flame front characteristics and reacting mixture composition. However, our focus in the present study is on a purely premixed model and hence we proceed with the above approximation. Accordingly the tabulation for $\overline{\dot{\omega}}$, $\overline{\dot{\omega}c}$, $C_{p_{reac}}$ and $\Delta h^o_{f_{reac}}$ is based only on laminar flame calculations of stoichiometric methane–air mixture.

7.3.2 Results and discussion

7.3.2.1 V–flame

The cross stream profiles of longitudinal and transverse velocities at three z locations from the V–flame calculations are compared with experimental data in Fig. 7.13. The velocity predictions of the unstrained and the strained flamelet formulations are very close to each other. The quantitative agreement with the experimental velocity profiles is good over most of the x range except a small disagreement (about 5%) for the longitudinal velocity in the vicinity of $x = 0$. A similar disagreement of centreline velocities were reported by Robin *et al.* (2008) as well as the V–flame DNS of Bell *et al.* (2005). This was attributed to the recirculation zone behind the rod. However the centreline velocity in Fig. 7.13 is qualitatively similar to the DNS result (Bell *et al.*, 2005) whereas the velocity profile calculated by Robin *et al.* (2008) (not shown here) has a local minimum at $x = 0$. This could be because the stabilising rod has a semi–circular cross section in Robin *et al.* (2008) whereas it is circular here. The reason for choosing a semi–circular cross section in Robin *et al.* (2008) is unclear. Nonetheless the velocity profiles are well predicted in the present calculations and in particular the transverse velocities induced due to the streamline divergence through the flame brush are close to the experimental values.

The computed Reynolds mean progress variable, $\overline{c}$, is compared with the experimental data for two z locations in Fig. 7.14. The experimental values obtained

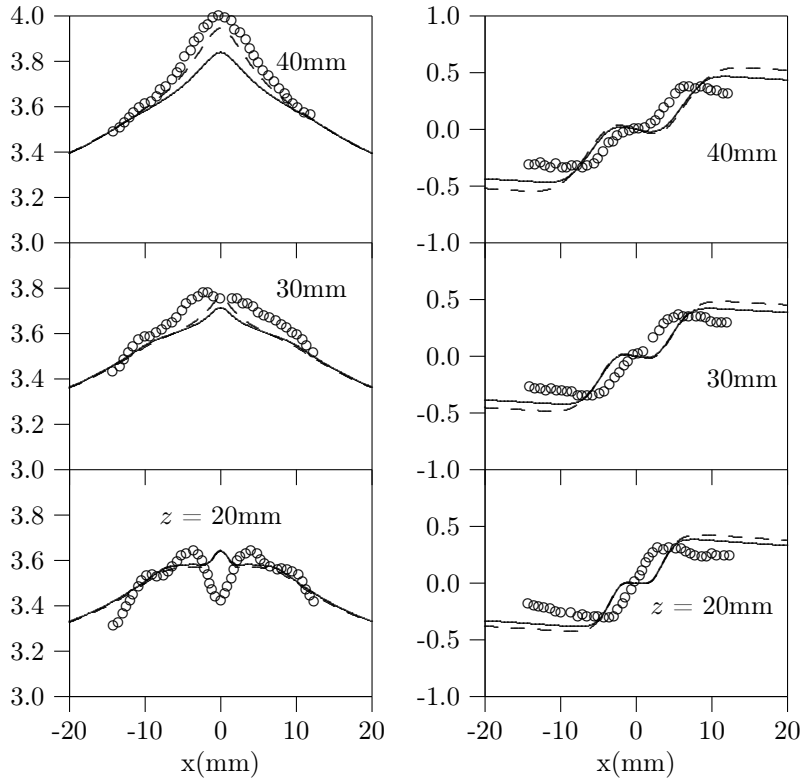

Figure 7.13: The calculated longitudinal (left) and transverse velocities (right) in m/s using the unstrained flamelets (dashed lines) and strained flamelets (solid lines) models are compared with the experimental data (∘) for the V–flame (Robin *et al.*, 2008) at three downstream locations.

from binarised tomographic images are shown in the figure. The Reynolds mean which is reported in the experiments, is obtained from the Favre mean using

$$\overline{c} = \tilde{c} + \frac{\tau \widetilde{c''^2}}{1 + \tau \tilde{c}}. \tag{7.15}$$

This equation results from the presumed β shape for $\widetilde{p}(\zeta)$ and it is derived in the Appendix A. Figure 7.14 suggests that the flame brush width is also well predicted by both the unstrained and the strained flamelet formulations although the former predicts slightly wider flame brush than the latter. The planar one–dimensional flame calculations in Section 7.2.2 showed similar trend in flame brush thickness predicted by the two models. The small difference in the unstrained and strained flamelets predictions is not surprising since the combustion conditions correspond

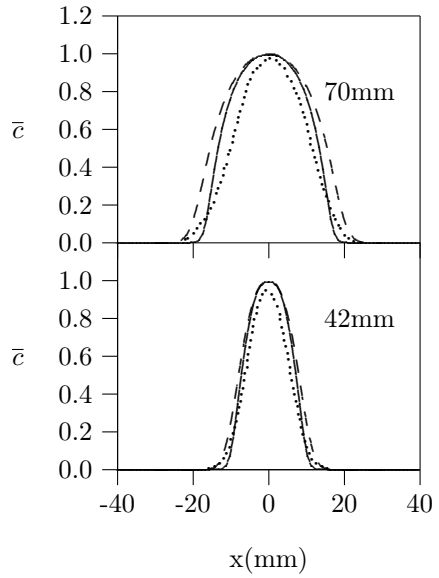

Figure 7.14: The calculated mean progress variable using the unstrained flamelets (dashed lines) and strained flamelets (solid lines) models are compared with the experimental data (dots) of the V–flame (Robin *et al.*, 2008) at two streamwise locations.

to the corrugated flamelets regime. The planar flame calculations have shown that for low turbulence intensities, the mean reaction rate values predicted by both the closures are not very different. The contours of $\overline{\dot{\omega}}/\overline{\rho}$ shown in Fig. 7.15 provide further evidence for this. The contours in the left half of Fig. 7.15 ($x < 0$) correspond to the strained flamelets and those in the right half ($x > 0$) correspond to the unstrained flamelets models. The values of $\overline{\dot{\omega}}/\overline{\rho}$ are nearly the same in the flame brush with the two models. The predictions of the reaction rate by these two models are likely to be significantly different for high turbulence intensities as observed in the planar flame calculations.

7.3.2.2 Bunsen flames

Calculations of non–reacting flow were performed to verify the turbulence modelling and the boundary conditions discussed in Section 7.3.1.2. Results for the F2 case are shown in Fig. 7.16, where the predictions of normalised mean axial velocity and mean turbulent kinetic energy, $\tilde{k}/k_o$ are compared to the experimental data. The bulk mean velocity at nozzle exit is U_o and the turbulent kinetic

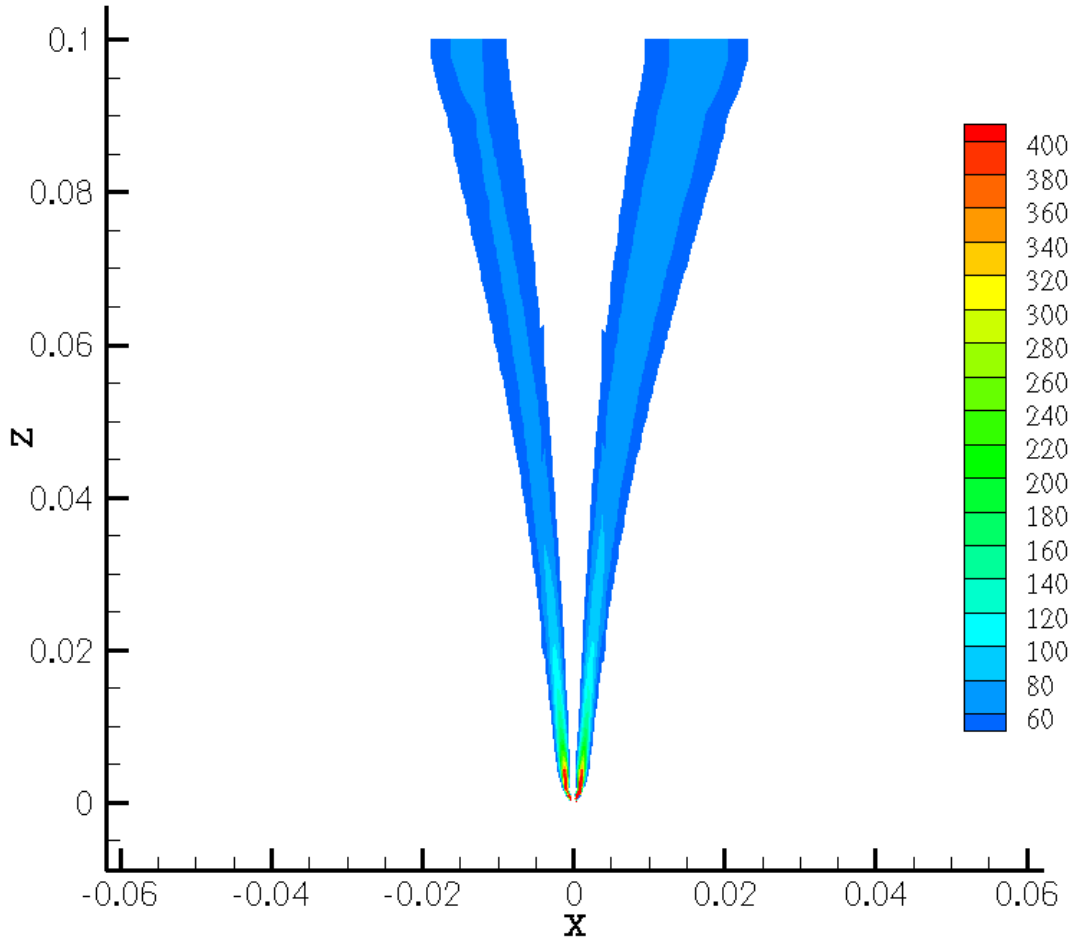

Figure 7.15: The contours of $\overline{\dot{\omega}}/\overline{\rho}$ (s^{-1}) from the V–flame calculations. The contours in $x < 0$ region are for the strained flamelets while those in $x > 0$ region are for the unstrained flamelets.

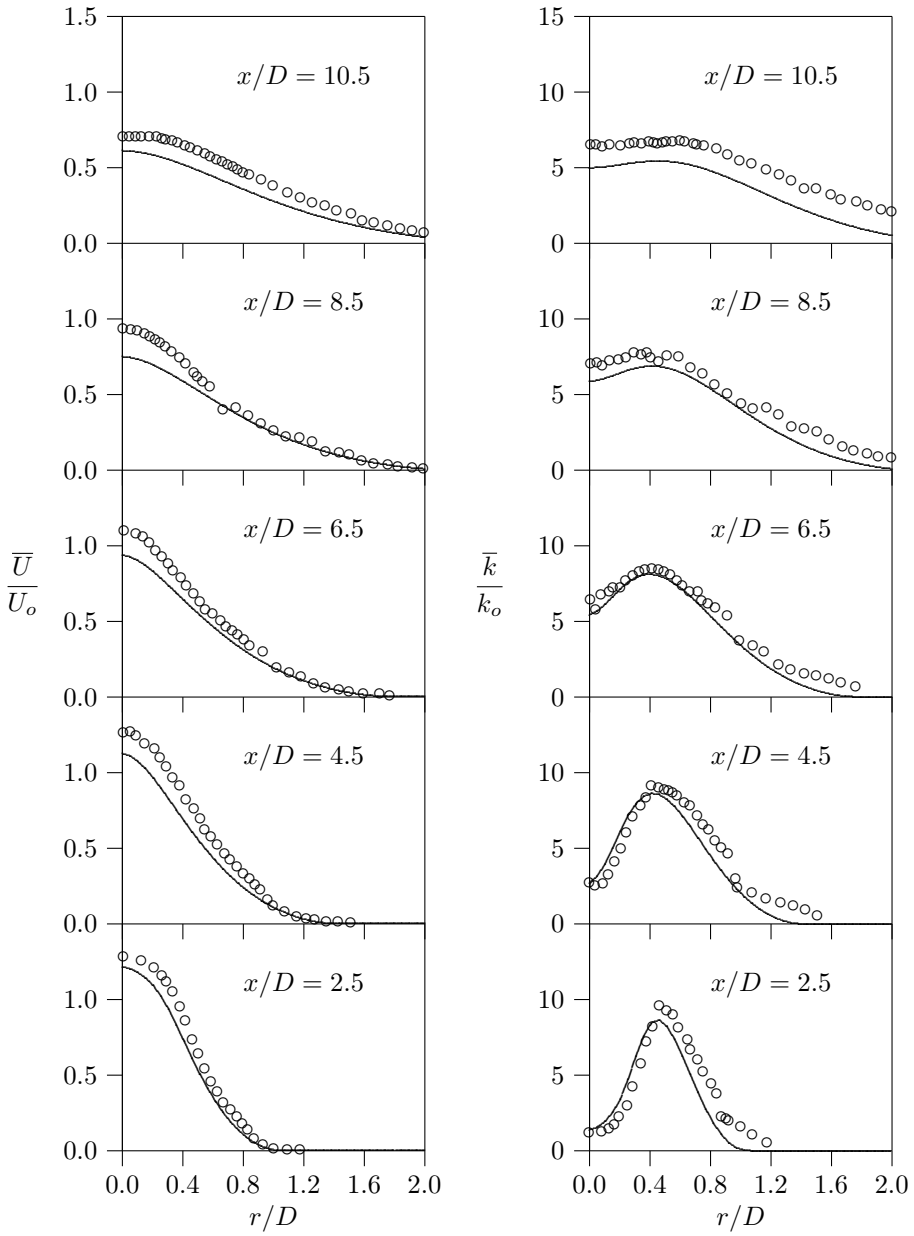

Figure 7.16: The normalised mean axial velocity and normalised mean turbulent kinetic energy from non–reacting flow calculations (solid lines) of case F2 are compared with the experimental data (○) of Chen *et al.* (1996).

energy at the centreline of the nozzle exit is k_o and their values for flame F2 are 50 m/s and 10.8 m^2/s^2 respectively (Chen *et al.*, 1996). The radial spread of the jet can be clearly seen in the velocity profiles which is in very good agreement with the experimental data. The centreline value seems to be slightly underpredicted at $x/D = 6.5$ and 8.5. The generation of turbulence in the shear layer is evident from the turbulent kinetic energy profiles showing a peak at roughly $r/D = 0.5$. Both the location and the magnitude of this peak are very well predicted upto $x/D = 8.5$. At $x/D = 10.5$, the predicted values are slightly lower than the experiment at all radial locations while the qualitative trend is well captured. Experimental data for F1 and F3 cases was not reported in (Chen *et al.*, 1996). However, assuming the jet obeys self–similarity, the experimental data of $\overline{U}/U_o$ and $\overline{k}/k_o$ for flame F2 are compared with the predictions for flames F1 and F3 in Figs. 7.17 and 7.18 respectively. The values of U_o are 65 m/s and 30 m/s and those of k_o are 12.7 m^2/s^2 and 3.82 m^2/s^2 for F1 and F3 respectively (Chen *et al.*, 1996). Figures 7.17 and 7.18 indeed show the self–similar behaviour of the jet and the predictions for these flames are also in good agreement with the experimental data. The overall good prediction of the non–reacting flow provides validation for the turbulence modelling.

The results of reacting flow calculations are presented next. Unless specified otherwise, the results in the following discussion are for the strained flamelets model. The normalised mean velocity, $\widetilde{U}/U_o$, and turbulent kinetic energy, $\tilde{k}/k_o$, computed for the three flames are compared to the experimental values in Figs. 7.19 and 7.20 respectively. While the mean velocities are well predicted at all axial locations, the values of the turbulent kinetic energy are overpredicted for locations close to the nozzle. At $x/D = 2.5$ this overprediction is about 40 % for the flame F1 while it is nearly a factor of 3 for the F3 flame. The agreement improves further downstream and for the flames F1 and F2, the agreement is very good at $x/D = 8.5$ and 10.5. Furthermore, even when the magnitudes are overpredicted, the radial location of the peak due to shear generated turbulence is well captured for all flames and at all locations. The values of $\tilde{k}$ predicted by Herrmann (2006) using a standard $\tilde{k}$–$\widetilde{\varepsilon}$ model with round jet correction, are lower than the values shown in Fig. 7.20. The present values, however, are closer to the predictions of Lindstedt & Vaos (2006) using Reynolds stress closure.

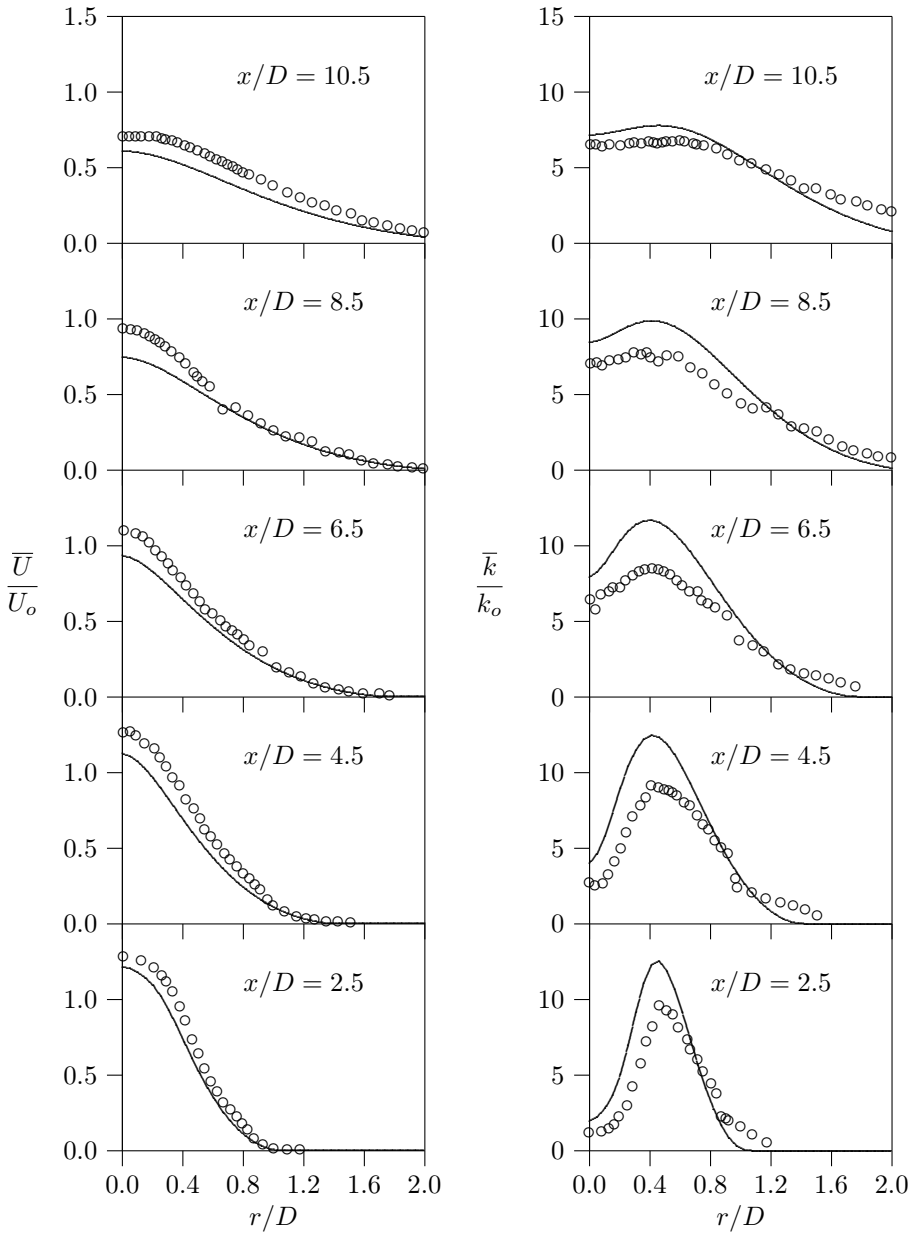

Figure 7.17: The normalised mean axial velocity and normalised mean turbulent kinetic energy from non–reacting flow calculations (solid lines) of case F1 are compared with the experimental data (○) of Chen *et al.* (1996).

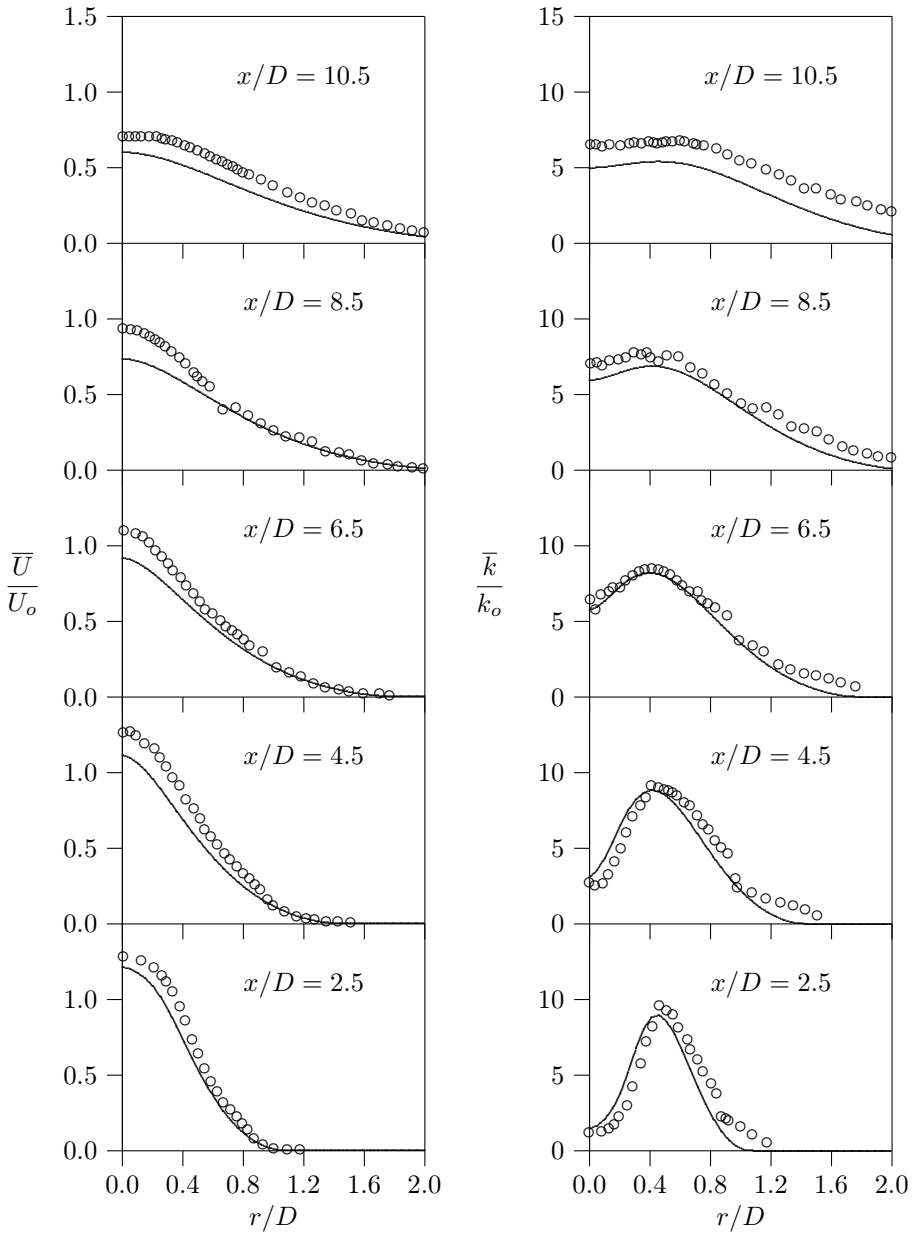

Figure 7.18: The normalised mean axial velocity and normalised mean turbulent kinetic energy from non–reacting flow calculations (solid lines) of case F3 are compared with the experimental data (○) of Chen *et al.* (1996).

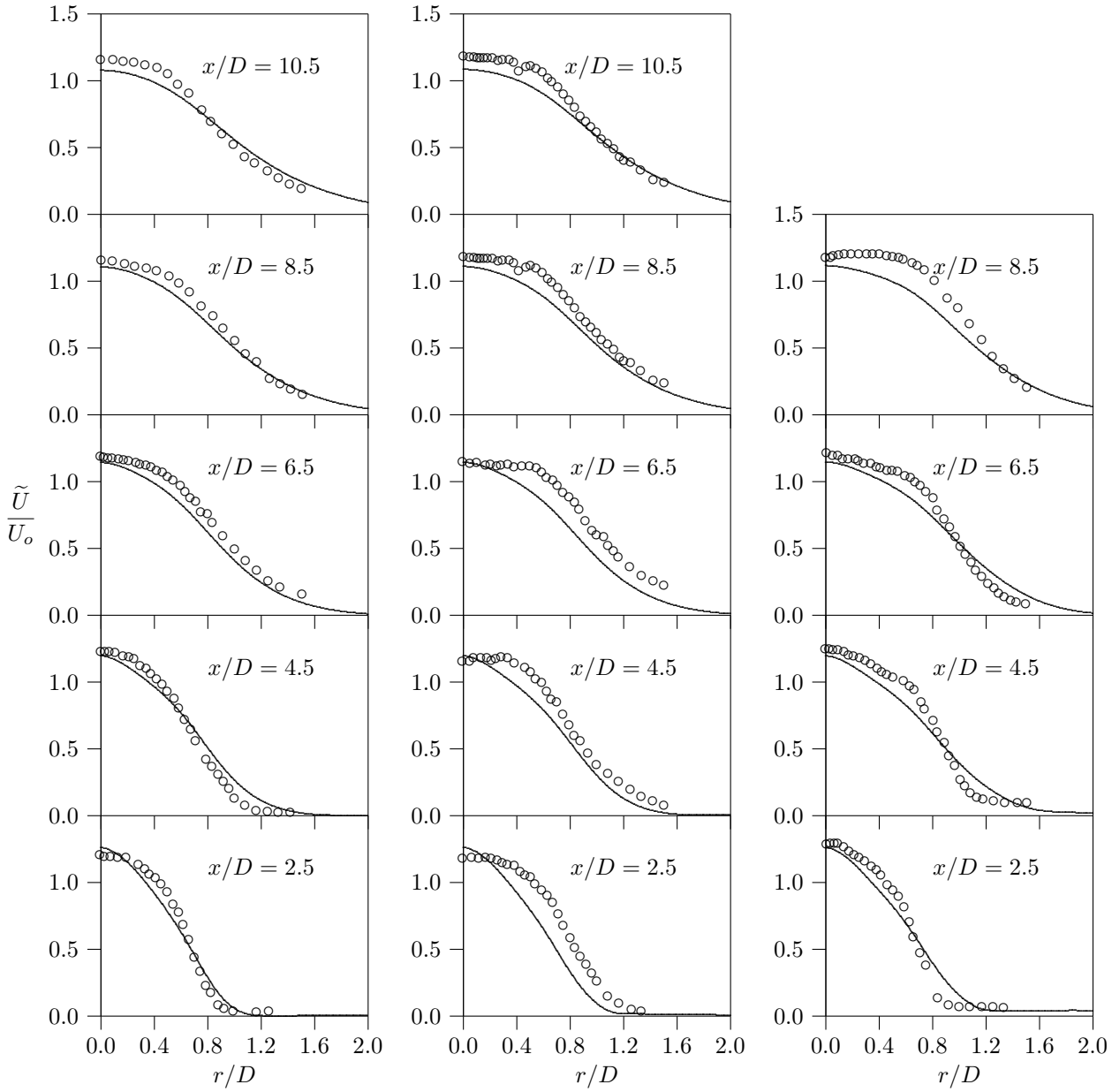

Figure 7.19: The normalised mean axial velocity from reacting flow calculations of flames F1 (left), F2 (center) and F3 (right) are compared with the experimental data of Chen *et al.* (1996).

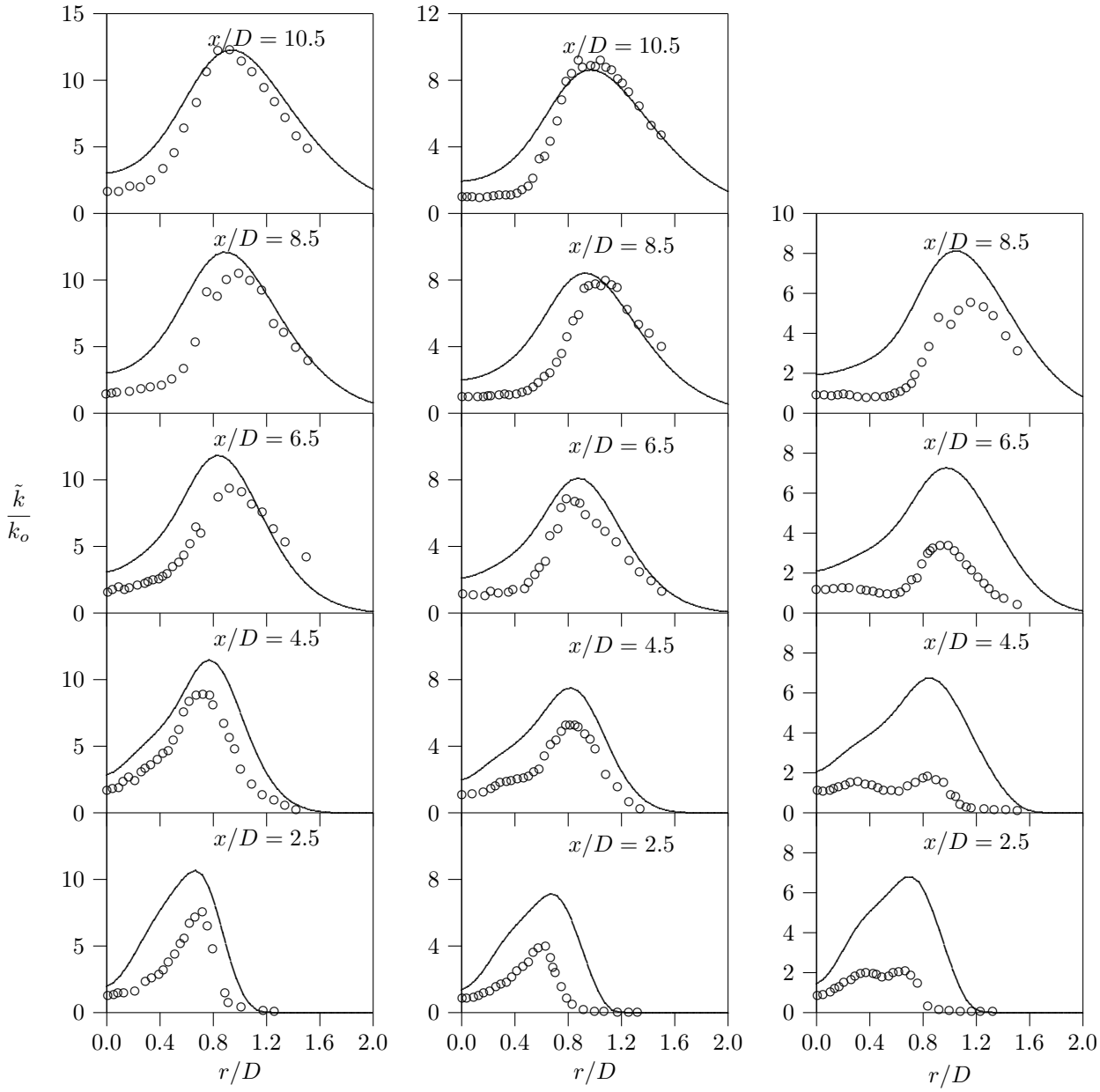

Figure 7.20: The normalised mean turbulent kinetic energy from reacting flow calculations using the strained flamelets model of flames F1 (left), F2 (center) and F3 (right) are compared with the experimental data of Chen *et al.* (1996).

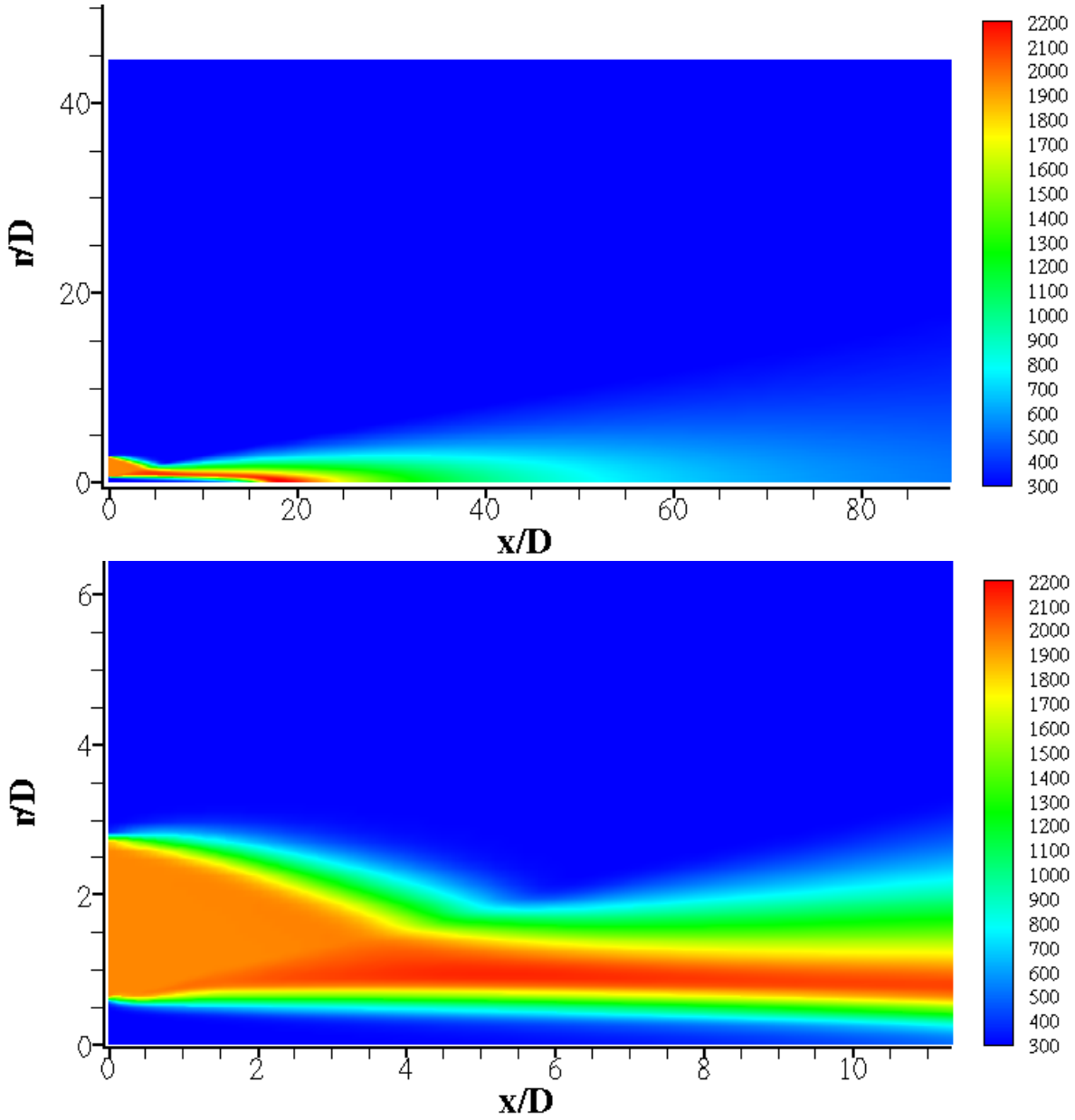

Figure 7.21: The contour plot of temperature (K) from the Bunsen flame calculations for case F3. The plot for the entire computational domain (top) and the region close to the nozzle exit (bottom) are shown.

In Fig. 7.21 the contour plots of temperature from the reacting flow calculations of flame F3 are shown. The plot above in Fig. 7.21 shows the temperature variation in the entire domain while the region close to the nozzle exit is shown in the plot below. This figure clearly shows that while the temperature at the pilot exit ($0.5 < r/D < 2.83$) is sub–adiabatic (1950 K), the temperature increases downstream as more heat is released from the chemical reactions. The measurements of Chen *et al.* (1996) show the same behaviour. This feature of the pilot–stabilised flames is very well captured in the calculations via the transport equation for the mean enthalpy, $\tilde{h}$. The interaction of burnt products with the ambient air and the resultant drop in temperature is also well captured in the simulation.

The calculated Reynolds mean progress variable, $\overline{c}$, and mean CH_4 mass fraction are compared with the experimental data for the three flames in Figs. 7.22 and 7.23 respectively. The agreement for CH_4 mass fraction is very good for all the cases indicating that the transport of $\widetilde{c_f}$ is well predicted. The quantity $\overline{c}$ from the calculations is obtained from Eq. (7.15) with an assumption $\widetilde{c''^2} \approx \widetilde{c_f''^2}$. Such an assumption seems, at first, reasonable since the diffusivities of c and c_f are nearly equal for methane–air mixtures. The radial decrease in calculated temperature due to mixing with the entrained cold air is clearly seen in Fig. 7.22. The prediction of $\overline{c}$ is reasonable and the rise in centreline temperatures is well predicted. However, there are some notable discrepancies between the calculated and measured values. For locations close to the burner exit, the calculated peak temperature is higher and the temperature rises quickly as in Fig. 7.22. The most plausible reason for this is the overprediction of $\tilde{c}$ and $\widetilde{c''^2}$, both of which are attributable to the pilot temperature boundary condition used. As noted earlier, the measured temperature at $r/D = 0.83$ is about 1500 K which is considerably lower than the value of 1950 K specified in the calculations. Consequently, at a given radial location in the flame brush, this leads to a higher mean temperature in the calculation compared to the experiment. Furthermore, the assumption $\widetilde{c''^2} \approx \widetilde{c_f''^2}$ results in an overprediction of $\widetilde{c''^2}$, because of sub-adiabatic pilot stream temperatures used to specify the boundary conditions for the enthalpy equation given in Eq. (7.10). These factors contribute to an overprediction of $\overline{c}$ through Eq. (7.15). A similar overprediction of mean temperature is seen in earlier studies

(Herrmann, 2006; Lindstedt & Vaos, 2006; Pitsch & de Lageneste, 2002; Schneider *et al.*, 2005) as well. Lindstedt & Vaos (2006) found that a pilot temperature of 2005 K was too high and hence performed calculations with a much lower value of 1785 K. However, this boundary condition mainly affects predictions close to the nozzle and its influence diminishes further downstream. For $x/D \geq 6.5$ the agreement is good for all three flames similar to previous study (Lindstedt & Vaos, 2006).

The overprediction of $\widetilde{c''^2}$ due to the pilot temperature boundary condition is evident in the comparisons of root mean square fluctuations, $\sqrt{\overline{c'^2}}$, with experimental data shown in Fig. 7.24. The $\overline{c'^2}$ value is obtained using

$$\overline{c'^2} = \frac{\tilde{c}^2 + \widetilde{c''^2}}{1+\tau\tilde{c}} \left\{ 1 + \tau \frac{\tilde{c}^2(1-\tilde{c}) + \widetilde{c''^2}(2-\tilde{c})}{\widetilde{c''^2} + \tilde{c}(1-\tilde{c})} \right\} - \overline{c}^2 \qquad (7.16)$$

and the computed value of $\widetilde{c''^2_f}$ which is taken equal to $\widetilde{c''^2}$. Equation (7.16) is derived in Appendix A. Similar to $\overline{c}$, values of $\overline{c'^2}$ are overpredicted at $x/D = 2.5$ and 4.5, but the prediction improves further downstream due to the reasons described above. However, the location of the peak in $\overline{c'^2}$ profiles is well predicted for all flames at all locations.

While Fig. 7.22 suggests some discrepancies in the prediction of mean temperature it will be interesting to compare the gradient of $\overline{c}$ with the experiments. Chen *et al.* (1996) define a flame brush thickness as $\delta_t \equiv (\partial\overline{c}/\partial r)^{-1}_{\max}$, and its calculated values are compared to the experimental data in Fig. 7.25. For flames F1 and F2 the experimental values of δ_t do not vary much while the calculated values show a slight increase with x/D. For flame F3, Chen *et al.* (1996) suggest that δ_t variation in the experiment follows the variation of peak $\overline{c'^2}$ value, which increases with x/D. The calculations show a similar correspondence between δ_t and the peak $\overline{c'^2}$ values. In general, the calculated flame brush thicknesses seem reasonably close to the experimental values for all flames.

The predictions of $\overline{c}$ and mean CH_4 mass fraction from the calculations using the unstrained flamelets closure are compared with the experimental data for the flame F2 in Fig. 7.26. The CH_4 comparisons indicate that the calculated flame is "hungrier" and consumes reactants much faster compared to the experiment. At $x/D = 8.5$ nearly all the fuel is consumed in the calculations, but a significant

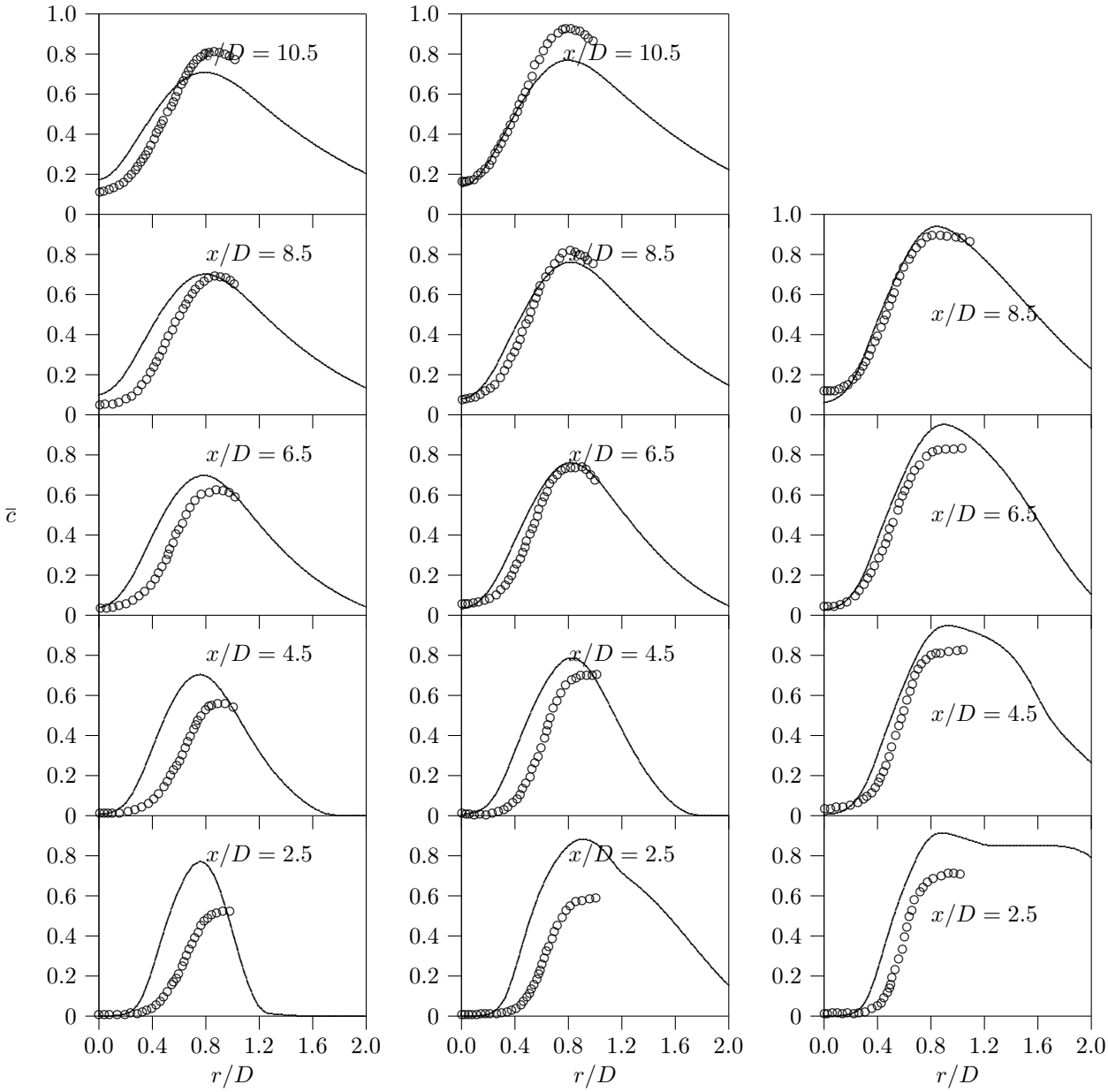

Figure 7.22: The mean progress variable, $\overline{c}$, using the strained flamelets model is compared with the experimental data of Chen *et al.* (1996) for flames F1 (left), F2 (center) and F3 (right).

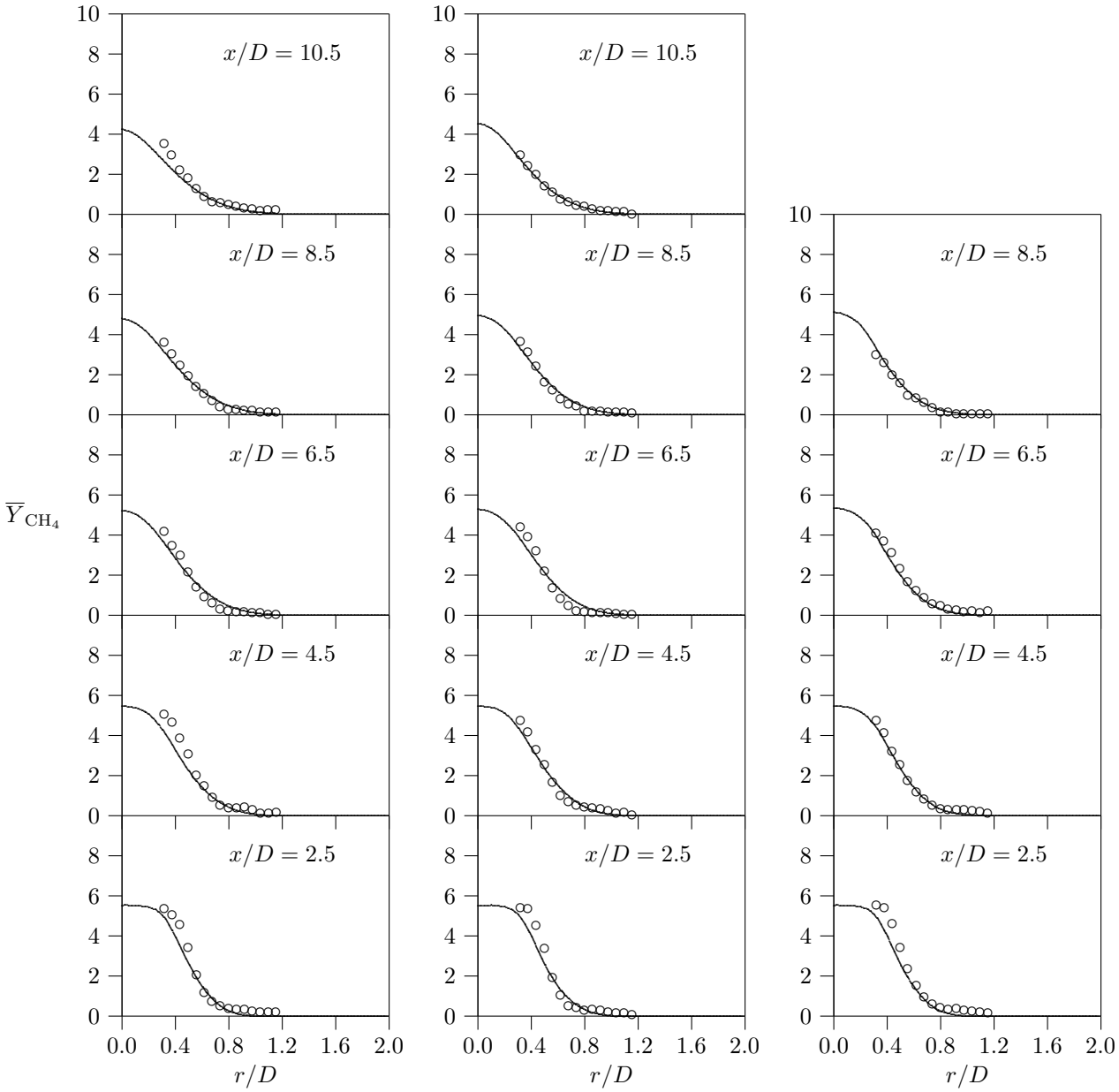

Figure 7.23: The mean CH_4 mass fractions from strained flamelets calculations are compared with the experimental data of Chen *et al.* (1996) for flames F1 (left), F2 (center) and F3 (right).

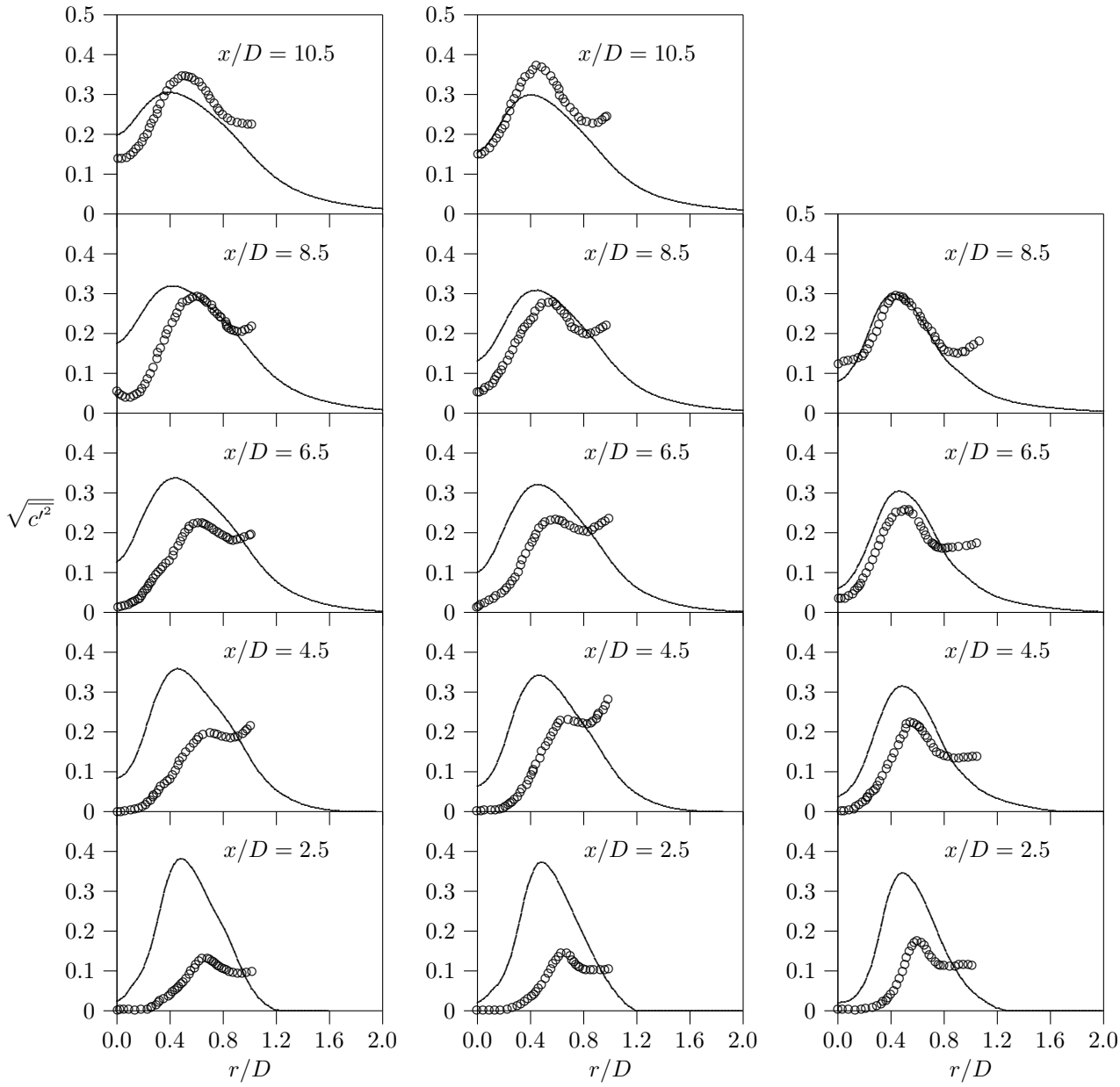

Figure 7.24: The root mean square progress variable fluctuations, $\sqrt{\overline{c'^2}}$, from strained flamelets calculations are compared with the experimental data of Chen *et al.* (1996) for flames F1 (left), F2 (center) and F3 (right).

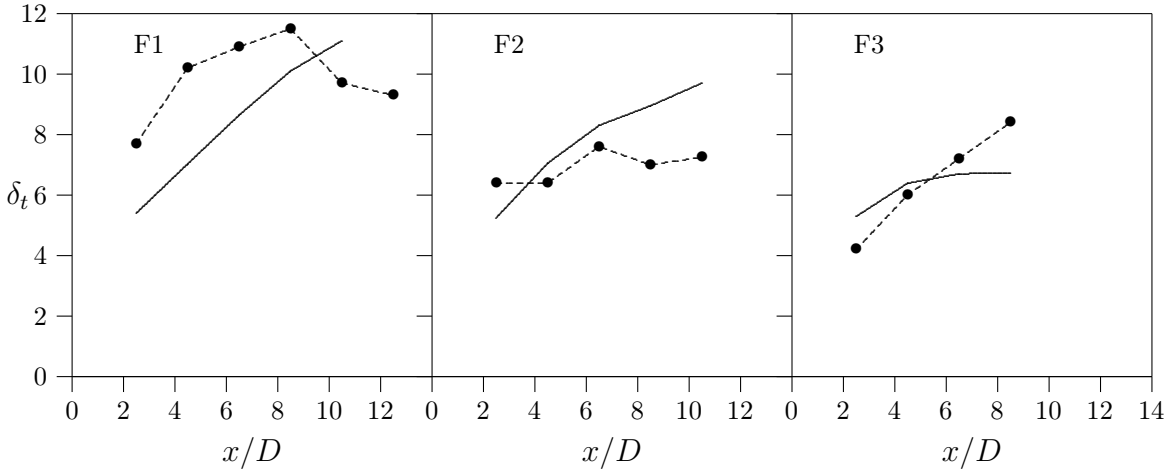

Figure 7.25: The turbulent flame brush thicknesses, δ_t (mm), from the strained flamelets calculations are compared with the experimental data (•) of Chen *et al.* (1996) for flames F1 (left), F2 (center) and F3 (right).

amount of fuel is present even at $x/D = 10.5$ in the experiment. The resultant temperature rise is also quicker compared to the experiment. The centreline value of the temperature at $x/D = 8.5$ is close to the fully burnt value in the calculations while it is close to the unburnt value in the experiment. This indicates that the mean fuel consumption rate is higher in the unstrained flamelets calculations resulting in a shorter and narrower flame brush compared to the experiment. The calculations of flames F1 and F3 (not shown) show similar results. Instantaneous experimental images in Chen *et al.* (1996) show that the flame front is strongly stretched by the turbulent eddies which are likely to attenuate the reaction rate. While the strained and unstrained flamelet models yield comparable mean reaction rates for low turbulence intensities (see Fig. 7.15), for very high turbulence intensities the unstrained flamelets overpredict the mean reaction rate as one would expect. This is consistent with the planar flame results reported earlier.

The major species predictions are compared to the experimental data in Fig. 7.27. As with Eq. (7.14), the influence of mixing with entrained air on the species mass fractions is accounted by $\overline{Y}_i \approx \widetilde{\xi}\,\overline{Y}_i^R + (1-\widetilde{\xi})Y_i^A$ where $\overline{Y}_i^R$ is for the reacting component of the mixture and Y_i^A is for air. Note that Y_i^A is zero for all species except O_2 and N_2. The agreement is quite good for flame F3

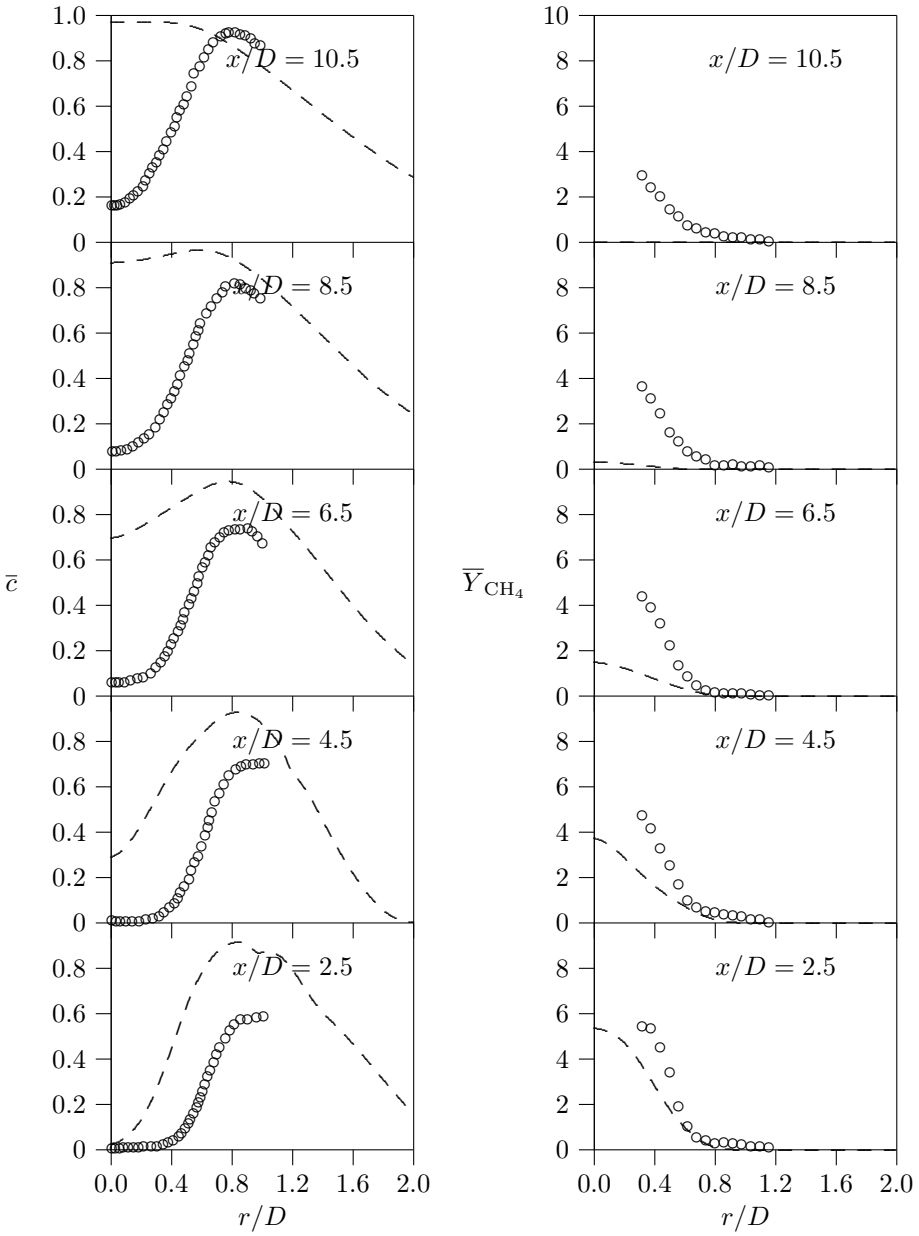

Figure 7.26: The mean progress variable, $\overline{c}$, (left) and mean CH_4 mass fraction (right) from the unstrained flamelet calculations are compared with the experimental data of Chen *et al.* (1996) for flame F2.

for all three major species: O_2, CO_2 and H_2O. For flames F1 and F2, H_2O is well predicted, but there is an overprediction of O_2 and underprediction of CO_2 for $x/D \geq 6.5$ which is probably due to the approximate treatment of mixing with entrained air. Nonetheless, the approximation seems reasonable since the qualitative trends are very well predicted. For instance, the rise in O_2 and drop in H_2O mass fractions in the radial direction due to mixing with entrainment air are well captured in the calculations. The O_2 mass fraction for flame F1 at $x/D = 2.5$ is overpredicted for $r/D \geq 0.8$, which is similar to the predictions of Herrmann (2006) and Lindstedt & Vaos (2006), the reasons for which are not clear. The overall level of agreement for the major species predictions is good.

The predictions of the minor species: CO, H_2 and OH, are compared with the experimental data in Fig. 7.28. While H_2 and OH are well predicted for all three flames, CO is considerably overpredicted. For flame F3 the CO overprediction is by nearly a factor of 2.5 while for flames F1 and F2 it is by a factor of 2. The CO predictions of Herrmann (2006) are similar to those shown in Fig. 7.28. The CO predictions of Lindstedt & Vaos (2006) are also similar to those shown in Fig. 7.28 for flame F1. However, their predictions are closer to experimental data for flame F3 and a typical comparison is shown in Fig. 7.29.

Figure 7.29 also shows typical sensitivity of minor species predictions to the RtP flamelets boundary conditions. The results using the equilibrium mixture composition for the product stream is shown in Fig.7.29a, whereas the Fig.7.29b shows the results when the product stream contains only CO_2 and H_2O. As one can observe in this figure, minor species predictions are sensitive to the flamelets boundary conditions, but the major species do not show such a sensitivity. For the results reported in this study, the equilibrium composition is used as product stream for the flamelets. This sensitivity may be reduced if one uses a second progress variable to represent the chemical species with slow time scales, since the progress variable used here represents the overall progress of the chemical reactions. The carbon monoxide is clearly identified to have a slow chemical time scale by Peters & Williams (1987). The choice for the second progress variable is unclear and will be explored in future. Since an overall progress variable is used to represent the combustion, its influence on CO prediction is verified using an

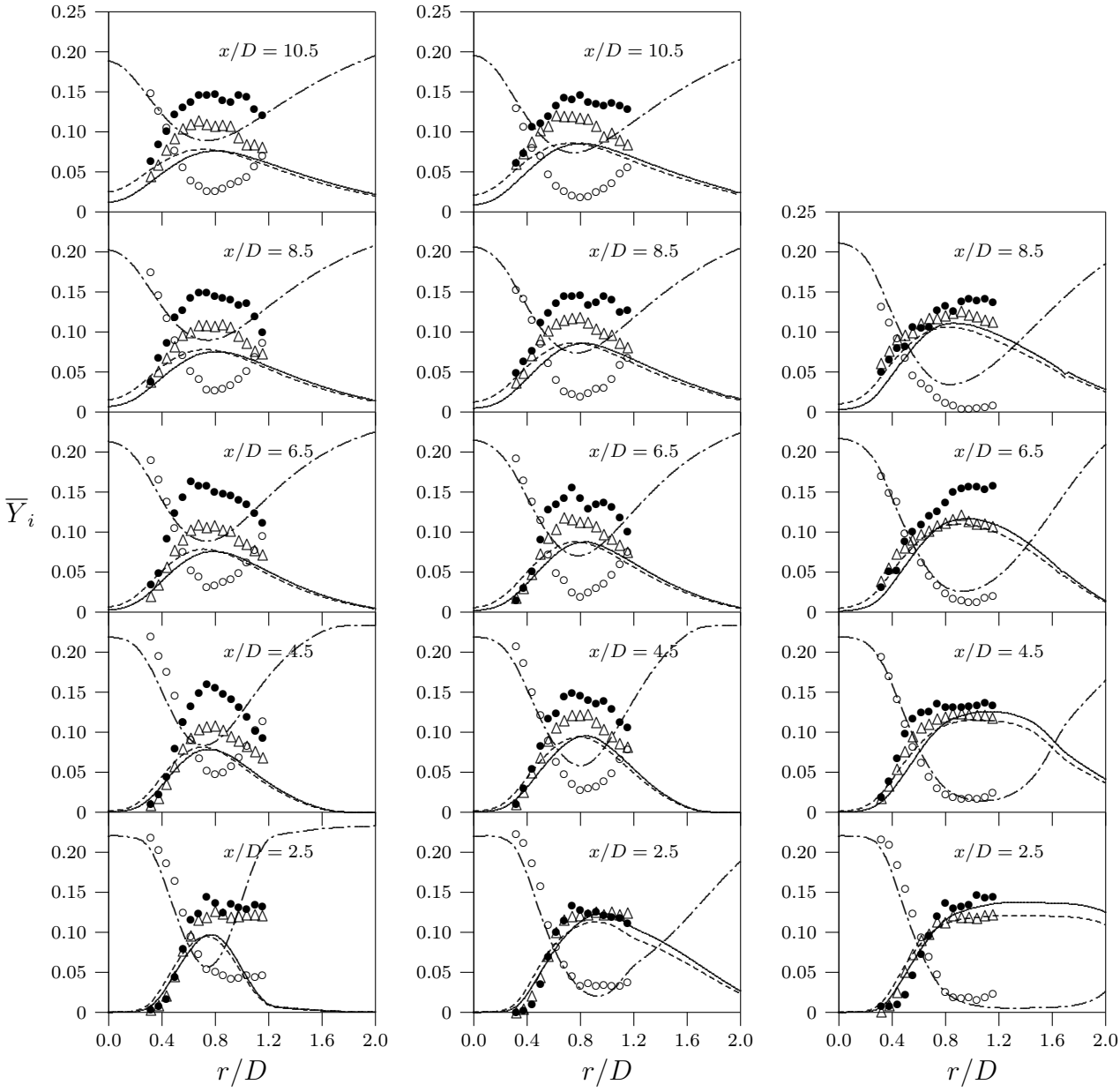

Figure 7.27: The major species mass fractions: O_2 (○, _ _ _), CO_2 (●, ___) and H_2O (△, _ _), from strained flamelets calculations are compared with the experimental data (symbols) of Chen *et al.* (1996) for flames F1 (left), F2 (center) and F3 (right).

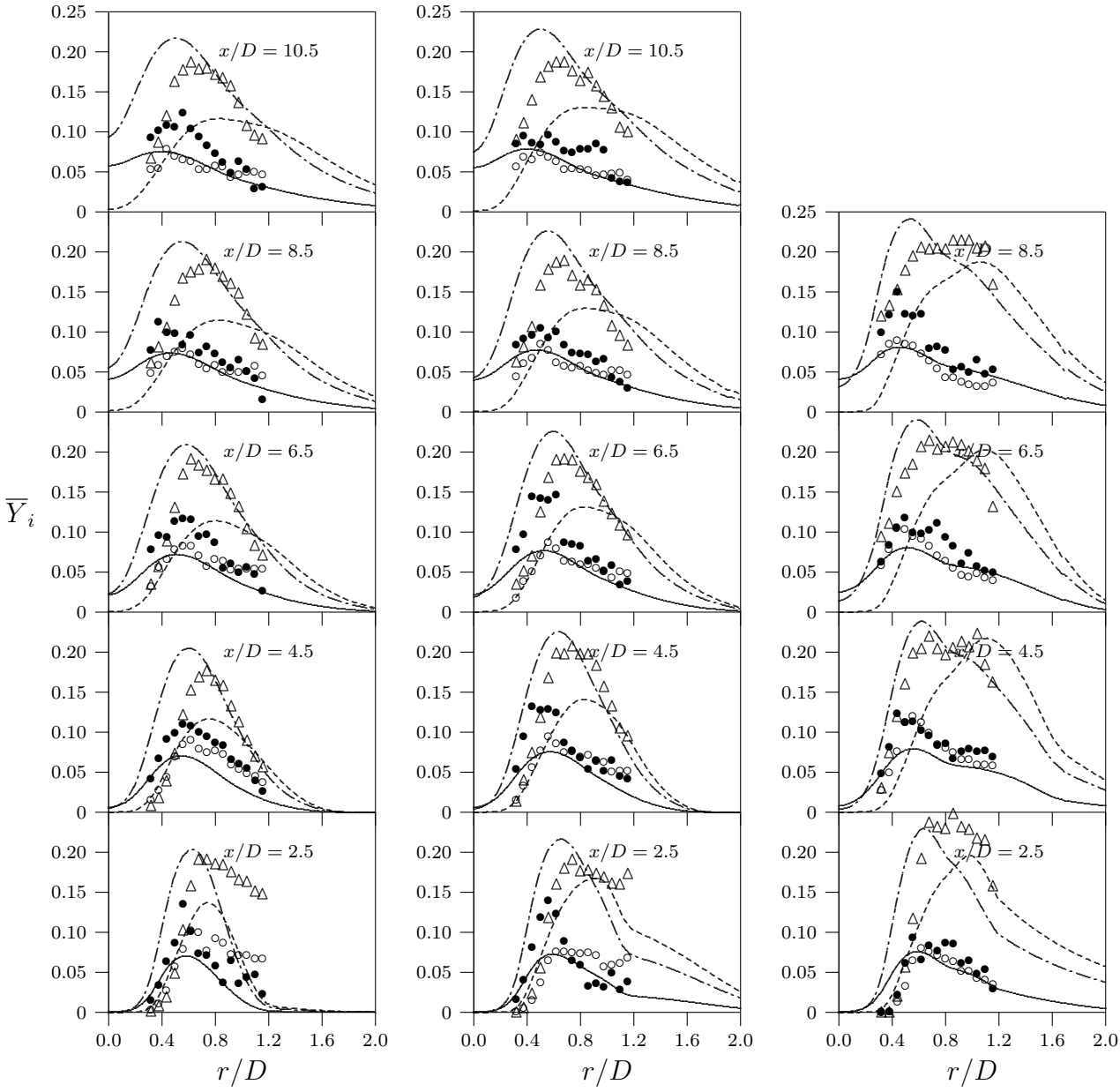

Figure 7.28: The minor species mass fractions: 10×CO (○, _ _ _) , 100×H_2 (●, __) and 75×OH (△, _ _), from strained flamelets calculations are compared with the experimental data (symbols) of Chen *et al.* (1996) for flames F1 (left), F2 (center) and F3 (right).

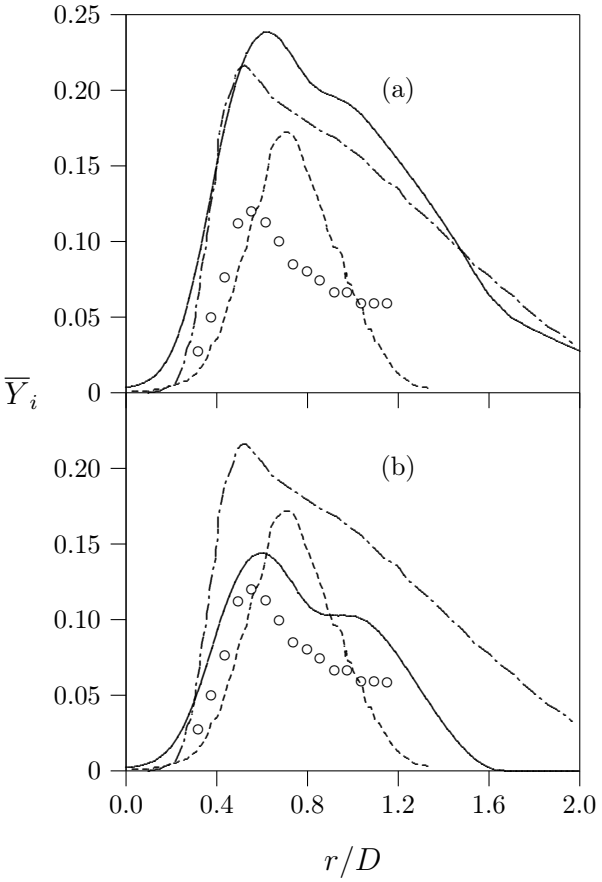

Figure 7.29: The predictions of $10 \times Y_{\mathrm{CO}}$ using strained flamelets model (—) are compared with predictions of Herrmann (2006) (_ - _) and Lindstedt & Vaos (2006) (_ _) for flame F3 at $x/D = 4.5$. The sensitivity of strained flamelets predictions to RtP flamelet boundary conditions are shown: (a) equilibrium mixture composition for product stream, (b) product stream comprising of only CO_2 and H_2O.

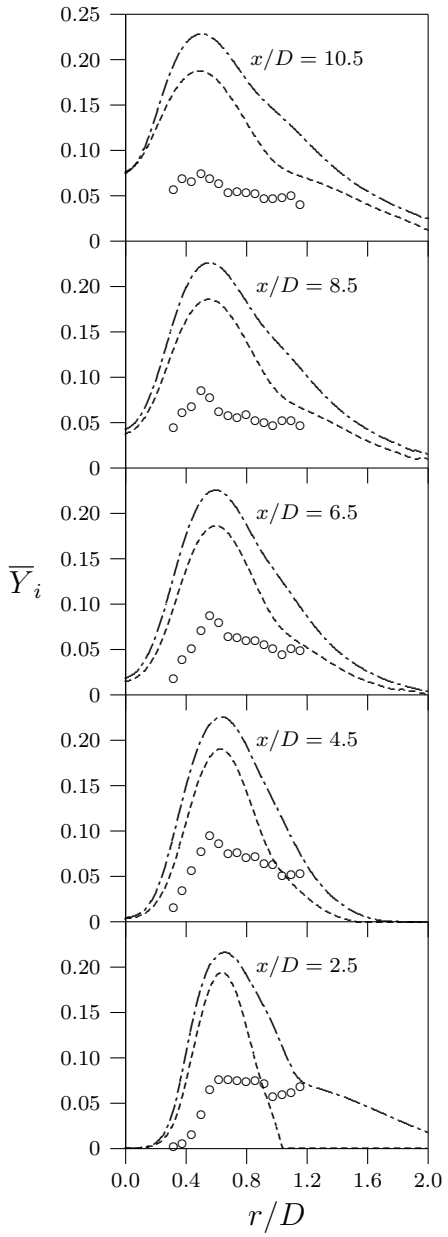

Figure 7.30: The predictions of 10×CO from strained flamelet calculations using two definitions of progress variable: c_f (_ _ _) and c_p (_ _) are compared with the experimental data of Chen *et al.* (1996) for flame F2.

alternative definition, given by Fiorina *et al.* (2003)

$$c_p = \frac{Y_{\mathrm{CO}} + Y_{\mathrm{CO_2}}}{Y_{\mathrm{CO,eq}} + Y_{\mathrm{CO_2,eq}}}. \tag{7.17}$$

It is necessary to include $Y_{\mathrm{CO_2}}$ in the above definition to ensure that c_p varies monotonically in the flamelets. The CO values calculated using the c_p progress variable are compared with those using c_f for flame F2 in Fig. 7.30. It appears that the improvement in CO predictions is marginal.

7.4 Summary

RANS calculations of turbulent premixed flames are performed to assess the strained flamelets model described in Chapter 4. The mean scalar dissipation rate, which is a modelling parameter, is closed via the algebraic model derived in Chapter 5. Calculations of statistically planar one–dimensional flames are performed to test the mean reaction rate closure and laboratory flame calculations are used to test the overall predictive ability of the model. A single set of model parameters is used in all the calculations.

Calculations of planar one–dimensional flames are performed to compare the predictions of the strained flamelets closure with those of algebraic closure of Bray (1979) and the unstrained flamelets closure. Two sets of flames, one in the corrugated flamelets regime with the value of flame stretch factor K = 0.15 and the other in the thin reaction zones regime with K = 1.0, are considered for stoichiometric methane–air mixtures. The results show that the flame brush thickness, δ_t, increases with u'/s_L^o for a given K value, as one would expect, for all three reaction rate closures. The algebraic closure viewing the flame front as a thin interface predicts the broadest flame brush while the closure proposed here predicts the narrowest flame brush. The turbulent flame speed, S_T, predicted by the three closures is compared to the experimental data of Abdel-Gayed *et al.* (1987). The algebraic closure overpredicts the mean reaction rate and hence the turbulent flame speed for all flames considered here. The unstrained flamelets closure predicts turbulent flame speed reasonably well for flames in the corrugated flamelets regime but overpredicts for flames in the thin reaction zones regime. This is because the fluid dynamic straining reduces the burning rate. This effect

is well captured by the strained flamelets closure and the flame speeds predicted by this closure are close to the experimental data for flames both in the corrugated flamelets and the thin reaction zones regimes. Calculations for lean propane–air mixture with a Lewis number greater than unity confirm the hypothesis of Bradley *et al.* (1992) that the flame speeds correlate better with the parameter KLe than with K.

The flame speeds predicted by this strained flamelets closure are close to the values of Bradley *et al.* (1994) who used stretch rate to parametrise the flamelets and employed second order turbulence closure by solving Reynolds stresses and turbulent scalar flux transport equations. The agreement in the flame speed values of Bradley *et al.* (1994) and that of the present study, despite a vast modelling difference, is likely due to insignificant quantitative differences in the predicted mean reaction rate values for the range of flow and flame conditions considered here. However, it is clear that the stretch effects are to be included in the modelling and the scalar dissipation rate based approach seems attractive for this.

Laboratory flames of two different configurations: rod stabilised V–flame of lean methane–air (Robin *et al.*, 2008) and pilot stabilised Bunsen flames of stoichiometric methane–air mixtures (Chen *et al.*, 1996) are also calculated. The conditions of the V–flame correspond to the corrugated flamelets regime and the Bunsen flame conditions correspond to the thin reaction zones regime. The results of V–flame calculations using the strained flamelets model are in good agreement with the experimental data. The longitudinal and transverse velocities and the Reynolds mean progress variable, $\overline{c}$, are well predicted. Results of an unstrained flamelets model are close to the results of the strained flamelets model. This is because the mean reaction rate values predicted by the two models are nearly equal for the V–flame, which is in the corrugated flamelets regime. This is consistent with the planar flame results.

Calculations of Bunsen flame with the unstrained flamelet model predicted a flame brush which is much shorter and narrower compared to the experiment, indicating an overprediction of the mean reaction rate. The flame front in these flames is strongly stretched by the turbulent eddies which are likely to attenuate

the reaction rate. This is not accounted by the unstrained flamelets model resulting in an overprediction of mean reaction rate. On the other hand, the strained flamelets model predictions of the flame brush dimensions are in good agreement with the experimental values. From flamelet modelling point of view, this underscores the importance of appropriately accounting for the local fluid–dynamic effects on the flamelet characteristics, and the scalar dissipation rate is a good parameter to represent this.

The mean velocity and turbulent kinetic energy of the Bunsen flame are reasonably well predicted by the strained flamelet calculations. The mean and RMS of the progress variable are also well predicted although a slight overprediction is observed at locations close to the nozzle which is attributed to the higher pilot temperatures used in the calculations as in earlier studies. However, the flame brush thickness, which is related to the gradient of the mean progress variable, is well predicted. The predicted major and minor species mass fractions are also in reasonable agreement with the experimental data. It is assumed in the present calculations that the combustion is in a purely premixed environment and the mixing of entrained air is only with the combustion products. This assumption yields good results for the lower Reynolds number flame F3 while for flames F1 and F2, some discrepancies in the major species predictions are observed due to such an approximate treatment. However, CO mass fraction is consistently overpredicted which is likely due to the misrepresentation of the slow CO oxidation in the flamelet by an overall progress variable. Calculations with a progress variable based on a combination of CO and CO_2 yielded little improvement over calculations with a fuel based progress variable. The predictions of minor species such as CO are also sensitive to the RtP flamelets boundary conditions. In the present calculations, the product stream in RtP flamelets has an equilibrium composition. However, considering RtP flamelets whose product stream comprises of only CO_2 and H_2O yields considerably different predictions for the minor species while the major species predictions are not affected. The current flamelet modelling needs to be improved to capture the statistics of the species with slow chemical time scales such as CO and the minor species.

Chapter 8

Conclusions and Future work

In this thesis laminar flamelet modelling of turbulent premixed flames was studied in the RANS context. A strained flamelet model is proposed and the scalar dissipation rate of the progress variable is used to parametrise the flamelets which are represented by Reactant–to–Product opposed flow laminar flames. Shapes are presumed for the pdfs of the progress variable and the conditional scalar dissipation rate. Using physical arguments, the conditional mean scalar dissipation rate is closed by relating it to the unconditional mean dissipation rate, which is a modelling parameter. An algebraic model for the unconditional mean scalar dissipation rate, valid for large Reynolds and Damköhler number flames, was derived based on recent findings of scalar dynamics in turbulent premixed flames which are different from the passive scalar scenario. The mean scalar dissipation rate model lead to an algebraic expression for the turbulent flame speed which, in this study, is defined as the propagation speed of the flame brush leading edge. The predictions of the mean scalar dissipation rate model were in reasonable agreement with DNS data of turbulent premixed flames in different combustion regimes. The predictions of the turbulent flame speed expression were also in good agreement with experimental data from a wide range of flame configurations and conditions, with the same set of model constants, providing an indirect validation for the scalar dissipation rate model.

RANS calculations of turbulent premixed flames provide evidence supporting the central hypothesis of the model formulation in this work; flamelet models that appropriately account for the turbulence fluid dynamics influence on the flame

front characteristics have a wider regime of applicability than those that do not. Calculations of statistically planar one–dimensional flames show that for conditions in the corrugated flamelets regime, the unstrained flamelets model predicts turbulent flame speeds reasonably close to experimental data, whereas for conditions in the thin reaction zones regime the flame speed is overpredicted. This is because the reaction rate attenuation due to fluid dynamic stretch, likely to be considerable in the latter regime, is not captured by the unstrained flamelets model resulting in an overprediction of the mean reaction rate. That the strained flamelets model using a scalar dissipation rate parametrisation is able to capture this is encouraging. Calculations of laboratory flames reflect the same characteristics of the models. For a flame in the corrugated flamelets regime, the V–flame, the strained and unstrained flamelets models predict flame brush structures in close agreement with experimental data but for the Bunsen flames which are in the thin reaction zones regime the unstrained flamelets model predicts a smaller flame brush as a result of the mean reaction rate overprediction. The flame brush structure predicted by the strained flamelets model is in much better agreement for these flames. The strained flamelets model is also able to give good predictions of the major species mass fractions although minor species predictions show room for improvement. The minor species predictions appear sensitive to product stream composition in RtP flamelets while major species predictions are not. Furthermore, for species such as CO which is known to have slow chemistry in the post flame region, a single progress variable is probably insufficient to capture its thermochemistry accurately. A formulation involving two progress variables, one representing the slow and the other representing the fast time scales, might be more successful in this regard and this could be explored in future studies.

8.1 Recommendations for future work

There are many topics worthy of further investigations based on the contributions of the present work. Some of these are discussed below.

8.1.1 Lewis number effects

The nature of the flamelet response to straining entailed considerations of the mixture Lewis number. This was appropriately addressed in the strained flamelet model, as evidenced from the one–dimensional flame calculations for the lean propane–air mixture in Chapter 7. However, non–unity Lewis number effects were not explicitly accounted for in the modelling of the mean scalar dissipation rate. Accordingly, data corresponding to mixtures with Lewis numbers close to unity were considered for the validation of this model in Chapters 5 and 6. The Lewis number dependence of the mean scalar dissipation rate needs to be investigated further. A recent study by Chakraborty *et al.* (2009) suggests that the turbulence–scalar interaction term, a leading order term in the transport of mean scalar dissipation rate, shows a Lewis number dependence. Such investigations can form the basis for incorporating an explicit Le dependence in the dissipation rate model.

8.1.2 Sensitivity to turbulence closure

The influence of the underlying turbulence model on the predictions using the strained flamelet model need to be investigated. In the present study all calculations employed the standard $\tilde{k}$–ε turbulence closure. The calculations of Bradley *et al.* (1994) using the stretch rate based flamelet model show that predictions with standard $\tilde{k}$–ε closure can be quite different from those with second order turbulence closure. The burning rate factor, P_b, a central quantity in the flamelet model of Bradley *et al.* (1994), is directly influenced by the turbulence quantities $\tilde{k}$ and $\widetilde{\varepsilon}$. In the scalar dissipation based model studied in the present work, the influence of the turbulence field on the mean thermochemical quantities is predominantly via the mean scalar dissipation rate. Hence it might be worthwhile to investigate the extent to which second order turbulence closures affects the predictions of the strained flamelets model.

8.1.3 Unsteady strain, non–adiabaticity and curvature

The strained flamelets model employs steady strained adiabatic RtP laminar flames as the canonical flamelet configuration. In reality however, the turbulent flame front experiences unsteady strain rate. Hawkes & Chen (2006) study the response of a laminar flamelet to unsteady strain by imposing inlet velocity oscillations at a particular frequency, and find that point–wise quantities in the flamelet are likely display quasi–steady behaviour. While this result is by no means general, it is encouraging and lends some validity to the use of steady strained flamelets. However, one suspects that beyond a certain frequency the quasi–steady behaviour might break down and unsteady response might have to be rigorously incorporated in the flamelet formulation. Such a formulation might be critical for instance in the prediction of thermo–acoustic oscillations of premixed flames.

Another important factor to consider is curvature. Traditionally turbulent eddies are thought to influence the flame front via strain rate and curvature, together imposing a total stretch rate. It can be argued that the present formulation prescribes the scalar dissipation rate description as an alternative to the strain rate + curvature description. Still, the flamelet structure in highly curved portions of a turbulent flame might not correspond to that given by the scalar dissipation parametrisation of a purely strained laminar flame. In other words, the choice of the RtP flamelet configuration, while accounting for the strain rate directly, does not explicitly account for curvature effects. Whether it is necessary at all to treat these two influences separately in the context of scalar dissipation rate parametrisation is worth examining using DNS data. If it is, then one could address this by considering a canonical curved laminar flamelet in addition to the purely strained flamelet.

Also, in many practical scenarios effects of non–adiabaticity could be important. For instance, such effects can occur for flames in confined geometries with significant flame wall interactions. The asymptotic analysis of Libby *et al.* (1983) considers non–adiabatic effects in RtP flames in great detail. For flamelet model formulation, following van Oijen & de Goey (2000), one could consider calculating RtP flamelets for different product stream enthalpies and generate a look–up

table with enthalpy as the additional dimension.

8.1.4 Stratified combustion

A similar approach can be adopted to extend the strained flamelets closure for application to stratified combustion. Working with the progress variable definition of Bray *et al.* (2005) that accounts for local stoichiometry, together with a mixture fraction, the strained flamelet model can be employed in calculations of stratified flames. This would then involve calculating RtP flamelets of various equivalence ratios and generating the look–up table with the mixture fraction moments as the additional dimensions.

8.1.5 Statistically non–planar flames

An interesting result obtained in the thesis from studying the applicability of KPP analysis to multi–dimensional flames is the influence of mean curvature on the propagation speed of flame brush leading edge. The analysis in Chapter 6 indicates that a positive mean curvature enhances the leading edge propagation speed (see Eq. (6.17)). While it is difficult to study statistically steady curved flames in experiments, the KPP result can still be compared with calculations of statistically non–planar one–dimensional flames. Such calculations would also facilitate investigating the effects of mean curvature in great detail.

8.1.6 Modelling for CMC

As noted in Chapter 2, implementation of CMC for premixed combustion involves two main modelling challenges: closure for the conditional mean dissipation rate and conditional mean reaction rate of the progress variable. The closure for the former based on physical arguments, presented in Chapter 4, can be evaluated for applicability with CMC. This closure can be described simply as estimating the conditional mean scalar dissipation rate from the unconditional mean quantity based on flamelet assumption. As a first step, this closure can be validated with DNS data by taking the unconditional mean dissipation rate value from the DNS.

If such a validation is promising, the closure together with the algebraic mean scalar dissipation rate model presented in Chapter 5 can be assessed by making comparisons with DNS data. Alternatively, obtaining a conditional mean scalar dissipation rate closure from the analysis of the pdf transport equation, Eq. (4.21), is also worth exploring.

8.1.7 Modelling for LES

For turbulent flames with complex flow features LES is becoming increasingly preferred. However, as noted in the Introduction, the chemical reactions occur at scales that are unresolved in LES and hence RANS type combustion models are relevant for LES. Indeed, many combustion models employed in LES are based on extension of RANS modelling ideas (Poinsot & Veynante, 2001). Typically, for LES of premixed flames, the balance equation for filtered progress variable is solved. In flame surface density based approaches the filtered reaction rate, combined with the diffusive flux term (terms on the r.h.s of Eq. (2.13)) are closed via the displacement speed s_d (see Eq. (6.8)) as (Boger *et al.*, 1998; Fureby, 2005)

$$\widehat{\rho s_d |\nabla c|} \approx \rho_u s_L^o \Xi |\nabla \widehat{c}| \ , \tag{8.1}$$

where a $\widehat{\ }$ denotes filtered quantities. The flame wrinkling factor, Ξ, is closed as in RANS models. Another approach is to provide a closure of the filtered reaction rate, $\widehat{\dot{\omega}}$, using an FPI tabulation (Domingo *et al.*, 2005)

$$\widehat{\dot{\omega}} = \int_0^1 \dot{\omega}_o(\zeta)\, \widehat{p}(\zeta)\, d\zeta \ , \tag{8.2}$$

where $\widehat{p}(\zeta)$ is the filtered pdf whose shape is presumed. The limitations of such a closure based only on unstrained flamelets are clearly documented in this thesis. The attenuation of reaction rate due to turbulence straining is likely to affect $\widehat{\dot{\omega}}$ just as it affects $\overline{\dot{\omega}}$. Therefore it will be worthwhile to extend the scalar dissipation based strained flamelet approach to provide a closure for the filtered reaction rate, $\widehat{\dot{\omega}}$.

Appendix A

Relations between Reynolds and Favre averaged quantities

The Reynolds average quantities can be obtained from Favre averaged quantities if the relation between $p(\zeta)$ and $\widetilde{p}(\zeta)$ and the shape of the latter is known. We know that

$$p(\zeta) = \frac{1+\tau\zeta}{1+\tau\tilde{c}}\,\widetilde{p}(\zeta),$$

and hence

$$\overline{c} \;=\; \int_0^1 \zeta\; p(\zeta)\; d\zeta \;=\; \frac{1}{1+\tau\tilde{c}} \int_0^1 \zeta(1+\tau\zeta)\;\widetilde{p}(\zeta) d\zeta. \tag{A.1}$$

The pdf $\widetilde{p}(\zeta)$ is presumed to be a β–pdf i.e. $\widetilde{p}(\zeta) = C\zeta^{a-1}(1-\zeta)^{b-1}$, where

$$C = \frac{1}{\beta(a,b)}, \quad a = \tilde{c}\left(\frac{1}{g}-1\right), \quad b = (1-\tilde{c})\left(\frac{1}{g}-1\right)$$

and the variance parameter is $g \equiv \widetilde{c''^2}/\tilde{c}(1-\tilde{c})$. The beta function is written in terms of the gamma functions (Davis, 1970) as $\beta(a,b) = \int_0^1 \zeta^{a-1}(1-\zeta)^{b-1}d\zeta = \Gamma(a)\Gamma(b)/\Gamma(a+b)$. Substituting for $\widetilde{p}(\zeta)$ in Eq. (A.1) and using the above definitions yields

$$\overline{c}(1+\tau\tilde{c}) = \frac{\Gamma(a+b)}{\Gamma(a)\Gamma(b)}\;\left\{\frac{\Gamma(a+1)\Gamma(b)}{\Gamma(a+b+1)} \;+\; \tau\frac{\Gamma(a+2)\Gamma(b)}{\Gamma(a+b+2)}\right\}. \tag{A.2}$$

Using the property of the gamma function $\Gamma(x+1) = x\Gamma(x)$ (Davis, 1970) and simplifying the above equation yields

$$\overline{c}(1+\tau\tilde{c}) \;=\; \frac{a}{a+b}\left\{1+\;\tau\frac{a+1}{a+b+1}\right\}\;. \tag{A.3}$$

After some algebra one gets

$$\overline{c} = \tilde{c} + \tau\frac{\widetilde{c''^2}}{(1+\tau\tilde{c})}\;. \tag{A.4}$$

It is interesting to note that the BML relationship (Bray, 1980), $\overline{c} = \tilde{c}(1+\tau)/(1+\tau\tilde{c})$, is recovered when $\widetilde{c''^2} = \tilde{c}(1-\tilde{c})$.

The variance can be written as

$$\overline{c'^2} = \int_0^1 \zeta^2 p(\zeta)d\zeta - \overline{c}^2\;. \tag{A.5}$$

Repeating the above steps yields

$$(\overline{c'^2} + \overline{c}^2)(1+\tau\tilde{c}) = \frac{a(a+1)}{(a+b)(a+b+1)}\left\{1+\tau\frac{a+2}{a+b+2}\right\} \tag{A.6}$$

with the final result as

$$\overline{c'^2} \;=\; \frac{\tilde{c}^2+\widetilde{c''^2}}{1+\tau\tilde{c}}\left\{1+\tau\frac{\tilde{c}^2(1-\tilde{c})+\widetilde{c''^2}(2-\tilde{c})}{\widetilde{c''^2}+\tilde{c}(1-\tilde{c})}\right\} \;-\; \overline{c}^2\;. \tag{A.7}$$

It is easy to see that for the case of constant density ($\tau = 0$), the above relations recover the equalities $\overline{c} = \tilde{c}$ and $\overline{c'^2} = \widetilde{c''^2}$.

Appendix B

List of Publications

- Kolla, H. & Swaminathan, N. (2010). Strained flamelets for turbulent premixed flames, I: formulation and planar flame results. *Combustion and Flame*, In press.
- Kolla, H. & Swaminathan, N. (2010). Strained flamelets for turbulent premixed flames, II: laboratory flame results. *Combustion and Flame*, Under review.
- Kolla, H., Rogerson, J.W. & Swaminathan, N. (2010). Validation of a turbulent flame speed model across combustion regimes. *Combustion Science and Technology*, In press.
- Kolla, H., Rogerson, J.W., Chakraborty, N. & Swaminathan, N. (2009). Scalar dissipation rate modeling and its validation. *Combustion Science and Technology*, **181**, 518–535.
- Kolla, H. & Swaminathan, N. (2009). Modelling of turbulent premixed flames using strained–flamelets. In 4^{th} *European Combustion Meeting, Vienna, Austria*, number 810106.

References

Abdel-Gayed, R.G. & Bradley, D. (1981). A two–eddy theory of premixed turbulent flame propagation. *Philosophical Transactions of the Royal Society of London A*, **301**, 1–25.

Abdel-Gayed, R.G., Bradley, D. & Lawes, M. (1987). Turbulent burning velocities: A general correlation in terms of straining rates. *Proceedings of the Royal Society of London A*, **414**, 389–413.

Akkerman, V. & Bychkov, V. (2005). Velocity of weakly turbulent flames of finite thickness. *Combustion Theory and Modelling*, **9**, 323–351.

Aldredge, R.C., Vaezi, V. & Ronney, P.D. (1998). Premixed-flame propagation in turbulent Taylor-Couette flow. *Combustion and Flame*, **115**, 395–405.

Anand, M., Zhu, J., Connor, C. & Razdan, M. (1999). Combustor flow analysis using an advanced finite-volume design system. *ASME, International Gas Turbine and Aeroengine Congress and Exhibition, Indianapolis, IN. Paper No. 99-GT-273.*.

Anand, M.S. & Pope, S.B. (1987). Calculations of premixed turbulent flames by PDF methods. *Combustion and Flame*, **67**, 127–142.

Andrews, G.E. & Bradley, D. (1972). The burning velocity of methane–air mixtures. *Combustion and Flame*, **19**, 275–288.

Ashurst, W.T., Kerstein, A.R., Kerr, R.M. & Gibson, C.H. (1987). Alignment of vorticity and scalar gradient with strain rate in simulated Navier-Stokes turbulence. *Physics of Fluids*, **30**, 2343–2353.

Batchelor, G. (1952). The effect of homogeneous turbulence on material lines and surfaces. *Proceedings of the Royal Society of London A*, **231**, 349.

Bell, J.B., Day, M.S., Shepherd, I.G., Johnson, M.R., Cheng, R.K., Grcar, J.F., Beckner, V.E. & Lijewski, M.J. (2005). Numerical simulation of a laboratory–scale turbulent v–flame. *Proceedings of the National Academy of Sciences of the United States of America*, **102**, 10006–10011.

Bilger, R.W. (1976). The Structure of Diffusion Flames. *Combustion Science and Technology*, **13**, 155–170.

Bilger, R.W. (1993). Conditional moment closure for turbulent reacting flow. *Physics of Fluids A*, **5**, 436.

Bilger, R.W. (2004a). Marker fields for turbulent premixed combustion. *Combustion and Flame*, **138**, 188–194.

Bilger, R.W. (2004b). Some aspects of scalar dissipation. *Flow, Turbulence and Combustion*, **72**, 93–114.

Bilger, R.W., Esler, M.B. & Starner, S.H. (1991). On reduced mechanisms for methane–air combustion. In M.D. Smooke, ed., *Reduced Kinetic Mechanisms and Asymptotic Approximations for Methane–Air Flames*, 86, Springer-Verlag, Berlin.

Bilger, R.W., Pope, S.B., Bray, K.N.C. & Driscoll, J.F. (2005). Paradigms in turbulent combustion research. *Proceedings of the Combustion Institute*, **30**, 21–42.

Boger, M., Veynante, D., Boughanem, H. & Trouvé, A. (1998). Direct numerical simulation analysis of flame surface density concept for large eddy simulation of turbulent premixed combustion. In *Twenty Seventh Symposium (International) on Combustion*, 917–925.

Borghi, R. (1988). Turbulent Combustion Modeling. *Progress in Energy and Combustion Science*, **14**, 245–292.

Borghi, R. (1990). Turbulent premixed combustion: Further discussions on the scales of fluctuations. *Combustion and Flame*, **80**, 304–312.

Bradley, D. (1992). How fast can we burn. In *Twenty Fourth Symposium (International) on Combustion*, 247–262.

Bradley, D. (2002). Problems of predicting turbulent burning rates. *Combustion Theory and Modelling*, **6**, 361–382.

Bradley, D., Kwa, L.K., Lau, A.K.C., Missaghi, M. & Chin, S.B. (1988). Laminar flamelet modeling of recirculating premixed methane and propane-air combustion. *Combustion and Flame*, **71**, 109–122.

Bradley, D., Lau, A.K.C. & Lawes, M. (1992). Flame stretch rate as a determinant of turbulent burning velocity. *Philosophical Transactions of the Royal Society of London A*, **338**, 359–387.

Bradley, D., Gaskell, P.H. & Gu, X.J. (1994). Application of a Reynolds stress, stretched flamelet, mathematical model to computations of turbulent burning velocities and comparison with experiments. *Combustion and Flame*, **96**, 221–248.

Bradley, D., Gaskell, P.H. & Gu, X.J. (1996). Burning Velocities, Markstein Lengths and Flame Quenching for Spherical Methane–Air Flames: A Computational Study. *Combustion and Flame*, **104**, 176–198.

Bradley, D., Gaskell, P.H. & Gu, X.J. (1998). The modeling of aerodynamic strain rate and flame curvature effects in premixed turbulent combustion. In *Twenty Seventh Symposium (International) on Combustion*, 849.

Bradley, D., Gaskell, P.H., Gu, X.J. & Sedaghat, A. (2005). Premixed flamelet modelling: Factors influencing the turbulent heat release rate source term and the turbulent burning velocity. *Combustion and Flame*, **143**, 227–245.

Bray, K.N.C. (1979). The interaction between Turbulence and Combustion. In *Seventeenth Symposium (International) on Combustion*, 223–233.

Bray, K.N.C. (1980). Turbulent flows with premixed reactants. In P.A. Libby & F.A. Williams, eds., *Turbulent Reacting Flows*, 115–183, Springer–Verlag, New York.

Bray, K.N.C. (1990). Studies of the turbulent burning velocity. *Proceedings of the Royal Society of London A*, **431**, 315–335.

Bray, K.N.C. & Cant, R.S. (1991). Some applications of Kolmogorov's turbulence research in the field of combustion. *Proceedings of the Royal Society of London A*, **434**, 217–240.

Bray, K.N.C. & Libby, P.A. (1976). Interaction effects in Turbulent Premixed Flames . *Physics of Fluids*, **19**, 1687–1701.

Bray, K.N.C. & Moss, J.B. (1977). A unified Statistical model of the Premixed Turbulent Flame. *Acta Astronautica*, **4**, 291–319.

Bray, K.N.C. & Swaminathan, N. (2006). Scalar dissipation and flame surface density in premixed turbulent combustion. *Comptes Rendus Mécanique*, **334**, 466–473.

Bray, K.N.C., Libby, P.A., Masuya, G. & Moss, J.B. (1981). Turbulence Production in Premixed Turbulent Flames. *Combustion Science and Technology*, **25**, 127–140.

Bray, K.N.C., Libby, P.A. & Moss, J.B. (1984). Flamelet Crossing Frequencies and Mean Reaction Rates in Premixed Turbulent Combustion. *Combustion Science and Technology*, **41**, 143–172.

Bray, K.N.C., Champion, M. & Libby, P.A. (1989). The interaction between turbulence and chemistry in premixed turbulent flames. In R. Borghi & S.N. Murthy, eds., *Turbulent reacting flows*, Lecture Notes in Engineering, 541–563, Springer Verlag.

Bray, K.N.C., Champion, M. & Libby, P.A. (1992). Premixed flames in stagnating turbulence part III - The $\tilde{k}$–$\widetilde{\varepsilon}$ theory for reactants impinging on a wall. *Combustion and Flame*, **91**, 165–186.

Bray, K.N.C., Domingo, P. & Vervisch, L. (2005). Role of the progress variable in models for partially premixed combustion. *Combustion and Flame*, **141**, 431–437.

Bray, K.N.C., Champion, M., Libby, P.A. & Swaminathan, N. (2006). Finite rate chemistry and presumed pdf models for premixed turbulent combustion. *Combustion and Flame*, **146**, 665–673.

Bychkov, V. (2000). Velocity of turbulent flamelets with realistic fuel expansion. *Physical Review Letters*, **84**, 6122–6125.

Cambray, P. & Joulin, G. (1992). On moderately–forced premixed flames. In *Twenty Fourth Symposium (International) on Combustion*, 61–67.

Candel, S.M. & Poinsot, T.J. (1990). Flame stretch and the balance equation for the flame area. *Combustion Science and Technology*, **70**, 1–15.

Cant, R.S. & Mastorakos, E. (2008). *An Introduction to Turbulent Reacting Flows*. Imperial College Press, London.

Chakraborty, N. & Swaminathan, N. (2007a). Influence of the Damköhler number on turbulence-scalar interaction in premixed flames. I. physical insight. *Physics of Fluids*, **19**, 045103.

Chakraborty, N. & Swaminathan, N. (2007b). Influence of the Damköhler number on turbulence-scalar interaction in premixed flames. II. model development. *Physics of Fluids*, **19**, 045104.

Chakraborty, N., Rogerson, J.W. & Swaminathan, N. (2008). *A Priori* assessment of closures for scalar dissipation rate transport in turbulent premixed flames using direct numerical simulation. *Physics of Fluids*, **20**, 045106.

Chakraborty, N., Klein, M. & Swaminathan, N. (2009). Effects of Lewis number on the reactive scalar gradient alignment with local strain rate in turbulent premixed flames. *Proceedings of the Combustion Institute*, **32**.

Chen, Y.C. & Bilger, R.W. (2001a). Simultaneous 2-d imaging measurements of reaction progress variable and OH radical concentration in turbulent premixed flames: Experimental methods and flame brush structure. *Combustion Science and Technology*, **167**, 131–167.

Chen, Y.C. & Bilger, R.W. (2001b). Simultaneous 2-d imaging measurements of reaction progress variable and OH radical concentration in turbulent premixed flames: Instantaneous flame-front structure. *Combustion Science and Technology*, **167**, 187–222.

Chen, Y.C. & Bilger, R.W. (2002). Experimental investigation of three-dimensional flame-front structure in premixed turbulent combustion-i: hydrocarbon/air bunsen flames. *Combustion and Flame*, **131**, 400–435.

Chen, Y.C., Peters, N., Schneeman, G.A., Wruck, N., Renz, U. & Mansour, M.S. (1996). The detailed flame structure of highly stretched turbulent premixed methane-air flames. *Combustion and Flame*, **107**, 223–244.

Chomiak, J., Hakberg, B. & Olsson, E. (1991). A note on the scalar dissipation rates in turbulent flows. *Combustion and Flame*, **83**, 412–414.

Clavin, P. (1985). Dynamic behavior of premixed flame fronts in laminar and turbulent flows. *Progress in Energy and Combustion Science*, **11**, 1–59.

Correa, S.M. (1992). A review of NOx formation under gas–turbine combustion conditions. *Combustion Science and Technology*, **87**, 329–362.

Correa, S.M. (1998). Power generation and aeropropulsion gas turbines: From combustion science to combustion technology. In *Twenty Seventh Symposium (International) on Combustion*, 1793–1807.

Corvellec, C., Bruel, P. & Sabel'nikov, V.A. (2000). Turbulent premixed flames in the flamelet regime: Burning velocity spectral properties in the presence of countergradient diffusion. *Combustion and Flame*, **120**, 585–588.

Curtiss, C.F. & Hirschfelder, J.O. (1949). Transport Properties of Multicomponent Gas Mixtures. *The Journal of Chemical Physics*, **17**, 550–555.

Damköhler, G. (1940). *Zeitschrift für Elektrochemie*, **46**, 601–652 (English Translation NACA TM 1112, 1947).

Davis, L.B. & Washam, R.M. (1988). Development of a dry low NOx combustor. No. ASME 89-GT-255 in Gas Turbine and Aeroengine Congress and Exposition, Toronto, Ontario, Canada.

Davis, P.J. (1970). Gamma function and related functions. In M. Abramowitz & I.A. Stegun, eds., *Handbook of Mathematical Functions*, 255–258, Dover, New York.

De, A. & Acharya, S. (2008). Combustor flow analysis using an advanced finite-volume design system. *Proceedings of ASME Turbo Expo 2008: Power for Land, Sea and air, Berlin, Germany, Paper No. GT 2008-51320.*.

Dixon-Lewis, G. (1990). Structure of laminar flames. In *Twenty Third Symposium (International) on Combustion*, 305–324.

Domingo, P., Vervisch, L. & Bray, K.N.C. (2002). Partially premixed flamelets in LES of nonpremixed turbulent combustion. *Combustion Theory and Modelling*, **6**, 529–551.

Domingo, P., Vervisch, L., Payet, S. & Hauguel, R. (2005). DNS of a premixed turbulent V flame and LES of a ducted flame using a FSD-PDF subgrid scale closure with FPI-tabulated chemistry. *Combustion and Flame*, **143**, 566–586.

Driscoll, J.F. (2008). Turbulent premixed combustion:flamelet structure and its effect on turbulent burning velocities. *Progress in Energy and Combustion Science*, **34**, 91–134.

Duclos, J.M., Veynante, D. & Poinsot, T.J. (1993). A comparison of flamelet models for premixed turbulent combustion. *Combustion and Flame*, **95**, 101–107.

Dunn, M.J., Masri, A.R. & Bilger, R.W. (2007). A new piloted premixed jet burner to study strong finite-rate chemistry effects. *Combustion and Flame*, **151**, 46–60.

Dunn, M.J., Masri, A.R., Bilger, R.W., Barlow, R.S. & Wang, G.H. (2009). The compositional structure of highly turbulent piloted premixed flames issuing into a hot coflow. *Proceedings of the Combustion Institute*, **32**, 1779–1786.

Eswaran, V. & Pope, S.B. (1988). Direct numerical simulations of the turbulent mixing of a passive scalar. *Physics of Fluids*, **31**, 506–520.

Filatyev, S.A., Driscoll, J.F., Carter, C.D. & Donbar, J.M. (2005). Measured properties of turbulent premixed flames for model assessment, including burning velocities, stretch rates and surface densities. *Combustion and Flame*, **141**, 1–21.

Fiorina, B., Baron, R., Gicquel, O., Thevenin, D., Carpentier, S. & Darabiha, N. (2003). Modelling non-adiabatic partially premixed flames using flame-prolongation of ILDM. *Combustion Theory and Modelling*, **7**, 449–470.

Fiorina, B., Gicquel, O., Vervisch, L., Carpentier, S. & Darabiha, N. (2005). Premixed turbulent combustion modeling using tabulated detailed chemistry and pdf. *Proceedings of the Combustion Institute*, **30**, 867–874.

Fureby, C. (2005). A fractal flame–wrinkling large eddy simulation model for premixed turbulent combustion. *Proceedings of the Combustion Institute*, **30**, 593–601.

Gao, F. & O'Brien, E.E. (1991). A mapping closure for multispecies Fickian diffusion. *Physics of Fluids A*, **3**, 956.

Gicquel, O., Darabiha, N. & Thévenin, D. (2000). Laminar premixed hydrogen/air counterflow flame simulations using flame prolongation of ILDM with differential diffusion. In *Twenty Eighth Symposium (International) on Combustion*, 1901–1908.

Gouldin, F.C. (1996). Combustion intensity and burning rate integral of premixed flames. In *Twenty Sixth Symposium (International) on Combustion*, 381–388.

Gouldin, F.C., Bray, K.N.C. & Chen, J.Y. (1989). Chemical closure model for fractal flamelets. *Combustion and Flame*, **77**, 241–259.

Gran, I.R., Echekki, T. & Chen, J.H. (1996). Negative flame speed in an unsteady 2-D premixed flame: A computational study. In *Twenty Sixth Symposium (International) on Combustion*, 323–329.

Gülder, O.L. (1990). Turbulent premixed flame propagation models for different combustion regimes. In *Twenty Third Symposium (International) on Combustion*, 743–750.

Hakberg, B. & Gosman, A.D. (1984). Analytical determination of turbulent flame speed from combustion models. In *Twentieth Symposium (International) on Combustion*, 225–232.

Hartung, G., Hult, J., Kaminski, C.F., Rogerson, J. & Swaminathan, N. (2008). Effect of heat release on turbulence and scalar-turbulence interaction in premixed combustion. *Physics of Fluids*, **20**, 035110.

Hawkes, E.R. & Chen, J.H. (2006). Comparison of direct numerical simulation of lean premixed methane-air flames with strained laminar flame calculations. *Combustion and Flame*, **144**, 112–125.

Hélie, J. & Trouvé, A. (2000). A Modified Coherent Flame model to describe turbulent flame propagation in mixtures with variable composition. In *Twenty Eighth Symposium (International) on Combustion*, 193–201.

Herrmann, M. (2006). Numerical simulation of turbulent Bunsen flames with a level set flamelet model. *Combustion and Flame*, **145**, 357–375.

Heywood, J.B. (1976). Pollutant formation and control in spark–ignition engines. *Progress in Energy and Combustion Science*, **1**, 135–164.

Il'yashenko, S.M. & Talantov, A.V. (1966). Theory and analysis of straight-through-flow combustion chambers. Edited machine translation, Wright Patterson AFB, Ohio, United States.

IPCC (2007). Climate change 2007: Synthesis report. Intergovernmental Panel on Climate Change, Geneva, Switzerland.

Jiménez, C., Cuenot, B., Poinsot, T. & Haworth, D. (2002). Numerical Simulation and Modeling for Lean Stratified Propane–Air Flames. *Combustion and Flame*, **128**, 1–21.

Jones, W.P. (1994). Turbulence modelling and numerical solution methods for variable density and combusting flows. In P.A. Libby & F.A. Williams, eds., *Turbulent Reacting Flows*, 309–374, Academic Press, London.

Jones, W.P. & Launder, B.E. (1972). The prediction of laminarization with a 2–equation model of turbulence. *International Journal of Heat and Mass Transfer*, **15**, 301.

Kee, R.J., Grcar, J.F., Smooke, M.D. & Miller, J.A. (1985). A fortran program for modeling steady laminar one–dimensional premixed flames. Tech. Rep. SAND85-8240, Sandia National Laboratories.

Kerstein, A.R. & Ashurst, W.T. (1992). Propagation rate of growing interfaces in stirred fluids. *Physical Review Letters*, **68**, 934–937.

Kim, S.H. & Bilger, R.W. (2007). Iso-surface mass flow density and its implications for turbulent mixing and combustion. *Journal of Fluid Mechanics*, **590**, 381–409.

Klimenko, A.Y. (1990). Multicomponent diffusion of various admixtures in turbulent flow. *Fluid Dynamics*, **25**, 327–334.

Klimenko, A.Y. & Bilger, R.W. (1999). Conditional moment closure for turbulent combustion. *Progress in Energy and Combustion Science*, **25**, 595–687.

Klimov, A.M. (1963). *Zhurnal Prikladnoi Mekhaniki i Tekhnicheskoi Fiziki*, **3**, 49–58.

KLIMOV, A.M. (1983). In J.R. Bowen, N. Manson, A.K. Oppenheim & R.I. Soloukhin, eds., *Flames, Lasers and Reactive Systems*, vol. 88 of *Progress in Aeronautics and Astronautics*, 133–146, American Institute of Aeronautics and Astronautics, New York.

KOBAYASHI, H. & KAWAZOE, H. (2000). Flame instability effects on the smallest wrinkling scale and burning velocity of high–pressure turbulent premixed flames. In *Twenty Eighth Symposium (International) on Combustion*, 375–382.

KOBAYASHI, H., TAMURA, T., MARUTA, K., NIIOKA, T. & WILLIAMS, F.A. (1996). Burning velocity of turbulent premixed flames in a high–pressure environment. In *Twenty Sixth Symposium (International) on Combustion*, 389–396.

KOBAYASHI, H., NAKASHIMA, T., TAMURA, T., MARUTA, K. & NIIOKA, T. (1997). Turbulence measurements and observations of turbulent premixed flames at elevated pressures up to 3.0 mpa. *Combustion and Flame*, **108**, 104–117.

KOBAYASHI, H., KAWAHATA, T., SEYAMA, K., FUJIMORI, T. & KIM, J.S. (2002). Relationship between the smallest scale of flame wrinkles and turbulence characteristics of high–pressure, high–temperature turbulent premixed flames. *Proceedings of the Combustion Institute*, **29**, 1793–1800.

KOLLA, H., ROGERSON, J.W., CHAKRABORTY, N. & SWAMINATHAN, N. (2009). Scalar dissipation rate modelling and its validation. *Combustion Science and Technology*, **181**, 518–535.

LAW, C.K. (1993). A compilation of experimental data on laminar burning velocities. In N. Peters & B. Rogg, eds., *Reduced Kinetic Mechanisms for Applications in Combustion Systems*, 15–26, Springer-Verlag, New York.

LAW, C.K. (2006). *Combustion Physics*. Cambridge University Press, New York.

LAW, C.K., ZHU, D.L. & YU, G. (1986). Propagation and extinction of stretched premixed flames. In *Twenty First Symposium (International) on Combustion*, 1419–1426.

Law, C.K., Zhu, D.L. & Yu, G. (1994). On the structural sensitivity of-purely strained planar premixed flames to strain rate variations. *Combustion and Flame*, **98**, 139–154.

Lee, C.H. & Lee, K.H. (2007). An experimental study on the combustion and emission characteristics of a stratified charge compression ignition (SCCI) engine. *Energy & Fuels*, **21**, 1901–1907.

Lefebvre, A.H. (1999). *Gas Turbine Combustion*. Taylor and Francis, Philadelphia, Pennsylvania, 2nd edn.

Libby, P.A. (1989). Characteristics of laminar lifted flames in a partially premixed jet. *Combustion Science and Technology*, **68**, 15–33.

Libby, P.A. & Williams, F.A. (1980). Fundamental aspects. In P.A. Libby & F.A. Williams, eds., *Turbulent Reacting Flows*, 1–43, Springer–Verlag, New York.

Libby, P.A. & Williams, F.A. (1982). Structure of laminar flamelets in premixed turbulent flames. *Combustion and Flame*, **44**, 287–303.

Libby, P.A. & Williams, F.A. (2000). A presumed pdf analysis of partially premixed turbulent combustion. *Combustion Science and Technology*, **161**, 351–390.

Libby, P.A., Linan, A. & Williams, F.A. (1983). Strained Premixed Laminar Flames with Nonunity Lewis Numbers. *Combustion Science and Technology*, **34**, 257–293.

Lieuwen, T., Neumeier, Y. & Zinn, B.T. (1998). The Role of Unmixedness and Chemical Kinetics in Driving Combustion Instabilities in Lean Premixed Combustors. *Combustion Science and Technology*, **135**, 193–211.

Lindstedt, R.P. & Vaos, E.M. (2006). Transported pdf modeling of high–Reynolds–number premixed turbulent flames. *Combustion and Flame*, **145**, 495–511.

Lipatnikov, A.N. & Chomiak, J. (2002). Turbulent flame speed and thickness: phenomenology, evaluation and application in multi-dimensional simulations. *Progress in Energy and Combustion Science*, **28**, 1–74.

Lutz, A.E., Kee, R.J., Grcar, J.F. & Rupley, F.M. (1997). OPPDIF: A fortran program for computing opposed–flow diffusion flames. Tech. Rep. SAND96-8243, Sandia National Laboratories.

Maas, U. & Pope, S. (1992a). Implementation of simplified chemical kinetics based on intrinsic low–dimensional manifolds. In *Twenty Fourth Symposium (International) on Combustion*, 103–112.

Maas, U. & Pope, S. (1992b). Simplifying Chemical Kinetics: Intrinsic Low–Dimensional Manifolds in Composition Space. *Combustion and Flame*, **88**, 239–264.

Maas, U. & Pope, S.B. (1994). Laminar Flame Calculations using Simplified Chemical Kinetics based on Intrinsic Low–Dimensional Manifolds. In *Twenty Fifth Symposium (International) on Combustion*, 1349–1356.

Mantel, T. & Bilger, R.W. (1995). Some conditional statistics in a turbulent premixed flame derived from direct numerical simulations. *Combustion Science and Technology*, **110-111**, 393–417.

Mantel, T. & Borghi, R. (1994). A new model of premixed wrinkled flame propagation based on a scalar dissipation equation. *Combustion and Flame*, **96**, 443–457.

Marble, F.E. & Broadwell, J.E. (1977). The coherent flame model for turbulent chemical reactions. Tech. Rep. TRW–9–PU.

Mason, H.B. & Spalding, D.B. (1973). In F.J. Weinberg, ed., *Combustion Institute European Symposium*, 601–606, Academic Press, New York.

Mitarai, S., Riley, J.J. & Kosály, G. (2005). Testing of mixing models for Monte Carlo probability density function simulations. *Physics of Fluids*, **17**.

Mongia, H.C. (1998). Aero-Thermal Design and Analysis of Gas Turbine Combustion Systems Current Status and Future Direction. *AIAA Paper 98–3982*.

Moss, J.B. (1980). Simultaneous measurements of concentration and velocity in an open premixed turbulent flame. *Combustion Science and Technology*, **22**, 119–129.

Muppala, S.P.R., Aluri, N.K., Dinkelacker, F. & Leipertz, A. (2005). Development of an algebraic reaction rate closure for the numerical calculation of turbulent premixed methane, ethylene, and propane/air flames for pressures up to 1.0 mpa. *Combustion and Flame*, **140**, 257–266.

Mura, A. & Borghi, R. (2003). Towards an extended scalar dissipation equation for turbulent premixed combustion. *Combustion and Flame*, **133**, 193–196.

Nada, Y., Tanahashi, M. & Miyauchi, T. (2004). Effect of turbulence characteristics on local flame structure of H_2-air premixed flames. *Journal of Turbulence*, **5:1**, 1–15.

O'Brien, E.E. (1980). The probability density function (pdf) approach to reacting turbulent flows. In P.A. Libby & F.A. Williams, eds., *Turbulent Reacting Flows*, 185–218, Springer–Verlag, New York.

Patankar, S.V. (1980). *Numerical Heat Transfer and Fluid Flow*. Taylor and Francis, London.

Paul, R.N. & Bray, K.N.C. (1996). Study of premixed turbulent combustion including Landau-Darrieus instability effects. In *Twenty Sixth Symposium (International) on Combustion*, 259–266.

Peters, N. (1984). Laminar diffusion flamelet models in non–premixed combustion. *Progress in Energy and Combustion Science*, **10**, 319–339.

Peters, N. (1986). Laminar Flamelet Concepts in Turbulent Combustion. In *Twenty First Symposium (International) on Combustion*, 1231–1250.

Peters, N. (1999). The turbulent burning velocity for large-scale and small-scale turbulence. *Journal of Fluid Mechanics*, **384**, 107–132.

PETERS, N. (2000). *Turbulent Combustion*. Cambridge University Press.

PETERS, N. & WILLIAMS, F.A. (1987). The asymptotic structure of stoichiometric methane–air flames. *Combustion and Flame*, **68**, 185–207.

PITSCH, H. & DE LAGENESTE, L.D. (2002). Large-eddy simulation of premixed turbulent combustion using a level-set approach. *Proceedings of the Combustion Institute*, **29**, 2001–2008.

POINSOT, T. & VEYNANTE, D. (2001). *Theoretical and Numerical Combustion*. Edwards, Philadelphia.

POINSOT, T., VEYNANTE, D. & CANDEL, S. (1991). Quenching Processes and Premixed Turbulent Combustion Diagrams. *Journal of Fluid Mechanics*, **228**, 561–605.

POPE, S.B. (1978). An explanation of the turbulent round-jet/plane-jet anomaly. *AIAA Journal*, **16**, 279–281.

POPE, S.B. (1985). PDF methods for turbulent reactive flows. *Progress in Energy and Combustion Science*, **11**, 119–192.

POPE, S.B. (1988). The evolution of surfaces in turbulence. *International Journal of Engineering Science*, **26**, 445–469.

POPE, S.B. (1990). Computations of Turbulent Combustion: Progress and Challenges. In *Twenty Third Symposium (International) on Combustion*, 591–612.

POPE, S.B. & ANAND, M.S. (1984). Flamelet and distributed combustion in premixed turbulent flames. In *Twentieth Symposium (International) on Combustion*, 403–410.

PRASAD, R.O.S. & GORE, J.P. (1999). An evaluation of flame surface density models for turbulent premixed jet flames. *Combustion and Flame*, **116**, 1–14.

REYNOLDS, W.C. (1986). The element potential method for chemical equilibrium analysis: Implementation in the interactive program STANJAN. Tech. rep., Department of Mechanical Engineering, Stanford University.

Ribert, G., Champion, M. & Plion, P. (2004). Modeling turbulent reactive flows with variable equivalence ratio: Application to the calculation of a reactive shear layer. *Combustion Science and Technology*, **176**, 907–923.

Robin, V., Mura, A., Champion, M. & Plion, P. (2006). A Multi–Dirac presumed pdf model for turbulent reactive flows with variable equivalence ratio. *Combustion Science and Technology*, **178**, 1843–1870.

Robin, V., Mura, A., Champion, M., Degardin, O., Renou, B. & Boukhalfa, M. (2008). Experimental and numerical analysis of stratified turbulent V-shaped flames. *Combustion and Flame*, **153**, 288–315.

Rogerson, J.W. & Swaminathan, N. (2007). Correlation between dilatation and scalar dissipation in turbulent premixed flames. In *Proceedings of the European Combustion Meeting*.

Rogerson, J.W., Swaminathan, N., Tanahashi, M. & Shiwaku, N. (2007). Analysis of progress variable variance equations using DNS data. In *Proceedings of the European Combustion Meeting*.

Rolls-Royce (2005). *The Jet Engine*. Rolls–Royce plc, London, England.

Ronney, P.D. & Yakhot, V. (1992). Flame broadening effects on premixed turbulent flame speed. *Combustion Science and Technology*, **86**, 31–43.

Rutland, C.J. & Cant, R.S. (1994). Turbulent transport in premixed flames. In *Proceedings of Summer Program, Centre for Turbulence Research*, 75–94, NASA Ames/ Stanford University.

Savarianandam, V.R. & Lawn, C.J. (2006). Burning velocity of premixed turbulent flames in the weakly wrinkled regime. *Combustion and Flame*, **146**, 1–18.

Schneider, E., Sadiki, A. & Janicka, J. (2005). Modeling and 3D-Simulation of the Kinetic Effects in the Post-Flame Region of Turbulent Premixed Flames Based on the G-Equation Approach. *Flow, Turbulence and Combustion*, **75**, 191–216.

Shepherd, I.G. & Cheng, R.K. (2001). The burning rate of premixed flames in moderate and intense turbulence. *Combustion and Flame*, **127**, 2066–2075.

Shepherd, I.G. & Kostiuk, L.W. (1994). The burning rate of premixed turbulent flames in divergent flows. *Combustion and Flame*, **96**, 371–380.

Shepherd, I.G., Bourguignon, E., Michou, Y. & Gokalp, I. (1998). The burning rate in turbulent bunsen flames. In *Twenty Seventh Symposium (International) on Combustion*, 909–916.

Shih, W.P., Lee, J.G. & Santavicca, D.A. (1996). Stability and Emissions Characteristics of a Lean Premixed Gas Turbine Combustor. In *Twenty Sixth Symposium (International) on Combustion*, 2771–2778.

Smith, K.O. & Gouldin, F.C. (1978). Experimental investigation of flow turbulence effects on premixed methane-air flames. *Progress in Astronautics and Aeronautics*, **58**, 37–54.

Somers, B. (1994). *The Simulation of Flat flames with Detailed and Reduced Chemical Models*. Ph.D. thesis, Technische Universiteit Eindhoven.

Spalding, D.B. (1971). Concentration fluctuations in a round turbulent free jet. *Chemical Engineering Science*, **26**, 95–107.

Subramaniam, S. & Pope, S.B. (1998). A mixing model for turbulent reactive flows based on Euclidean minimum spanning trees. *Combustion and Flame*, **115**, 487–514.

Sung, C.J., Liu, J.B. & Law, C.K. (1996). On the scalar structure of nonequidiffusive premixed flames in counterflow. *Combustion and Flame*, **106**, 168–183.

Sung, C.J., Li, B., Law, C.K. & Wang, H. (1998). `http:/www.princeton.edu/~cklaw/kinetics/slw001`.

Swaminathan, N. & Bilger, R.W. (2001a). Analyses of conditional moment closure for turbulent premixed flames. *Combustion Theory and Modelling*, **5**, 241–260.

Swaminathan, N. & Bilger, R.W. (2001b). Scalar dissipation, diffusion and dilatation in turbulent H_2–air premixed flames with complex chemistry. *Combustion Theory and Modelling*, **5**, 429–446.

Swaminathan, N. & Bray, K.N.C. (2005). Effect of dilatation on scalar dissipation in turbulent premixed flames. *Combustion and Flame*, **143**, 549–565.

Swaminathan, N. & Grout, R.W. (2006). Interaction of turbulence and scalar fields in premixed flames. *Physics of Fluids*, **18**, 045102.

Swaminathan, N., Bilger, R.W. & Reutsch, G.R. (1997). Interdependence of the instantaneous flame front structure and the overall scalar flux in turbulent premixed flames. *Combustion Science and Technology*, **128**, 73–97.

Takagi, Y. (1998). A new era in spark–ignition engines featuring high–pressure direct injection. In *Twenty Seventh Symposium (International) on Combustion*, 2055–2068.

Trouvé, A. & Poinsot, T. (1994). The evolution equation for the flame surface density in turbulent premixed combustion. *Journal of Fluid Mechanics*, **278**, 1–31.

Vagelopoulos, C.M., Egolfopoulos, F.N. & Law, C.K. (1994). Further considerations on the determination of laminar flame speeds with the counterflow twin–flame technique. In *Twenty Fifth Symposium (International) on Combustion*, 1341–1347.

van Oijen, J.A. & de Goey, L.P.H. (2000). Modelling of premixed laminar flames using flamelet–generated manifolds. *Combustion Science and Technology*, **161**, 113–137.

Vervisch, L., Hauguel, R., Domingo, P. & Rullaud, M. (2004). Three facets of turbulent combustion modelling: DNS of premixed V-flame, LES of lifted nonpremixed flame and RANS of jet-flame. *Journal of Turbulence*, **5:1**, 1–36.

VEYNANTE, D. & POINSOT, T. (1997). Effects of pressure gradients on turbulent premixed flames. *Journal of Fluid Mechanics*, **353**, 83–114.

VEYNANTE, D. & VERVISCH, L. (2002). Turbulent combustion modeling. *Progress in Energy and Combustion Science*, **28**, 193–266.

WESTBROOK, C.K., MIZOBUCHI, Y., POINSOT, T.J., SMITH, P.J. & WARNATZ, J. (2005). Computational combustion. *Proceedings of the Combustion Institute*, **30**, 125–157.

WILLIAMS, F.A. (1976). Criteria for existence of wrinkled laminar flame structure of turbulent premixed flames. *Combustion and Flame*, **26**, 269–270.

WILLIAMS, F.A. (1985a). *Combustion Theory*. The Benjamin/Cummings Publishing Company, California.

WILLIAMS, F.A. (1985b). Turbulent combustion. In J.D. Buckmaster, ed., *The Mathematics of Combustion*, 97–131, SIAM, Philadelphia.

YAKHOT, V. (1988). Propagation velocity of premixed turbulent flames. *Combustion Science and Technology*, **60**, 191–214.

YAO, M., ZHENG, Z. & LIU, H. (2009). Progress and recent trends in homogeneous charge compression ignition (HCCI) engines. *Progress in Energy and Combustion Science*, **In Press**.

ZELDOVICH, Y.B., BARENBLATT, G.I., LIBROVICH, V.B. & MAKHVILADZE, G.M. (1985). *The mathematical theory of combustion and explosions*, 278–286. Consultants Bureau, New York.

ZHANG, S. & RUTLAND, C.J. (1995). Premixed flame effects on turbulence and pressure-related terms. *Combustion and Flame*, **102**, 447–461.

ZHAO, F., LAI, M.C. & HARRINGTON, D.L. (1999). Automotive spark ignited direct–injection gasoline engines. *Progress in Energy and Combustion Science*, **25**, 437–562.

Zimont, V.L. (2000). Gas premixed combustion at high turbulence. Turbulent flame closure combustion model. *Experimental Thermal and Fluid Science*, **21**, 179–186.

Zimont, V.L. & Lipatnikov, A.N. (1995). A numerical model of premixed turbulent combustion of gases. *Chemical Physics Reports*, **14**, 993–1025.